Studies on Nonlinear Dynamics of Ferroresonance in Transformers

Thesis Submitted by

Rajat Shubhra Pal

Doctor of Philosophy (Engineering)

Electrical Engineering Department,
Faculty Council of Engineering & Technology
Jadavpur University
Kolkata, India
2024

Jadavpur University

Faculty of Engineering and Technology

INDEX NO. - 163/17/E

1. **Title of the Thesis**:

Studies on Nonlinear Dynamics of Ferroresonance in Transformers

2. Name, Designation & Institution of the Supervisors:

Dr. Madhab Roy
Associate Professor
Electrical Engineering Department
Jadavpur University

3. List of Publications:

i. Journals:

- **Pal Shubhra Rajat**, Roy Madhab, "Investigation on the Stability of an Electric Power Circuit under Ferroresonance Based on Nonlinear Dynamic Model of Transformer", Recent Advances in Electrical & Electronic Engineering 2022; 15(7). https://dx.doi.org/10.2174/2352096515666220817123902

- **Pal, R.S**., Roy, M. "Verification of Period-Doubling Behavior of Ferroresonance Circuit with the Jacobian Matrix and Eigenvalues". J. Inst. Eng. India Ser. B (2022). https://doi.org/10.1007/s40031-022-00835-2

ii. Book Chapter:

- **Pal, R.S**., Roy, M. (2022). "Investigation on the Occurrence of Ferroresonance with the Variation of Degree of Transformer Core Saturation". In: Mahajan, V., Chowdhury, A., Padhy, N.P., Lezama, F. (eds) Sustainable Technology and Advanced Computing in Electrical Engineering . Lecture Notes in Electrical Engineering, vol 939. Springer, Singapore. https://doi.org/10.1007/978-981-19-4364-5_53

iii. Conferences:

- **R. S. Pal** and M. Roy, "Study and Verification of Ferroresonance Simulated with Rudenburg's Method," 2021 Innovations in Energy Management and Renewable Resources(52042), Kolkata, India, 2021, pp. 1-5, doi: https://doi.org/10.1109/IEMRE52042.2021.9386880

- **R. S. Pal** and M. Roy, "Investigation on the Occurrence of Ferroresonance with the Variation of Core Loss of a Transformer using Nonlinear Dynamic Model of the Transformer," 2021 7th International Conference on Electrical Energy Systems (ICEES), Chennai, India, 2021, pp. 445-447, doi: https://doi.org/10.1109/ICEES51510.2021.9383708

4. List of Patents: None

5. List of Presentations in National / International Conferences

i. "Study and Verification of Ferroresonance Simulated with Rudenburg's Method," Innovations in Energy Management and Renewable Resources - 2021, Organized by Institute of Engineering & Management, Kolkata, India, 5-7 February, 2021

ii. "Investigation on the Occurrence of Ferroresonance with the Variation of Core Loss of a Transformer using Nonlinear Dynamic Model of the Transformer," 7th International Conference on Electrical Energy Systems (ICEES), Organized by Sri Sivasubramaniya Nadar College of Engineering, Chennai, India, 11-13 February, 2021

iii. "Investigation on the Occurrence of Ferroresonance with the Variation of Degree of Transformer Core Saturation', International Conference on Sustainable Technology and Advanced Computing in Electrical Engineering (ICSTACE)), Organized by Sardar Vallabhbhai National Institute of Technology (SVNIT), Surat, India, 11 - 12 November, 2021

Statement of Originality

I, **Rajat Shubhra Pal,** registered on 02/06/2017 do hereby declare that this thesis entitled "***Studies on Nonlinear Dynamics of Ferroresonance in Transformers***" contains literature survey and original research work done by the undersigned candidate as part of Doctoral studies.

All information in this thesis have been obtained and presented in accordance with existing academic rules and ethical conduct. I declare that, as required by these rules and conduct, I have fully cited and referred all materials and results that are not original to this work.

I also declare that I have checked this thesis as per the "Policy on Anti Plagiarism, Jadavpur University, 2019", and the level of similarity as checked by iThenticate software is ___3___%.

Signature of Candidate: Rajat Shubhra Pal

Date: 18. 1. 24

Certified by Supervisor:

(Signature with date, seal)

18.01.2024.

.....

(**Dr. Madhab Roy**)

Associate Professor
Electrical Engg. Dept.
Jadavpur University
Kolkata - 700 032

CERTIFICATE FROM THE SUPERVISOR

This is to certify that the thesis entitled ***"Studies on Nonlinear Dynamics of Ferroresonance in Transformers***" submitted by Shri **Rajat Shubhra Pal**, who got his name registered on 02/06/2017 for the award of **Ph. D. (Engineering)** degree of Jadavpur University is absolutely based upon his own work under the supervision of **Dr. Madhab Roy** and that neither his thesis nor any part of the thesis has been submitted for any degree/diploma or any other academic award anywhere before.

M Madhab Roy 18.01.2024.

(**Dr. Madhab Roy**)

Signature of the Supervisor and date with Office Seal

Associate Professor
Electrical Engg. Dept.
Jadavpur University
Kolkata - 700 032

ACKNOWLEDGEMENT

The work presented in this thesis would not have been possible without my close association with many people. I take this opportunity to extend my sincere gratitude and appreciation to all those who have been instrumental in the successful completion of this thesis.

First and foremost, I would like to extend my sincere gratitude to my research guide **Dr. Madhab Roy, Associate Professor, Electrical Engineering Department, Jadavpur University**, for his dedicated help, advice, inspiration, encouragement and continuous support throughout my course work. His enthusiasm, integral view on research and his mission for providing high-quality work have made a deep impression on me.

I would like to pay my special thanks to the **HOD, Electrical Engineering Department, Jadavpur University** for the cooperation during the research. I am grateful for her constant support and help. I would also like to thank all the members of my **thesis committee** for their encouragement and insightful comments. I gratefully acknowledge all the **faculty members of Electrical Engineering Department of Jadavpur University**.

Finally, my sincere gratitude to my father and mother for their continuous and unparalleled love, help and support through the years. I am forever indebted to my father for giving me opportunities and experiences that have made me who I am. My mother selflessly encouraged me to explore new directions in life and seek my own destiny.

I offer my regards and blessings to all those who supported me in any respect during the completion of my research.

18.1.24.

Rajat Shubhra Pal

Preface

The phenomena of ferroresonance in the electrical power system is the subject of this thesis. Ferroresonance may occur if transmission line capacitance is in series with the magnetizing inductances of transformer with no load at a critical value in a AC Power System when the following conditions arise due to a fuse blown or unsynchronized 3-phase switching device that failed to connect all phases:

- 3-phase system grounded at the source, but having no ground at the transformers banks or vice versa.
- Underground cable length or overhead conductor length is sufficient to create the capacitance necessary.
- The degree of nonlinearity in the magnetic characteristics of the transformer.
- Transformers are unloaded or lightly loaded.
- VT is energized through the grading capacitance of the circuit breaker when circuit breakers disconnect the phases.

The sustained Ferroresonant over-voltages across the power system equipment may cause outages of the distressed transformers as well as line equipment, such as surge arresters, etc. Therefore, it is difficult to conduct experimental studies of ferroresonance in the commercial power system.

Thus, there have been a continuous research initiatives on ferroresonance over the years, to know it properly and attempts to predict or validate ferroresonance in vulnerable networks as well as mitigation strategies. The research focuses on designing ferroresonance in a laboratory setting to make it experimentally and creating a simulation models of ferroresonance incorporating transformer-nonlinear magnetizing characteristics mathematically for computer-based analysis. Considering ferroresonance-phenomenon as a nonlinear dynamical system, due to the intricacy of a nonlinear mathematical differential equations arising out of the saturable core of a transformer: the multiple stability of the system under ferroresonance to be a challenging topic for researchers today. Therefore, research on ferroresonance using nonlinear dynamical mathematics to ascertain how a Bifurcation or Chaos in the stability of the system results in fluctuations in the parameters of the system and ac source voltages is still needed.

Thus, this research work has been done on 'Studies on Nonlinear Dynamics of Ferroresonance in Transformers'.

The ferroresonance experiment was devised and developed in a lab setting. The ferroresonance incident experimentally has been captured successfully in the oscilloscope. Time domain waveform of capacitor-voltage and transformer-voltage at various source voltages are taken on the non-creation to creation of ferroresonance at various line conditions.

A simulation mathematical model of the experimental ferroresonance is developed to investigate ferroresonance further in a simulation environment where experiment is not permissible level. At first, existing 'Rudenburg's Method' is verified with present simulation model. The effect of the variation of different circuit parameters on ferroresonance occurrence was checked. Utilizing the nonlinear dynamic model of ferroresonance, an investigation is conducted on the occurrence of ferroresonance with variations in core loss and the variation of the degree of the transformer-core saturation and the results published.

An analysis of the stability of a power circuit under ferroresonance using a nonlinear dynamic model of the transformer has been performed. Analysis established the fact that the system ultimately landed in 'Chaos' after successive 'Period-Doubling' when the supply voltage was increased as parameter. Calculation of 'Feigenbaum Constant' also supports root-to-Chaos behavior of the system. 'Period-Doubling' behavior of the ferroresonance circuit is verified using a method of ‘Eigenvalues’ and the 'Jacobian Matrix' analysis for the 'Limit Cycles'. To investigate the stability, a small 'Perturbation' is injected into the system deliberately and the 'Jacobian Matrix' was calculated with the 'Poincare' values near 'Perturbation'. Finally, the 'Finite Element Method' is applied to study the flux-distribution in the magnetic core of the transformer under the ferroresonance condition.

The findings from simulation show that a minute variation of the system parameter in a nonlinear system can result in a different state of operations. It has also been demonstrated that chaotic ferroresonance states are likely to arise within a wide range of system parameters, even though fundamental frequency and sub-harmonic ferroresonance situations may occur under common-place operating settings. An Engineer must have a thorough understanding of these ferroresonance possibilities so they may plan for the expansion of their systems without increasing the likelihood of ferroresonance and can avoid the hazardous areas.

Contents

List of Figures

List of Tables

List of Symbols

V_a, V_b, V_c	Phase voltages
X_c	Capacitive impedance
X_m	Magnetizing impedance of the transformer
L	Inductance of magnetic circuit
C	Capacitance
f_0	Fundamental frequency
E	Impressed sinusoidal voltage
E_C	Voltage across constant Capacitor
E_L	Voltage across saturated Inductance
I	Circuit current.
I_λ	Charging current of the condenser
γ	Slope of the condenser line
I_μ	Magnetizing current of the saturated inductance
ω	Angular frequency of supply voltage
$f(I)$	Non-linear function of current
f	Supply voltage frequency
R	Resistance
$+ve$	Positive
$-ve$	Negative
V_S	Source voltage
R_C	Core loss resistance
i_λ	Magnetizing current of transformer
i_R	Current through core loss resistance
λ	Flux linkage
V_C	Voltage across capacitor
V_R	Voltage across resistance R
V_r	Voltage across resistance r
V_L	Voltage across inductor / transformer primary
i_φ	Transformer primary current

φ	Magnetic flux
n	Degree of core saturation
J	Jacobiam matrix
τ	Trace of Jacobiam matrix
Δ	Determinant of Jacobiam matrix
δ_n	Feigenbaum constant
$\tilde{\varphi}$	Potential function
$\upsilon_i(x, y)$	Shape functions
$[K^{(m)}]$	Characteristic matrix of m^{th} element
$\tilde{P}^{(m)}$	Characteristic vector of m^{th} element
$\tilde{A}$	Magnetic vector potential
J_e	Current density
R_{w1}	Resistance of primary winding of transformer
R_{w2}	Resistance of secondary winding of transformer
L_{L1}	Primary winding leakage inductance of transformer
L_{L2}	Secondary winding leakage inductance of transformer
L_H	Nonlinear inductance of transformer core
I_{EX}	Excitation current of transformer primary at no load
W_m	Stored magnetic energy
B	Magnetic flux density
H	Magnetic field intensity
μ	Permeability
L_{Fe}	Iron length of the transformer
Φ_0	Main flux of transformer at no load
L_0	No-load inductance
M	mutual inductance
N_1, N_2	Primary and secondary turns of transformer
i_1, i_2	Primary and secondary current of transformer
σ	Conductivity

List of Abbreviations

2D	Two dimensional
3D	Three dimensional
AC	Alternating current
C.B.	Circuit Breaker
CCVT	Coupling capacitor voltage transformers
CRO	Cathode ray oscilloscope
DC	Direct current
EMTP	Electromagnetic Transients Program
FEM	Finite Element Method
Fig.	Figure
GO	Grain Oriented
Hz	Hertz
i.e.	That is
Km	Kilometer
KV	Kilo volt
KVL	Kirchhoff's voltage law
MF	Multiplication factor
ms	Mili second
MVA	Mega Volt Ampere
MW	Mega Watt
nF	Nano farad
OCC	Open circuit characteristic
ODE	Ordinary differential equations
p.u.	Per unit
PDE	Partial differential equations
pF	Pico Farad
RMS	Root mean square
s	Second
SDE	Stochastic differential equations

T	Tesla
UI	United Illuminating
V	Volt
VT	Voltage transformer
Wb	Weber
ZnO	Zinc oxide
μF	Micro farad

1. Introduction

1.1 General Introduction

Ferroresonance is a phenomenon that can occur in electrical power systems when there is a combination of non-linear inductance and capacitance. It can result in a sustained oscillation of voltage and current in the system, leading to high voltages and currents that can cause damage to equipment and power outages. Ferroresonance occurs when the magnetic core of a transformer or reactor becomes saturated, causing a non-linear relationship between the applied voltage and the resulting magnetic flux. This can lead to the buildup of energy in the magnetic field, which can cause the voltage to oscillate at a frequency that is a multiple of the power system frequency. Ferroresonance can be triggered by a number of factors, including switching operations, lightning strikes, and faults in the power system. It is important to design power systems with care and to use appropriate protection devices to prevent or mitigate the effects of ferroresonance.

1.2 Research Gaps

Resonance in a transformer circuit was first reported in 1907 [1] and the term ferroresonance was first used in1920 [2]. Ferroresonance is possible in a series L-C circuit. Here the L can be the saturable iron core of a transformer and C is the capacitive effect of the line or some equipment. At the beginning, ferroresonance has been considered as an unknown phenomenon due its unpredictable nature, lack of mathematical tools to analyze its overall behavior. The first detailed analysis was provided by R. Rudenberg [3] in 1950. However, with the important developments in nonlinear dynamics and chaos theory the situation changed. Some useful engineering works on ferroresonance began to be published from late 1980s [4].

Although ferroresonance could be found due to abnormal situations like single pole switching in 3 phase, presence of PT with grading capacitance of C.B. but on the occurrence of that resulting in sustained ferroresonant over voltages and currents across the power system equipment; which may cause outages of distressed transformer along with line equipment- surge arrester, etc. So ferroresonance research activities are not possible in the commercial power system.

So over the years, there have been ferroresonance research activities like efforts to forecast or confirm the occurrence of ferroresonance in susceptible networks and mitigation measures [5-7]. The studies pertain recreation of ferroresonance in a laboratory environment and the development of mathematically suitable transformer models for simulations and analysis using the computer [8-10]. Nevertheless, the complexity of a non-linear mathematical equation representing the saturable core of a transformer making ferroresonance as a nonlinear dynamical system, still poses a challenge for researchers to understand the stability of the system under ferroresonance. So the study on ferroresonance and transformer experiencing it applying nonlinear dynamical mathematics to determine how the stability of the system changes, by a bifurcation, chaos, having variations of system(circuit) parameters is still under demand.

If we look at the research work done on ferroresonance in India in recent decades, we will found a series of papers published by R. Ramanujam and co-authors on the analytical study of ferroresonance. The dependency of single and double open conductor configurations [11], iron core loss nonlinearity [12] and arrestor [13] on the chaotic behavior of the ferroresonance circuit were discussed.

Experimental study on ferroresonance and its dependencies on various circuit parameters, initial conditions and instant of switching angle of the source voltage were done by M. Roy and his co-authors [14, 15]. Simulation done with the nonlinear model of the transformer [16]. Damping technique is also investigated [17].

Detailed work on the stability analysis of ferroresonance circuit with the help of nonlinear dynamic model of the transformer is not very common in India. So the studies on nonlinear dynamics of ferroresonance in transformers will have to be performed to explore this gap of ferroresonance study.

1.3 Objective of the Work

Objective of the research work can be divided into two phases. In the first phase, a nonlinear dynamic model of a ferroresonance system is to develop with the help of experimental data of the transformer. Generation of ferroresonance in the laboratory setup experimentally and validation of the ferroresonance model outputs by experimental ferroresonance results. In the second phase of the work, analysis to be done to understand the nonlinear dynamic model of the

ferroresonance system and to find out how stability of the system changes with the change of the system parameters.

1.4 Contribution of the Thesis

The following work has been performed under this thesis:

1. An experimental setup was developed and ferroresonance observed in laboratory
2. A suitable nonlinear dynamic model of the transformer was designed.
3. That model was tested in MATLAB and the results are compared with the experimental results.
4. The simulation model was examined for the effect of variation of different circuit parameters on the occurrence of ferroresonance. Results matched with the analysis given by R. Rudenberg.
5. Investigation on the stability of the electric power circuit under ferroresonance was carried out based on the nonlinear dynamic model of transformer. The output showed period doubling bifurcation of the system while supply voltage is increased in steps.
6. The period-doubling behavior of ferroresonance circuit was verified with both numerical simulation and mathematical analysis by Jacobian Matrix and corresponding Eigenvalues. Both the results agreed with each other.
7. System modelling was done in finite element method (FEM). Ferroresonance recreated in the Comsol Multiphysics simulator and the distribution of magnetic field under ferroresonance was observed.

1.5 Organization of the Thesis

This thesis work is divided into ten (10) chapters. The chapter-wise organization of this thesis is as follows:

Chapter 1 gives an overall introduction to the thesis. It discusses the current scenario of the ferroresonance study and the necessity of the proposed work. This is explained in a nutshell with the basic works that have been performed under the current thesis.

Chapter 2 on the definition of ferroresonance. It discusses the effects of ferroresonance that have been listed in different publications. The study says that the circuit consists of saturable

inductance, capacitance, and an alternating voltage source is prone to ferroresonance. How this combination can be achieved in the power system that also discussed in this chapter. In 1950, a German engineer R. Rudenberg presented a graphical analysis of ferroresonance which is the stepping stone of ferroresonance analysis. This chapter provides an overview of Rudenberg's analysis. Analysis shows, how the system jumps into ferroresonance from normal value while changing any of the circuit parameters. At the end of this chapter, a comprehensive study is made on the different types of works on ferroresonance that have been performed for decades. Four main categories have been discussed - examples & case studies, experimental investigations, damping, and analysis of ferroresonance.

Chapter 3 describes the details of a laboratory experiment that has been developed and performed to observe ferroresonance in a controlled environment. At first, the core magnetic characteristics of the transformer under the ferroresonance test is extracted from the open circuit test of the transformer. The series capacitance value is designed and calculated using R. Rudenberg's graphical method. To protect the digital oscilloscope a potential divider made of capacitor is used. To prevent the line equipment from extended exposure to overvoltage at ferroresonance, an auto cut-off switch is used which cuts off the circuit after a pre-defined time. The ferroresonance incident has been captured successfully. Time domain Waveform of capacitor voltage and transformer voltage at different source voltages are taken on the creation of ferroresonance at various line conditions.

Chapter 4 explains the process of building up the simulation model of ferroresonance incorporating experimental transformer magnetic characteristics. A wide experimental study on ferroresonance in a real setup is difficult and also hazardous for the equipment used as it involves power frequency and very high over-voltages. So for further study of ferroresonance, a suitable simulation model is developed. The B-H loop data of the transformer obtained from the experiment is used to find an approximated mathematical equation to represent the transformer core magnetism for the ferroresonance circuit model. Then that mathematical nonlinear differential equations for ferroresonance is simulated in a MATLAB software platform. The ferroresonance result obtained from the simulation model is compared with the experimental results where both the results match with a minor deviation.

Chapter 5 continues the study with the MATLAB model for ferroresonance developed in the previous chapter. Here some circuit parameters like supply voltage, supply frequency, series

capacitance, core loss resistance of transformer, degree of transformer core saturation, initial flux linkage in the core of the transformer are varied and the voltage across series capacitor and transformer for ferroresonance are observed. For each of the cases it has been found at a certain point when the circuit parameter and other condition matches, voltages jump to a high value at ferroresonance. Using Rudenberg's graphical analysis it has been shown how the stable operating point of the system switches from 1st quadrant to 3rd quadrant of V-I characteristic and builds up ferroresonance oscillation.

Chapter 6 briefs the nonlinear dynamical method and its application for ferroresonance in the thesis work. It describes the use of a phase plane diagram in the analysis of a nonlinear system. For a periodic function for nonlinear ferroresonance, the 'Phase-Plane' analysis produces 'Limit Cycles'. The method to determine the 'Stability' of a nonlinear ferroresonance system is to provide a small 'Perturbation' at a steady state and if the system returns to its previous 'Phase Plane' path then the system will be called 'Stable' otherwise 'Unstable'. So a 'Stability domain of nonlinear ferroresonance' has been studied. Mathematically, the linearization method that is used to determine the 'Stability of a Fixed Point' cannot be applied to the 'Stability of Limit Cycles'. The 'Stability of Limit Cycles' problem has been converted into a 'Stability of a Fixed Point' problem by using the concept of 'The Poincare method' and 'Floquet theory' for the stability of periodic orbit. The study of the Poincare plot also reveals how a system 'Bifurcate from one Stable state to another Stable state'.

Chapter 7 shows the simulation study of the model ferroresonance system used in Chapter 5. In this case, the system is under ferroresonance and the supply voltages are increased in steps. The Poincare plots of different ferroresonance system voltages are also observed. At first system generates a single point on the Poincare plane. As the supply voltage is increased, it generates two points, then four, eight and so on leading to the Period-Doubling Behavior of ferroresonance. At a very high supply voltage, the Poincare plot shows a 'Strange Attractor' which changes with the change of initial condition. The behavior of the system at this stage is moving to 'Chaos'. The bifurcation plot, which holds all the Poincare plots for all supply voltages in a single diagram, shows a period-doubling behavior of the system. The calculation of 'The Feigenbaum Constant' also establishes the fact that the system will ultimately land in chaos after successive period doubling. In the end, the bifurcation study with series capacitance as the 'Bifurcation' parameter is also made.

Chapter 8 deals with the stability of the system at different periodic oscillations as obtained in the bifurcation diagram in the previous chapter. For determining the stability at the period-1 region of the bifurcation diagram, a small perturbation is injected in the flux linkage while the system is in a steady state. Poincare plots and phase plane diagram shows that the system iterates back to its previous operating condition. To verify this condition mathematically, the Jacobian matrix was calculated with the Poincare values near perturbation. The magnitude of the Eigenvalues of the Jacobian matrix falls within the unity value. A similar investigation was carried out in the period-2 region and mathematical calculation shows the system lost its period-1 stability. For period-2 oscillation, the relations $x_{(i+2)} = x_i$ and $y_{(i+2)} = y_i$ hold, and the Eigenvalues of the Jacobian matrix fall within the value 1. Analysis with period-4 oscillation is also performed and verified.

Chapter 9 gives the details of finite element analysis done on the ferroresonance circuit. To know the magnetic field distribution in the core of the transformer during ferroresonance conditions, the finite element method is used. The transformer model is built up in the Comsol Multiphysics simulator. The core characteristic equation that was used in the previous chapters is injected into the core properties. Then to build up the ferroresonance circuit, the magnetic field model of the transformer is coupled with the electric circuit model consisting of an alternating voltage source, capacitor in series, and resistance in parallel which will act as core loss resistance. The current developed in the circuit is used as the excitation parameter of the primary of the transformer keeping the secondary of the transformer open. The simulation was done with different supply voltages. At a certain supply voltage ferroresonance is observed. The results match with the experimental outputs given in Chapter 3. The magnetic flux density distribution during ferroresonance is also observed.

Chapter 10, the last chapter, contains the conclusion and prospects of the present work. The study of ferroresonance in real systems is not possible because it leads to the destruction of the equipment. So a laboratory study of ferroresonance is performed in this research work on a miniature scale. To study the system behavior under ferroresonance, simulation, and numerical analysis has been done with the background of nonlinear mathematics. Numerical simulations and analysis showed how the ferroresonance circuit lost its stability moving from a stable period-one response to a period-two response and towards chaos through a period double bifurcation.

2. Review on Ferroresonance

2.1 What is Ferroresonance?

For power companies, ferroresonance - a complex electrical phenomenon - has long been an issue. It can happen in power transformers, voltage transformers, reactors, and other devices having saturable inductors fed by capacitive coupling from nearby sources. With an overvoltage several times higher than the typical voltage ratings, it can be quite dangerous.

The term "ferroresonance" was first used by Boucherot [2] in 1920 to characterize the occurrence of two stable operating points coexisting in a circuit comprising a capacitor, nonlinear inductor, and series resistor. In addition to the leap to a higher current fundamental frequency state, ferroresonance analysis is now used to examine subharmonic, quasi-periodic, and even chaotic oscillations in any circuit with a nonlinear inductance.

2.2 Generation of Ferroresonance

According to literature, a ferroresonance circuit consists of capacitors connected in series with iron-core transformers operating at no load. The coupling capacitance between transmission lines or cables, circuit breaker grading capacitors, power factor improvement capacitors connected either in series or shunt and other sources can all contribute to capacitance in a power system. If the circuit parameters match, the transformer may be forced to operate in a non-linear zone of magnetizing characteristics due to the appropriate magnitude and initial state of the supply voltage. This could result in ferroresonance oscillation.

Some typical transformer connections having ferroresonance risk are reported in the various literature [18-21]. A few simplified configurations of the line for the ferroresonance system are explained in the following sections.

2.2.1 Grounded Source and Ungrounded Transformer Windings

A circuit depicted in Fig. 2.1, 2.2, and 2.3, which includes an ungrounded 3-phase transformer (either in a wye or delta configuration), undergoes the formation of a series network comprising inductance and capacitance within a 3-phase power system under various circumstances. These circumstances include the blowing of one or two fuses, the action of a

lineman disconnecting an elbow connector for switching purposes, or one or two phases being left open during the manual energization of a 3-phase transformer bank, while connected to a cable line at a new construction site. In such scenarios, one or two of the 3-phase ungrounded transformers, connected either in a star or delta configuration at the primary side, establish a return path through the grounding capacitance of the cables when the 3-phase supply is grounded through its neutral. In a three-phase line, this phenomenon is frequently referred to as an "open-phase condition". When the transformers are operating at no load and the overall circuit losses are low, the length of the cable between the transformer and the location of the open conductor may have a critical capacitance that can result in ferroresonance.

In each of these cases, the equivalent circuit consists of both inductance and capacitance in series as the dashed lines show. In these circuits, V_a, V_b, $and\ V_c$ denote the voltage across the entire circuit, not across any individual circuit elements. So the voltage across the open-phase (i.e., across X_c) or the transformer primary winding (X_m) may be high enough with respect to the ground such that it poses a potential risk to surge arresters and the associated insulation. Here X_m represents the magnetizing impedance of the transformer, while X_c signifies the line capacitance impedance.

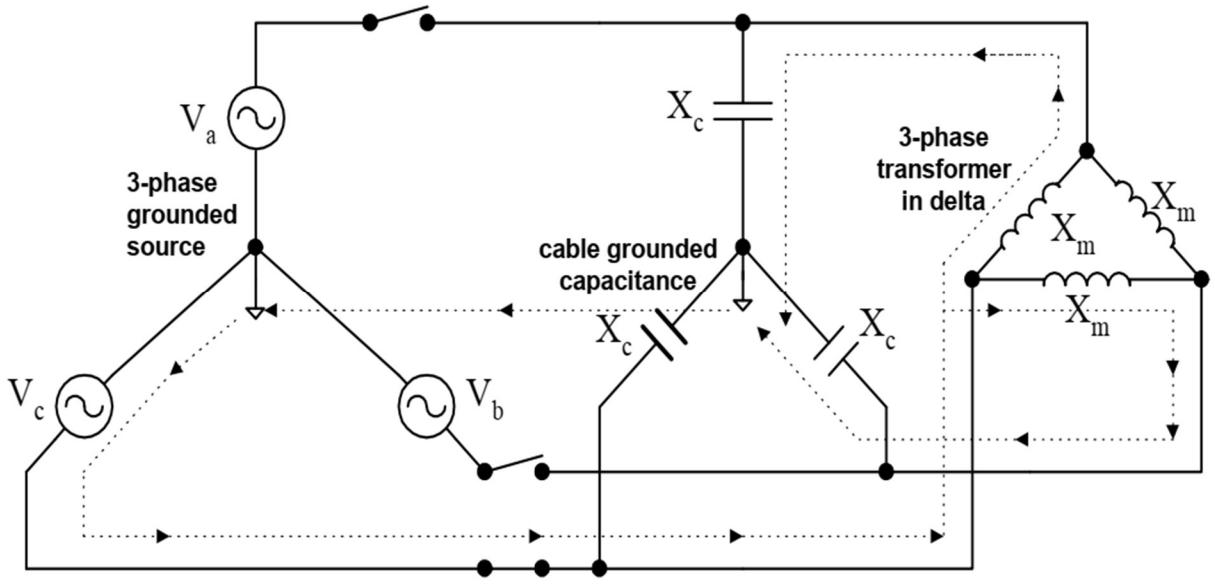

Fig. 2.1. Transformers in delta supplied by a star-grounded source at one-pole switching

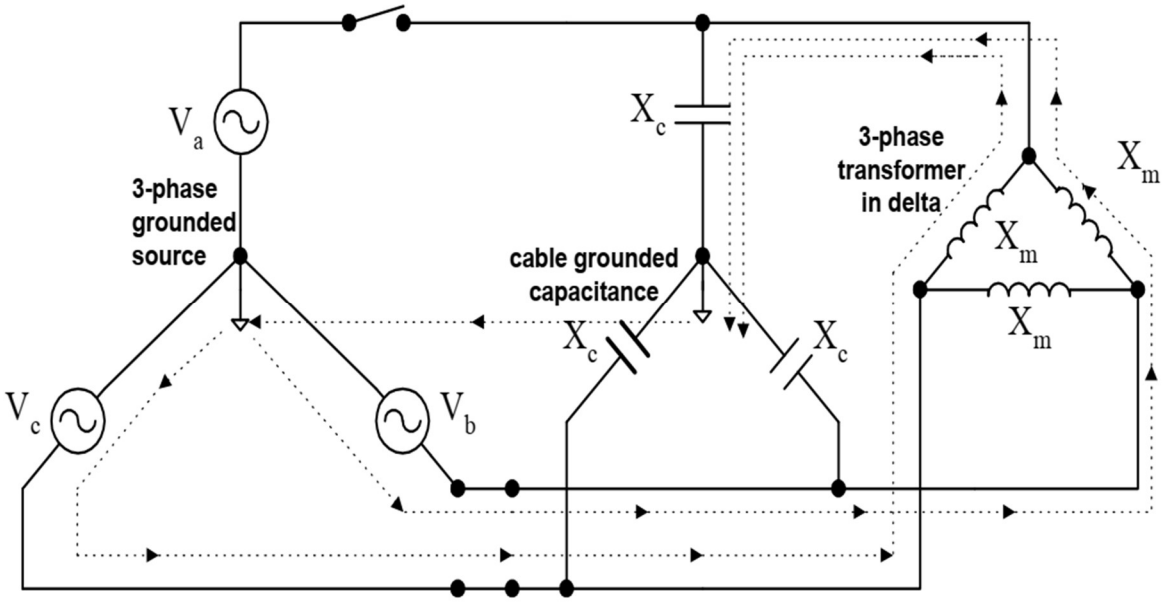

Fig. 2.2. Transformers in delta supplied by a star-grounded source at two-pole switching

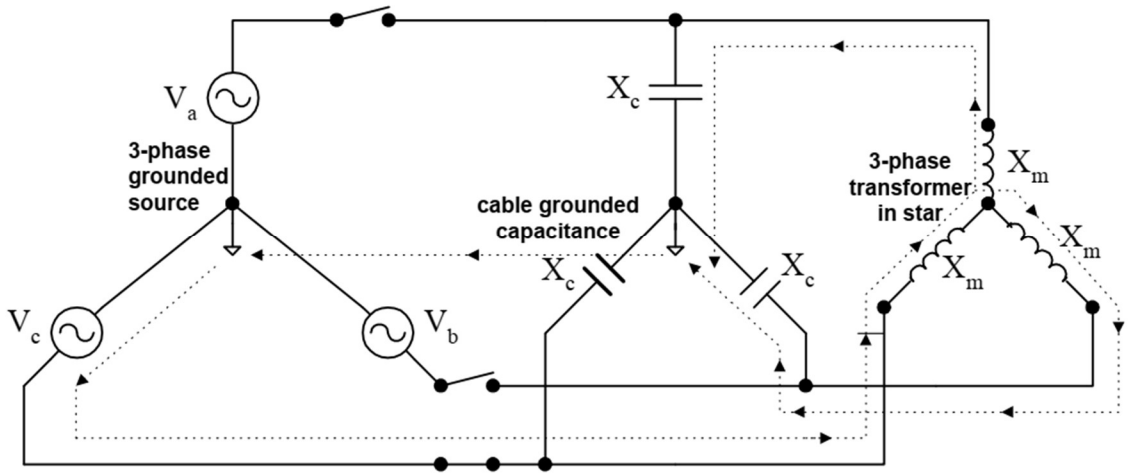

Fig. 2.3. Transformer in ungrounded star supplied by a star-grounded source at one-pole switching

2.2.2 Grounded Source and Grounded Transformer Winding with Ungrounded Capacitor Banks

The arrangement is shown in Fig. 2.4 and 2.5 closely resembles the previous example, with the only difference being that the system voltages and excited branch of grounded transformers are linked through an ungrounded power factor correction capacitor bank.

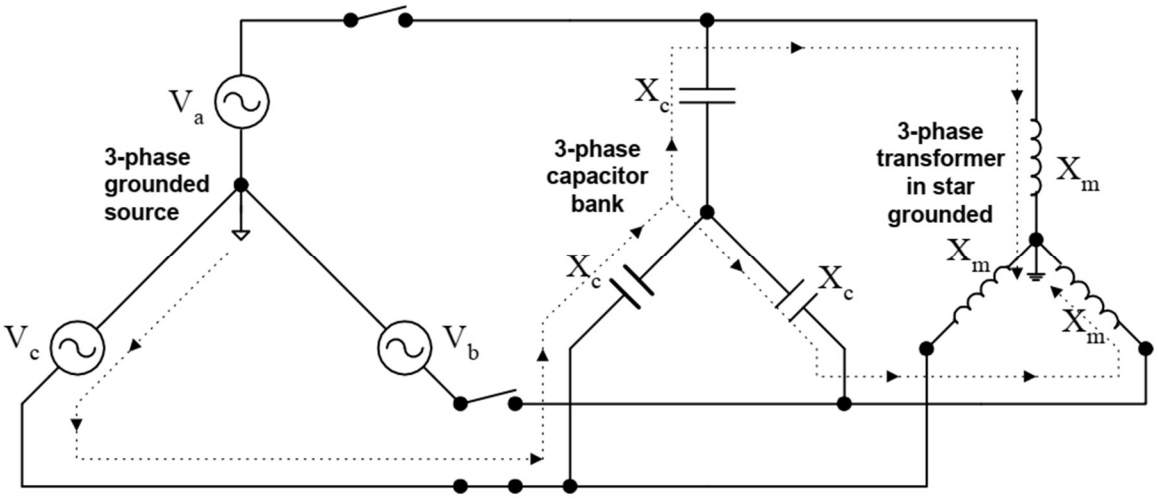

Fig. 2.4. Single-pole switching of transformer with grounded primary winding along with ungrounded capacitor banks from a grounded source

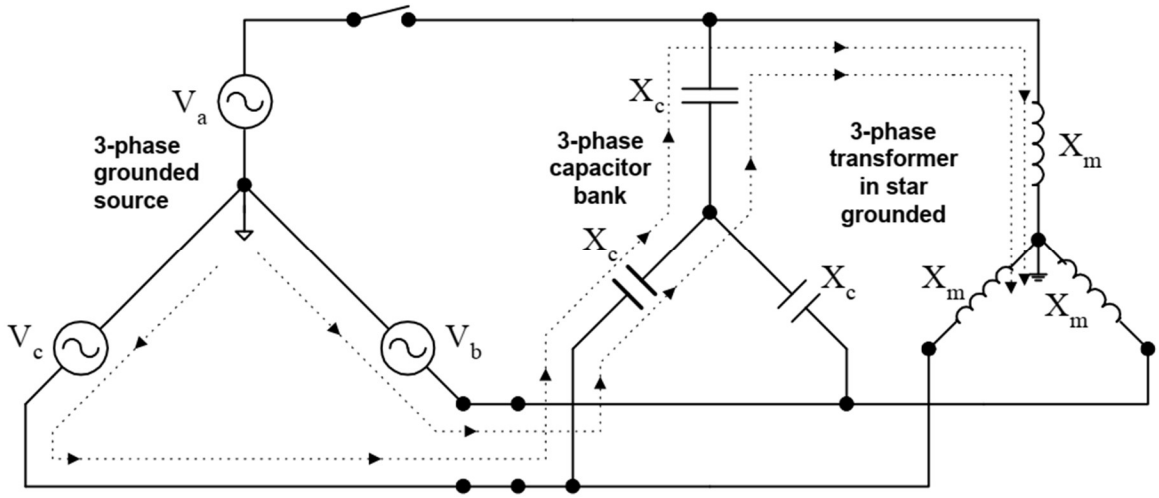

Fig. 2.5. Two-pole switching of transformer with grounded primary winding along with ungrounded capacitor banks from a grounded source

2.2.3 Breaker Contact Capacitance with Voltage Transformer

In a power system, the circuit breakers illustrated in Fig. 2.6 can energize a deactivated bus by utilizing the capacitance present across the open contacts of the circuit breakers. When this occurs it creates a ferroresonance series network consisting of inductance (L) and capacitance (C) due to the grading capacitance, which interacts with the voltage transformer (VT).

Although the utilization of multiple circuit breakers is diminishing, there are still some being manufactured and put into use, and an existing inventory of such devices remains in operation. The capacitance across open contacts is lower for a circuit breaker without grading capacitors. However, for multiple break circuit breakers, the grading capacitance is typically in the range of around 1000 pF, and this level of capacitance can instigate ferroresonance within the system.

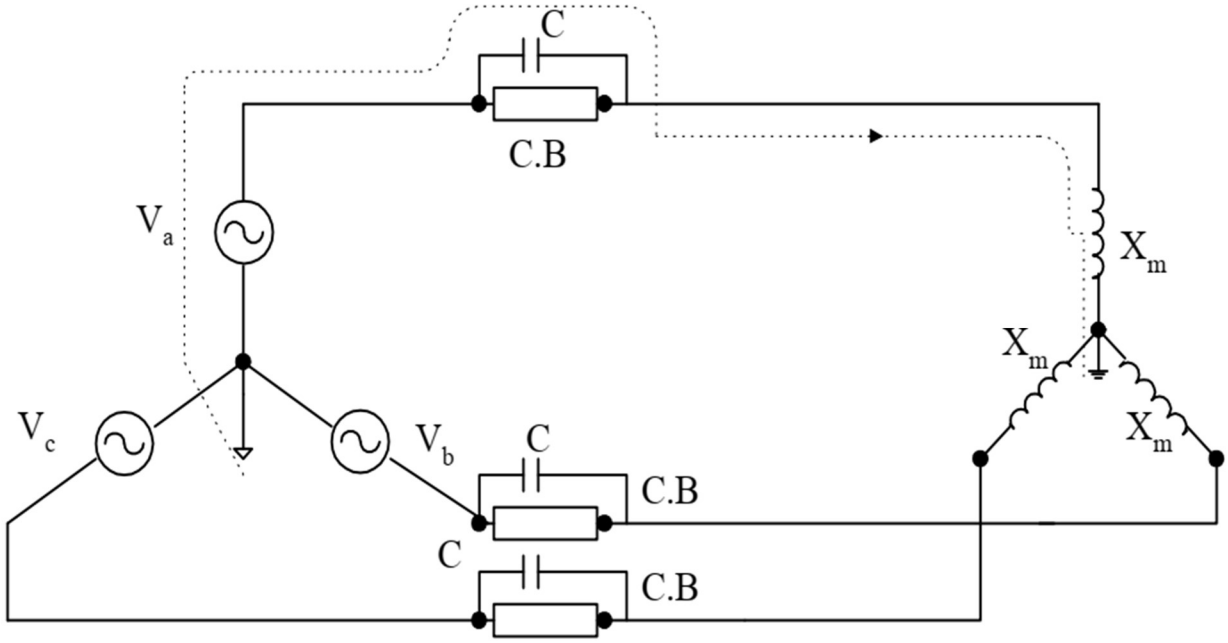

Fig. 2.6. Grounded wye transformers (VT) with grading capacitor(C) of C.B. connected to a star-grounded source

2.3 Effects of Ferroresonance

Ferroresonance can lead to high overvoltage and overcurrent and corresponding harmonics that can harm equipment and cause power failure [22, 23]. Some of the associated issues of ferroresonance include:

2.3.1 Peak Voltages and Currents

The primary concern associated with ferroresonance is the generation of high peak voltage, which can lead to damage in line equipment. In cases where transformers are connected in delta-wye configurations, and the primary side is ungrounded while being supplied by a grounded source, it has been observed that peak voltages of up to 2 times the normal sine wave

peaks (referred to as "per unit") can easily occur during ferroresonance events. Occasionally, these peaks can even spike to as high as 4 or 5 times the normal peak voltage.

Ferroresonance is still possible with the more common configuration of a three-phase 5-legged wye-wye grounded transformer but typically results in much lower peak voltages. Peak voltages in these scenarios are typically in the range of 1 to 1.5 times the rated peak voltage, with occasional short spikes reaching up to 2 times the normal peak voltage.

It's worth noting that most reports on ferroresonance incidents do not include data on currents. Therefore, it's possible that in some cases, current levels may be high during ferroresonance events, but these levels are not always documented.

2.3.2 Protective Relaying

Relays are typically not positioned within the power system at locations specifically intended for detecting ferroresonance occurrences in the distribution network. Moreover, the primary purpose of a relay is often to trigger the operation of a circuit breaker. As a result, if a relay is present, it may not be configured to detect single-phase switching events that can lead to ferroresonance. In some instances, the conditions that induce ferroresonance may not be sensed by a relay. For instance, a relay might be capable of detecting ferroresonance on the voltage transformer (VT) used for monitoring a circuit [24].

Another challenge is that protective relays are typically designed in such a way that they can sense the fundamental frequency only. Ferroresonant circuits, however, produce distorted waveforms with harmonics that may exhibit high peaks but possess low fundamental frequency components. That is why, a conventional relay may struggle to recognize the presence of a ferroresonant condition.

One potential solution could involve configuring the relay such that it can trip if detects random high-voltage spikes repeatedly, which could serve as an indicator of potential ferroresonance.

2.3.3 Surge Arresters

Ferroresonance conditions pose a significant risk to surge arresters, as the voltage peaks and the associated energy levels can often be so high that cannot be effectively absorbed by surge arresters in a reliable manner [25].

However, in the case of grounded wye transformers with 4 or 5 legs, the voltage peaks and energy generated under ferroresonance are generally not so excessive. If a surge arrester has enough energy absorption capacity, it may tolerate the ferroresonant state for these particular transformer configurations. In some instances, it may even play a role in damping the ferroresonance event, helping to mitigate potential damage and instability [26].

2.3.4 Issues with Distributed Generation

The increased popularity of distributed generation raises the probability of receiving power from sources not originally intended [27]. This increases the of risk single-phasing issues in the power system.

When a substantial power factor correction capacitance is added in induction generators, an unanticipated ferroresonance condition may arise. Induction generators and motors could not turn off automatically when the utility opens the breaker. In fact, in such cases, sustained high voltages may persist in the system.

2.3.5 Transformer Damage

There have been different reports of ferroresonance-related transformer damage, however, insulation damage rather than core heating effects are most likely to occur. Eddy current losses [28] and hysteresis losses are significant when ferroresonance drives the transformer into high saturation. On the other hand, ferroresonance on an unloaded transformer would produce a loud, audible noise as well as bubbling and burned paint on the tank of the transformer. This could be caused by an unusually large magnetic flux that is going through the tank wall during ferroresonance and saturating the magnetic core.

To prevent ferroresonance, it is important to design power systems with care, using appropriate equipment and protection devices. Proper grounding, overvoltage protection, and the use of surge arresters can also help mitigate the effects of ferroresonance.

2.4 Different Modes of Ferroresonance

Experiments conducted in the laboratory, and the numerical simulations with practical parameters help to classify four different modes of ferroresonance at steady-state conditions. The

transient ferroresonant state is not considered as it is difficult to differentiate it from the normal transient state. Transient ferroresonance may also be harmful to electrical equipment. After multiple system periods of an incident, dangerous transient overvoltage may develop and last for multiple power system cycles.

There are four distinct types of ferroresonance modes [29]: the fundamental mode, the subharmonic mode, the quasi-periodic mode, and the chaotic mode.

Below is an explanation of each type of ferroresonance.

2.4.1 Fundamental Mode

The system resonates at the fundamental frequency of the power supply, which is normally 50 or 60 Hz depending on the region, in the fundamental mode of ferroresonance. The frequency spectrum will contain the dominant fundamental frequency component along with the decreasing contents of odd harmonic components. Fig. 2.7 shows the periodic signal and corresponding frequency response for a fundamental ferroresonance.

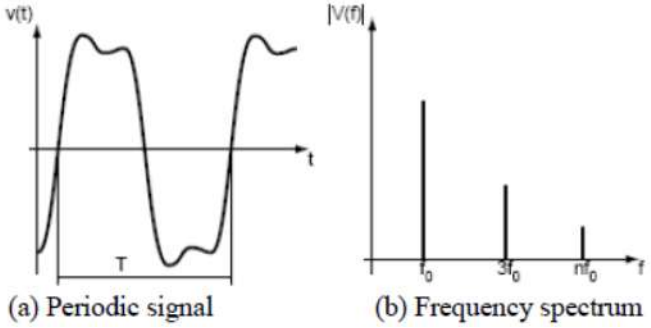

Fig. 2.7 Fundamental mode

2.4.2 Subharmonic Mode

In the subharmonic mode, the system resonates at frequencies that are integer fractions (subharmonics) of the supply frequency. For example, if the power system operates at 50 Hz, the subharmonic frequencies could be 25 Hz, 16.67 Hz, 12.5 Hz, and so on. The fundamental frequency ferroresonance is referred to as the First Period (i.e. f_0/1 Hz) and N – Period (i.e. f_0/N Hz) ferroresonance is defined as a sub-multiple of the power system frequency [30]. Fig. 2.8 shows the periodic signal and corresponding frequency response for a subharmonic ferroresonance.

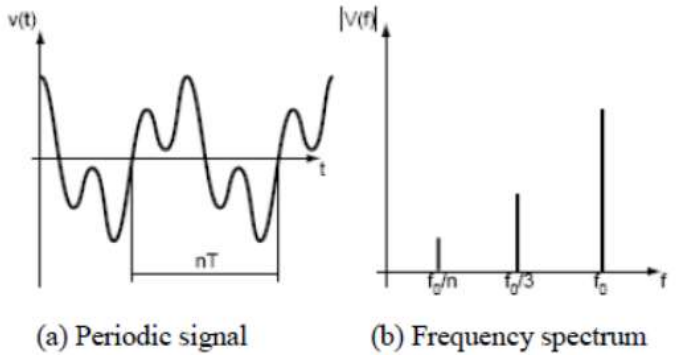

Fig. 2.8 Subharmonic mode

2.4.3 Quasi-periodic Mode

This mode of ferroresonance can be challenging to predict and analyze due to its non-linear and intermittent nature. It often involves a combination of different frequencies, including the fundamental frequency, harmonics, and subharmonics, resulting in a broad range of spectral components. The frequencies are denoted as $nf_1 + mf_2$ (where n and m are integers and f_1/f_2 is an irrational real number).

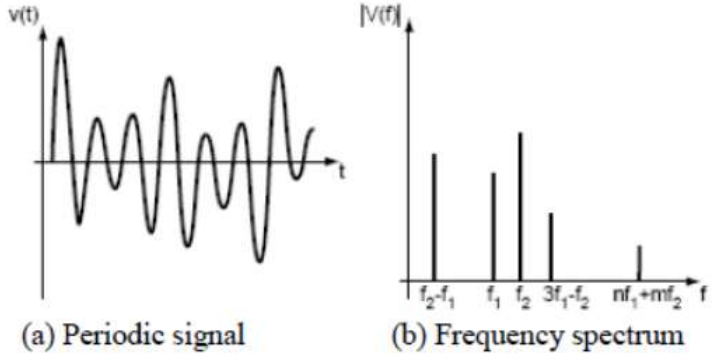

Fig. 2.9. Quasi-periodic mode

2.4.4 Chaotic Mode

The system exhibits highly irregular and unpredictable behavior in the chaotic mode of ferroresonance. This nature makes it difficult to determine or analyze its exact trajectory. The oscillations in voltage and current can display a complex pattern that appears random, with no discernible periodicity or repetitive structure. Analysis of chaotic mode required highly specialized mathematical brunches like chaos, bifurcation stability, and domain of nonlinear system. Fig. 2.7 shows the periodic signal and corresponding frequency response for a chaotic ferroresonance.

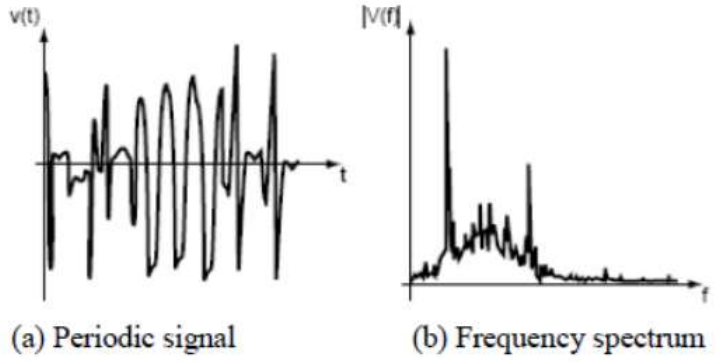

Fig. 2.10. Chaotic mode

2.5 Rudenburg's Graphical Method

The graphical method for analyzing ferroresonance phenomena was first proposed by R. Rudenburg [3] in 1950.

When given electromotive force '*E*' of sinusoidal shape feeds a circuit consisting, as in Fig. 2.11, of a constant capacitance '*C*' in series with a coil '*L*', wound around a closed iron magnetic circuit (transformer at no load),

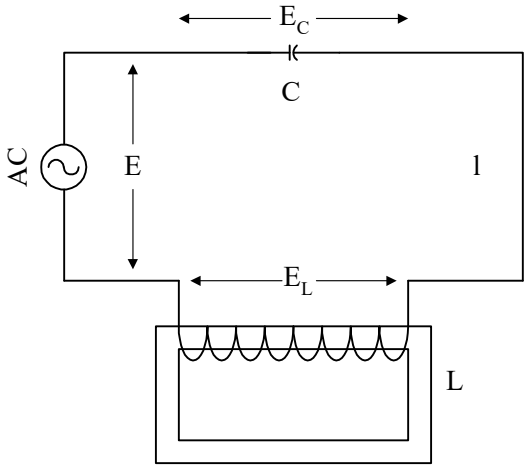

C : Constant capacitance

L : Inductance of magnetic circuit (saturated inductance)

E : Impressed sinusoidal voltage

E_C : Voltage across constant Capacitor

E_L : Voltage across saturated Inductance

I : Circuit current.

Fig. 2.11. Ferroresonance series circuit

As the transformer is considered at no load, the voltage drop due to the series resistance and leakage reactance of the circuit can be neglected. Therefore, following KVL, the supply voltage needs to balance the voltage across the saturable inductance and the voltage across the capacitance. Considering merely the fundamental sinusoidal waves of voltage and current neglecting any distortion of wave shape due to iron saturation is

$$E = E_L + E_C \qquad (2.1)$$

The voltage-current relationship for the inductance (L) of the circuit is not linear here, rather it depends on the magnetic characteristic of the iron core as plotted in Fig. 2.12. The characteristic of the amplitudes E_L and I is slightly dependent on the measurement, whether may be performed by sinusoidal voltage and a distorted current by sinusoidal current and a distorted voltage, or by both distorted current and voltage.

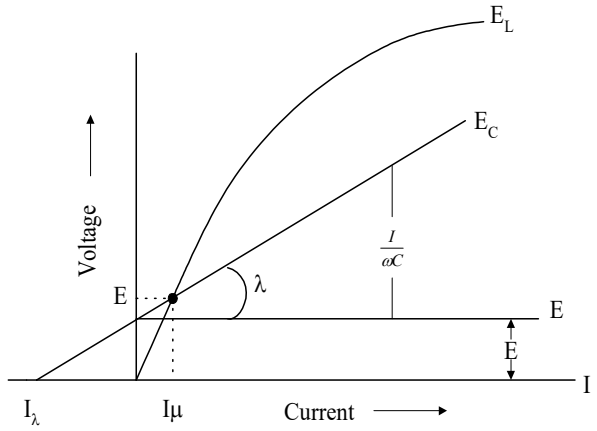

Fig. 2.12. Intersection of coil and capacitor characteristics

E: System voltage represented as the horizontal line

E_L: Voltage of saturated inductance

E_C: Capacitance voltage as a straight line (ascending)

I_λ: Charging current of the condenser under the sole influence of the supply voltage E

γ: slope of the condenser line

Iμ: Magnetising current of the saturated inductance under the sole influence of the voltage E.

The voltage-current relationship for the inductance may be represented by

$$E_L = \omega f(I) \qquad (2.2)$$

Where $f(I)$ is a non-linear function of current that is specific to ferro-inductance and only depends on the number of turns of the winding as well as the size and magnetic properties of iron core. The voltage across the capacitor is inversely proportional to the frequency and capacitance and proportional to the current through it. By its property, the capacitor voltage will be in phase opposition with the inductor voltage. If all losses and resistance in the circuit are neglected, this is given by

$$E_C = -\frac{I}{\omega C} \qquad (2.3)$$

Thus the equilibrium in the circuit of Fig. 2.11 is given, by substituting (2.2) and (2.3) in (2.1), as

$$E_L = \omega f(I) = E + (\frac{I}{\omega C}) \qquad (2.4)$$

The relation (2.4) indicates that the sum of the supply voltage E and capacitive voltage E_C must always be equal to the saturated inductance voltage E_L. A simple graphical solution of (2.4) is shown in Fig. 2.12. In this figure, the voltages are plotted along the x-axis and current along y. The system voltage is represented by a horizontal line, to which E_C is superimposed as a straight ascending line.

The slope angle of the line is determined by

$$\tan\gamma = \frac{1}{\omega C} \qquad (2.5)$$

Hence the slope is steeper for smaller capacitance of the line capacitance. If we extend the straight line E_C to the left-hand side, it intersects the negative axis of current at a distance from the origin at I_λ

Where, $I_\lambda = -(\frac{E}{\tan\gamma}) = -\omega CE$ (2.6)

This, therefore, is the charging current of the condenser under the sole influence of the voltage E. On the other hand, the magnetizing current I_μ of the inductance under the sole influence of the voltage E is given by the intersection of the E line with the magnetizing characteristic, as shown in Fig. 2.12. A different current develops under the joint action of both these elements in the circuit. There appears a rise of the inductive voltage above the system voltage to an amount as determined by the point of intersection of the two characteristics.

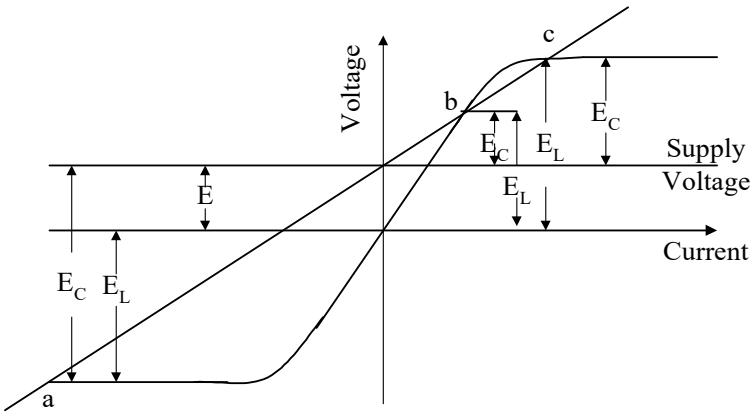

Fig. 2.13. Rudenberg's graphical method for ferroresonance analysis

The condenser line if increased in both directions will intercept the inductor voltage line at three different points '*a*' and '*b*' & '*c*' as shown in Fig. 2.13. However points '*a*' and '*b*' are stable operating points, whereas point '*c*' denotes an unstable operation. With larger voltages

(E_L & E_C) across the circuit elements, the operation at 'a' in the third quadrant is termed ferroresonance. So an appropriate magnitude of supply voltage may shift the operating point of the transformer into the non-linear region of magnetizing characteristics if the capacitance of the circuit and the initial conditions also match.

The stability of the operating point 'b' will be realized by the following consideration. If at point 'b' a small deviation occurs by a slight increase or decrease of current, E_C acting in the direction of the impressed voltage E, would change linearly with the current. However, the counteracting inductive voltage E_L changes more intensely with the current, its slope being steeper, and thus the current would be brought back to its original value at 'b'. Here the rate of change condenser voltage with respect to the current will be less than the rate of change inductor voltage with respect to the current i.e. $\frac{dE_C}{dI} \langle \frac{dE_L}{dI}$ for stability in the first quadrant at 'b' $E_L = E + E_C$. Similarly, at a deviation from point 'a' E_L which here acts in the direction of E as shown in Fig. 2.14, is not changing so intensely as the opposing voltage E_C, and therefore again, the current will return to point 'a'. Here $E_C = E + E_L$.

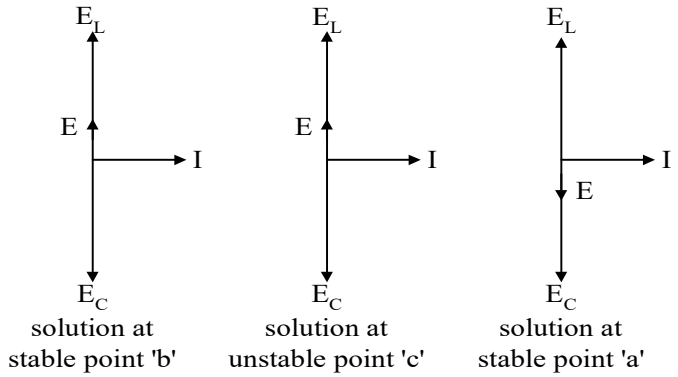

Fig. 2.14. Phasor diagrams at point of operation 'b', 'c' & 'a'

Completely different are the relations at point 'c'. Here, with every deviation of the current from the intersection, the condenser voltage E_C, acting in the direction of the driving voltage E as shown in Fig. 2.14, changes more intensely than the opposing voltage E_L, and thus the deviation of current will increase and separate the working state farther from point 'c'. For a complete survey the unstable branch of the voltage curve, corresponding to intersections of the point 'c', is plotted in a dashed line in Fig. 2.15.

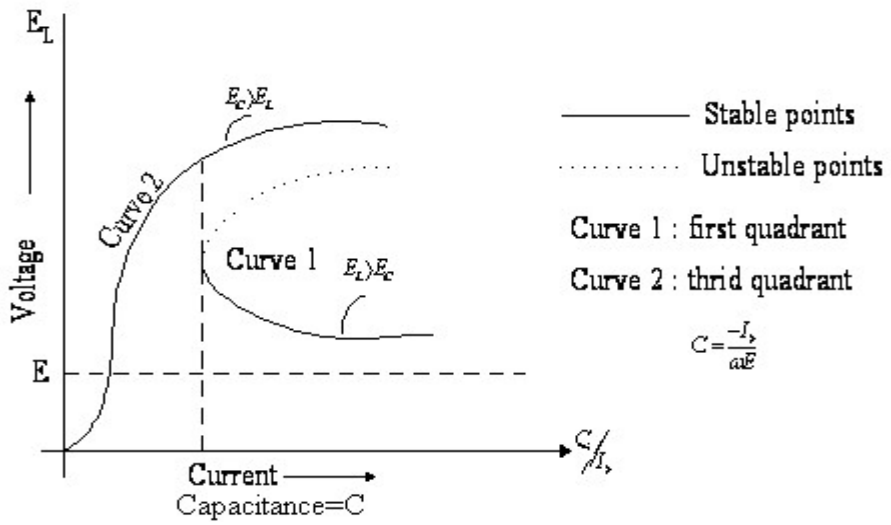

Fig. 2.15. The voltage across the iron coil is plotted against the capacitance

2.5.1 Change in Capacitance

The behavior of the working point at the intersection of the two characteristics is shown in Fig. 2.16, keeping unchanged the saturated inductance coil but changing the magnitude of the capacitance, when the supply voltage is constant. Here a large capacitance with a large charging current I_λ acts like a short circuit. So the transformer voltage becomes equal to the supply voltage. As the capacitance is decreasing the operating point slides up along the inductor line to higher voltages. This will carry on, nevertheless, until the capacitor line hits the first quadrant as a tangent rather than intersecting the characteristics due to its curvature. If the capacitance is decreased further, no operating point is possible in the first quadrant, with a positive voltage at the inductance receiving lagging magnetizing current from the source.

However, if the capacitor line is extended completely in Fig. 2.16, it intersects the magnetic characteristics at a second point, namely at negative values of current and voltage. With small capacitance such a state of operation actually will occur. In this condition, the current is now the leading charging current, whose amplitude will significantly rise, as opposed to the lagging magnetizing current of the earlier state. Correspondingly, the voltage at the inductance to be measured from the current (I) axis and still more the voltage at the condenser to be measured from the E line, will be greatly increased, and thus high voltages will develop in the circuit. As capacitance decreases, the operating point moves upward along the coil characteristics' negative branch, resulting in decreasing voltages between capacitance and inductance. Ultimately, the

inductive voltage vanishes and the capacitor voltage aligns with the supply voltage at very low capacitive values.

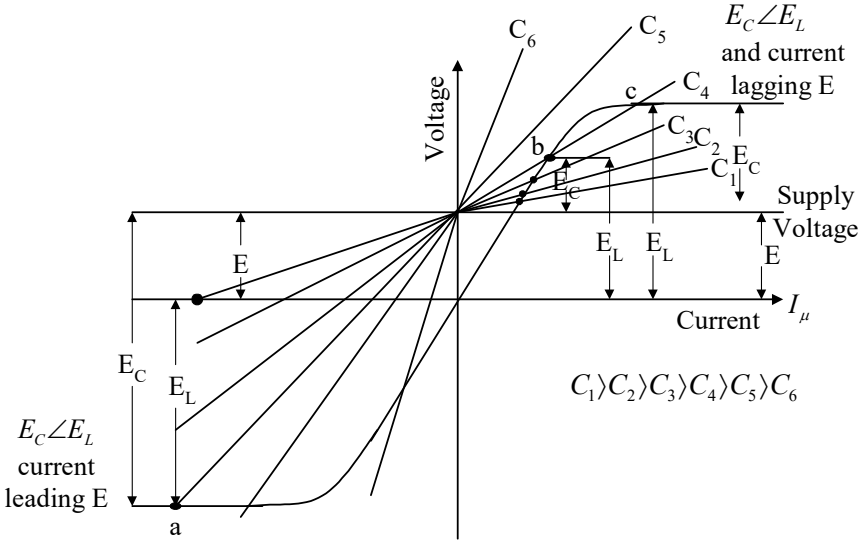

Fig. 2.16. Change of operating point with the variation of capacitance

In Fig. 2.15 the voltage across the iron coil is plotted against the capacitance, omitting the direction or phase of the voltage. Finite voltages occur through the entire region of capacitances. However, by the effect of the saturation there is a point of discontinuity at which, with a decrease in capacitance, the voltage will jump from a smaller value to a higher value.

Fig. 2.16 shows that for large capacitance the condenser line will also intersect the negative branch of the magnetic characteristics. Hence in this range, two different states of oscillation are possible, one of lagging current with low voltage and another one of leading current with high voltage. Both of these states are indicated in Fig. 2.15 by solid curves. Which of them occurs is a matter of chance and will be determined by the switching condition of the supply voltage.

In the case of small voltages and currents in the first quadrant, the inductive voltage is greater than the condenser voltage by the value of system voltage, whereas, in the case of large voltages and currents in the third quadrant, the reverse is true. Operation 'a' denotes a steady state of circuit operation that produces "ferroresonance," with high voltages across circuit elements.

2.5.2 Change in Supply Frequency

The usual linear resonance curves show the performance of current and voltage depending on the impressed frequency. For a direct comparison of the ferroresonance with those curves, (2.4) when divided by the frequency ' ω ' gives

$$f(I) = \frac{E}{\omega} + \left(\frac{1}{\omega^2 C} \right) \tag{2.7}$$

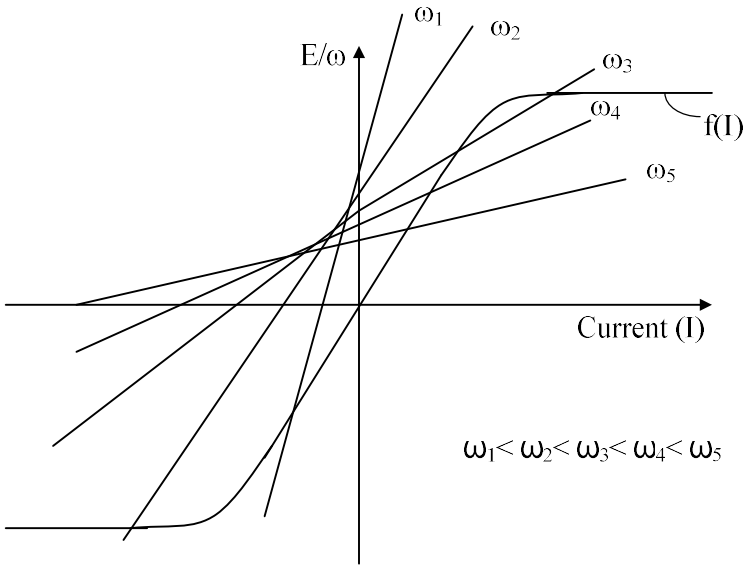

Fig. 2.17. Change of operating point with the variation of supply frequency

Fig. 2.17 shows that the magnetic characteristic $f(I)$ remains the same for all frequencies, but with the change of frequency, slope, and the position of the capacitor line change greatly. The capacitor line is sharp at low frequencies (ω_1) and crosses the magnetic characteristic on the negative branch. As a result, the circuit has a single-valued state and a leading charging current. When the frequency increases, the capacitor line touches the positive branch of the magnetic characteristic first and then intersects it. As a result, two more possible states come into existence with high frequency (for example ω_3). Though both of them operate with lagging magnetizing current only one is stable. With further increasing in the frequency (ω_5), the stable point slides downward on the characteristic. As derived from Fig. 2.17, the dependence of current and condenser voltage on the frequency is plotted in Fig. 2.18 and 2.19.

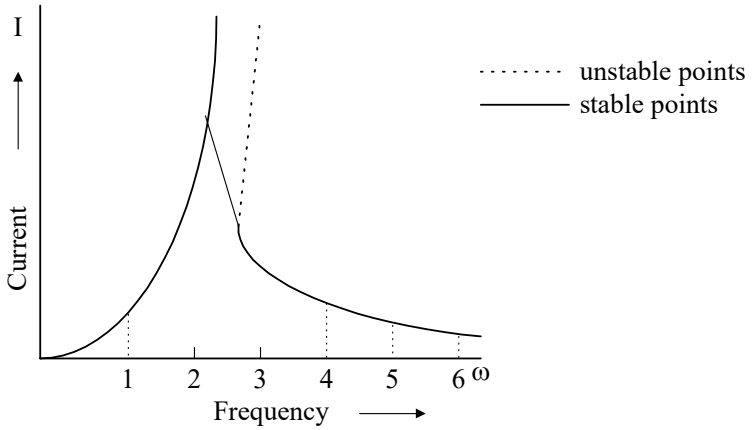

Fig. 2.18. Variation of current with the supply frequency

Those branches of the curves that correspond to the unstable intersection are plotted dashed in Fig. 2.18 and Fig. 2.19.

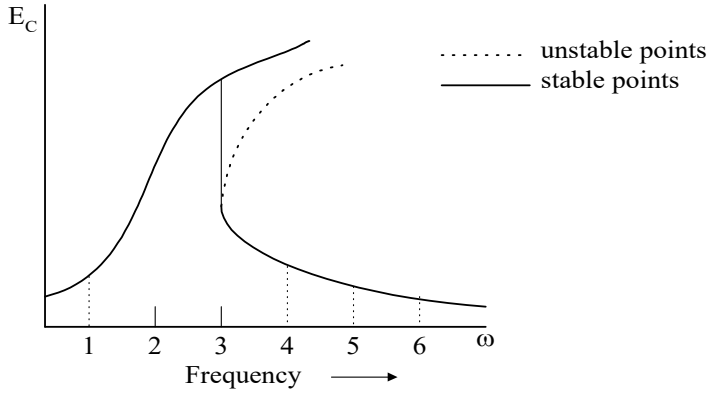

Fig. 2.19. Variation of voltage across constant capacitance with supply frequency

2.5.3 Change in the Supply Voltage

By a variation of the driving voltage, the state of oscillation on the magnetic characteristic can be widely displaced, whereas in non-saturated circuits currents and voltages simply change proportionally. In Fig. 2.20 several condenser lines are plotted for different supply voltages, according to (2.7). In Fig. 2.21 the voltage across capacitance, depending on the driving voltage, is derived from Fig. 2.20. As the voltage is raised, the functionality of the circuit abruptly shifts from an inductive to a capacitive state between E_2 and E_3. An irreversible ferroresonance jump can be observed if the voltage is decreased.

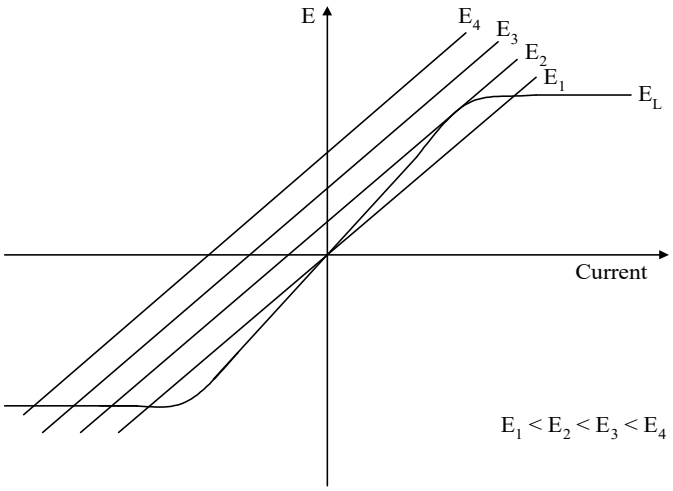

Fig. 2.20. Change of operating points with the variation of supply voltage

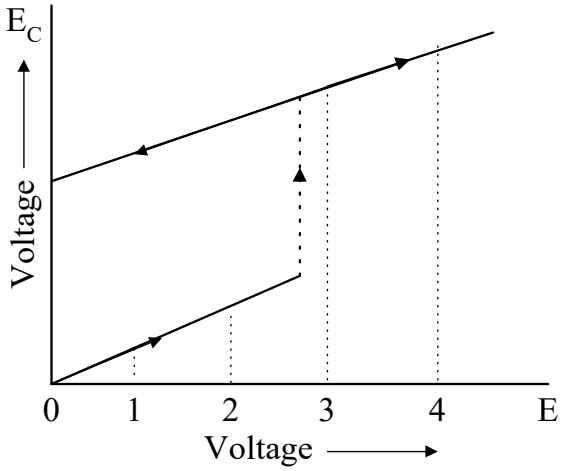

Fig. 2.21. Variation of voltage across the capacitance with supply voltage

2.6. Literature Survey

Work on ferroresonance was carried out in the following main areas:

- Examples & Case Studies
- Experimental Investigations
- Damping and mitigation.
- Analysis

Papers on examples and case studies explain different events of ferroresonance that occur in factories or power stations and suggest some probable causes of occurrence. A few examples of such kinds of papers are discussed below.

J. Pienaar and P. H. Swart [31] addressed a ferroresonance problem that happened at two 30 MVA submerged-arc furnaces which resulted in an unnecessary furnace shutdown. The process by which the electrical supply causes saturation in the core of the furnace transformer was explained mathematically. A. Noosuk and co-authors [32] shared the observations of the test performed from April to September 2001 during the commissioning of the interconnection of two 300 MW converter stations in Thailand-Malaysia. Ferroresonance was observed in the potential transformer during the disconnection from the converter transformer. P. E. Sutherland in his paper [33] recorded a ferroresonance observation that happened in 2002 at UI's New Haven Meter Shop. The ferroresonance started due to the single phasing occurring with a broken conductor in one phase. The incidents continued from 4 cycles to 120 seconds, and over-voltages rose to 113% - 126% of nominal. It was stated that the existence of power-factor correction capacitors was the likely culprit. The paper [34] investigated an event called "318 Blackout Incident" which happened at the Maanshan Nuclear Power Station in Taiwan on March 18, 2001. It has been found that 4 hours before the blackout event there was a ferroresonant overvoltage. Due to the loss of power supply, the motors started to act as generators and they built up ferroresonance by interacting with power-line capacitance and power transformers.

D. A. N. Jacobson [35] and R. C. Dugan [34] in their papers provided several examples of practical ferroresonance phenomena that occurred in high voltage transmission systems.

Works on experimental investigations recreate ferroresonance in a controlled environment either in the laboratory or in the field and analyze different features of ferroresonance. They also employed some simulating software and compared the simulation results with the practical results.

M. Rioual and C. Sicre [37] made a field study with a 900 MW generator, positioned near Paris in France and a 96 MVA test transformer located 140 Km away from the power station. This paper also performed an EMTP simulation and compared the results. J. Z. Vernieri, M. B. Barbieri, and P. L. Arnera [38] performed a study of the zero sequence behavior of a transformer excited under unbalanced conditions. The study was made with a 40 MVA, 132 KV / 13.86 KV transformer. It was then validated with ATP model simulation. Temperature rise of a potential transformer in underground mines investigated experimentally in [39]. D. Femandes [40] did one laboratory experiment to capture the frequency response of a 230 KV coupling capacitor voltage transformer.

Some papers deal with the damping and mitigation of ferroresonance when it already occurred. They suggest some damping techniques and validate them either real field study or by simulating the ferroresonance model circuit.

The use of damping resistors coupled to transformer secondary windings has been examined and studied in numerous publications [41]. But there are some other methods also suggested by many researchers. M. Graovac and co-authors in their paper [42] provided a method for quickly suppressing the ferroresonance phenomenon in coupling capacitor voltage transformers (CCVT) and clearing the ferroresonance quickly by modifying the secondary overvoltage protection and filter circuit parameters. A practical example of inductive load application in Hydro Que'bec's Deschambault substation is demonstrated in [43]. Equivalent linearization algorithm [44] was suggested to indicate the ferroresonance zone and safe zone of operation. In this way, the ferroresonance can be avoided. The continuous burden of the damping resistance can be removed by connecting a thermistor having a positive temperature coefficient [45]. ZnO nonlinear resistance has been considered as a preventive measurement for ferroresonance [46]. Paper [47] shows the effect of the DC reactor in limiting the fault current and stabilizing ferroresonance oscillation.

Some researchers do some mathematical analysis of ferroresonance with the help of suitable simulating software and try to predict the behavior of circuits under ferroresonance. They use a nonlinear dynamic method to build up the system equation and investigate the stability of the system.

A. Ben-Tal and co-authors in their paper [48] explains the existence of period-doubling bifurcation and the chaotic behavior of the ferroresonance circuit. Fractal dimension methods are used to analyze the chaotic response of a ferroresonance circuit [49]. B. Tanggawelu, and co-authors in their work [50] suggested the construction of bifurcation diagrams and phase plane portraits to verify the type of nonlinearity in an overvoltage scenario. Paper [51] introduces the power frequency excitation characteristic instead of the traditional excitation characteristic which was generally used to represent the nonlinear inductor. As per the authors, the latter method has the drawback of having a harmonic current. Paper [52] discussed the advantages of the flux reflection method for simulating ferroresonance over a full numerical solution. Application of fault current limiter in the mitigation of chaotic ferroresonance is discussed in [53] with bifurcation and phase plane diagram.

2.7 Summary

In this chapter, the basics of ferroresonance phenomena are explained. The combination of circuit elements that may cause ferroresonance in the power system is discussed. That means how the capacitive effect from various sources along with saturable inductors can create a ferroresonance-prone network that has been explained. The effect of ferroresonance on the power system and its equipment is also narrated. One of the oldest but most effective analyses of ferroresonance was given by R. Rudenberg. The theory of Rudenberg's has been explained in this chapter. Analysis shows, how the system jumps into ferroresonance from normal value while changing any of the circuit parameters. This theory does not include any complex nonlinear mathematics, thus easy to understand. At the end, a details literature survey is provided to understand the trend of work that has been done on ferroresonance so far.

3. Development of Experimental Setup and Experiment on Ferroresonance

3.1 Steps for Ferroresonance Study in Laboratory

The experimental study of ferroresonance in the laboratory required a single phase transformer operating at no load condition. The transformer, acting as a non-linear inductor is connected with a capacitor in series. A switching device connects the non-linear inductor and capacitance in series with an AC power source (Fig. 3.1).

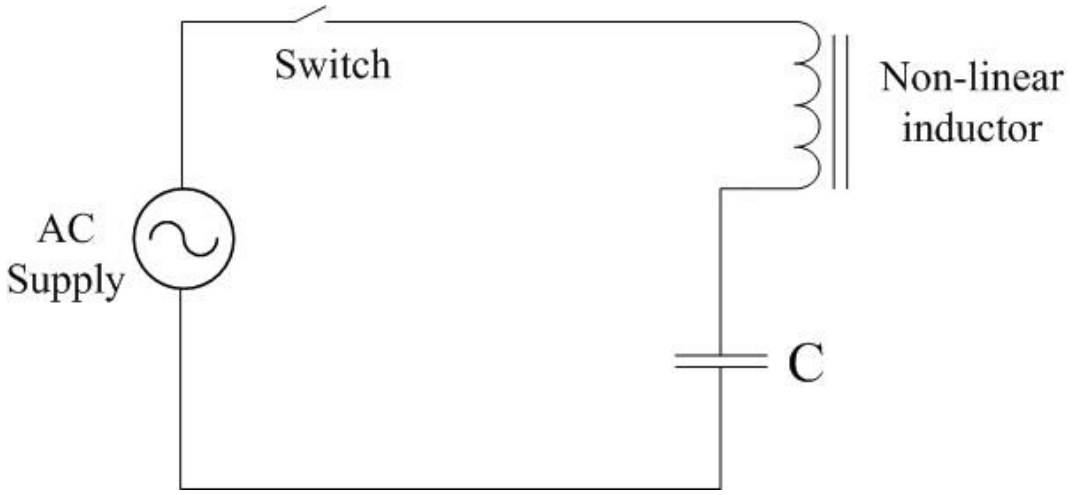

Fig. 3.1. Ferroresonance circuit

The following steps are followed for ferroresonance study in the laboratory:

1. Identifying a circuit configuration that is prone to ferroresonance.
2. Simplifying the circuit.
3. Determination of Open Circuit Characteristic of Transformer
4. Calculation of the value of capacitance by graphical method for a particular supply voltage.
5. Execution of experiment using calculated value of capacitance at specified voltage.
6. Study of the results of experimental observation.

3.2 Determination of Transformer Open Circuit Characteristic

The following transformer is used as a test transformer:

Single phase, 200 VA, 230V / 24-0-24V / 0-12 V, 50 Hz

The low voltage side is left open while the supply is connected to the high voltage side of the test transformer to acquire its open circuit characteristics. The supply voltage gradually increased and the corresponding current value is noted. To attain the non-linearity of the magnetizing curve, it is required to capture the knee point of saturation. For that the supply voltage is increased almost up to 150% of the rated value. The per-unit plot is shown in Fig. 3.2.

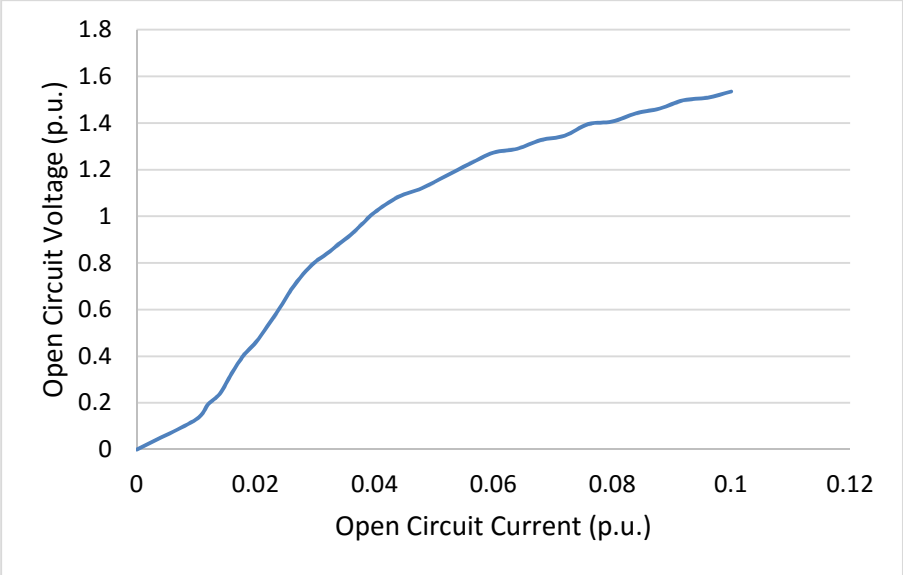

Fig. 3.2. Transformer OCC curve

3.3 Calculation of the Capacitance for Ferroresonance

One major ferroresonance circuit parameter is the series capacitance (Fig. 3.1). To calculate this, Rudenberg's graphical method is used. As per Rudenberg at ferroresonance, the circuit will have an operating point in the third quadrant in the V-I characteristic. So as a limiting condition, the capacitor line which is tangent to the magnetization curve at the first quadrant can be considered as experimental capacitance. For a desired supply voltage, a tangent is drawn to the open circuit characteristic of the transformer.

The slop of the tangent $= \frac{1}{\omega C}$, where $\omega = 2\pi f$

From this relation, the capacitance can be calculated. Fig. 3.3 shows the method of slop calculation at rated supply voltage. Table 3.1 shows calculated values of capacitance obtained graphically for different supply voltages.

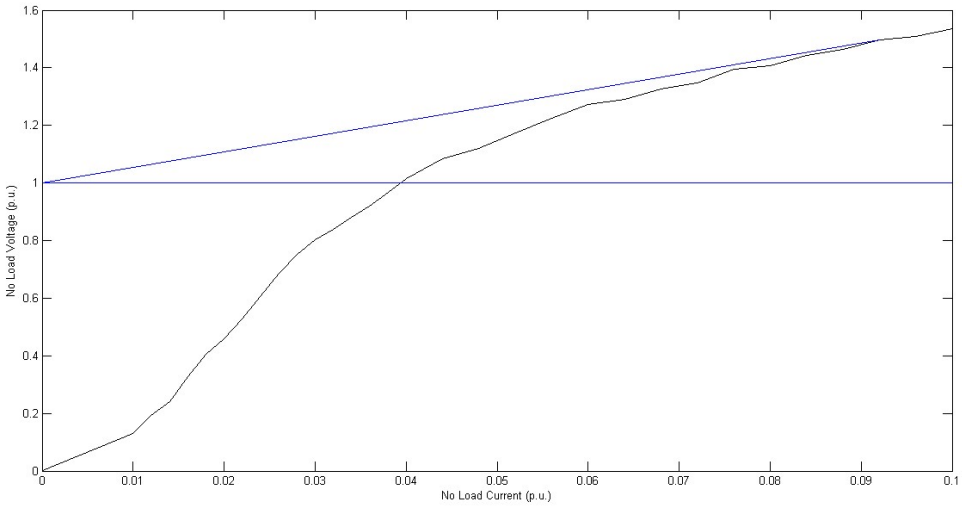

Fig. 3.3. Calculation of slop at rated voltage

Table 3.1: Variation of voltages with source voltage (p.u. values)

HV Side Voltage (p.u.)	Capacitance calculated from slope (μF)
0.35	1.0342
0.40	1.1575
0.45	1.2849
0.50	1.4085
0.55	1.5758
0.60	1.7684
0.65	1.9545
0.70	2.1425
0.75	2.4219
0.80	2.7852
0.85	3.2715
0.90	3.7992
0.95	4.711
1.00	6.1987

In the experimental setup, 20 capacitors were taken with each capacitor having a rating of 25 μF, 500 V. All the capacitors are connected in series with a target to achieve a resultant capacitance of 1.25 μF. The ultimate achievement was 1.272 μF.

3.4 The Experimental Setup

The test circuit for study ferroresonance and its recording arrangement is shown in Fig. 3.4. In the experimental setup the following apparatus are used:

1. Isolating transformer: single phase, 450VA, 0-230-433V / 0-230-433V, 50Hz, major insulation at 25KV level.
2. Variac; input voltage 230V, output voltage 270V
3. Digital oscilloscope
4. Multimeter to measure the voltages
5. Switching device
6. Measuring unit

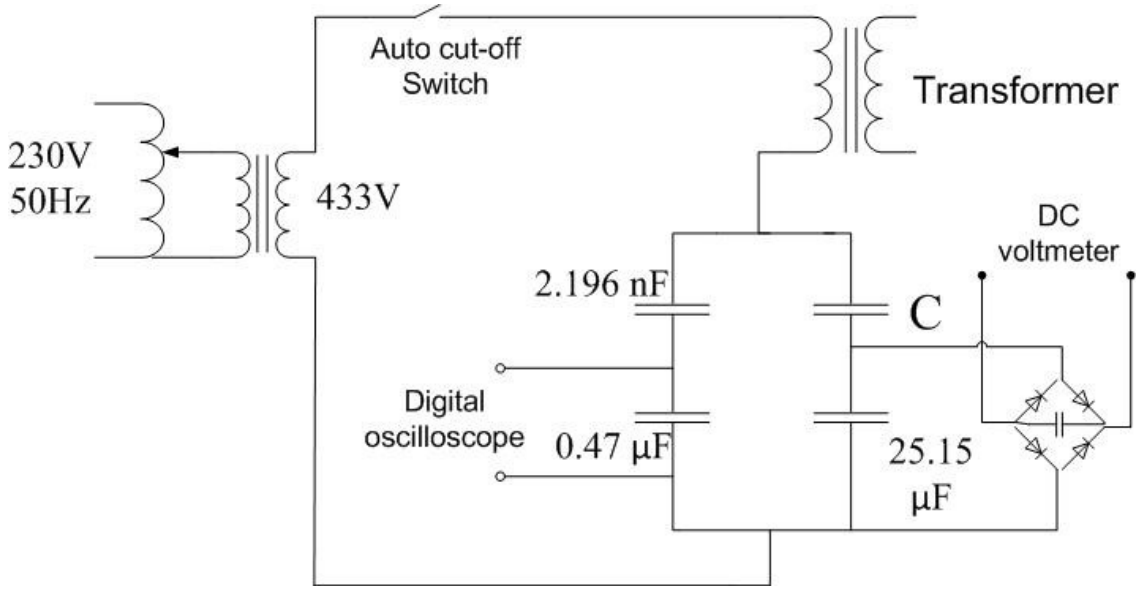

Fig. 3.4. Experimental circuit diagram for studying ferroresonance

3.4.1 Development of Auto Cutoff Switch

Instant of switching plays an important role in ferroresonance. A good switching device s necessary to identify the instant of switching and its effect on ferroresonance. The switching circuit developed for this experiment has the following features:

1. Switching is possible at different angles over a full cycle of 360 electrical degrees.
2. ON duration of the switch can be set to any value depending on the requirement.
3. Instant of switching can be easily identified by CRO recording.

The whole circuit is divided into several blocks as shown in Fig. 3.5.

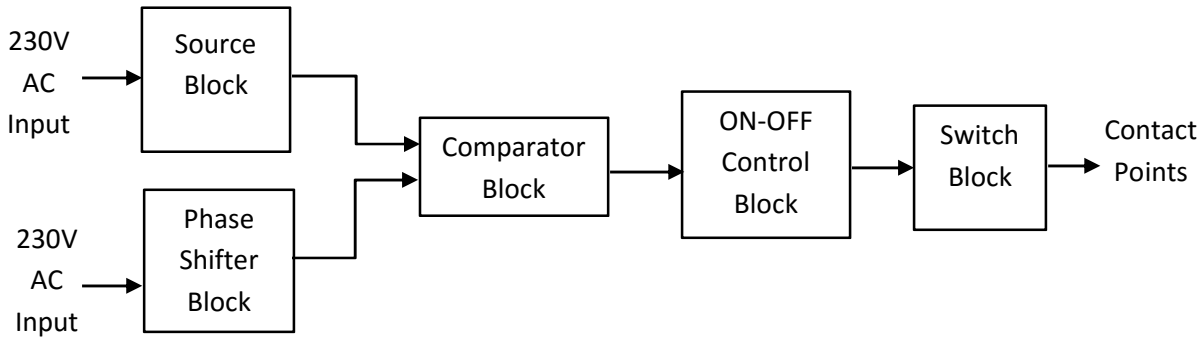

Fig. 3.5. Auto cut-off switch – block diagrams

The source block generates 12 volt DC stable voltage. This is used as the variable reference signal to the comparator block. It also supplies the ICs. The phase shifter block uses an R-C circuit. Phase shifting is done by varying the resistance R. The output of the phase shifter block is fed to the positive input of the comparator. The comparator generates a pulse signal. Pulse width is varied by varying reference input, which is done by a 100K pot in the source block. The output of the comparator is at positive saturation voltage when the reference DC voltage at the negative input terminal is larger than the AC input at the positive input terminal. The output is at negative saturation voltage when the AC input is greater than the reference DC input. Thus the comparator block produces a pulse output with controllable width by varying reference input.

The ON-OFF control block is comprised of an NPN transistor and a 555 timer. The output pulse of the comparator is given to an NPN transistor through a base resistance to amplify the pulse magnitude so that the timer can operate properly. The output of the 555 timer is fed to the gate of a MOSFET in the switch block. A contactor coil is attached to the drain of the MOSFET. For a high output of the timer, a voltage signal is sent to the gate of MOSFET and it is turned on. So the contactor coil is closed and the coil is energized to make contact.

The function of the auto cut-off switch can be observed from the CRO output shown in Fig. 3.6. It shows that the circuit gets cut off after 920ms (approx.). This time duration is sufficient to decide whether sustained ferroresonance occurs in the system or not. And also prevents the circuit equipment from experiencing high voltage and current for a long time.

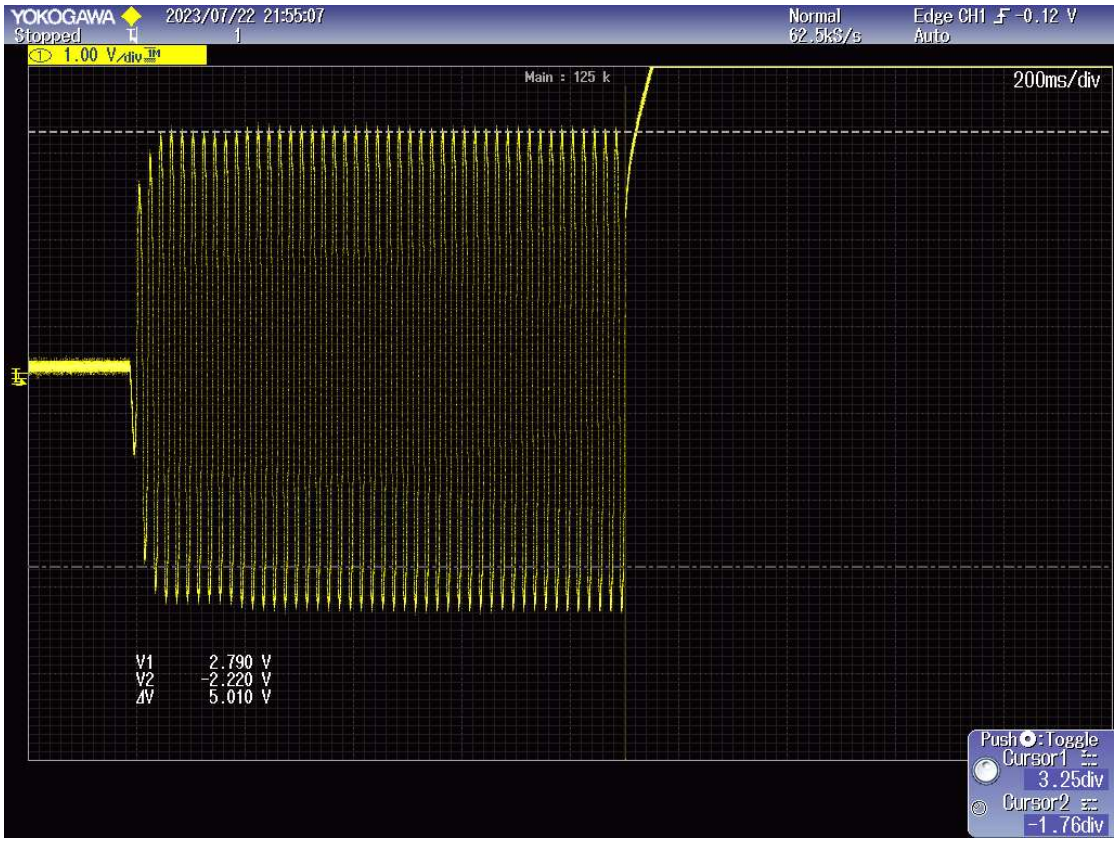

Fig. 3.6. Auto cut-off switch – operation

3.4.2 Development of Measuring Unit

It is required to measure a high voltage during ferroresonance. To measure the capacitor voltage safely through the digital oscilloscope a capacitive potential divider comprised of 0.47μF and 2.196nF capacitors is placed in parallel with the series capacitance (Fig. 3.4). Connecting the CRO channel across a 0.47μF capacitor the voltage across the series capacitor (C) under ferroresonance conditions is recorded. So the actual ferroresonance voltage will be MF times the recorded value. Where

$$MF = \frac{0.47+0.002196}{0.002196} = 215$$

Another capacitive potential divider is created with a 25.15μF capacitor connecting in series with the main capacitor C. The ferroresonance voltage is measured by a DC voltmeter that is

connected across 25.15μF through a bridge circuit. DC voltmeter is used to check whether ferroresonance has occurred or not.

To record the voltage across the transformer in ferroresonance condition the CRO channel is connected across the tertiary winding of the transformer with a 1:10 probe setting.

Fig. 3.7. Experimental setup in laboratory

3.5 Experiment at Various Supply Voltages

The ferroresonance phenomenon depends on certain circuit parameters like supply voltage, supply frequency, series capacitance, non-linear inductance, etc. Ferroresonance overvoltage is generated when the value of capacitance matches with the non-linear inductor present in the circuit for a particular impressed alternating voltage. In the laboratory experiment, the effect of supply voltage on ferroresonance is observed. Results recorded by a digital CRO are also displayed in the following sections to arrive at a conclusion about the effect of supply voltage on ferroresonance overvoltage generation.

The value of series capacitance is taken as 1.272μF.

For supply voltage 130V ferroresonance does not occur. Fig 3.8 shows the voltage across the transformer and capacitor as obtained from CRO. At 147V supply voltage high peaks appear in the transformer and capacitor voltages in the first 3-4 cycles and then it decays down to normal voltage (Fig. 3.9).

A strange situation arises near the 153V source voltage. A sustained ferroresonance occurs in some cases again it disappears when a similar condition is tried repeatedly. Fig. 3.10 and 3.11 show the capacitor and transformer voltages for two such cases when ferroresonance occurs in the first case and does not occur in the second case. For both cases, circuit parameters

remain the same. Only the switching instants are different. The RMS value of the capacitor voltage at steady-state ferroresonance is almost 2.48 times the supply voltage.

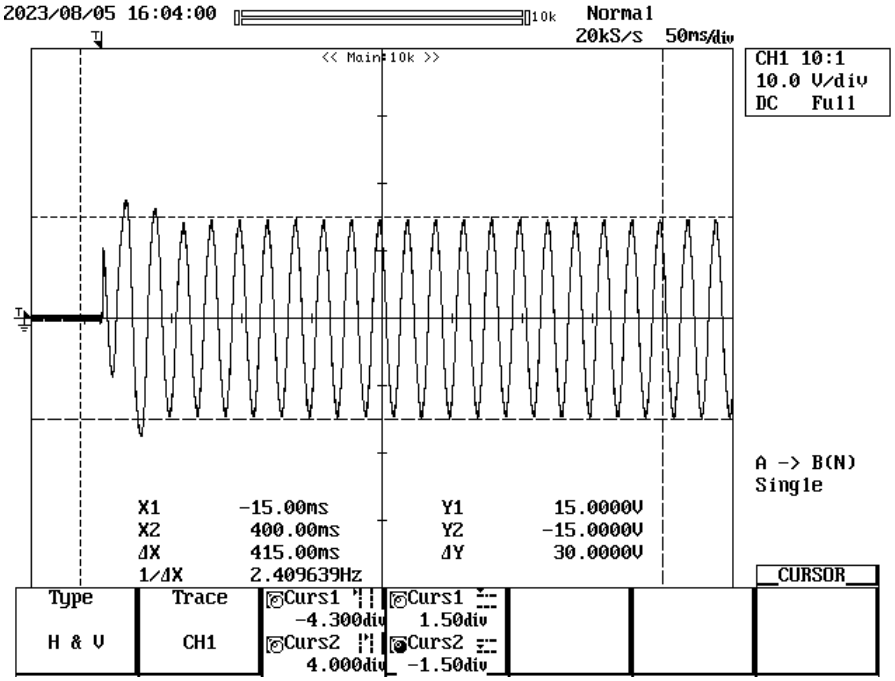

(a)

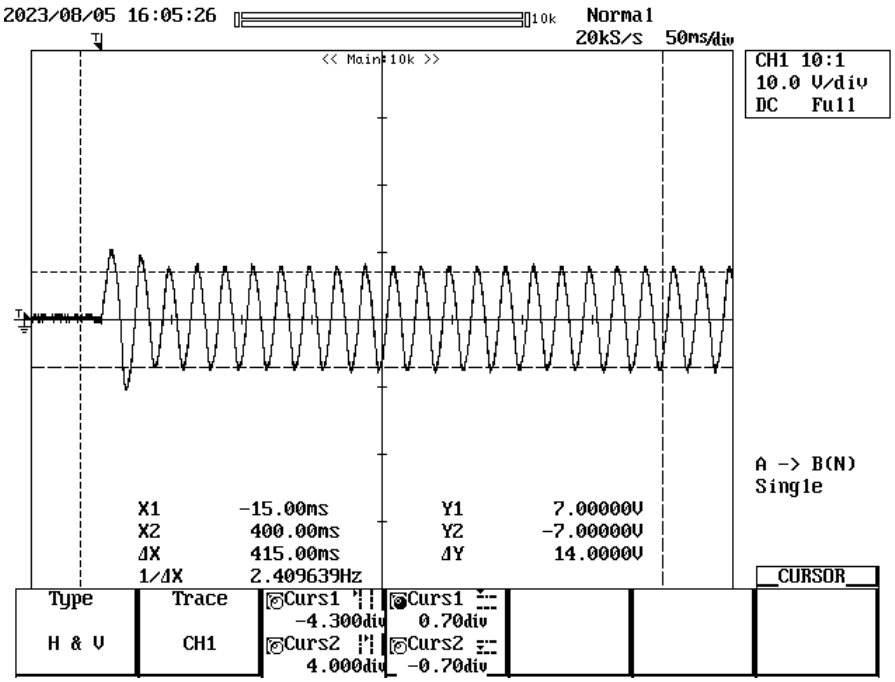

(b)

Fig. 3.8. (a) Transformer voltage and (b) capacitor voltage at 130V

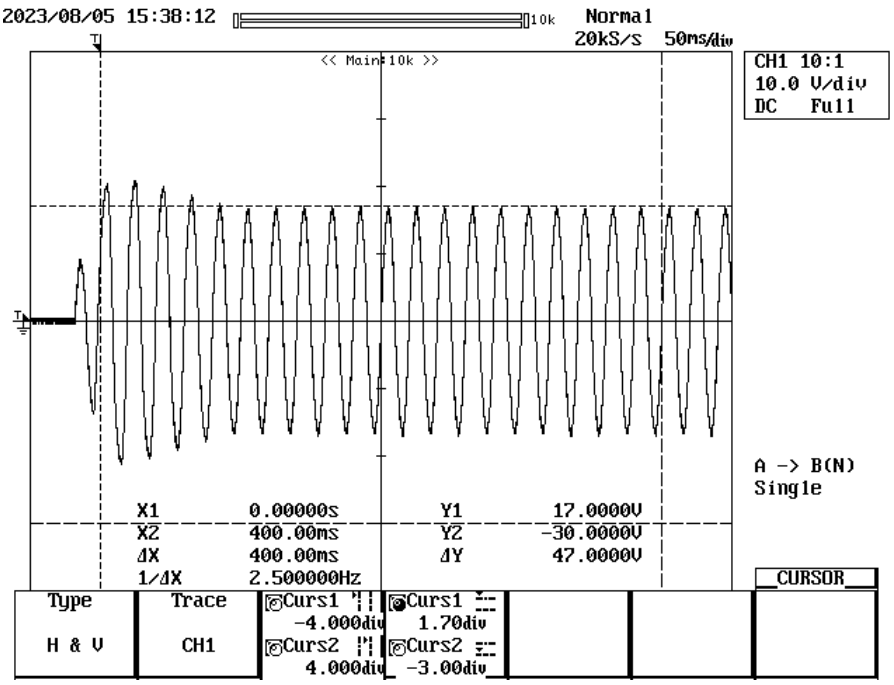

(a)

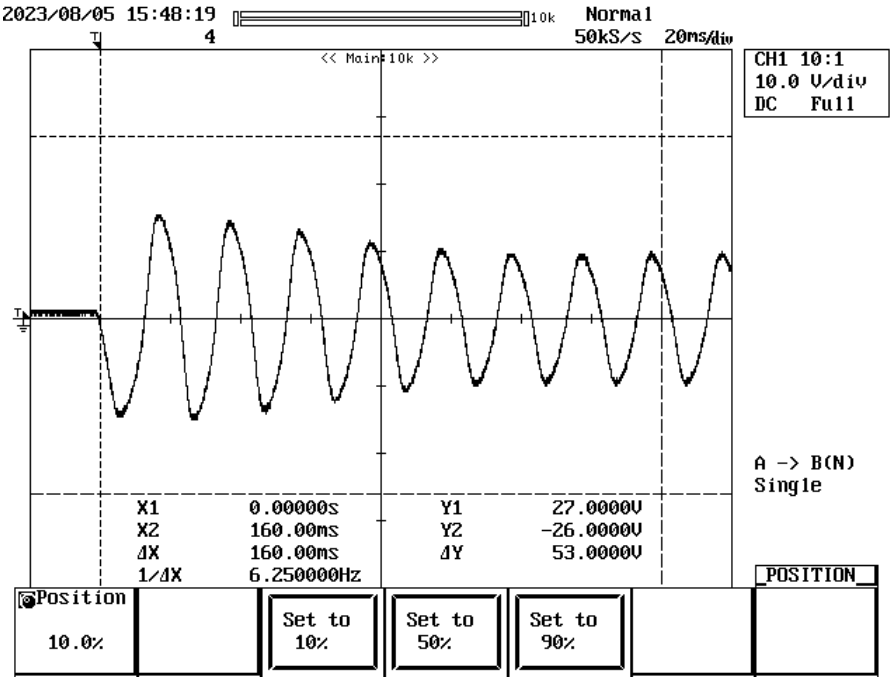

(b)

Fig. 3.9. (a) Transformer voltage and (b) capacitor voltage at 147V

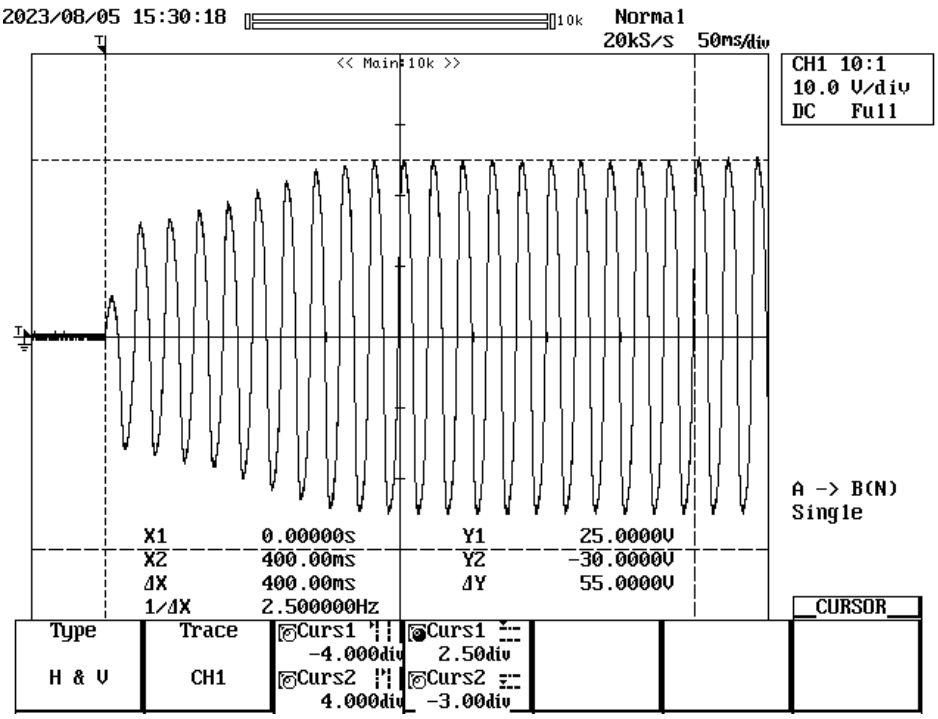

(a)

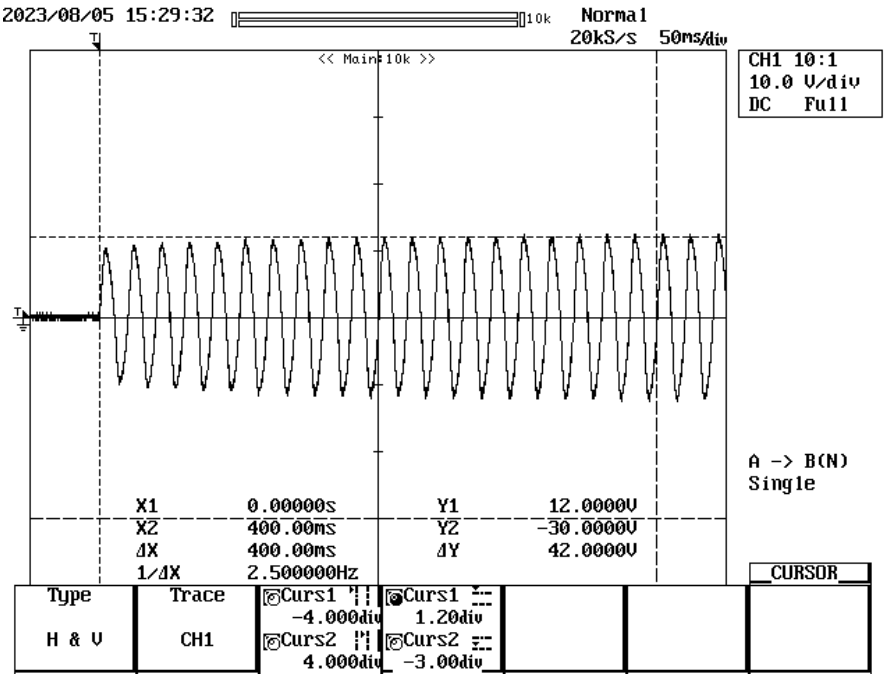

(b)

Fig. 3.10. Capacitor voltage (a) when ferroresonance occurs and (b) when no ferroresonance occurs at 153V supply voltage

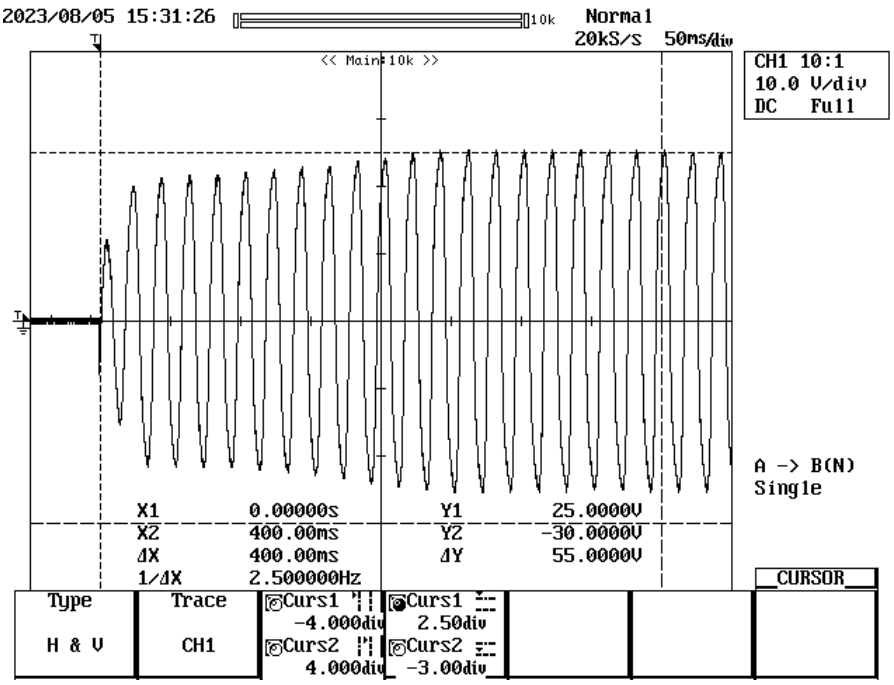

(a)

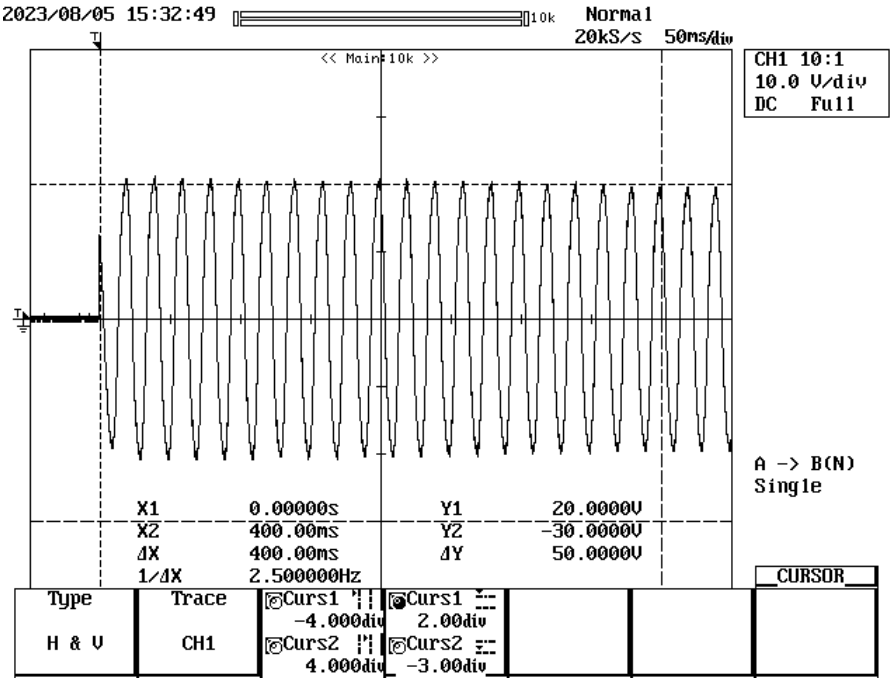

(b)

Fig. 3.11. Transformer voltage (a) when ferroresonance occurs and (b) when no ferroresonance occurs at 153V supply voltage

Fig. 3.12 shows sustained ferroresonance at 154V supply voltage. The steady-state ferroresonance voltage across the capacitor is 2.48 times the supply voltage. And steady state ferroresonance voltage across the transformer is 2.21 times the supply voltage. This data also ensures that at ferroresonance, the circuit behaves as a capacitive circuit. This phenomenon matches Rudenberg's graphical prediction explained in section 2.5.

With further increase in the supply voltage, the ferroresonance state continues to appear. Fig. 3.13 shows the transformer and capacitor voltage at 165V supply voltage. The RMS values at steady-state ferroresonance are 2.58 and 2.14 times the supply voltage respectively.

To observe the rising of capacitor voltage during ferroresonance, keeping the supply voltage at 170 V first few cycles are recorded in CRO as shown in Fig. 3.14. It takes 4.5 cycles to reach the steady state ferroresonance and the time to reach the steady state is 83.2 ms. The peaks are given in table 3.2.

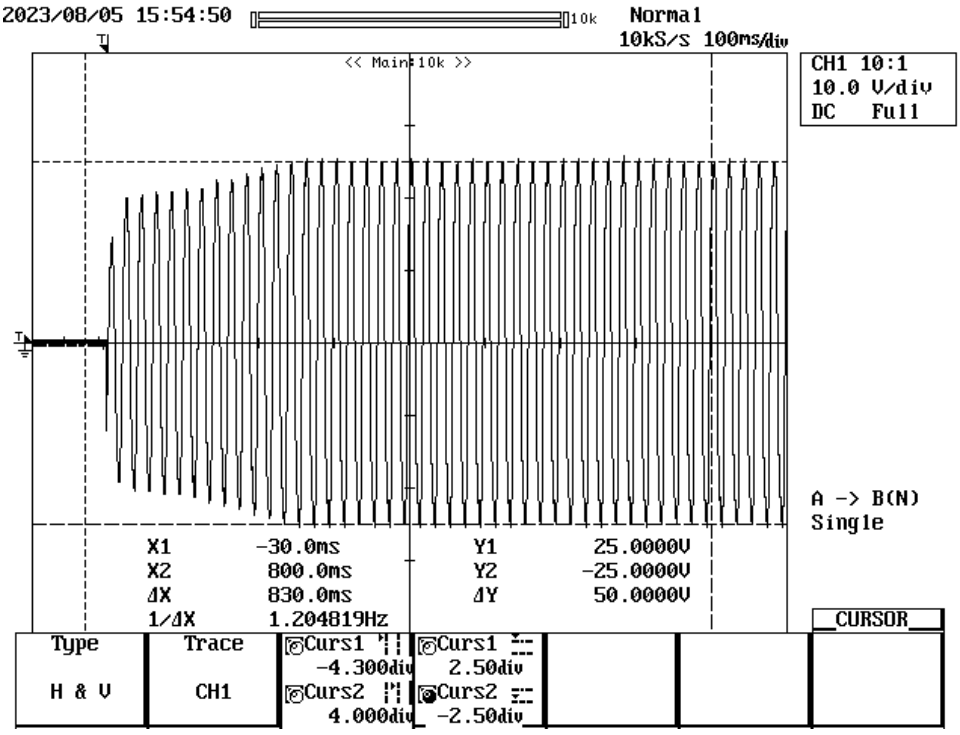

(a)

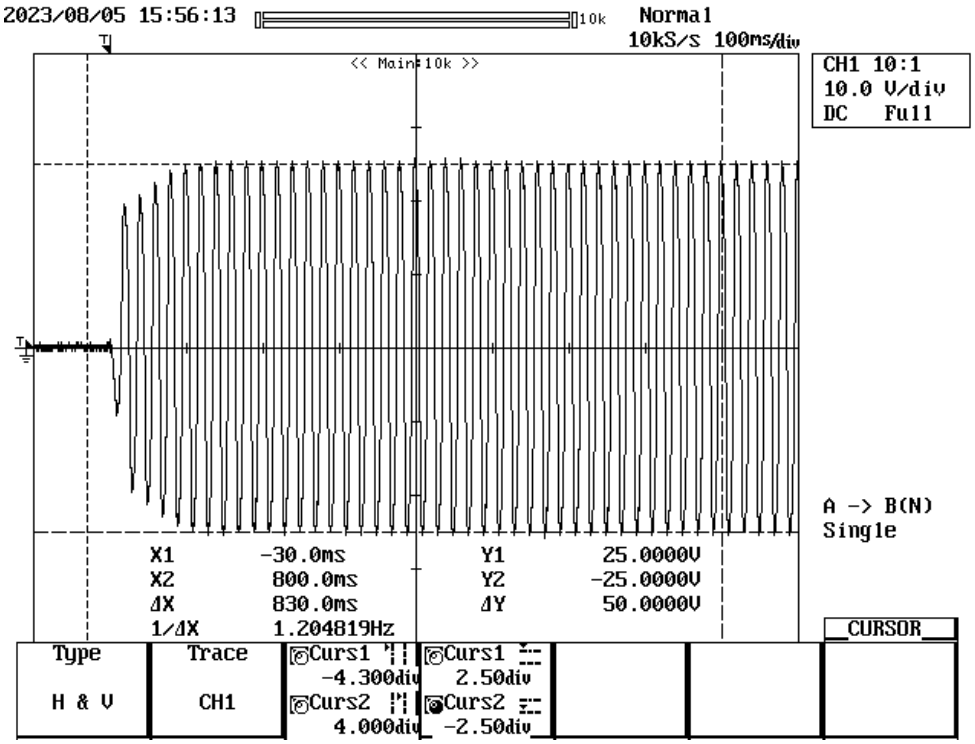

(b)

Fig. 3.12. (a) Transformer voltage and (b) capacitor voltage at 154V

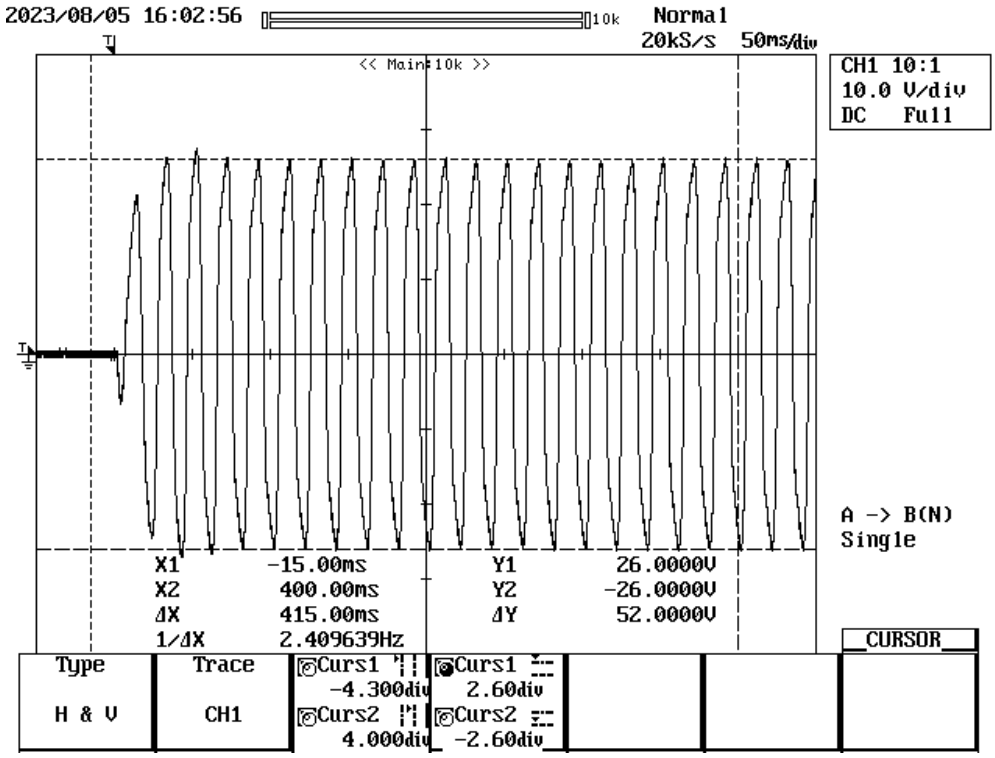

(a)

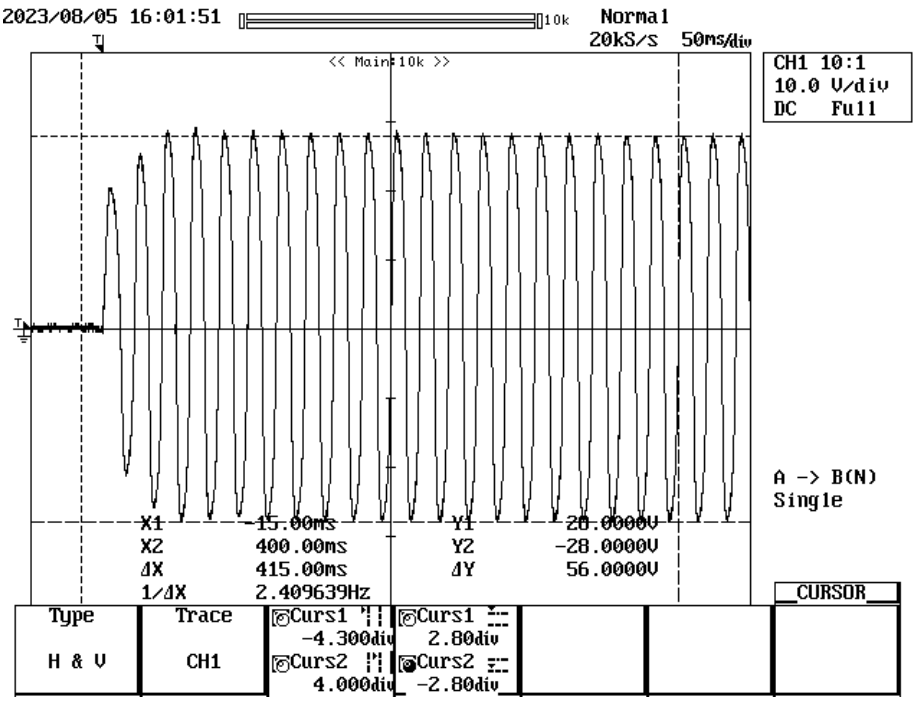

(b)

Fig. 3.13. (a) Transformer voltage and (b) capacitor voltage at 165V

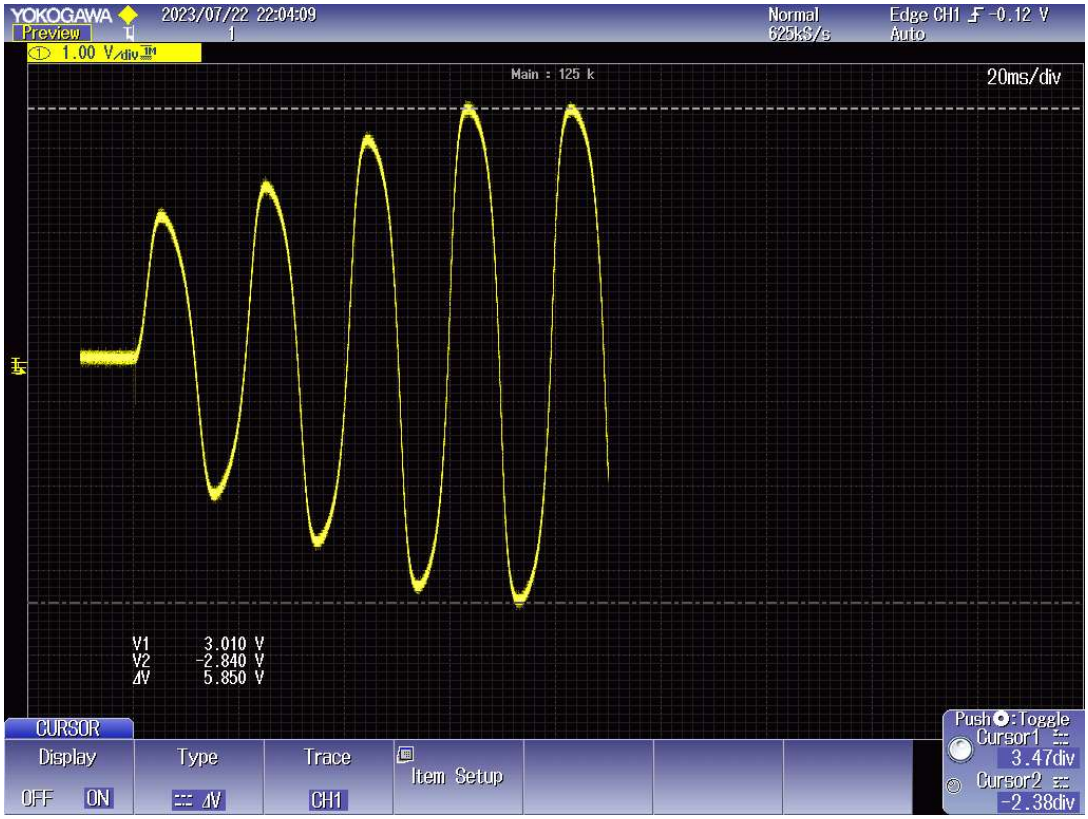

Fig. 3.14. Rising of capacitor voltage during ferroresonance at 170V

Table 3.2: Rising of capacitor voltage peaks at source voltage 170 V

Peak	Magnitude as a multiplier of supply voltage
$1st\ +ve\ peak$	2.27
$1st - ve\ peak$	-2.40
$2nd\ +ve\ peak$	2.65
$2nd\ -ve\ peak$	-2.78
$3rd\ +ve\ peak$	3.35
$3rd\ -ve\ peak$	-3.39
$4th\ +ve\ peak$	3.80
$4th\ -ve\ peak$	-3.59
$5th\ +ve\ peak\ (steady\ state)$	3.81

Increasing the supply voltage further shows that the steady state is achieved more quickly. Table 3.3 shows how the time to reach a steady ferroresonance state after switching on the circuit is varying with the supply voltage. It can be found from the observation that the time is decreasing with the increase of supply voltage. For the safety of the equipment and laboratory personnel, we restrict ourselves to the rated voltage that is 220V. Table 3.4 shows all the observations that are obtained from the experiment with different supply voltages.

Table 3.3: Time to reach steady state

Supply voltage	Time to reach steady state
190 V	80 ms
200 V	60 ms
210 V	52 ms
220 V	30 ms

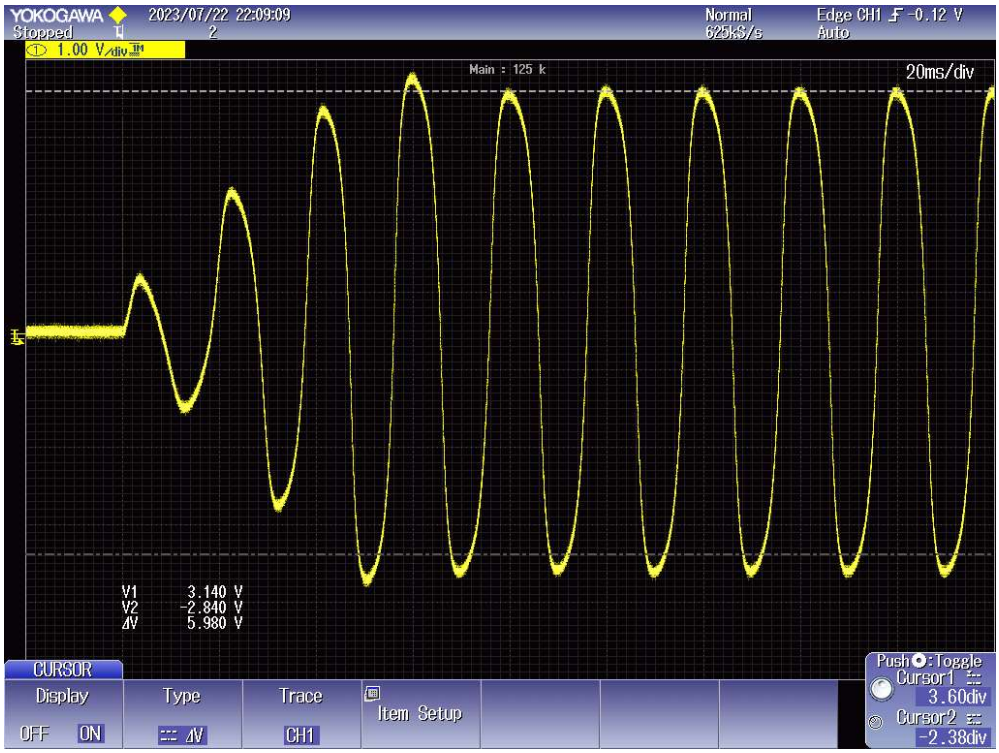

Fig. 3.15. Capacitor voltage at 190 V supply voltage

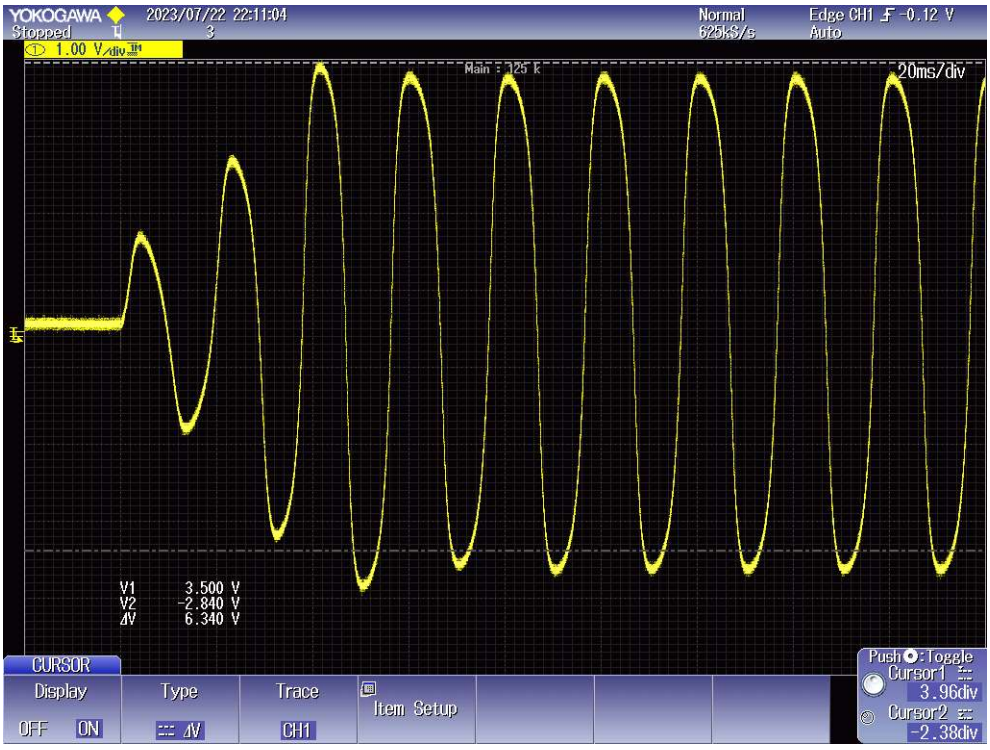

Fig. 3.16. Capacitor voltage at 200 V supply voltage

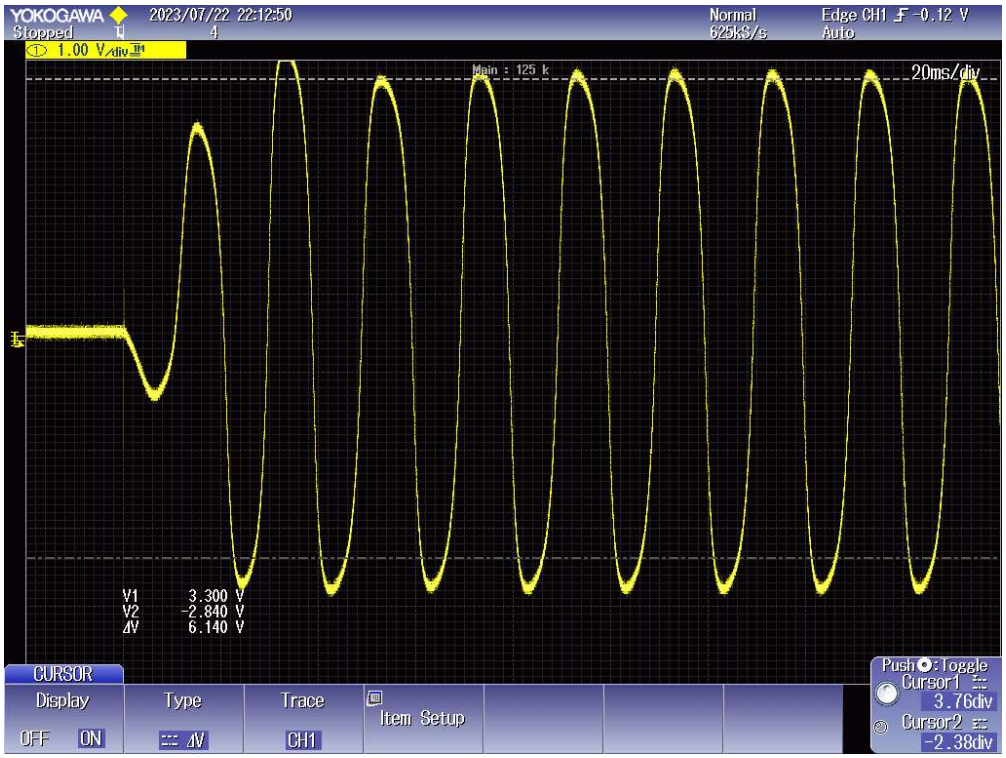

Fig. 3.17. Capacitor voltage at 210 V supply voltage

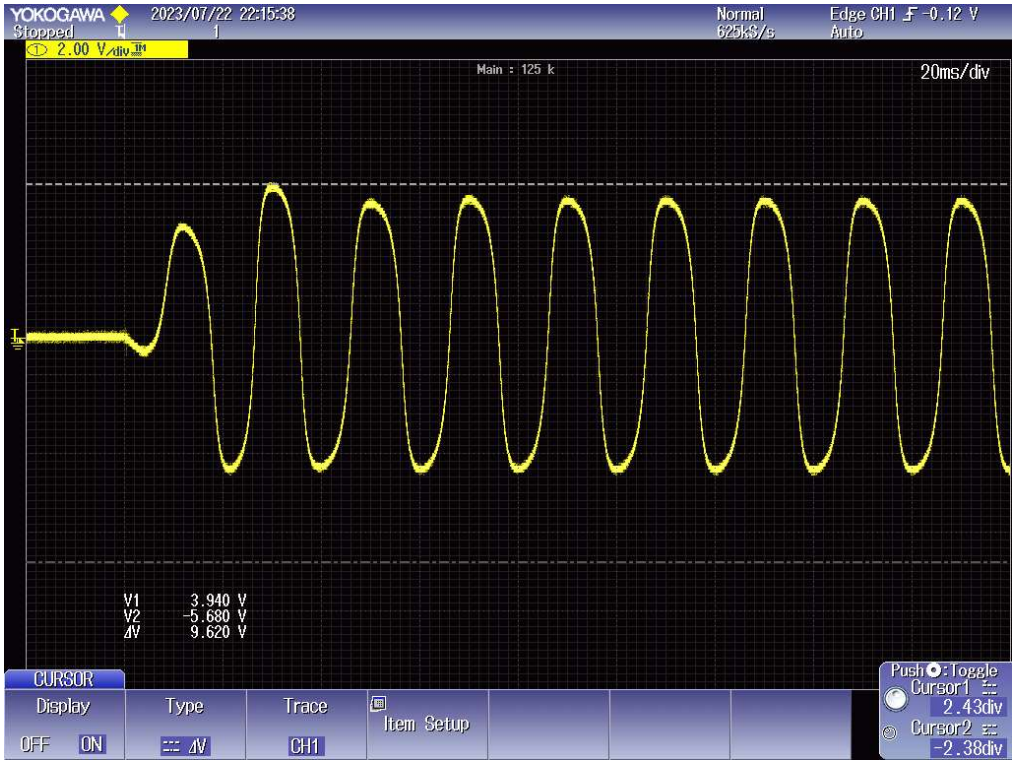

Fig. 3.18. Capacitor voltage at 220 V supply voltage

Table 3.4: Experimental result at different source voltages

Sl No.	Supply Voltage (V)	RMS voltage across (× Supply voltage)		Ferroresonance observed?	Remarks
		Series Capacitor	Transformer Secondary		
1	130	0.94	1.56	no	No occurrence of ferroresonance
2	147	0.94	1.59	no	
3	153	2.58	2.21	yes	Critical voltage for ferroresonance to occur
4	153	2.48	2.21	yes	
5	153	1.19	1.77	no	
6	153	2.48	2.21	yes	
7	153	2.48	2.21	yes	
8	153	1.19	1.77	no	
9	153	2.58	2.21	yes	
10	153	2.58	2.21	yes	
11	153	2.58	2.21	yes	
12	160	2.57	2.12	yes	Sustained ferroresonance
13	165	2.58	2.14	yes	
14	170	2.71	2.2	yes	
15	180	2.62	2.18	yes	
16	190	2.52	2.13	yes	
17	210	2.38	1.92	yes	
18	220	2.47	2.07	yes	

3.6 Summary

This chapter describes the details of a laboratory experiment that has been developed and performed to observe ferroresonance in a controlled environment. Initially, the open circuit test of the transformer is used to extract the core magnetic characteristics of the transformer during the ferroresonance test. R. Rudenberg's graphical method is used to develop and determine the series capacitance value. A potential divider composed of capacitors is employed to safeguard the digital oscilloscope. An auto cut-off switch is utilized, which shuts off the circuit after a certain amount of time, to protect the line equipment from prolonged exposure to overvoltage at ferroresonance. The ferroresonance event has been effectively recorded. When ferroresonance is created at different line conditions, the waveforms of the transformer and capacitor voltages at various source voltages are recorded.

4. Comparison of Experimental and Simulation Results

4.1 Preparation of Simulation Model

To verify the experimental observation discussed in Chapter 3, a suitable transformer model is required. Also before starting the in-depth stability analysis of a ferroresonance circuit, it is required to validate the working model with the experimental results.

The conventional equivalent circuit of a transformer consists of a series resistance and inductance representing copper loss and leakage flux of the transformer windings and a parallel resistance and inductance representing core loss and transformer magnetizing flux. If we stick to the no-load condition only in our whole analysis, we can neglect the series components. This assumption is necessary as it is reported many times that ferroresonance occurs in the low or no load condition of a transformer.

The critical part is to represent the magnetizing flux characteristic of the transformer as in conventional equivalent circuit it is assumed as linear. Whereas ferroresonance study requires the nonlinear behavior of the core.

4.2 Transformer Model Structure

Being a static device, a transformer is used in almost every sector of electric power transmission. It consists of two parts, one is insulated windings and the second is the magnetic core. Two or more sets of windings are placed on a solid core structure. The core ensures good magnetic coupling between the windings. The popular equivalent circuit model of a transformer represents the copper loss and leakage flux as series components and core loss as parallel components along with an inductor representing the basic transformer action. For the full utilization of the core material, a transformer is designed in such a way that its rated operating point falls near the knee point of its core magnetizing curve. At this stage, the core characteristic can be considered linear and can be represented with a linear equation. The problem arises when due to fault like ferroresonance the operating point slips into the saturation region. The behavior now cannot be characterized by linear relations. Here comes the main challenge to find out a

suitable nonlinear equation for the transformer core. Many researchers have proposed various nonlinear models to solve this purpose. All the models have their advantages and disadvantages.

Papers [54, 55] uses the harmonics balance method to find out the appropriate core characteristics of a transformer. Some papers [56, 57] suggested a piecewise linear inductance method for the modeling of the saturation characteristic of a transformer. Some popular simulator like EMTP also comes with an inbuilt non-linear transformer model based on the piecewise linearization technique [58]. Preisach theory has been used to develop the nonlinear model of the transformer inductance [29]. Different duality-based approaches were compared for modeling low-frequency transformers in [59, 60]. Equivalent winding capacitance obtained from standard test data has been proposed for the accurate modeling of the transformer [61].

To represent the B-H loop analytically various approaches can be taken. It can be represented with a nonlinear single-valued inductance with constant core loss resistance [62, 63]. To capture the variation of the core loss resistance, non-linear single-valued inductance can be coupled with a nonlinear core loss resistance [12, 64]. Another approach can be the full hysteresis information along with constant core loss resistance [65]. The paper [66] gave an analytical comparison of above mentioned three different core modeling.

4.3 Finding the Nonlinear Equation for Transformer Core

The open circuit characteristic obtained in the open circuit test of the transformer is needed to feed to the mathematical model of the transformer. This is done with the help of the MATLAB program. The curve fitting tool is used to predict the suitable polynomial for the experimental curve. The following equation of order 7 is found suitable:

$$x = ay + by^7 \tag{4.1}$$

Where $a = 0.038$, and $b = 0.0022$. and x and y are open circuit current and voltage respectively. The approximated graph is shown in red color in the Fig. 4.1 along with the experimental curve in blue.

4.4 Development of Ferroresonance Nonlinear Model

As observed from different literature [67, 68] circuit shown in Fig. 4.2 is taken as a ferroresonance circuit. This consists of a voltage source V_S, a series capacitance C, and a single-

phase transformer. The transformer is represented with its parallel branches only where resistance R_C represents core loss and a saturable inductance represents the primary winding of the transformer. It is assumed that the transformer is working under no load condition. For that, the secondary winding and the series resistance and inductances are neglected.

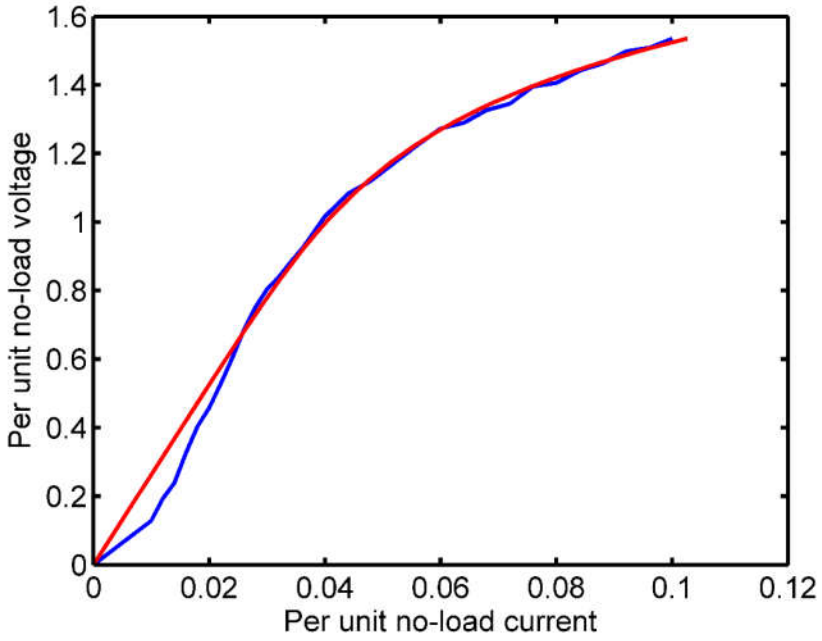

Fig. 4.1. Experimental (blue) and simulated (red) OCC curves

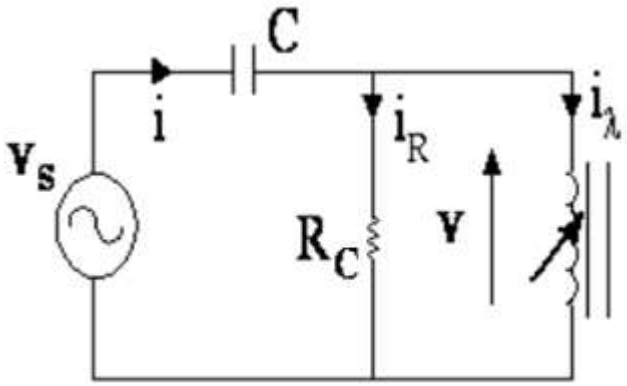

Fig. 4.2. Model circuit for ferroresonance

By applying KVL for the circuit shown in Fig. 4.2

$$V_s = V_C + V \qquad (4.2)$$

Where

V_s = source voltage

$V_C = \frac{1}{C}\int i\,dt$ = Voltage across capacitor

$V = \frac{d\lambda}{dt}$ = Voltage across saturable inductor or transformer voltage which is equal to the rate of change of flux λ.

From (4.2)

$$V_s = \frac{1}{C}\int i\,dt + \frac{d\lambda}{dt} \quad (4.3)$$

Differentiating both sides of (4.3) with respect to time

$$\frac{dV_s}{dt} = \frac{1}{C}(i) + \frac{d^2\lambda}{dt^2} \quad (4.4)$$

Now $i = i_R + i_\lambda$

Where, $i_R = \frac{v}{R_C}$ = Current through the resistive branch and

$i_\lambda = 0.038\lambda + 0.0022\lambda^7 =$ The magnetizing current from (4.1)

Rearranging (4.4)

$$\frac{d^2\lambda}{dt^2} = \frac{dV_s}{dt} - \frac{1}{C}\left(\frac{v}{R_C}\right) - \frac{1}{C}(0.038\lambda + 0.0022\lambda^7) \quad (4.5)$$

Equation (4.5) is a 2nd-order differential equation. As the dependent variable λ contains a term with power 7, and the supply voltage V_S is sinusoidal, those make the equation highly non-linear and difficult to solve in conventional methods. It is required to prepare a simulation model based on (4.5) which can be used for the analysis of ferroresonance. MATLAB Simulink toolbox is chosen for this purpose and the working model is developed based on the following algorithm as shown in Fig. 4.3.

In this model, the three terms of the right-hand side of (4.5) are added to get the 2nd derivative of flux linkage. Then it is integrated to get the first derivative of flux linkage which is transformer voltage. This term again integrated 2nd time to get the flux linkage. Then (4.1) is used to calculate the magnetizing current.

4.5 Results from Simulation

As per the laboratory experiment conducted, the following parameters are used for MATLAB simulation:

C = 1.275 μF

R_C = 15.81 KΩ

f = 50 Hz

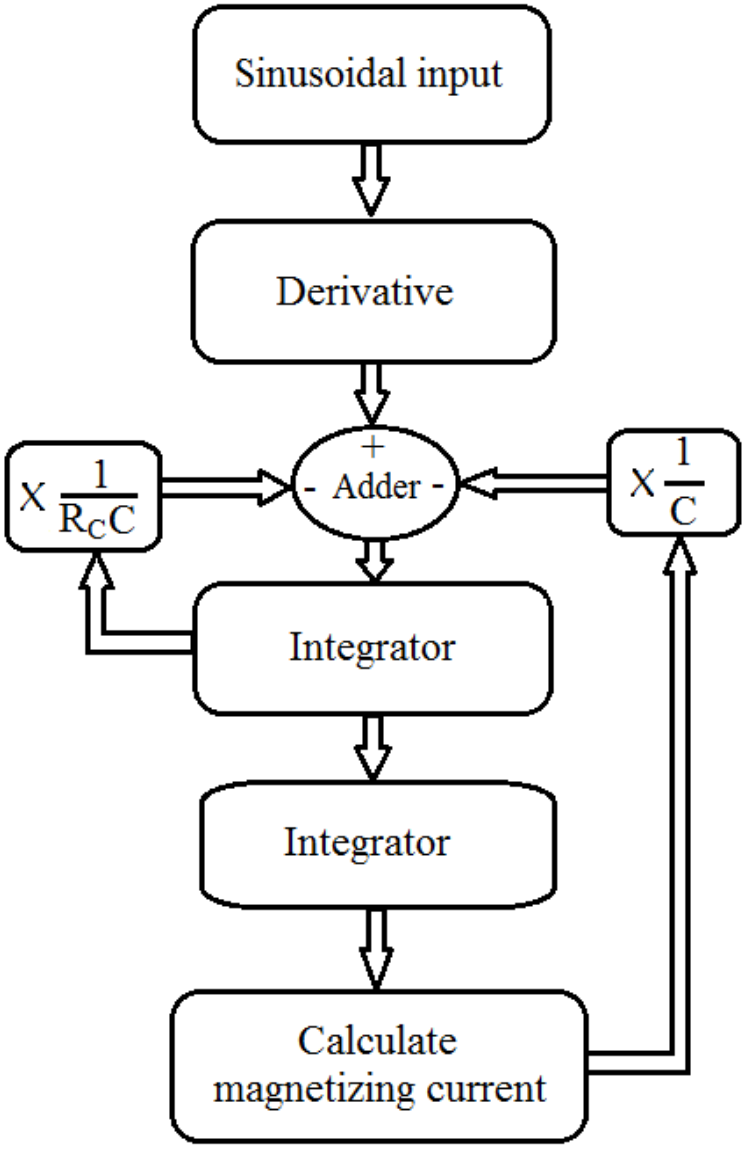

Fig. 4.3. MATLAB Simulink model

The value of the supply voltage is increased gradually from a very low value like 100V. At 130 V supply voltage, the transformer and capacitor voltage show no ferroresonance (Fig. 4.4). The RMS values of capacitor and transformer voltages are only 0.24 and 1.13 times of the supply voltage respectively. At 147 V supply voltage, the transformer and capacitor voltage shows no ferroresonance (Fig. 4.5). The RMS value is only 0.25 and 1.14 times of the supply voltage.

From 152 V to 155 V supply voltage, the simulation shows 2 -3 initial spikes before the system returns to a steady state. But no sustained ferroresonance was observed as Fig. 4.6 to 4.8

indicate. It is to be mentioned that the experimental setup showed sustained ferroresonance at 153 V supply voltage.

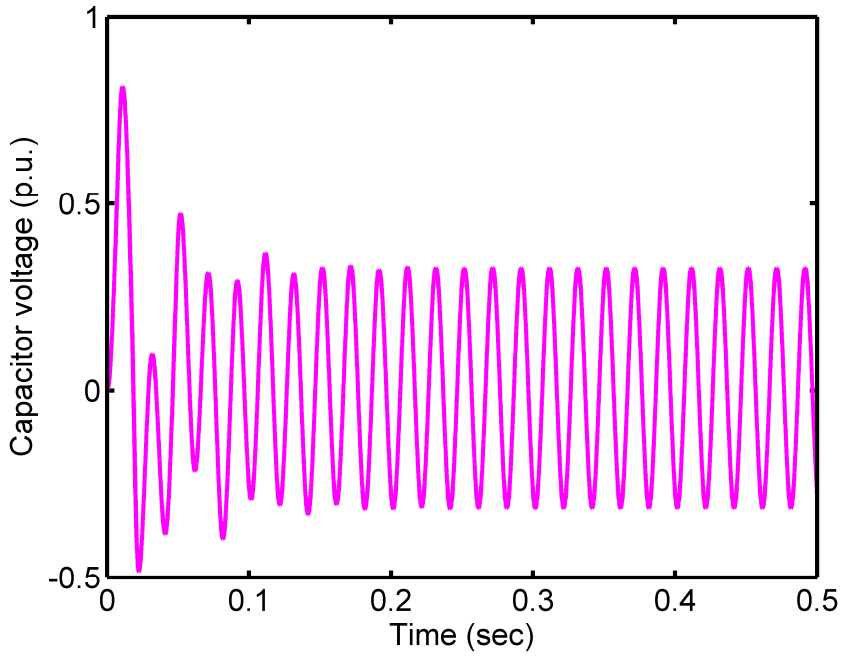

(a)

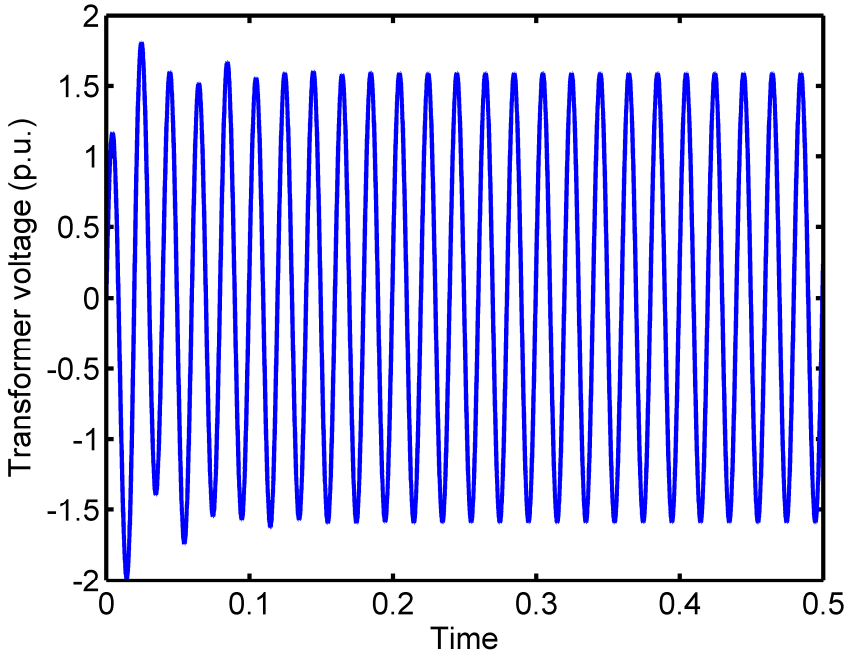

(b)

Fig. 4.4. (a) Capacitor voltage and (b) transformer voltage at 130 V supply voltage

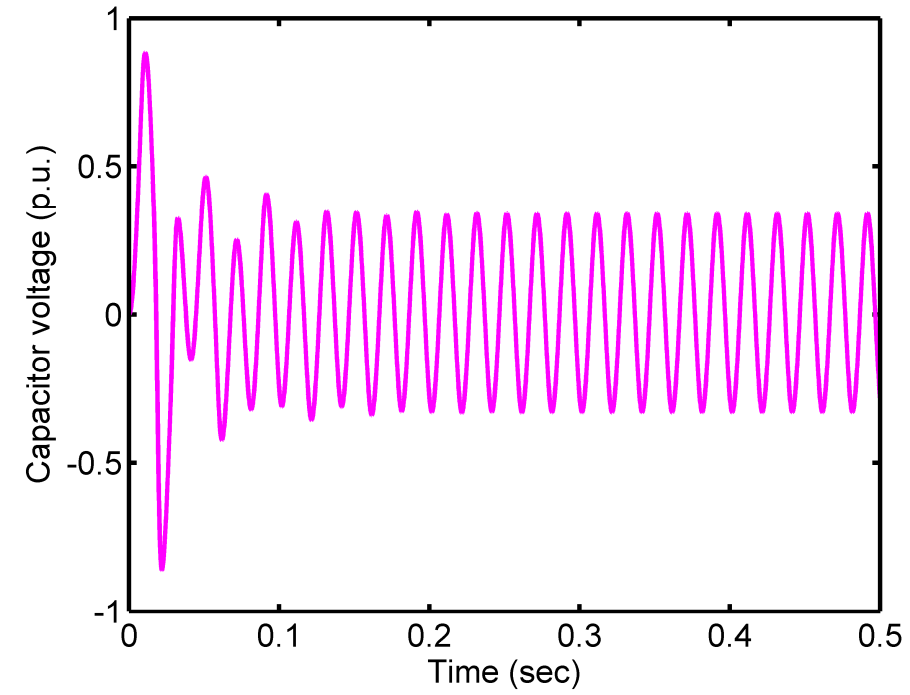

(a)

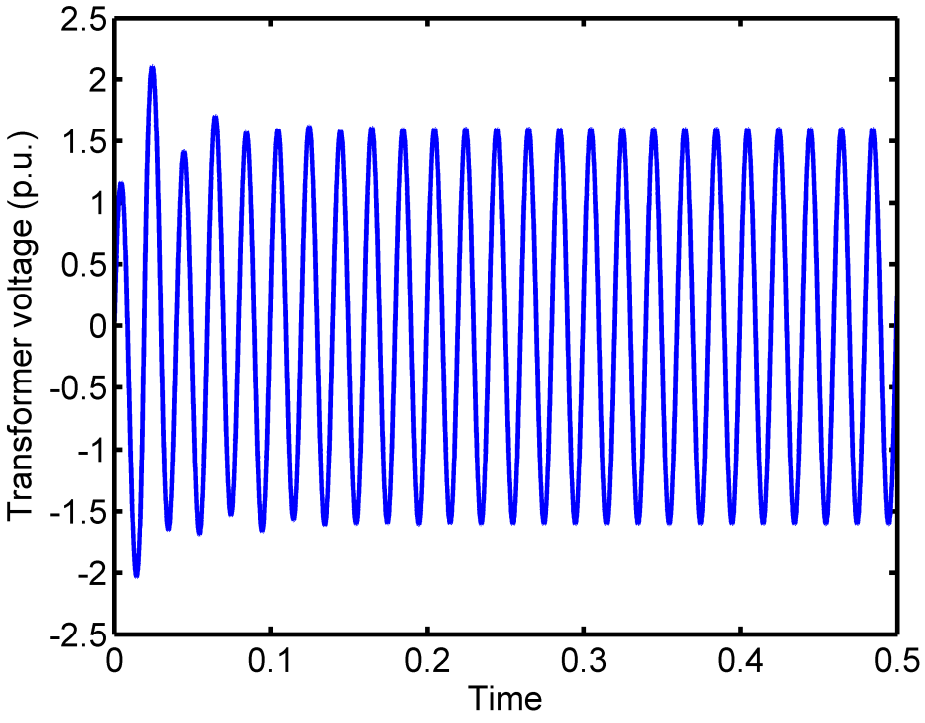

(b)

Fig. 4.5. (a) Capacitor voltage and (b) transformer voltage at 147 V supply voltage

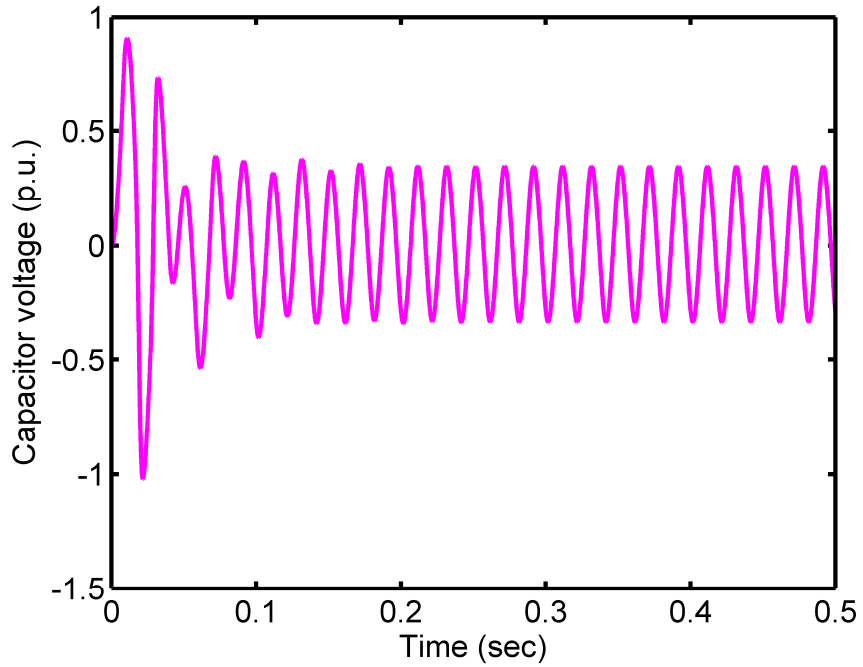

(a)

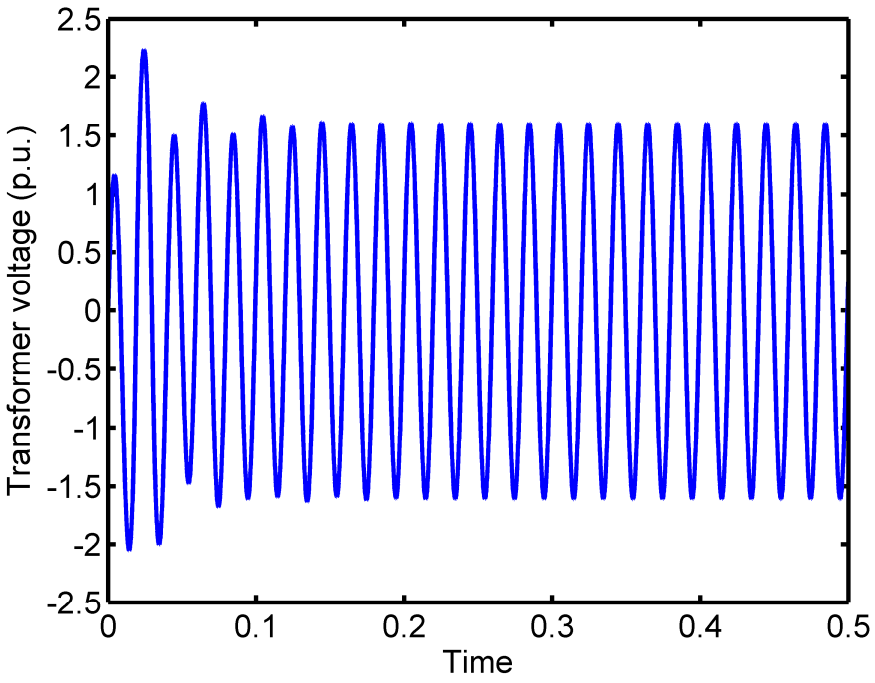

(b)

Fig. 4.6. (a) Capacitor voltage and (b) transformer voltage at 152 V supply voltage

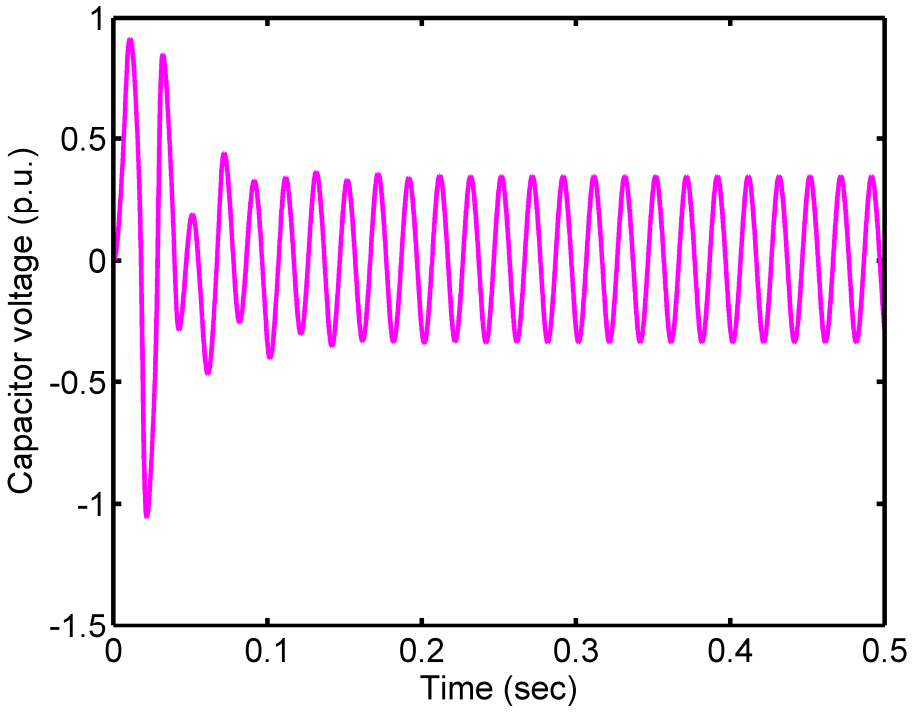

(a)

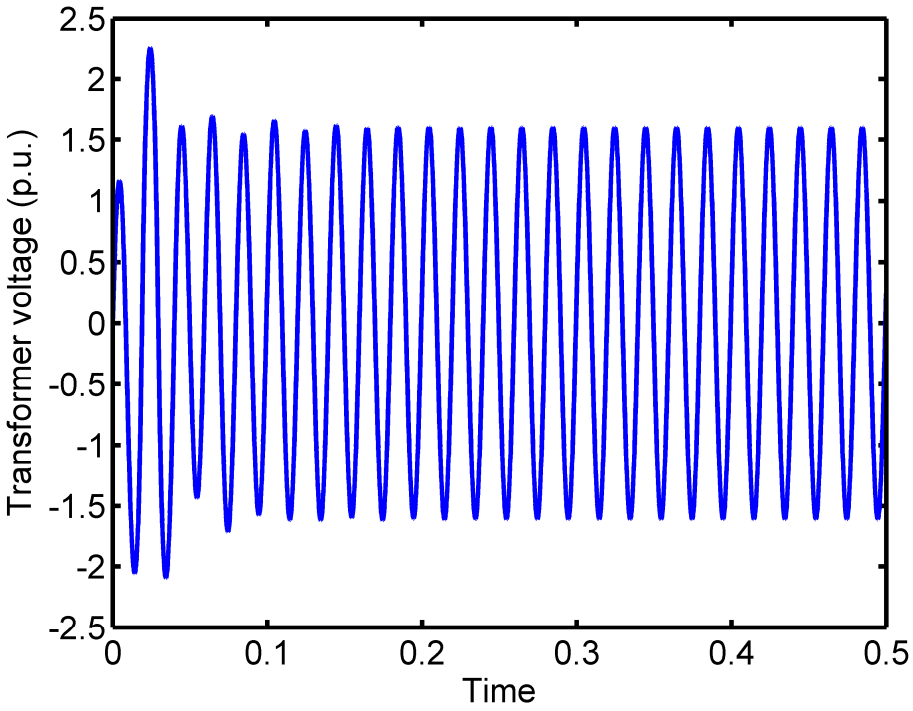

(b)

Fig. 4.7. (a) Capacitor voltage and (b) transformer voltage at 153 V supply voltage

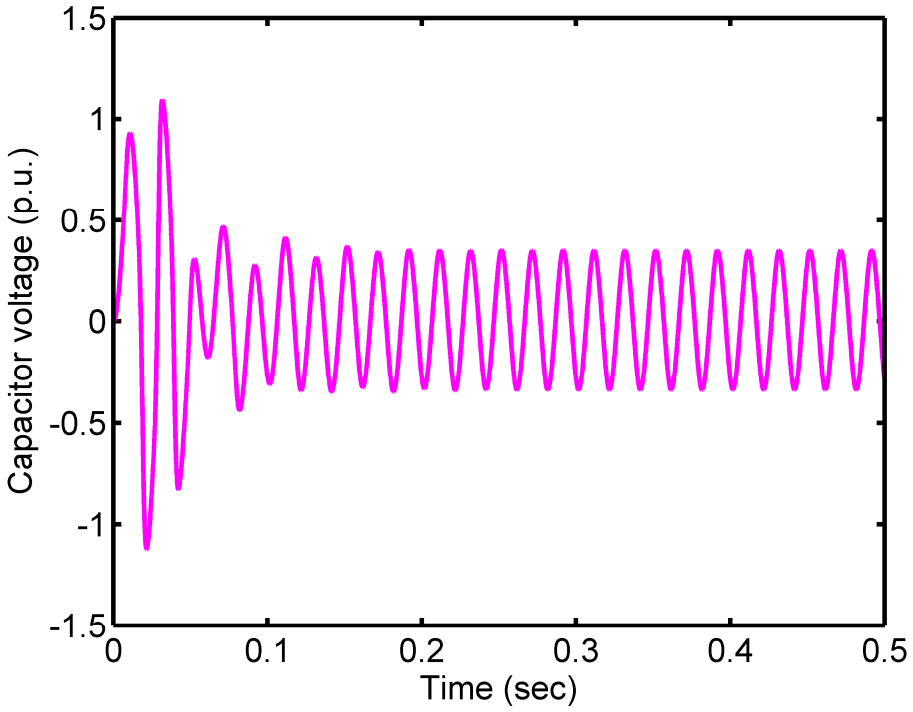

(a)

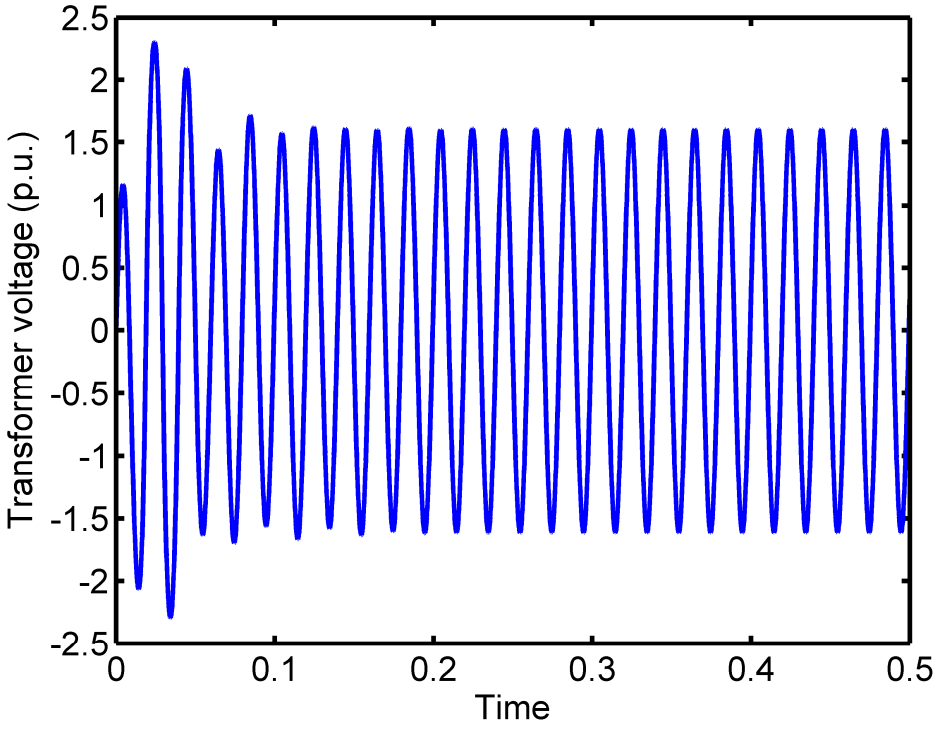

(b)

Fig. 4.8. (a) Capacitor voltage and (b) transformer voltage at 155 V supply voltage

Sustained ferroresonance was observed at 156 V supply voltage. Here the capacitor voltage jumps to 2.97 times of supply voltage, whereas the transformer voltage takes an RMS value 2.21 times of the supply voltage. The output is shown in Fig. 4.9. Corresponding capacitor and transformer voltages obtained from the experimental setup are shown in Fig. 4.10. Though this observation was obtained at 153 V supply voltage onwards. A closer look reveals that the nature of the output voltages does not match exactly. It may be due to the approximation of the non-linear core characteristics of the transformer. Also, the core loss is taken as constant in the simulation, which is actually not. The transformer voltage in Fig. 4.9 (b) shows some harmonics that were not present in the experimental observations.

Response at 157 V are shown in Fig. 4.11. The RMS value of the capacitor voltage is 3.06 times of supply voltage and the RMS value of the transformer voltage is 2.22 times of supply voltage. The time taken to reach a steady state is almost 150 ms.

Comparison of capacitor voltages for 170 V, 190 V and 210 V supply voltage are presented from Fig. 4.12 to 4.14.

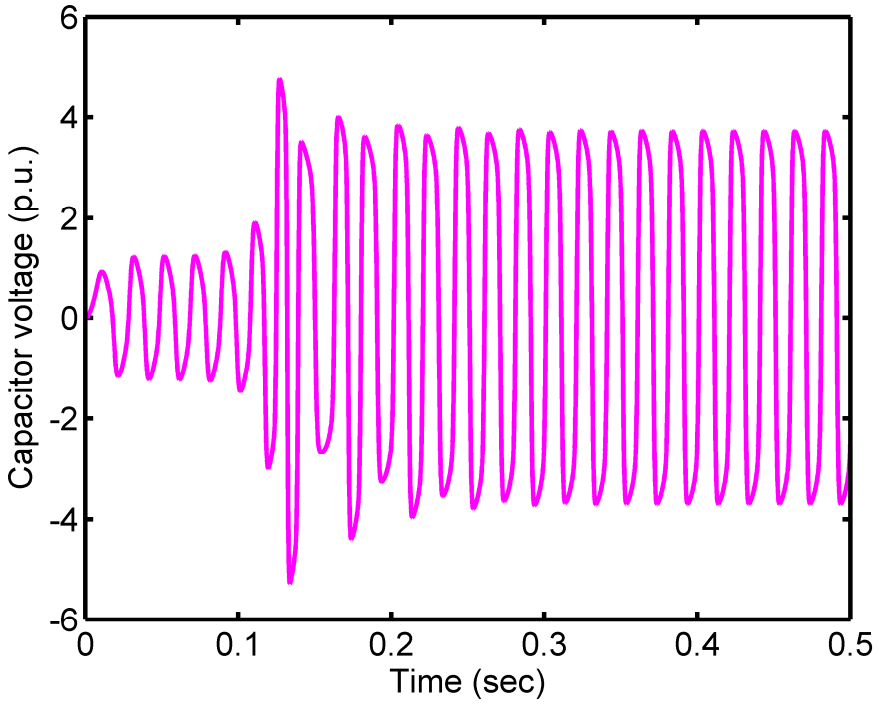

(a)

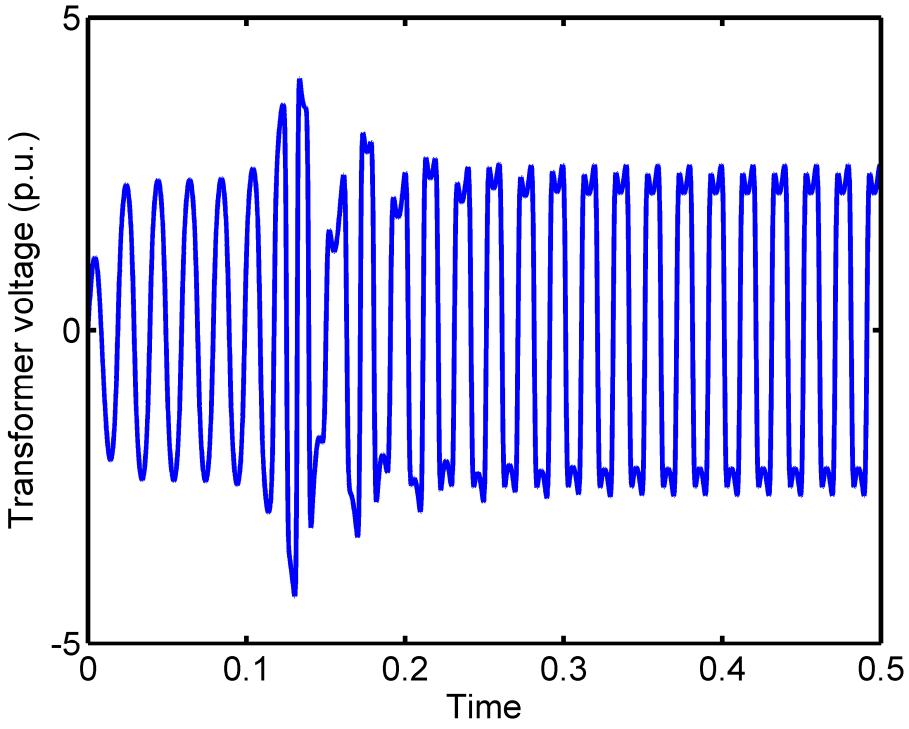

(b)

Fig. 4.9. (a) Capacitor voltage and (b) transformer voltage at 156 V supply voltage

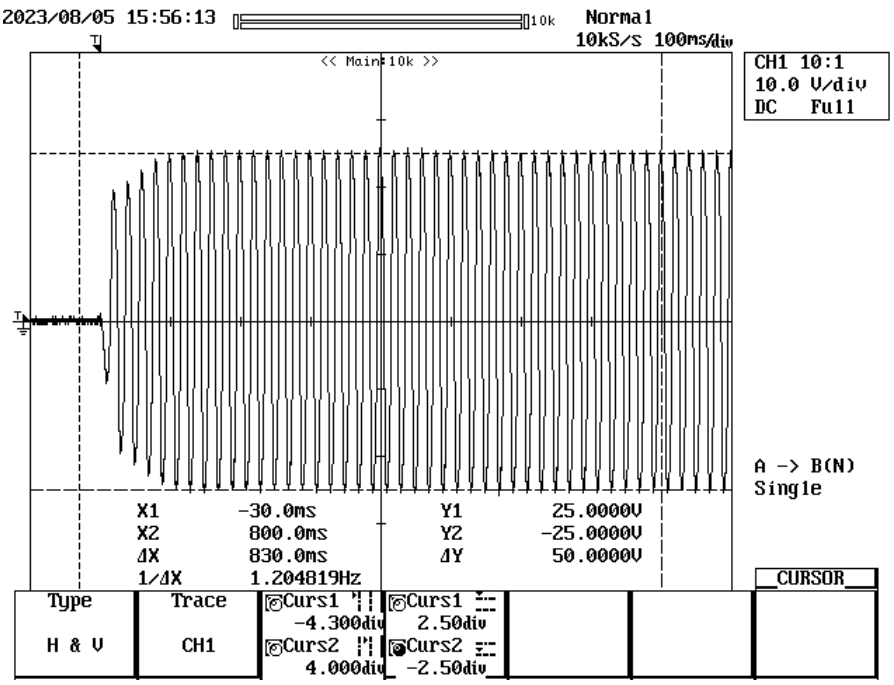

(a)

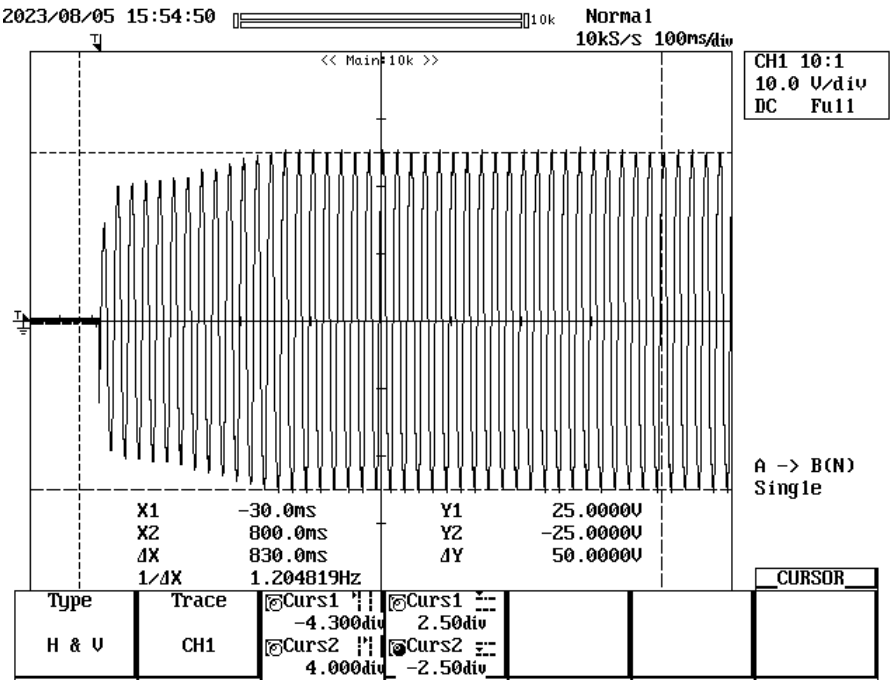

(b)

Fig. 4.10. (a) Capacitor voltage and (b) transformer voltage at 153 V supply voltage from experimental arrangement

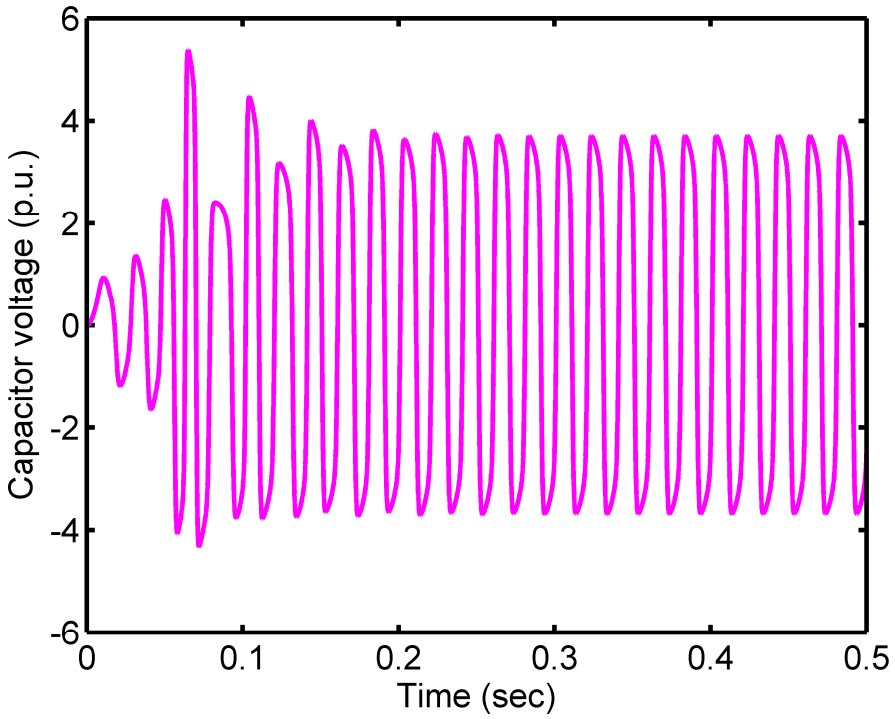

(a)

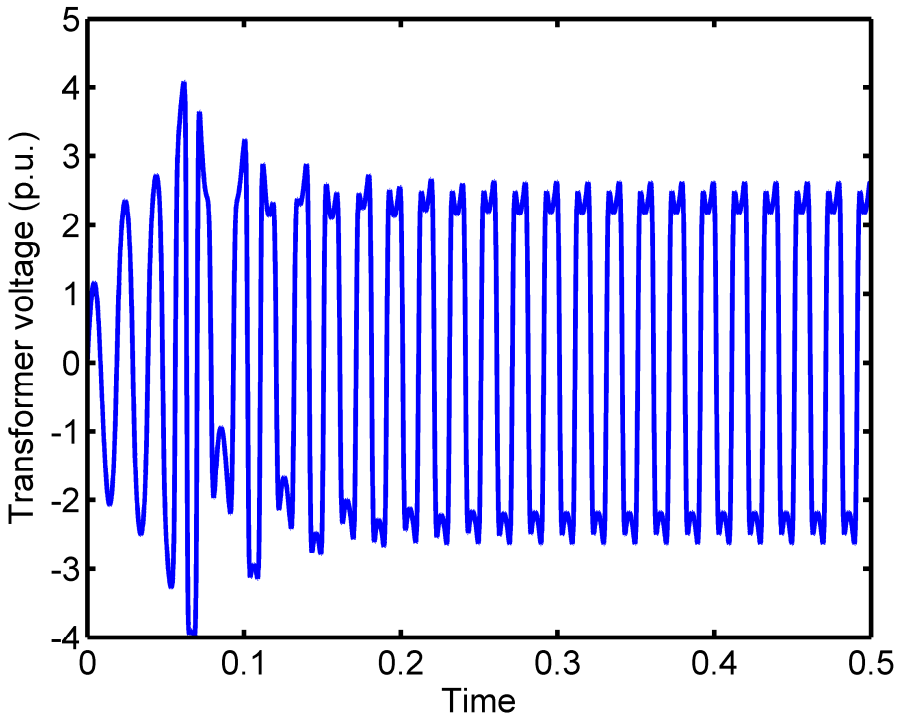

(b)

Fig. 4.11. (a) Capacitor voltage and (b) transformer voltage at 157 V supply voltage

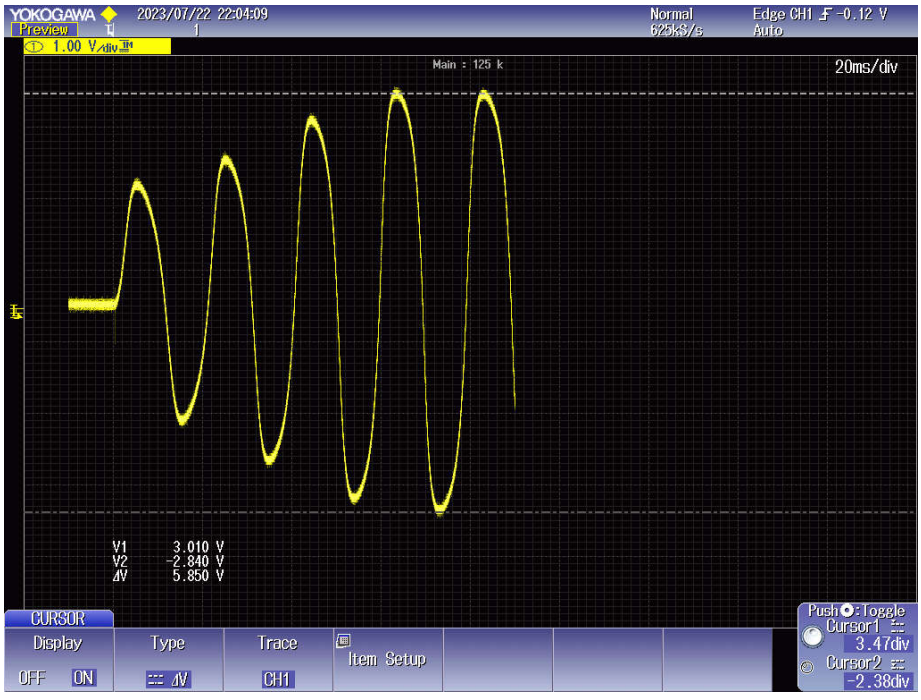

(a)

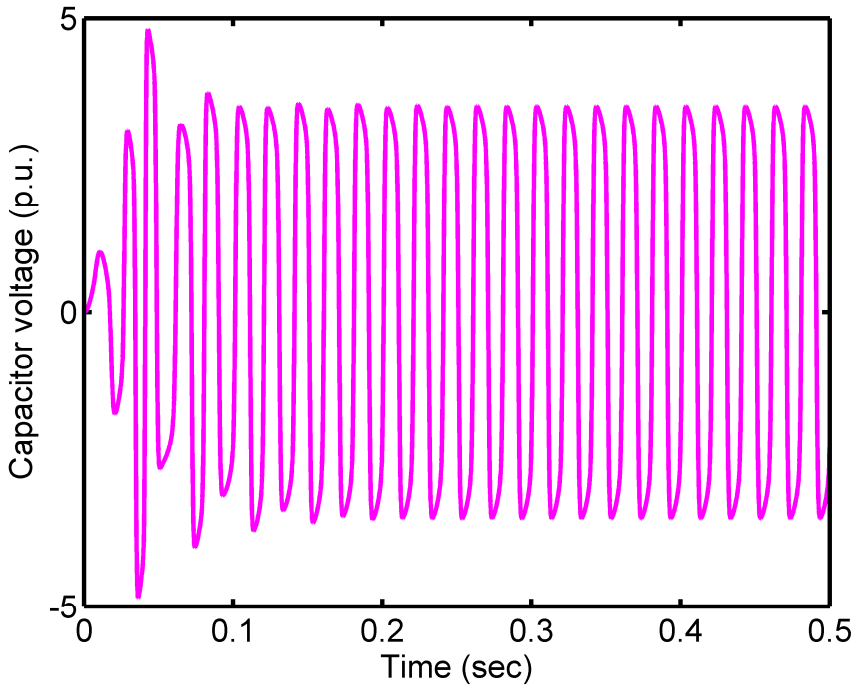

(b)

Fig. 4.12. Capacitor voltage (a) experimental and (b) simulated at 170 V supply voltage

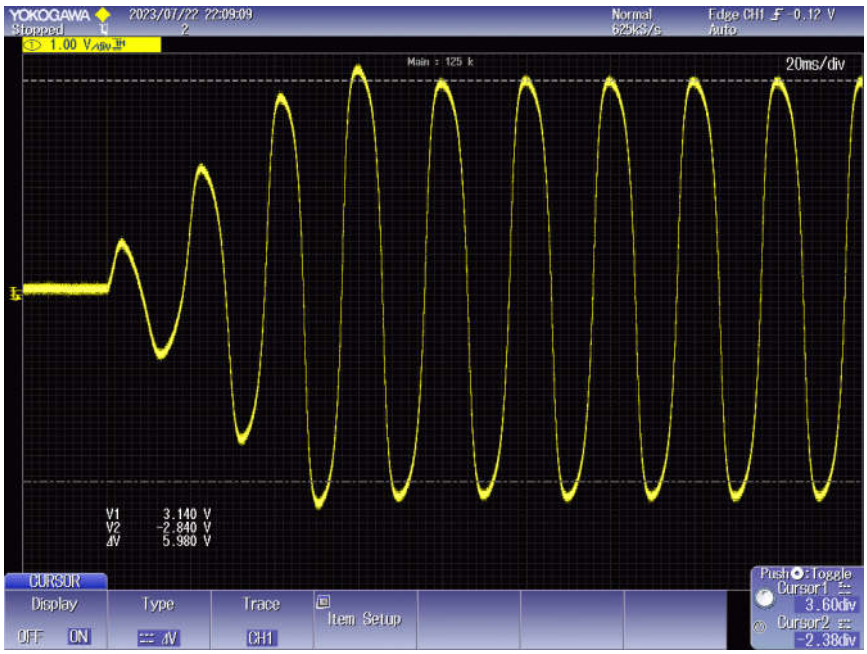

(a)

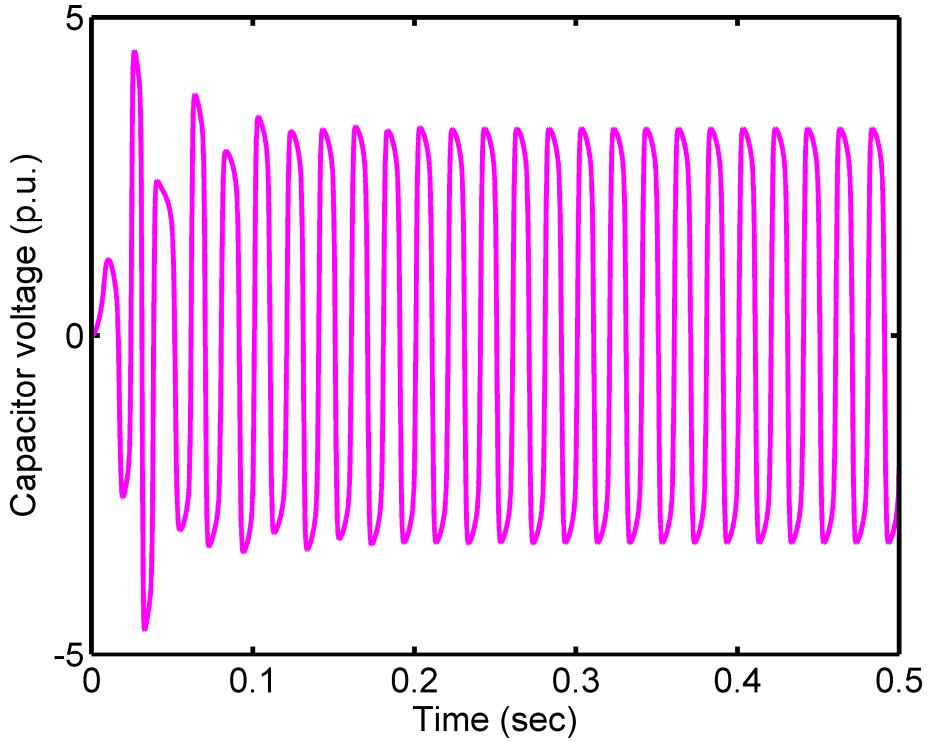

(b)

Fig. 4.13. Capacitor voltage (a) experimental and (b) simulated at 190 V supply voltage

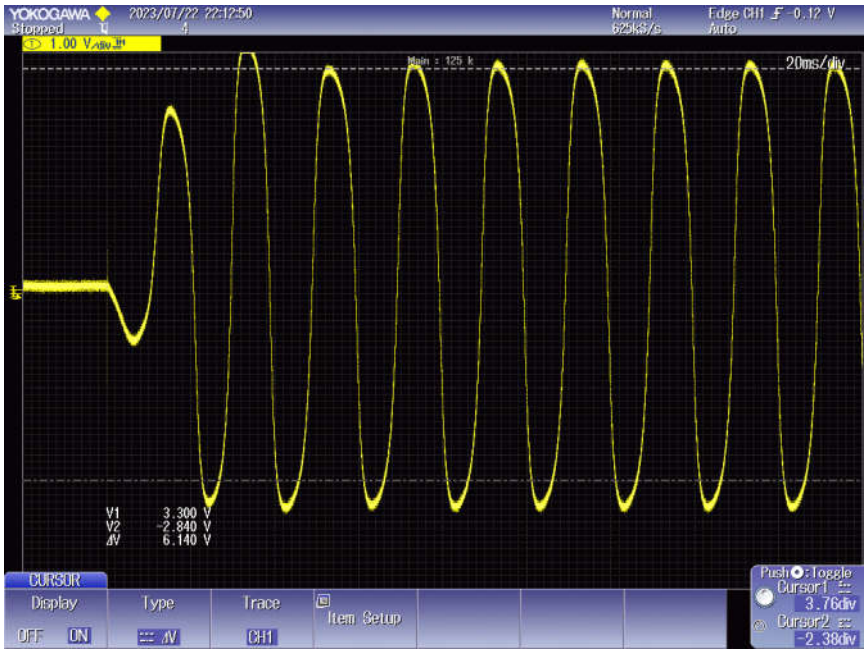

(a)

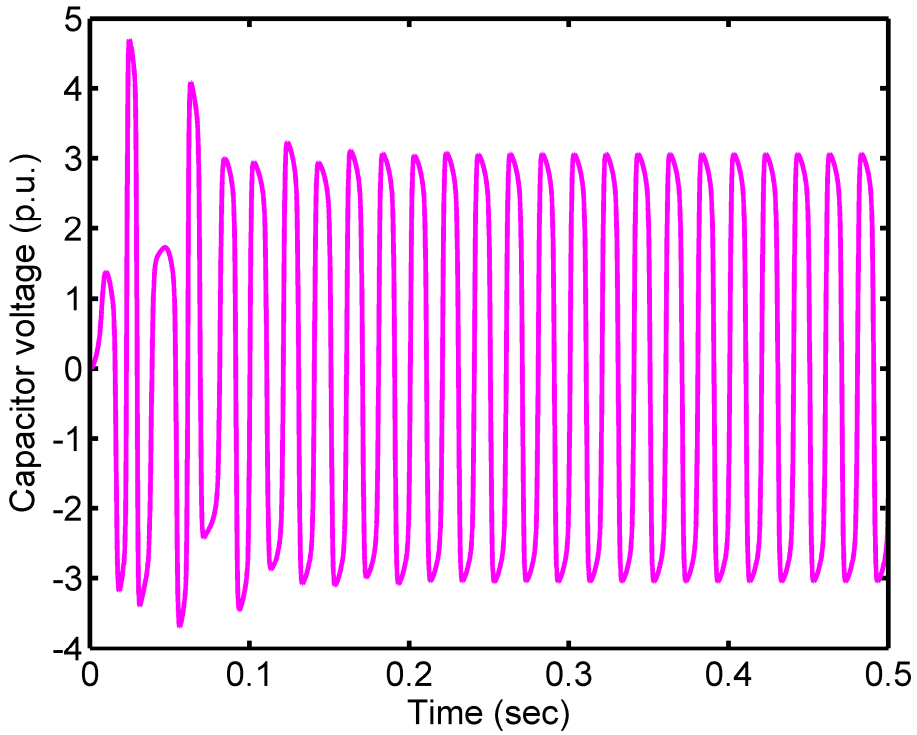

(b)

Fig. 4.14. Capacitor voltage (a) experimental and (b) simulated at 210 V supply voltage

Table 4.1 below shows all the observations that are obtained from the MATLAB simulation with different supply voltages.

Table 4.1: Simulated result at different source voltages

Sl No.	Supply Voltage (V)	RMS voltage across (× Supply voltage)		Ferroresonance observed?	Remarks
		Series Capacitor	Transformer Secondary		
1	130	0.24	1.13	No	No occurrence of ferroresonance
2	147	0.25	1.14	No	
3	152	0.26	1.15	No	
4	153	0.27	1.15	No	
5	154	0.27	1.16	No	
6	155	0.28	1.16	No	

Table 4.1: Simulated result at different source voltages (Contd.)

Sl No.	Supply Voltage (V)	RMS voltage across (× Supply voltage)		Ferroresonance observed?	Remarks
		Series Capacitor	Transformer Secondary		
7	156	2.97	2.21	Yes	Sustained ferroresonance
8	157	3.06	2.22	Yes	
9	165	2.99	2.13	Yes	
10	170	2.95	2.07	Yes	
11	180	2.85	1.97	Yes	
12	190	2.76	1.87	Yes	
13	200	2.68	1.79	Yes	
14	210	2.61	1.72	Yes	
15	220	2.54	1.65	Yes	

4.6 Summary

The procedure of importing experimental transformer magnetic properties into the simulation model of ferroresonance is explained in this chapter. As ferroresonance involves power frequencies and extremely high overvoltages, conducting thorough experimental research on it in a real setting is challenging and dangerous for the equipment involved. So an appropriate simulation model is constructed for the further investigation of ferroresonance. For the ferroresonance circuit model, an approximate mathematical equation representing the transformer core magnetism is found using the B-H loop data of the transformer that was received from the experiment. Next, using the MATLAB software platform, the mathematical nonlinear differential equations for ferroresonance are simulated. The ferroresonance result obtained from the simulation model is compared with the experimental results where both the results match with a minor deviation.

5. 1 Experimental Determination of Hysteresis Loop

The open circuit characteristic of the transformer is in terms of RMS values. So it is difficult to extract the instantaneous value of voltage and current from the OCC of a transformer. This problem can be shorted out by recording instantaneous voltage and current against time with a special laboratory arrangement [69] as shown in Fig. 5.1.

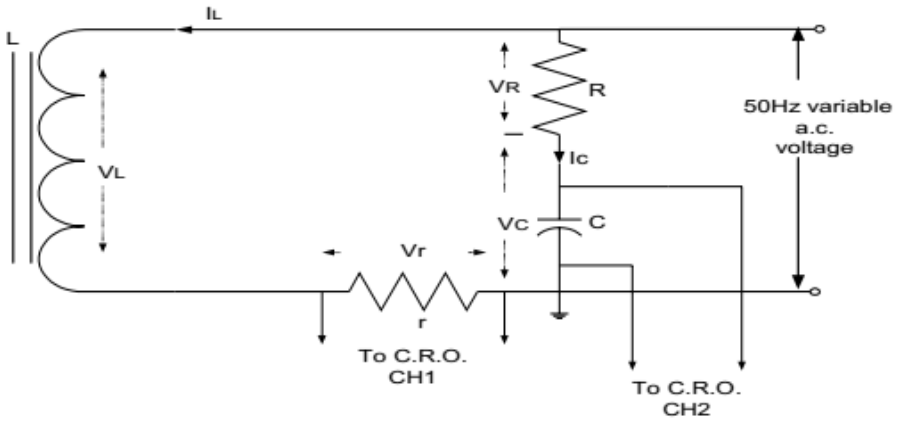

Fig. 5.1. Circuit to extract the B-H loop

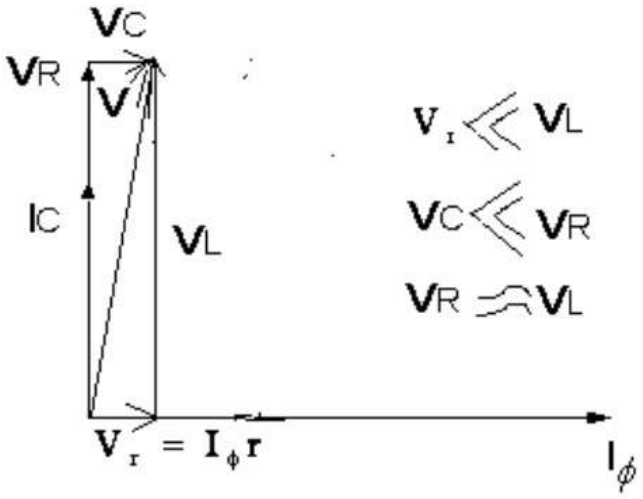

Fig 5.2. Phasor diagram of the circuit of Fig. 5.1 to determine the B-H loop

A small resistance *r* is connected in series with the primary to measure the magnetizing current. A series combination of resistance *R* and capacitance *C* are connected in parallel to the

transformer. The circuit is energized with an alternating voltage of 50 Hz. The phasor diagram (Fig.5.2) shows that the voltage across the capacitor (V_C) is in phase with the current through transformer primary current I_φ.

The voltage across capacitor C will be

$$V_C = \frac{V}{\sqrt{R^2+\frac{1}{\omega^2C^2}}} \times \frac{1}{\omega C} = \frac{V}{\sqrt{(\omega RC)^2+1}} \quad (5.1)$$

To make $R^2\omega^2C^2 >> 1$ the values of R, L & C are chosen accordingly. So (5.1) is reduced to

$$V = \omega RCV_C \quad (5.2)$$

But for transformer, $V_L \propto \varphi$ and $V_L \propto V$, as resistance r is very small,

Therefore, $V \propto \varphi$

Hence from (5.2),

$$\varphi \propto \omega RCV_C \quad (5.3)$$

In (5.3) ω, R and C are constant therefore magnetic flux (φ) is proportional to the voltage across the capacitor and they are in phase. Again the voltage across the resistor r, connected in series with the primary coil, is proportional to the magnetizing current. Now, by applying the voltage across the resistor r to channel I and the voltage across the capacitor to channel II of the CRO, a hysteresis loop may be formed from the CRO in dual mode. Changing the supply voltage hysteresis loops at various saturation levels can be created. These loops are saved to a computer, and the data is utilized to simulate a hysteresis model to analyze ferroresonance via digital computation. The transformer core becomes more saturated as the voltage increases.

Rating of the transformer used in the laboratory:

Single phase, 450 VA, 50 Hz, 0-250-433V / 0-250-433V / 2 V, major insulation at 25 KV level

Plots of flux density and magnetizing current against time for 175V are shown in Fig. 5.3 and Fig. 5.4 respectively. Plots show that the voltage waveform is purely sinusoidal whereas the current waveform takes a non-sinusoidal nature.

The *B-H* loop was thus obtained by plotting the magnetizing current along the X-axis and flux along the Y-axis as shown in Fig 5.5.

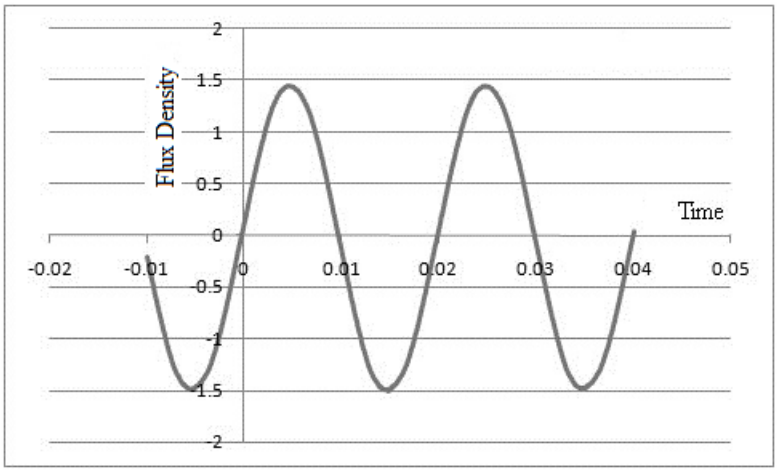

Fig. 5.3. Flux density vs. time for 175V

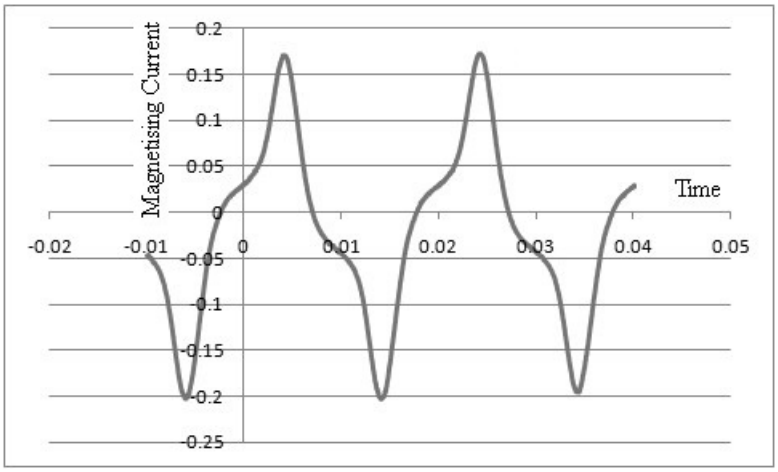

Fig. 5.4. Magnetizing current vs. time for 175V

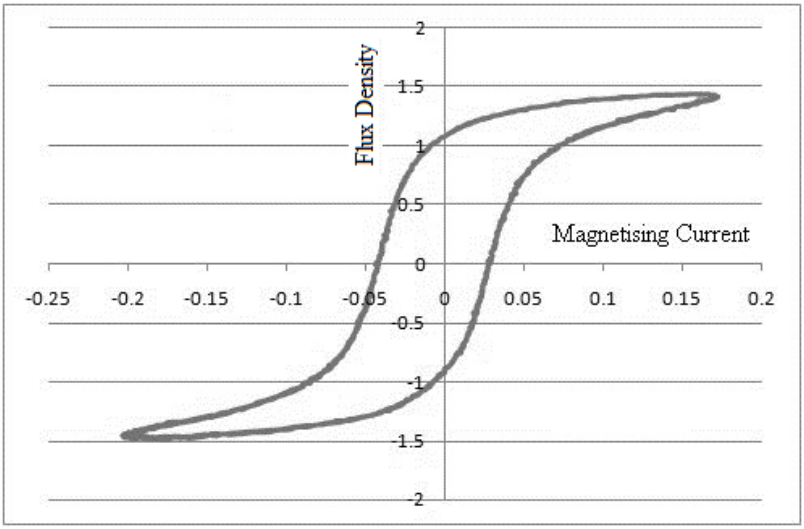

Fig. 5.5. B-H loop of the transformer for 175V

The polynomial relation suitable for the approximation of the *B-H* loop is the following.

$$i_\lambda = a\lambda + b\lambda^7 \quad (5.4)$$

Here

λ = flux linkage in Wb

i_λ = magnetizing current in Amp.

a = 0.015

b = 0.013

Fig. 5.6 shows that the plot from (5.4) matches with the plot from experimental data. The experimentally obtained B-H loop is presented in a solid line and the mathematical relation is obtained from curve fitting in a dashed line.

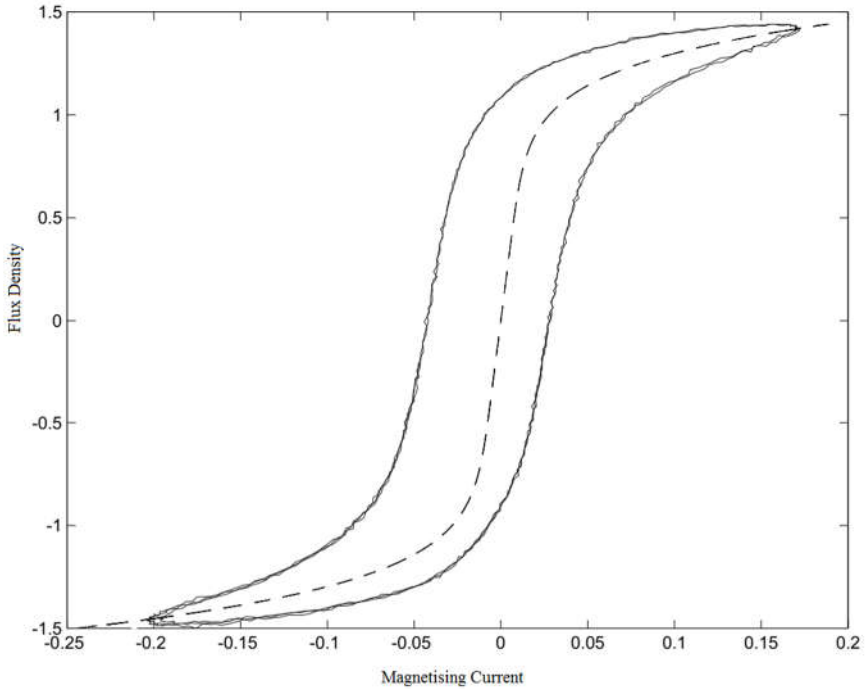

Fig. 5.6. Experimental (solid line) and simulated (dashed line) current vs. flux linkage

5.2 Analysis with Different Circuit Parameters

The generation of ferroresonance by a nonlinear circuit is primarily determined by the circuit characteristics, the amplitude and switching instant of the supply voltage, and its initial conditions [14, 68, 70]. The ferroresonance and its dependence on different circuit parameters have been examined and analyzed in this part by modeling the following system equation obtained as per the derivation shown in the previous chapter.

$$\frac{d^2\lambda}{dt^2} = \frac{dV_s}{dt} - \frac{1}{C}\left(\frac{v}{R_C}\right) - \frac{1}{C}(a\lambda + b\lambda^7) \quad (5.5)$$

The work following parameters were examined:

- Supply voltage;
- Series capacitance;
- Supply frequency;
- Core loss;
- Degree of core saturation
- Initial flux linkage

The effects of variation of supply voltage, supply frequency, and series capacitance on the occurrence of ferroresonance have already been discussed theoretically by R. Rudenberg [3]. As Rudenberg's ferroresonance model is already well established, the similarity of the results will strengthen the applicability of our model.

5.3 Analysis with Source Voltage

MATLAB software is used to simulate (5.5). The initial residual flux linkage (λ) of the transformer is taken as 1Wb. The series capacitance value is taken as 1.272μF with the initial stored charge assumed as zero. In the simulation the occurrence of ferroresonance is searched by the increase of source voltage in steps. Up to 107.7 V, no ferroresonance was found. The transformer voltage, capacitor voltage along source voltage are shown in Fig 5.7.

The plots show that a transient over-voltage appears just after switching, but it decays down to a steady state within 0.1s. At steady state voltage that appears across capacitance is 0.8 times and the voltage that appears across the transformer is 1.4 times of supply voltage. As the capacitor voltage is small compared to the transformer voltage, the circuit behaves as an inductive circuit.

However, the ferroresonance is caused by a little rise in source voltage. At 107.8 V, the voltage across the capacitor (C) and transformer appears as much higher than the supply voltage and is not dying down; rather, it is sustained as ferroresonance over-voltage in line, where the capacitor voltage is greater than the transformer voltage, as shown in Fig. 5.8.

Taking 107.7 V as the base voltage of the system, the steady-state over-voltage across the capacitor and transformer is calculated as 3.6 p.u. and 3.1 p.u respectively, when the

ferroresonance jump appears at the source voltage of 107.8 V. The detailed result of capacitor voltage and transformer voltage with the variation of the source voltage is shown in Table 5.1.

Fig. 5.9 shows the variation of RMS values of capacitor voltage (V_C) and transformer voltage (V_L) with supply voltage (V_s).

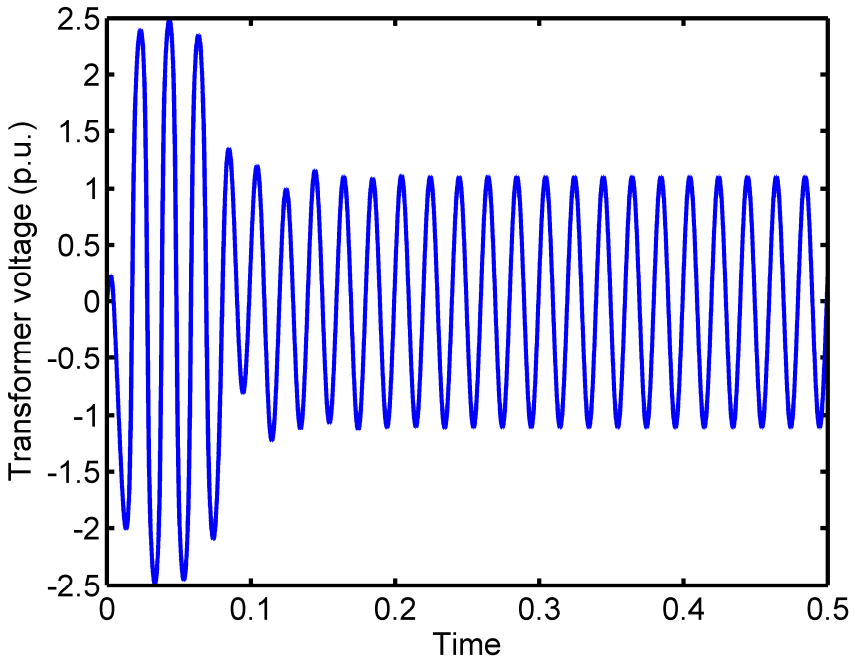

(a)

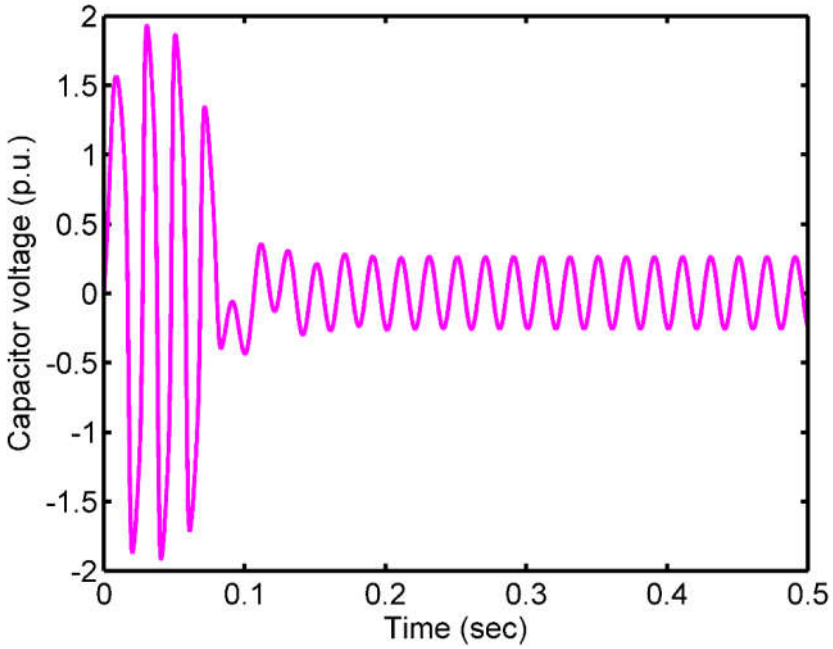

(b)

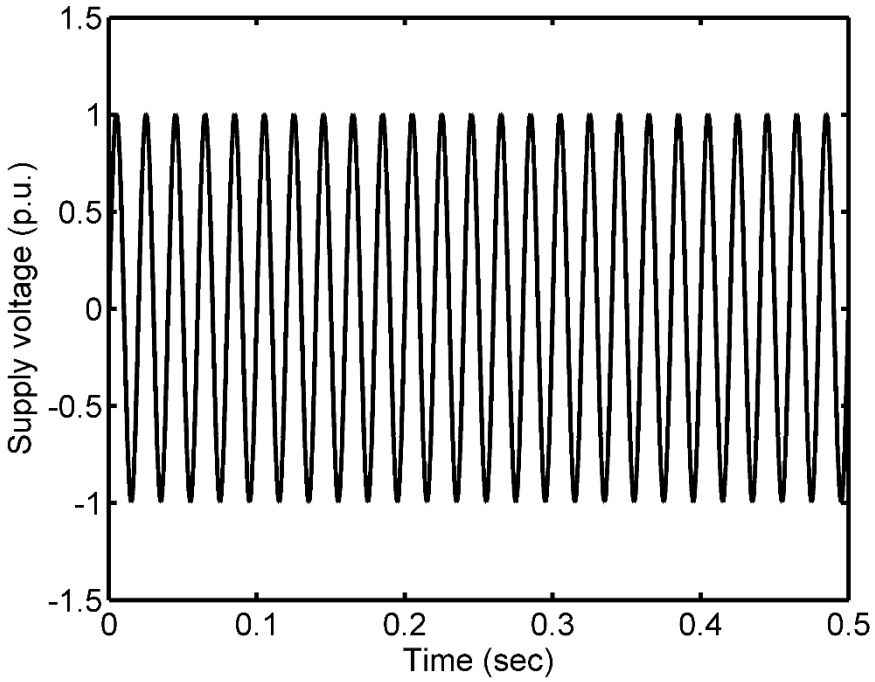

(c)

Fig. 5.7. (a) Transformer voltage, (b) capacitor voltage, and (c) source voltage waveform at a supply voltage of 107.7 V when ferroresonance does not occur

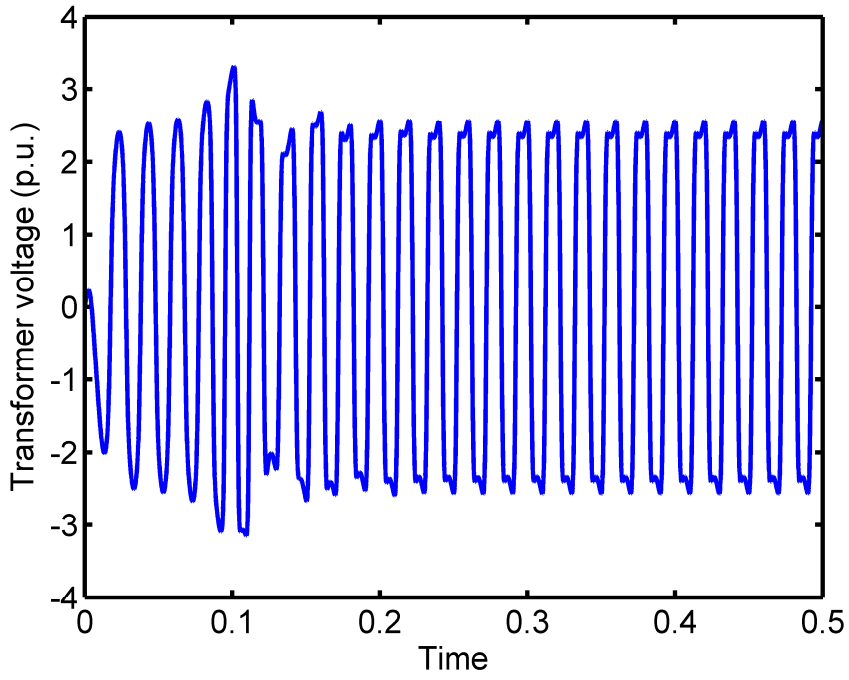

(a)

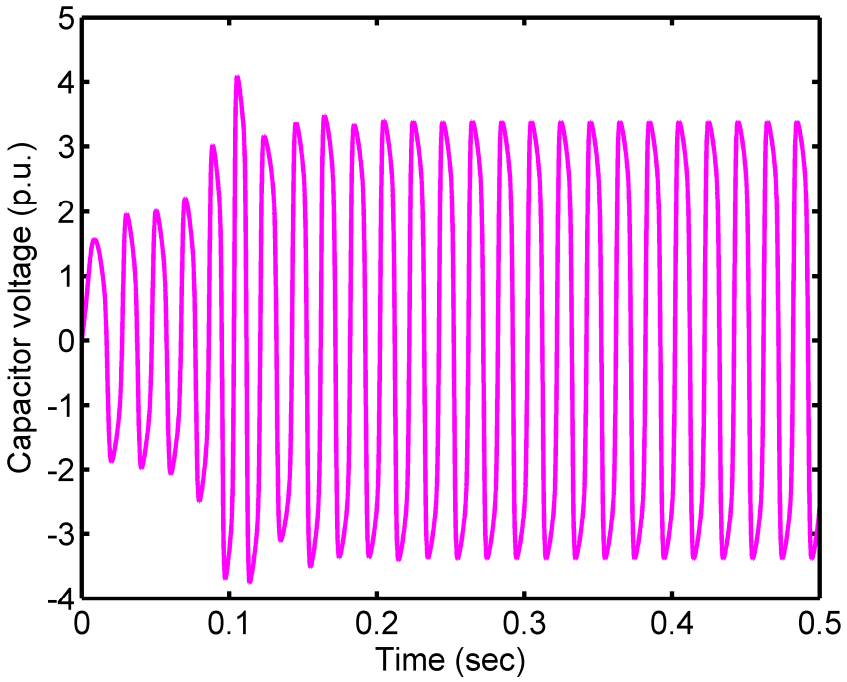

(b)

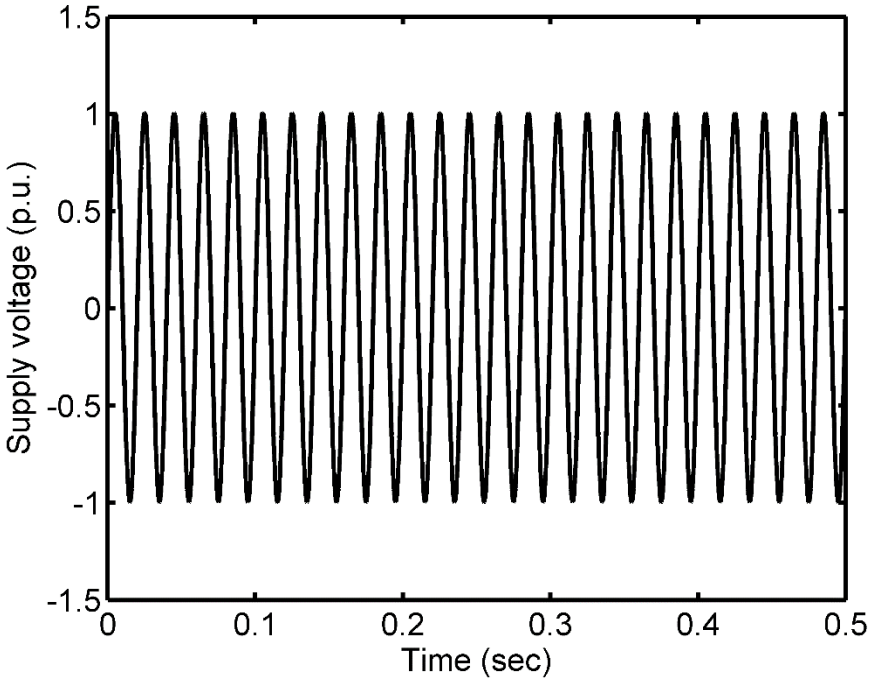

(c)

Fig. 5.8. (a) Transformer voltage, (b) capacitor voltage, and (c) source voltage waveform at a supply voltage of 107.8 V when ferroresonance occurs

Table 5.1: Variation of voltages with source voltage (p.u. values)

Source Voltage (V_S)	Capacitor Voltage (V_C)	Transformer Voltage (V_L)	Remarks
0.66	0.30	0.77	No sustained ferroresonance observed, $V_C < V_L$
0.69	0.31	0.81	
0.72	0.33	0.84	
0.76	0.37	0.90	
0.79	0.37	0.93	
0.82	0.37	0.96	
0.85	0.39	1.01	
0.89	0.41	1.05	
0.92	0.47	1.12	
0.95	0.50	1.17	
0.98	0.53	1.22	
0.99	0.58	1.26	
1.00	0.70	1.36	
1.00	0.77	1.42	
1.00	0.85	1.49	
1.00	3.65	3.10	Sustained ferroresonance observed, $V_C > V_L$
1.00	3.68	3.11	
1.00	3.76	3.12	
1.01	3.80	3.13	
1.02	3.84	3.14	
1.05	3.90	3.15	
1.08	3.97	3.16	
1.12	4.02	3.17	
1.15	4.06	3.17	
1.18	4.11	3.18	
1.21	4.16	3.19	
1.25	4.21	3.20	

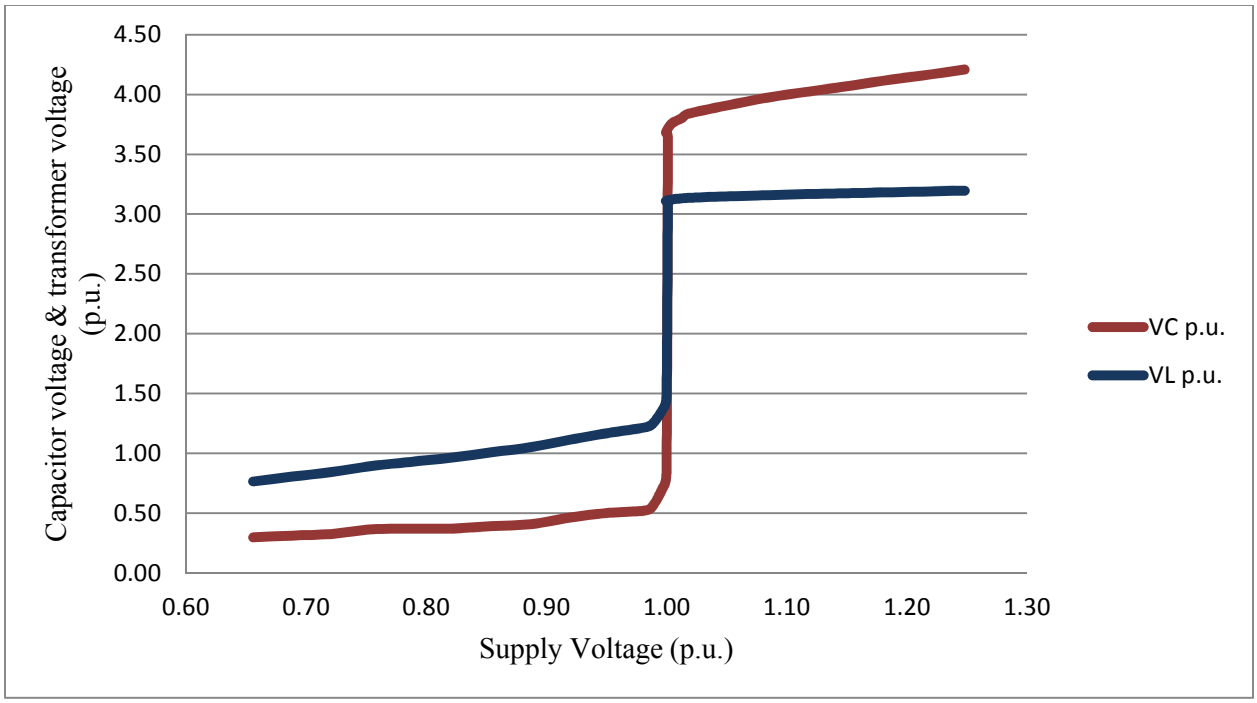

Fig. 5.9. Variation of capacitance voltage and transformer voltage with supply voltage

The observations that can be made from Fig. 5.9 are as follows: below 107.7 V supply voltage the capacitor and transformer voltages take rated values and the circuit behaves like an inductive circuit as V_C is less than V_L. But after 107.8 V capacitor and transformer voltages show a sudden jump in their values. And from here the circuit starts behaving like a capacitive circuit as V_C is greater than V_L. This zone of operation has been defined as a ferroresonance zone. This behavior agrees with the explanation given by R. Rudenburg which is depicted in Fig. 2.21.

5.4 Analysis with Series Capacitance

The effect of the variation of series capacitance on the occurrence of ferroresonance is discussed in Section 2.5. A similar observation in Fig. 2.15 was obtained while changing the value of capacitance in the analysis of the Simulink model prepared from (5.5). The variation of transformer voltage (V_L) against capacitance (C) is shown in Fig. 5.10.

The supply voltage is kept here fixed as 107.7 V and frequency as 50Hz. Initial flux is taken as 1 Wb. It has been observed that for very small capacitance like 1 nF the capacitor voltage is almost the same as that of supply voltage whereas the transformer voltage is very small like 0.1 p.u. While increasing, at 1.28 μF ferroresonance was observed. The capacitance

voltage suddenly jumps from 0.6 p.u. to 3.7 p.u. Simultaneously, transformer voltage jumps from 1.3 p.u. to 3.1 p.u. Again ferroresonance disappears at a capacitance of 2.49 μF. It again appears at 3.5 μF. This observation shows that the circuit alternates between ferroresonance and non-ferroresonance while the capacitor is increased. That means the circuit is choosing between two stable operating points one in the 1st quadrant which is non-ferroresonant and another in the 3rd quadrant of the V-I plane which is ferroresonant. The bottom curve of Fig. 5.10 shows the 1st quadrant operation and the top curve 3rd quadrant operation. The occurrence of ferroresonance is totally depends on the matter of chance and the point on the sinusoidal curve where the circuit is switched on [3]. This type of observation was also reported in the previous literature [71].

The voltages at 7 nF where no ferroresonance occurred and at 2.1 μF where ferroresonance occurred are shown in Fig. 5.11 and 5.12 respectively. Per unit values are shown in Table 5.2.

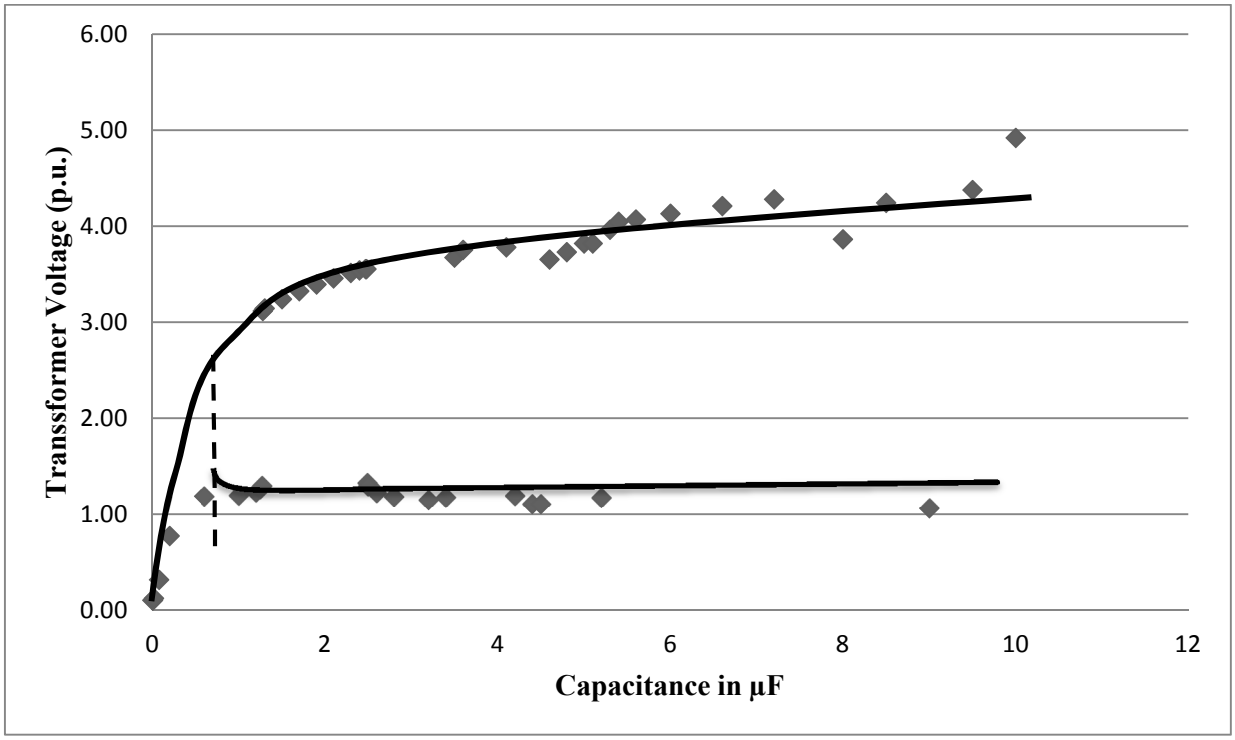

Fig. 5.10. Transformer voltage is plotted against the capacitance

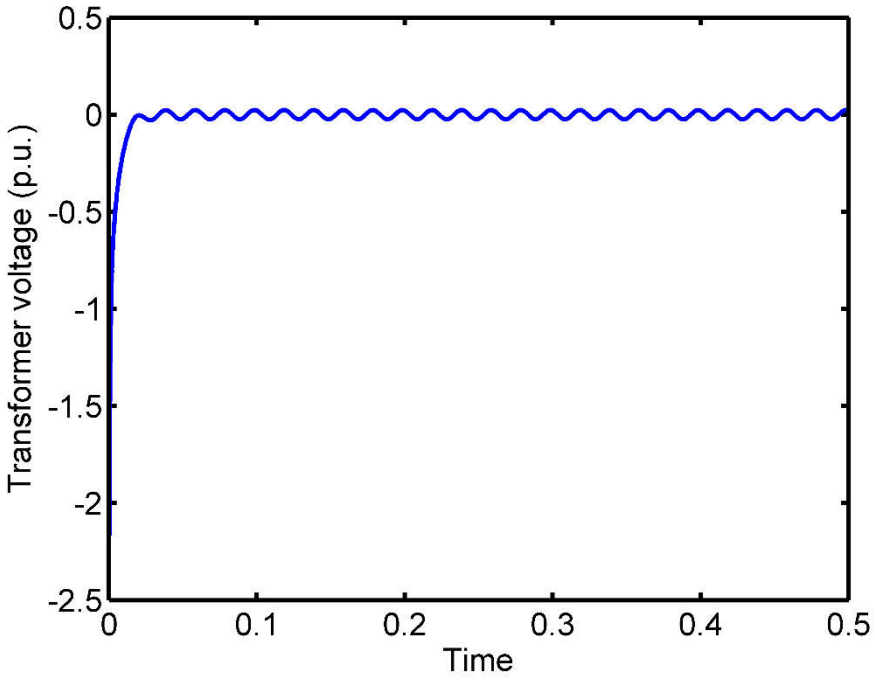
0.5
0
-0.5
-1
-1.5
-2
-2.5
Transformer voltage (p.u.)
0
0.1
0.2
0.3
0.4
0.5
Time

(a)

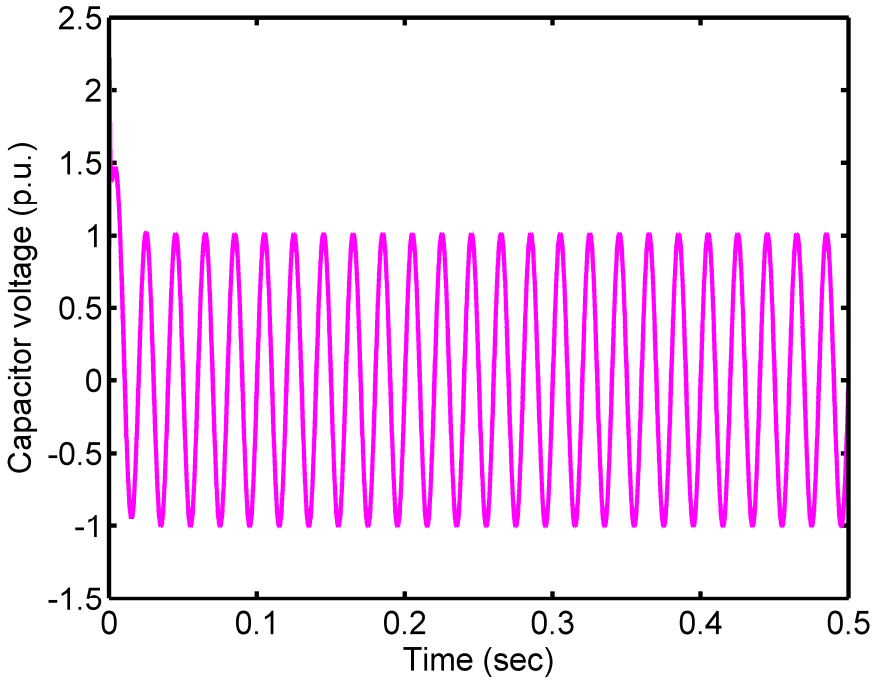
2.5
2
1.5
1
0.5
0
-0.5
-1
-1.5
Capacitor voltage (p.u.)
0
0.1
0.2
0.3
0.4
0.5
Time (sec)

(b)

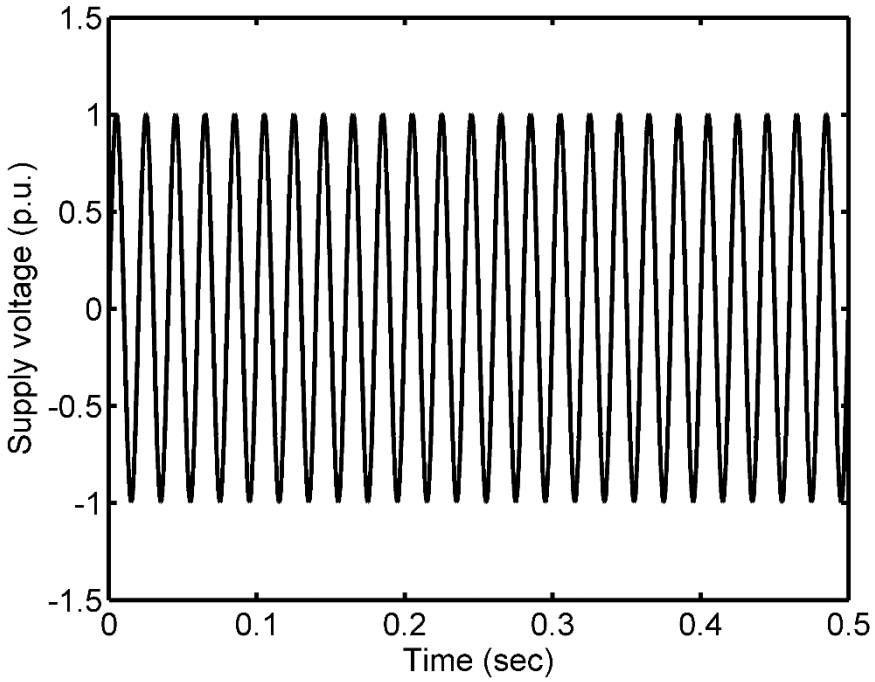

(c)

Fig. 5.11. (a) Transformer voltage, (b) capacitor voltage, and (c) source voltage waveform at a capacitance 7nF when ferroresonance does not occur

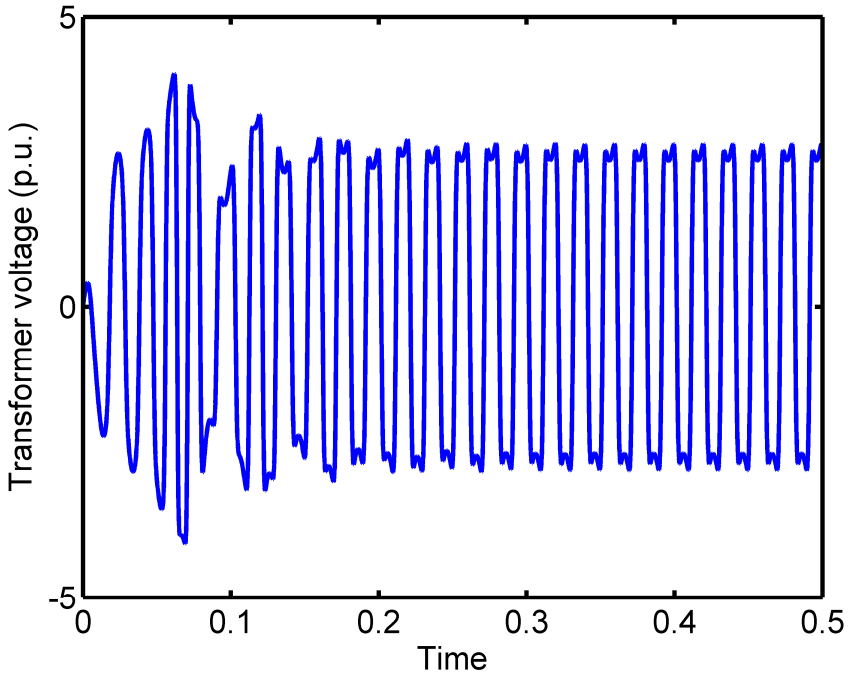

(a)

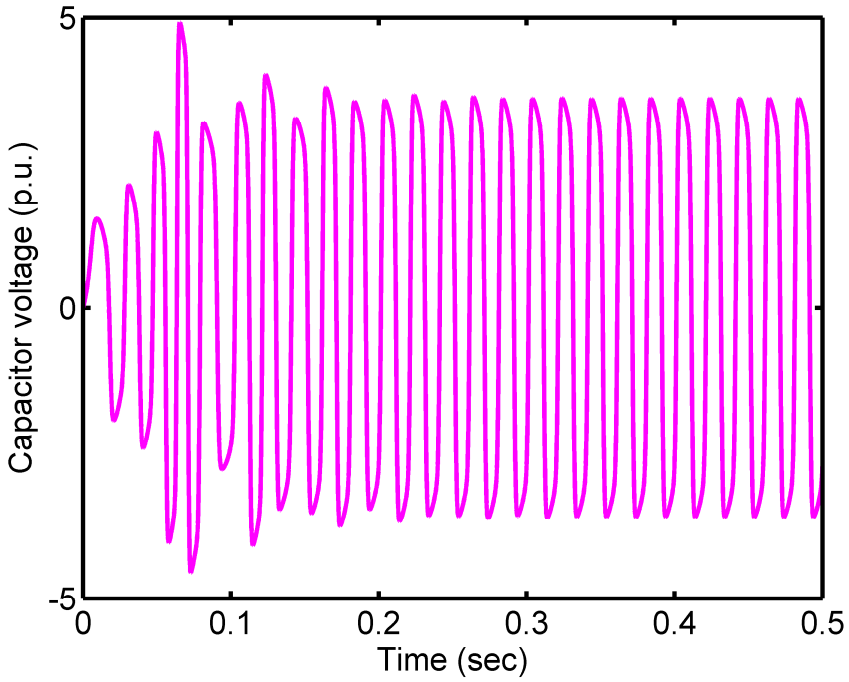

(b)

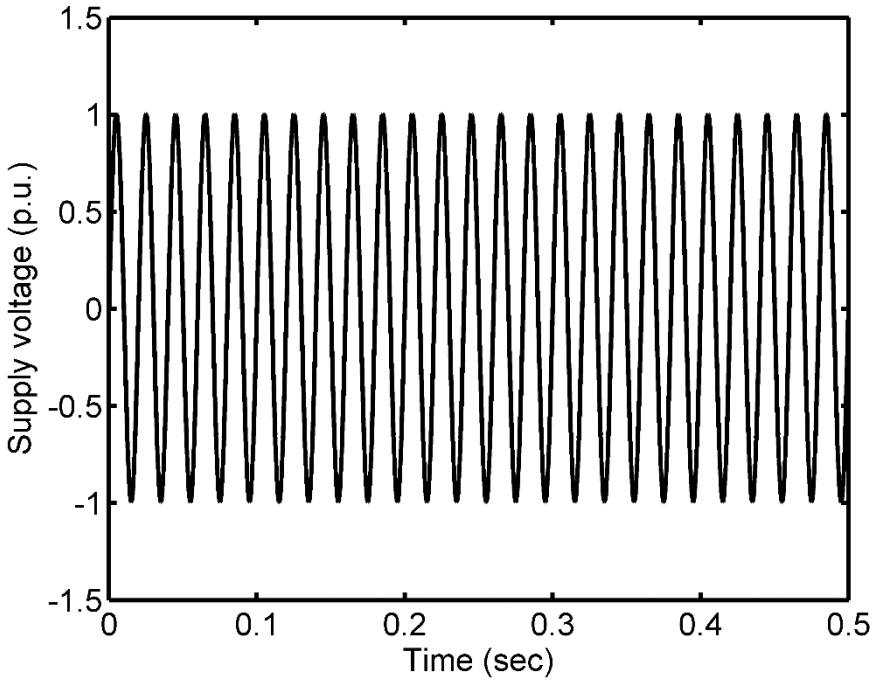

(c)

Fig. 5.12. (a) Transformer voltage, (b) capacitor voltage, and (c) source voltage waveform at a capacitance of 2.1μF when ferroresonance occurs

Table 5.2: Variation of voltages with capacitance

Capacitance in μF	Capacitor Voltage V_C (p.u.)	Transformer Voltage V_L (p.u.)	Magnetizing current I_λ (p.u.)	Ferroresonance observed or not
0.001	1.01	0.10	0.04	No
0.007	1.02	0.10	0.04	No
0.02	1.04	0.12	0.04	No
0.2	1.16	0.77	0.17	No
1	0.48	1.20	0.47	No
1.2	0.52	1.23	0.73	No
1.27	0.61	1.30	1.00	No
1.28	3.75	3.12	8.12	Yes
1.3	3.84	3.14	8.48	Yes
1.7	4.11	3.32	12.13	Yes
1.9	4.20	3.39	13.94	Yes
2.3	4.33	3.51	17.56	Yes
2.4	4.34	3.54	18.46	Yes
2.48	4.32	3.55	18.99	Yes
2.49	0.63	1.33	2.28	No
2.5	0.59	1.29	2.10	No
2.8	0.44	1.18	1.56	No
3.4	0.44	1.18	1.56	No
3.5	4.46	3.68	28.00	Yes
3.6	4.58	3.75	29.64	Yes
4.1	4.58	3.78	33.89	Yes
4.2	0.47	1.19	2.09	No
4.4	0.32	1.11	1.46	No
4.5	0.32	1.11	1.45	No
4.6	4.37	3.65	36.57	Yes
5	4.56	3.82	41.63	Yes

Table 5.2: Variation of voltages with capacitance (Contd.)

Capacitance in μF	Capacitor Voltage V_C (p.u.)	Transformer Voltage V_L (p.u.)	Magnetizing current I_λ (p.u.)	Ferroresonance observed or not
5.1	4.56	3.82	42.45	Yes
5.2	0.46	1.17	2.23	No
5.3	4.75	3.96	45.98	Yes
5.6	4.91	4.07	50.21	Yes
6	4.96	4.13	54.81	Yes
7.2	5.07	4.28	68.27	Yes
8	4.44	3.86	67.29	Yes
8.5	4.92	4.24	79.79	Yes
9	0.26	1.06	1.67	No
9.5	5.14	4.38	91.65	Yes
10	4.92	4.92	94.48	Yes

5.5 Analysis with Supply Frequency

The effect of the variation of supply frequency over the occurrence of ferroresonance is explained in section 2.5. The dependency of current and condenser voltage on the frequency is plotted in Fig. 2.18 and 2.19. Similar plots are attempted with the simulation of the ferroresonance model circuit.

Here the supply voltage is kept constant at 107.7 V and capacitance is kept at 1.27 μF. the frequency is made to vary from very low value like 10 Hz. The voltage output is shown in Fig. 5.13. At low frequencies, the circuit behaves like a capacitive circuit with a capacitive voltage of 1.3 p.u. and transformer voltage of 0.3 p.u. With the increase of the frequency capacitor voltage, transformer voltage, and magnetizing current gradually increase as shown in Table 5.3.

At a frequency of 49.98 Hz a sudden jump is observed where the capacitive voltage jumps from 3.8 p.u. at 49.97 Hz to 0.7 p.u. and transformer voltage jumps from 3.1 p.u. at 49.97 Hz to 1.3 p.u. Also from 49.98 Hz circuit starts behaving as an inductive circuit. Both the

variations of capacitive voltage and magnetizing current with supply angular frequency are shown in Fig. 5.14 and 5.15 respectively.

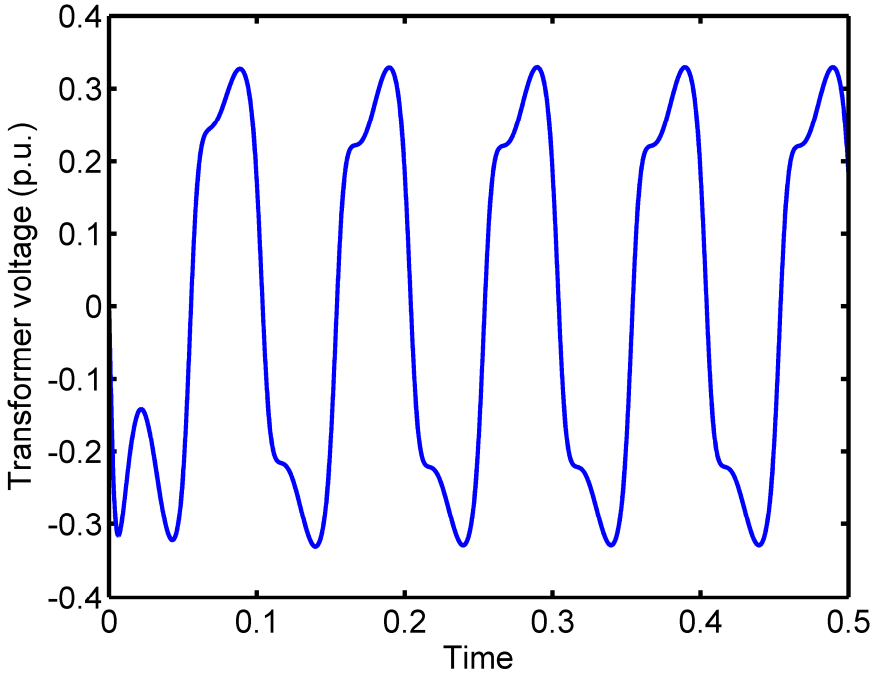

(a)

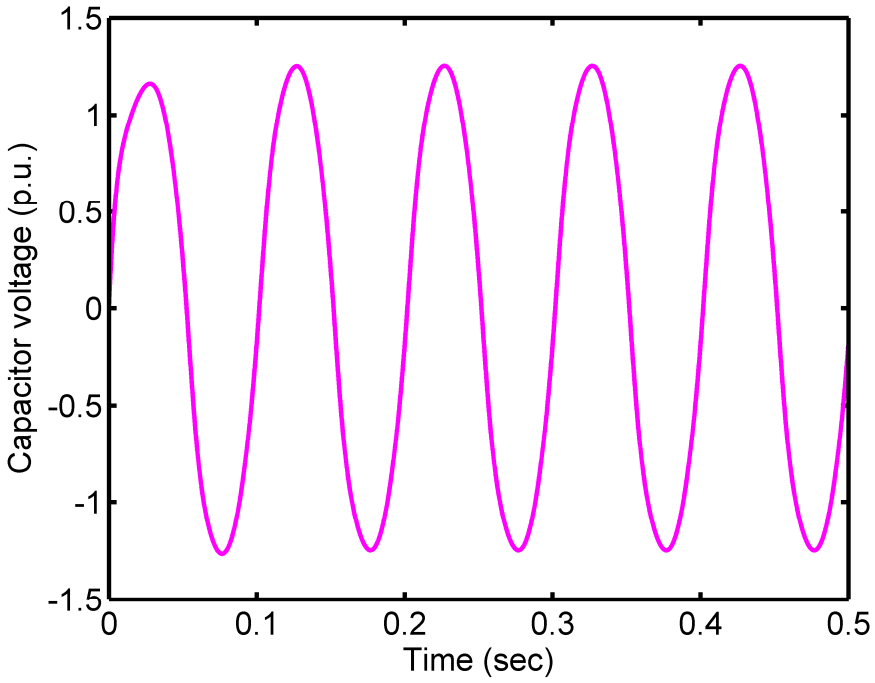

(b)

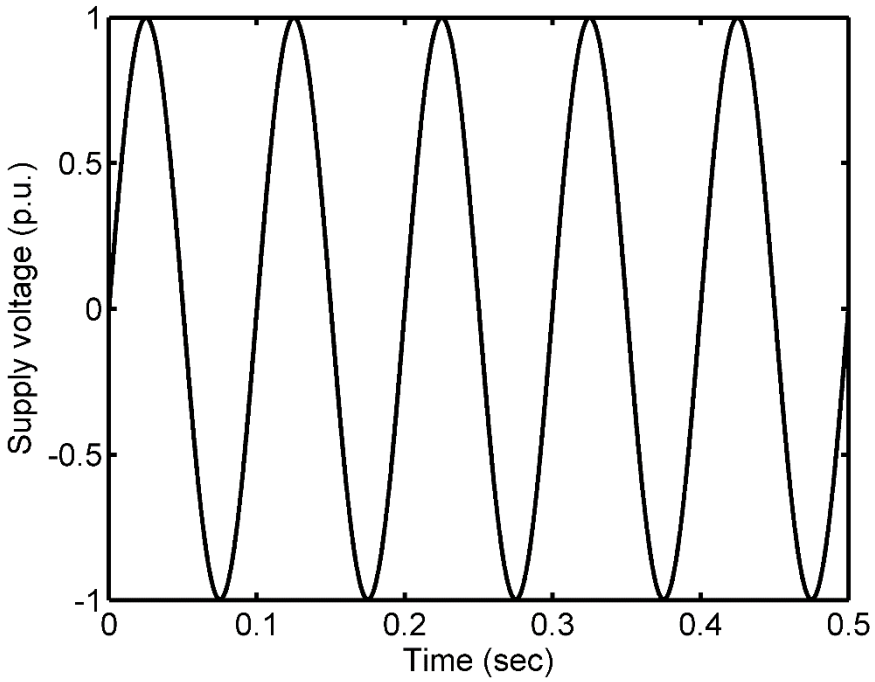

(c)

Fig. 5.13. (a) Transformer voltage, (b) capacitor voltage, and (c) source voltage waveform at a frequency of 10Hz when ferroresonance does not occur

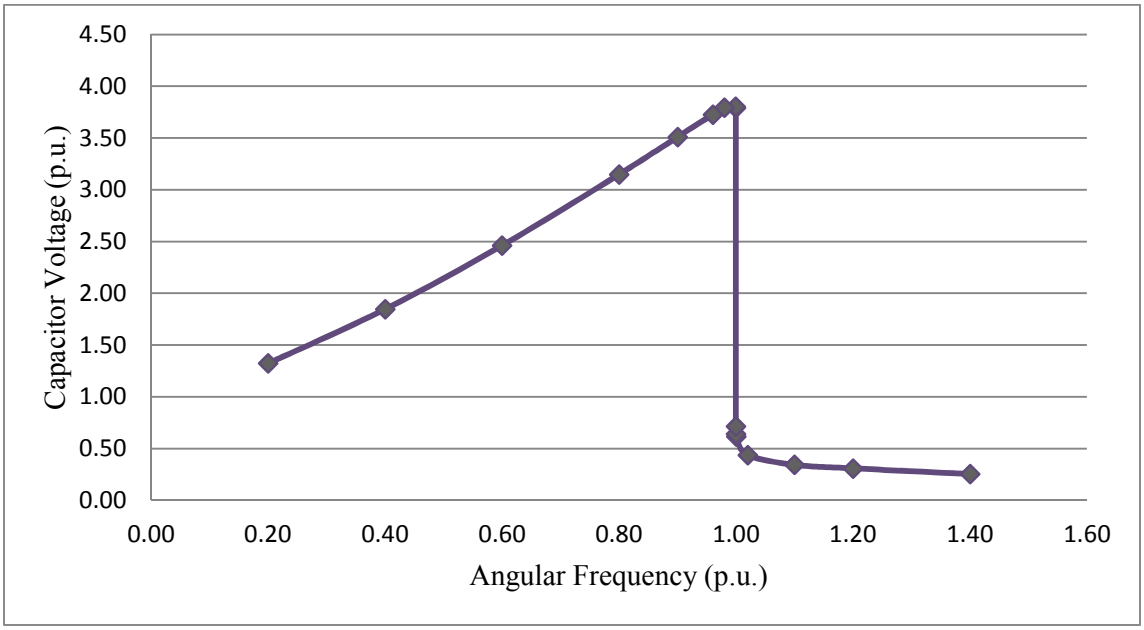

Fig. 5.14. Variation of capacitor voltage with supply frequency

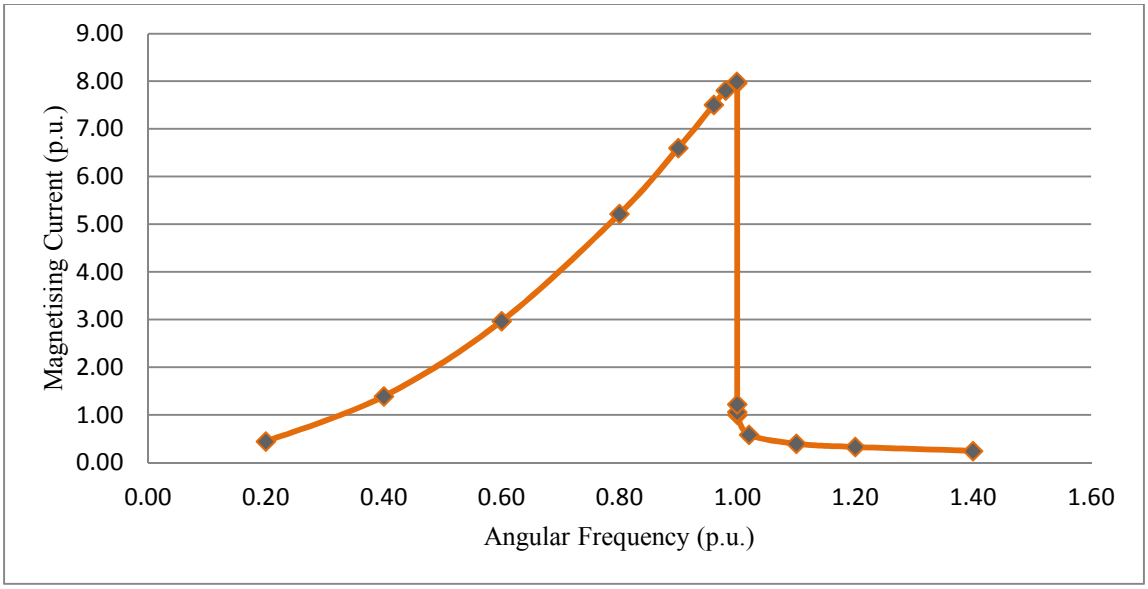

Fig. 5.15. Variation of magnetizing current with supply frequency

Table 5.3: Variation of voltages with supply frequency

Angular frequency (p.u.)	Capacitor Voltage V_C (p.u.)	Transformer Voltage V_L (p.u.)	Magnetizing current I_λ (p.u.)
1.40	0.25	1.07	0.24
1.20	0.31	1.10	0.33
1.10	0.34	1.13	0.39
1.02	0.44	1.18	0.59
1.00	0.62	1.30	1.00
1.00	0.64	1.32	1.06
1.00	0.72	1.38	1.22
1.00	3.79	3.12	7.96
1.00	3.80	3.12	7.99
0.98	3.79	3.06	7.81

Table 5.3: Variation of voltages with supply frequency (Contd.)

Angular frequency (p.u.)	Capacitor Voltage V_C (p.u.)	Transformer Voltage V_L (p.u.)	Magnetizing current I_λ (p.u.)
0.96	3.73	2.98	7.51
0.90	3.51	2.74	6.60
0.80	3.15	2.35	5.22
0.60	2.46	1.61	2.97
0.40	1.85	0.94	1.39
0.20	1.32	0.35	0.44

5.6 Analysis with Core Loss Resistance

In the model circuit of ferroresonance shown in Fig. 4.2, the core loss is shown as a parallel resistance R_C. Keeping the source voltage constant at 107.7 V, frequency at 50 Hz, and capacitance at 1.272 μF, the resistance is made to vary from a very low value like 50 Ω.

At 50 Ω it has been seen that the capacitor voltage is almost equal to the supply voltage and transformer voltage takes a negligible value like 0.02 p.u. The circuit behaves like a capacitive circuit. With the increase of the resistive value, at 3,125 Ω transformer voltage becomes greater than the capacitor voltage and the circuit becomes inductive. Ferroresonance was observed at a resistance of 12,520 Ω where capacitor voltage, transformer voltage, and current suddenly jump to a higher value, and the circuit again becomes capacitive (Fig. 5.16).

The observations are shown in Table 5.4 in per-unit values. The variation of capacitor voltage (V_C) and transformer voltage (V_L) along with the parallel resistance (R) are presented in Fig. 5.17. Fig. 5.18 displays the variation in magnetizing current. Fig. 5.19 displays the change of magnetizing current with core loss. It can be seen that a decrease in core loss will increase the probability of occurrence of ferroresonance. Though Rudenberg [3] did not provide any analysis of ferroresonance with transformer core loss, this observation matches with the work presented by R. A. Walling [72].

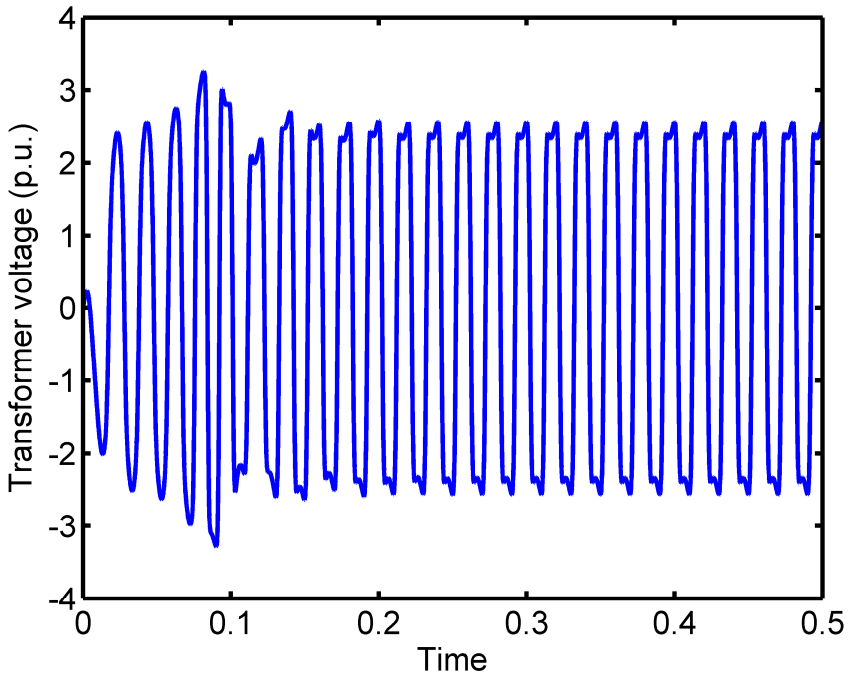
Transformer voltage (p.u.)
Time
4
3
2
1
0
-1
-2
-3
-4
0
0.1
0.2
0.3
0.4
0.5

(a)

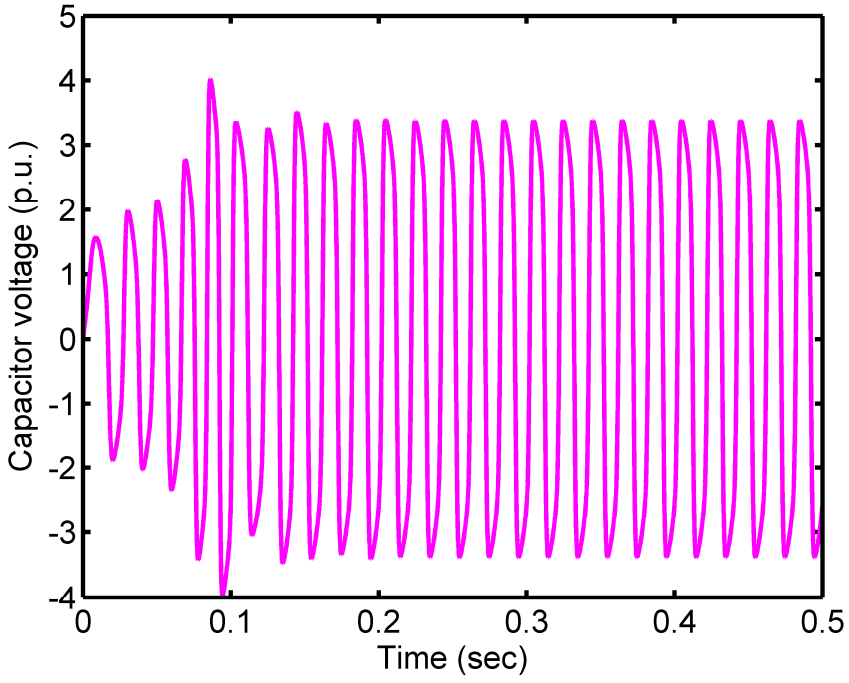
Capacitor voltage (p.u.)
Time (sec)
5
4
3
2
1
0
-1
-2
-3
-4
0
0.1
0.2
0.3
0.4
0.5

(b)

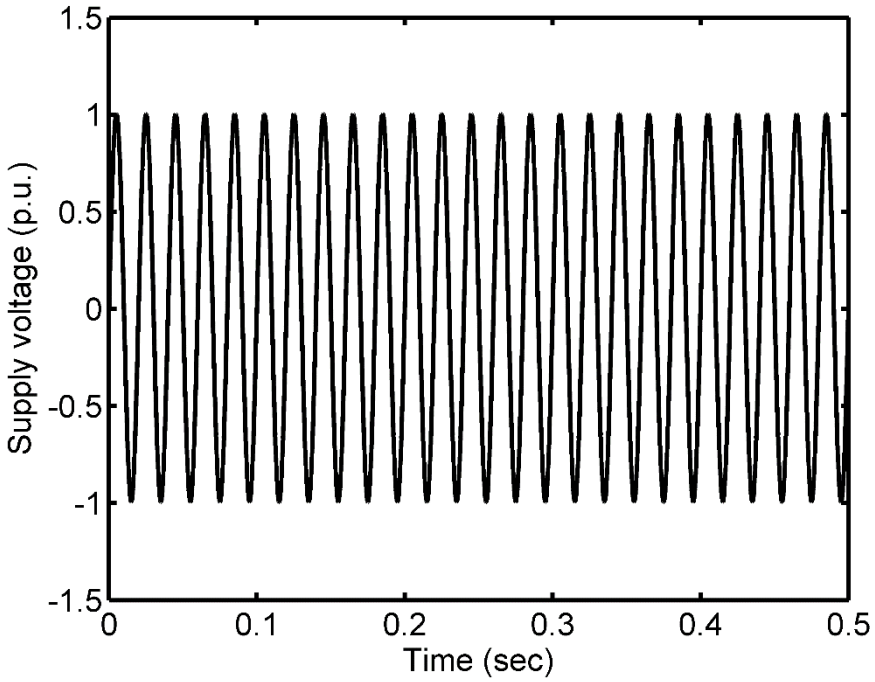

(c)

Fig. 5.16. (a) Transformer voltage, (b) capacitor voltage, and (c) source voltage waveform at a resistance value 12.52 KΩ when ferroresonance occurs

Table 5.4: Variation of voltages with parallel resistance (Base resistance 12.5KΩ)

Resistance (p.u.)	**Capacitor Voltage V_C (p.u.)**	**Transformer Voltage V_L (p.u.)**	**Magnetizing current I_λ (p.u.)**	**Core Loss (p.u.)**	**Remarks**
0.004	1.00	0.02	0.51	250.00	No ferroresonance $V_C > V_L$
0.010	1.00	0.05	0.35	100.00	
0.048	0.98	0.24	0.18	20.83	
0.100	0.92	0.46	0.17	10.00	
0.250	0.69	0.84	0.22	4.00	No ferroresonance $V_C < V_L$
0.520	0.46	1.05	0.27	1.92	
1.000	0.62	1.30	1.00	1.00	
1.001	0.66	1.33	1.09	1.00	

Table 5.4: Variation of voltages with parallel resistance (Base resistance 12.5KΩ) (Contd.)

Resistance (p.u.)	Capacitor Voltage V_C (p.u.)	Transformer Voltage V_L (p.u.)	Magnetizing current I_λ (p.u.)	Core Loss (p.u.)	Remarks
1.002	3.79	3.12	7.96	1.00	Sustained ferroresonance $V_C > V_L$
1.008	3.84	3.13	8.08	0.99	
1.040	3.88	3.14	8.19	0.96	
1.216	3.97	3.16	8.44	0.82	
1.680	4.05	3.18	8.72	0.60	
2.440	4.09	3.20	8.91	0.41	
7.240	4.13	3.26	9.37	0.14	
12.000	4.13	3.28	9.52	0.08	

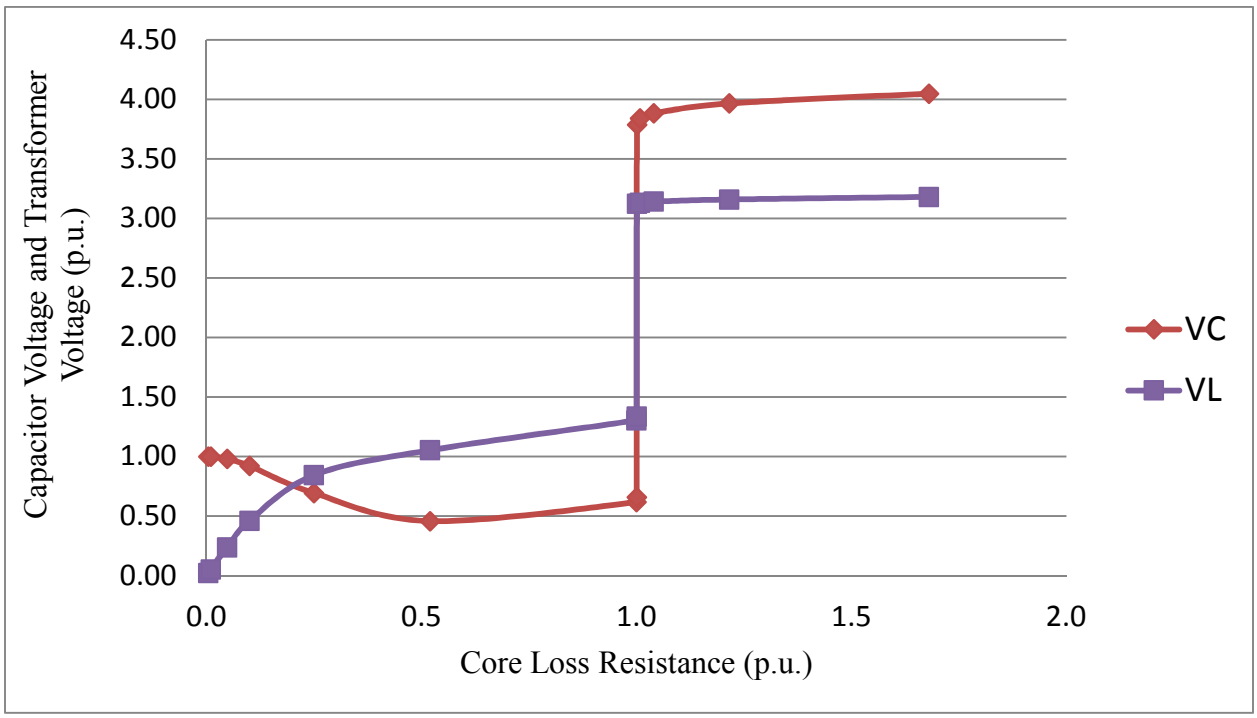

Fig. 5.17. Variation of voltages with core loss resistance

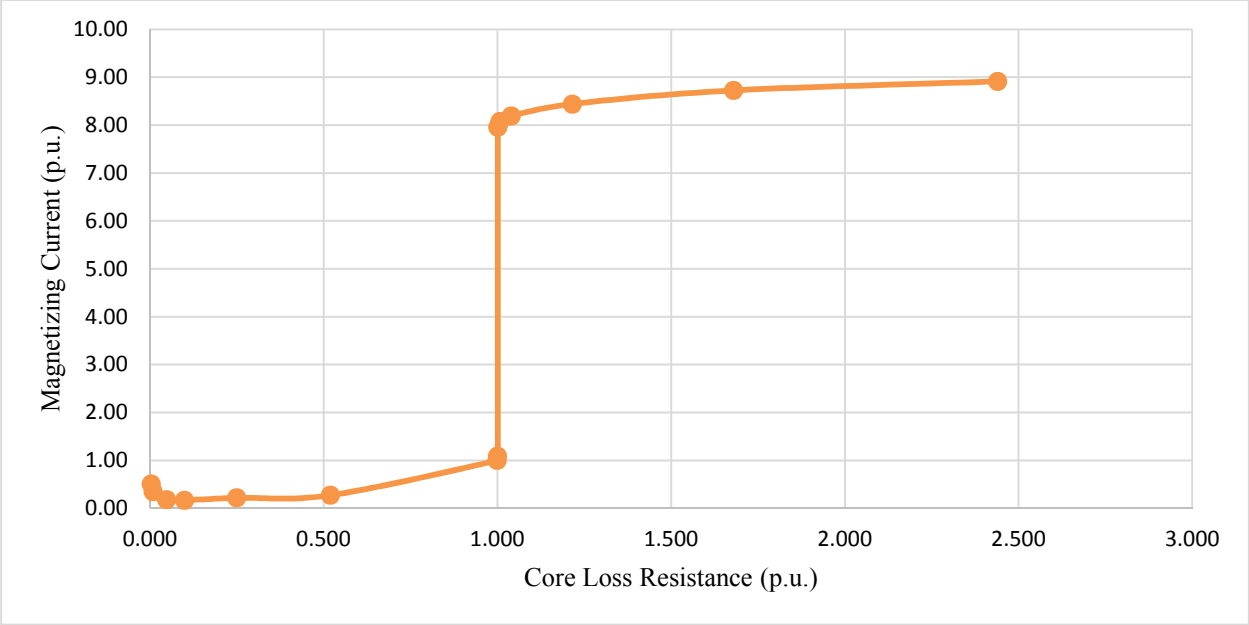

Fig. 5.18. Variation of magnetizing current with resistance

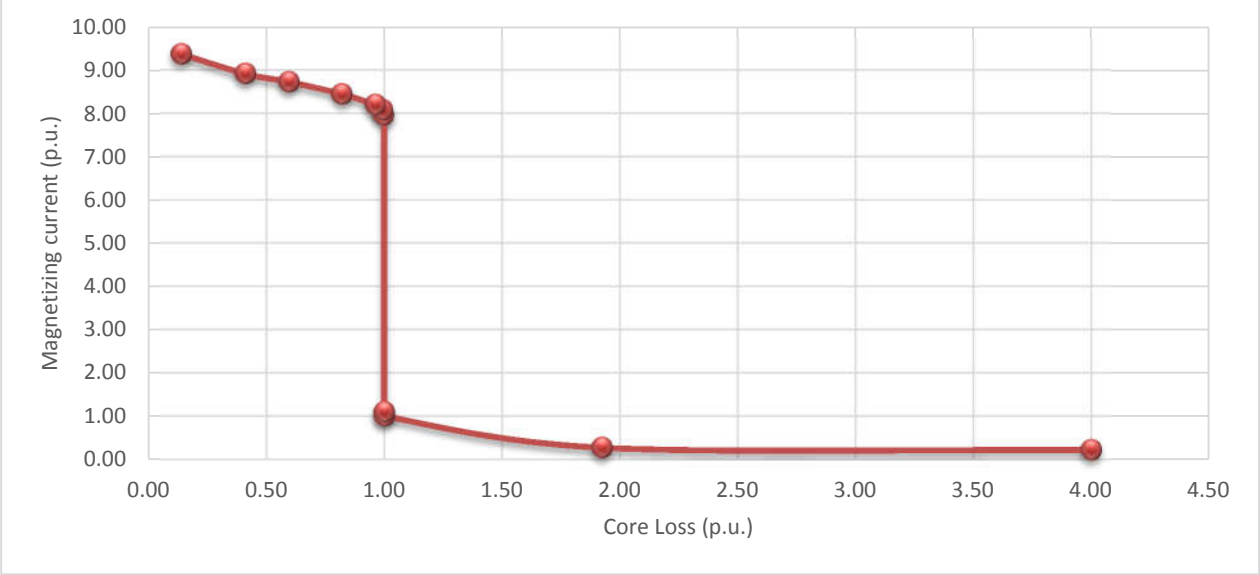

Fig. 5.19. Variation of magnetizing current with core loss

5.7 Analysis with Degree of Core Saturation

In (5.5) the power of magnetic flux linkage (λ) is 7. This is called the degree of core saturation (n) which decides how quickly the core will get saturated. The degree of core saturation is determined by the transformer core material used. Transformer core materials are

chosen based on design variables such as core loss, efficiency, and cost. Core losses in amorphous alloys, for example, are several orders of magnitude lower than in grain-oriented silicon steel. As a result, the amorphous core outperforms the regular one [73]. The amorphous core has a higher saturation level than electrical steel. [74]. Analysis of ferroresonance with two different core materials namely, M5 and ZDKH has been discussed in [75].

Fig. 5.20 shows the variation of the transformer magnetization curve with the change of degree of core saturation. Analysis starts with $n = 1$. Then it gradually increases with a step of 2. The other circuit parameters are kept unaltered. Up to $n = 7$, the system does not show any sustained ferroresonance. Fig. 5.21 shows the transformer voltage and capacitor voltage with $n = 7$. This shows an initial high value which decays down after 3-4 cycles.

Now when $n = 9$ is taken as the degree of core saturation, the system shows a sustained ferroresonance as appeared in Fig. 5.22.

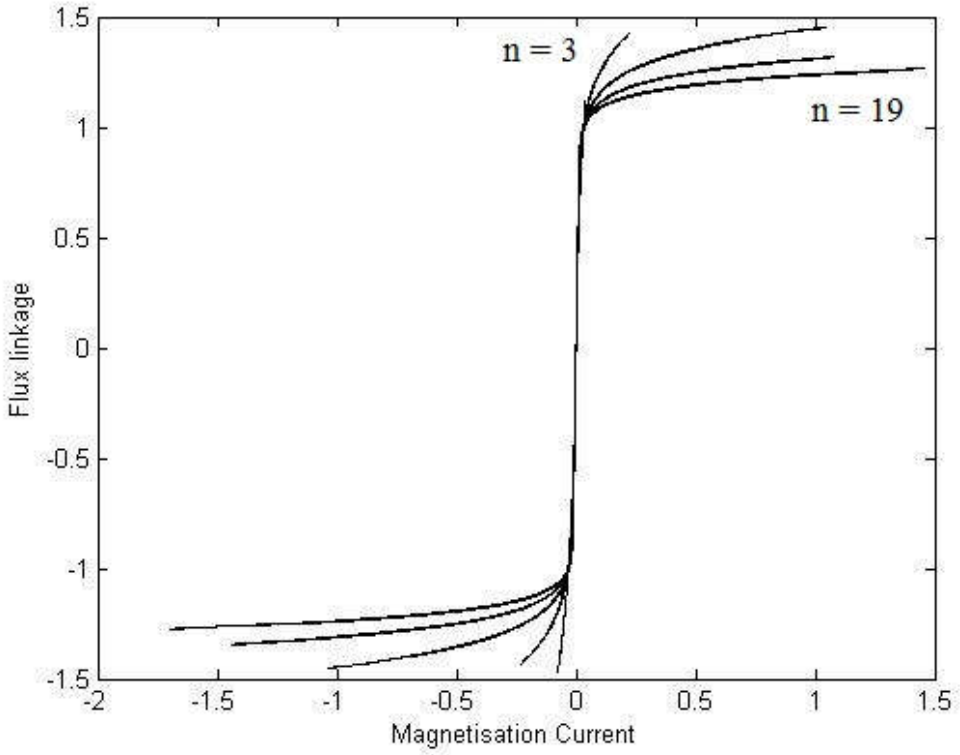

Fig. 5.20. Magnetizing curves for different degrees of core saturation

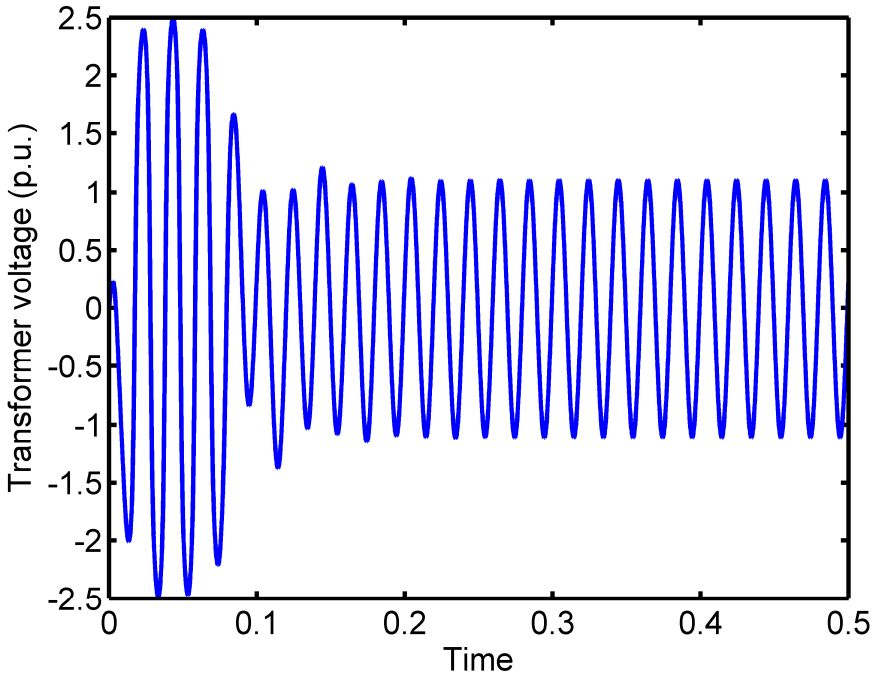

(a)

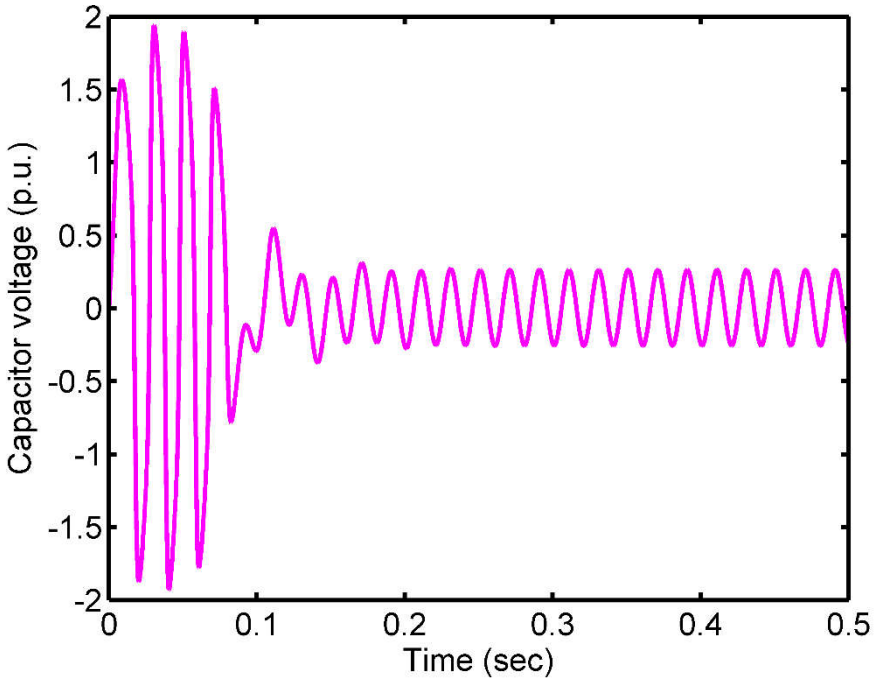

(b)

Fig. 5.21. (a) Transformer voltage and (b) capacitor voltage at $n = 7$ when ferroresonance does not occur

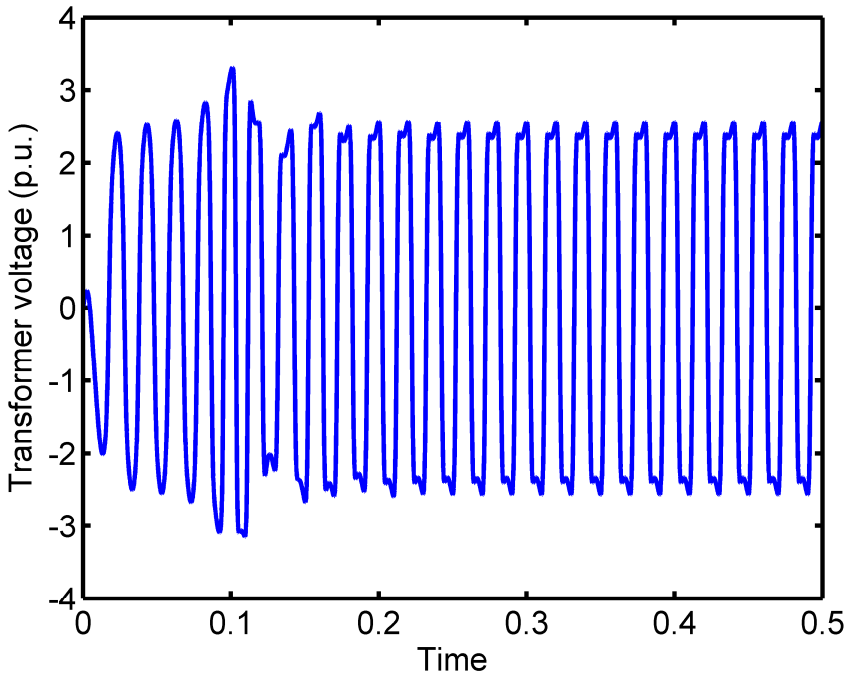

(a)

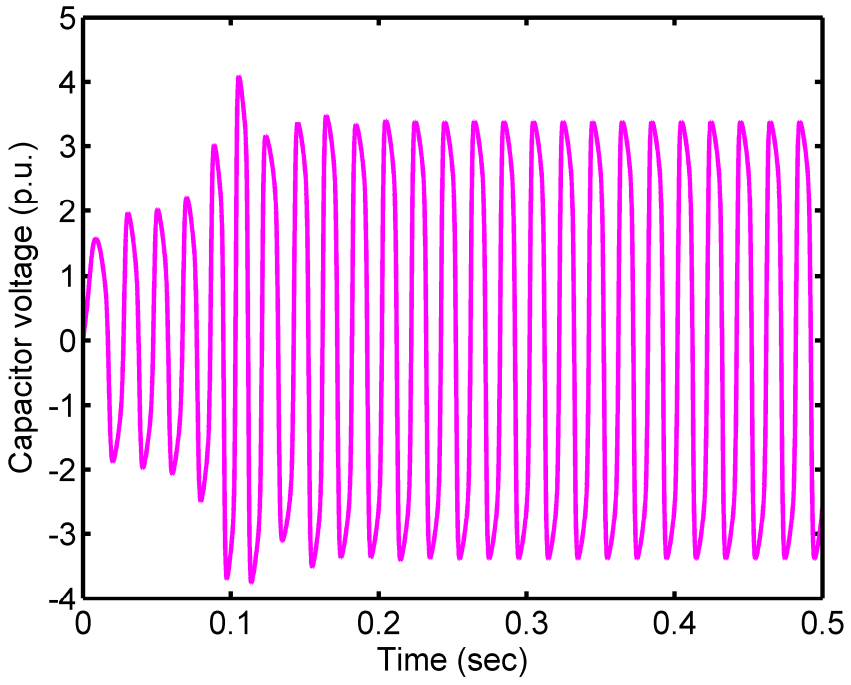

(b)

Fig. 5.22. (a) Transformer voltage and (b) capacitor voltage at $n = 9$ when sustained ferroresonance occurs

Table 5.5: Variation of voltages and current with the degree of core saturation (n)

Degree of core saturation (n)	Capacitor Voltage V_C (p.u.)	Transformer Voltage V_L (p.u.)	Magnetizing current I_λ (p.u.)	Remarks
1	0.47	1.31	0.59	No ferroresonance $V_C < V_L$
3	0.38	1.17	0.38	
5	0.39	1.16	0.42	
7	0.62	1.30	1.00	
9	3.62	2.84	8.26	Sustained ferroresonance $V_C > V_L$
11	3.46	2.66	8.48	
13	3.35	2.55	8.76	
15	3.27	2.46	9.06	

The jump of voltages and magnetizing current while changing the degree of core saturation are well observed in Fig. 5.23.

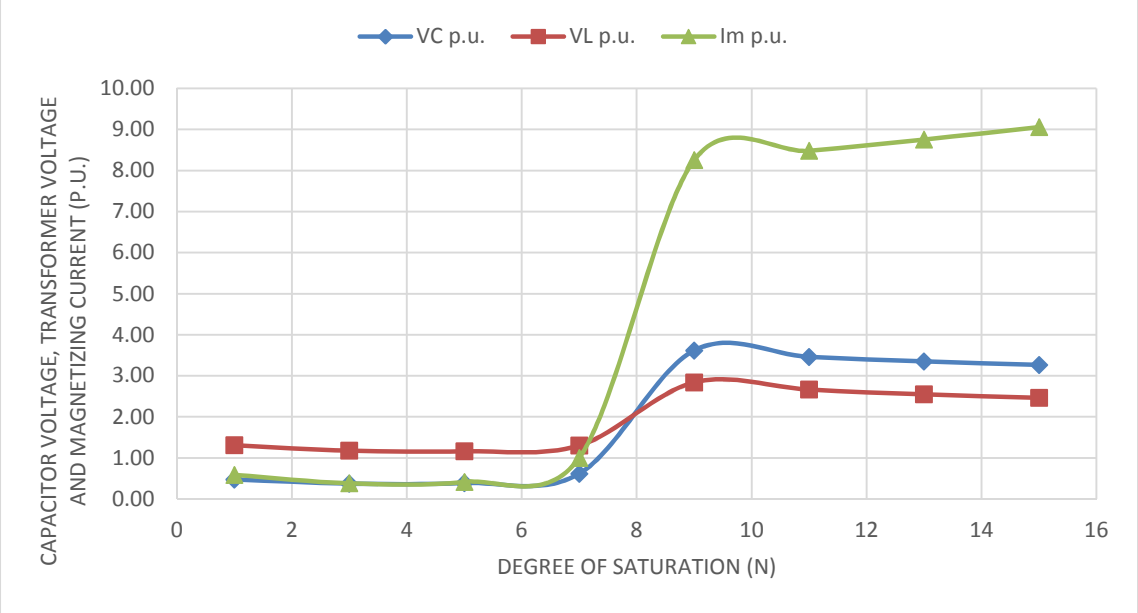

Fig. 5.23. Variation of voltages with the degree of core saturation (n)

The explanation can be obtained from Rudenberg's [3] graphical method. As depicted in Fig. 5.24, with a smaller value of n, such as n_1, one stable operating point (b_1) will appear in the first quadrant. But with a higher value of n, for example, n_2, no operating point is available in quadrant 1. While a stable operating point a_2 appears in quadrant 3. This operating point a_2 produces large oscillation in the system.

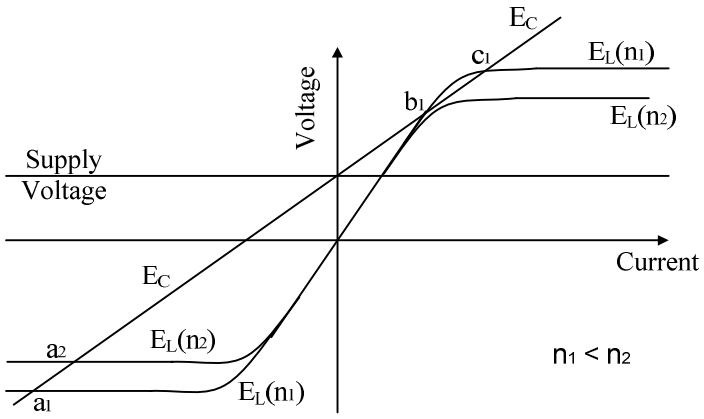

Fig. 5.24. Variation with different degrees of core saturation

5.8 Analysis with Initial Flux Linkage

Different literatures [14] show that the occurrence of ferroresonance highly depends on the initial condition of the circuit parameters. In this part of the study, an analysis was done with the variation of initial flux linkage (λ). That means if the transformer core has a certain remedial flux then what will be the effect of that on the occurrence of ferroresonance?

In this study the initial flux linkage was varied from -3 to 3 with a step of 0.5. With initial flux linkage -3, the ferroresonance occurs at 0.83 p.u. supply voltage. With -2.5 flux linkage, the ferroresonance occurs at 1.51 p.u. supply voltage. It again decreases to 0.72 p.u. supply voltage with -2 initial flux linkage. From -1 to +1.5 initial flux linkage, the ferroresonance occurrence voltage follows a decreasing pattern. After that it again at +2 initial flux voltage increases slightly to 0.96 p.u. Table 5.6 shows the supply voltage at which the ferroresonance jump occurred while initial flux linkage was increased with a step of 0.5. Fig. 5.25 to 5.29 shows the ferroresonance jump for different initial flux linkage. Fig. 5.30 shows the variation of supply voltage where ferroresonance occurs with flux linkage graphically.

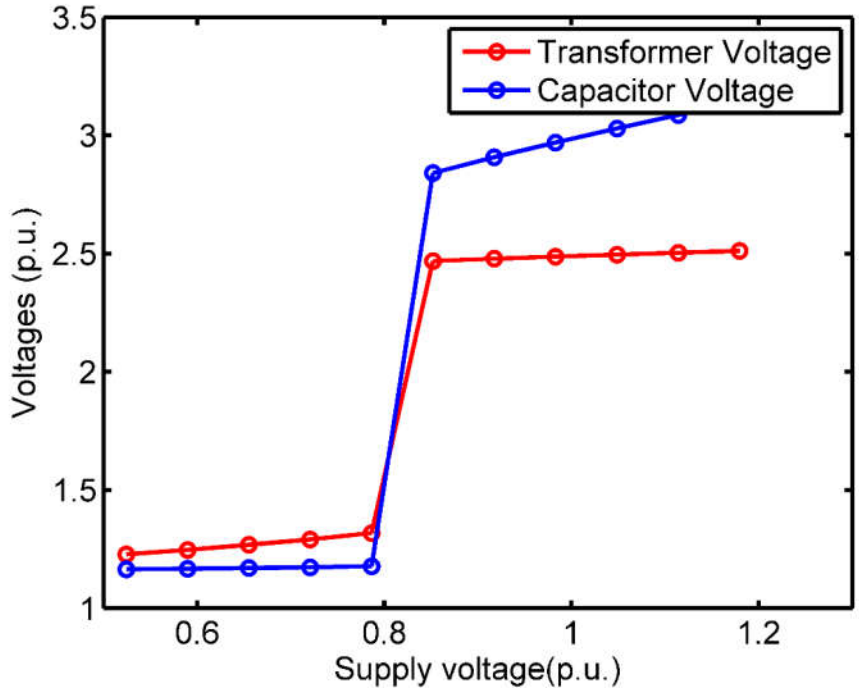

(a)

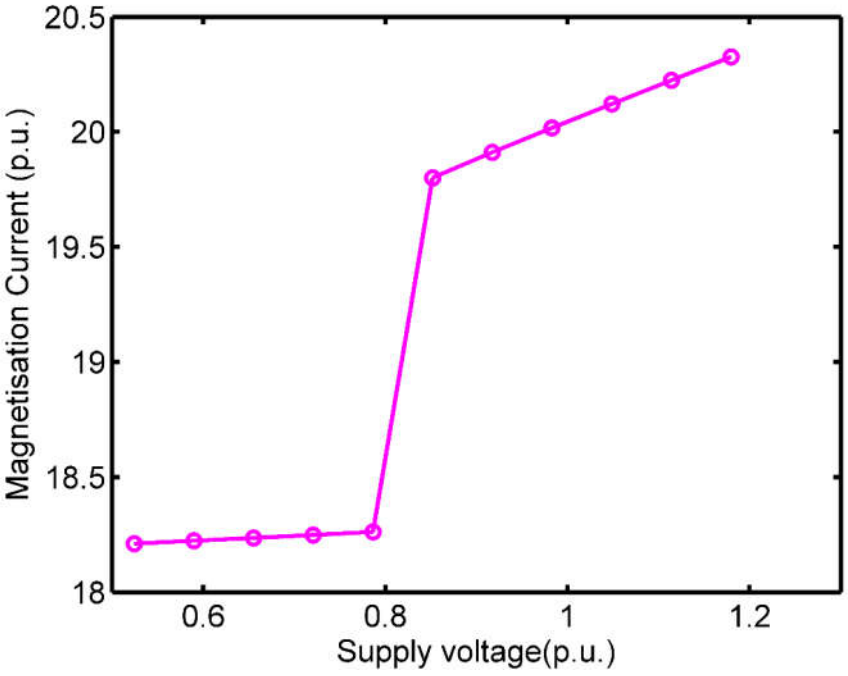

(b)

Fig. 5.25. Ferroresonance jump in (a) voltages and (b) current with initial $\lambda = -3$

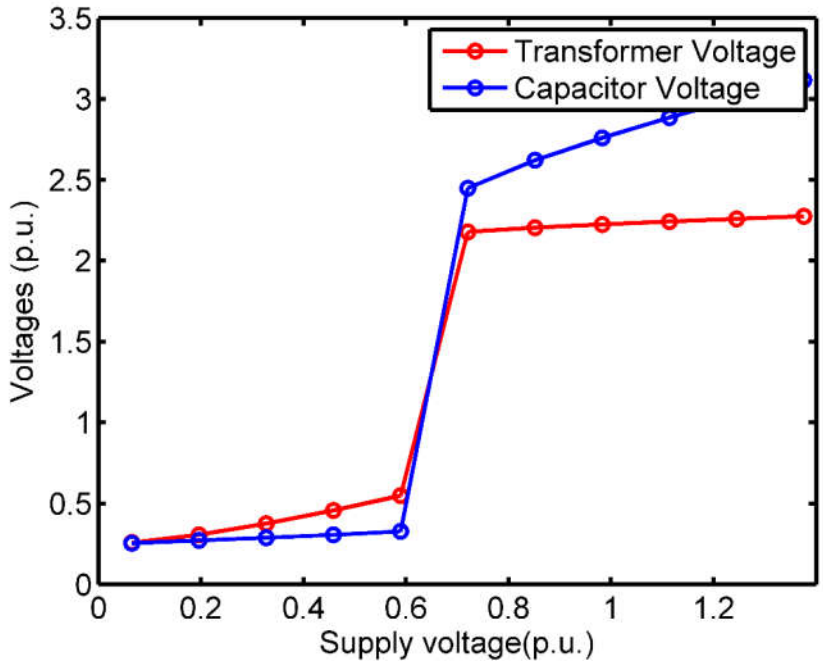

(a)

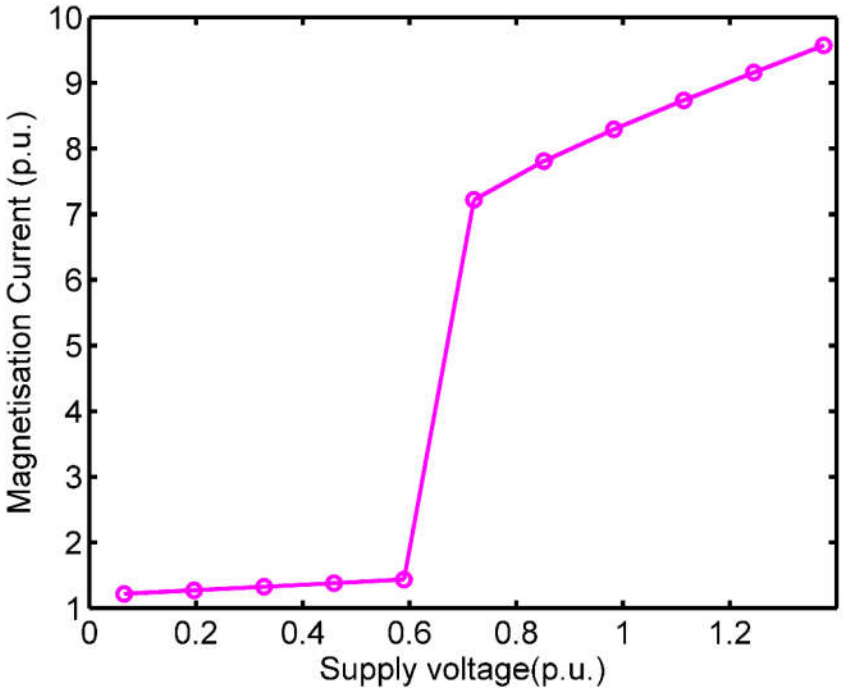

(b)

Fig. 5.26. Ferroresonance jump in (a) voltages and (b) current with initial $\lambda = -2$

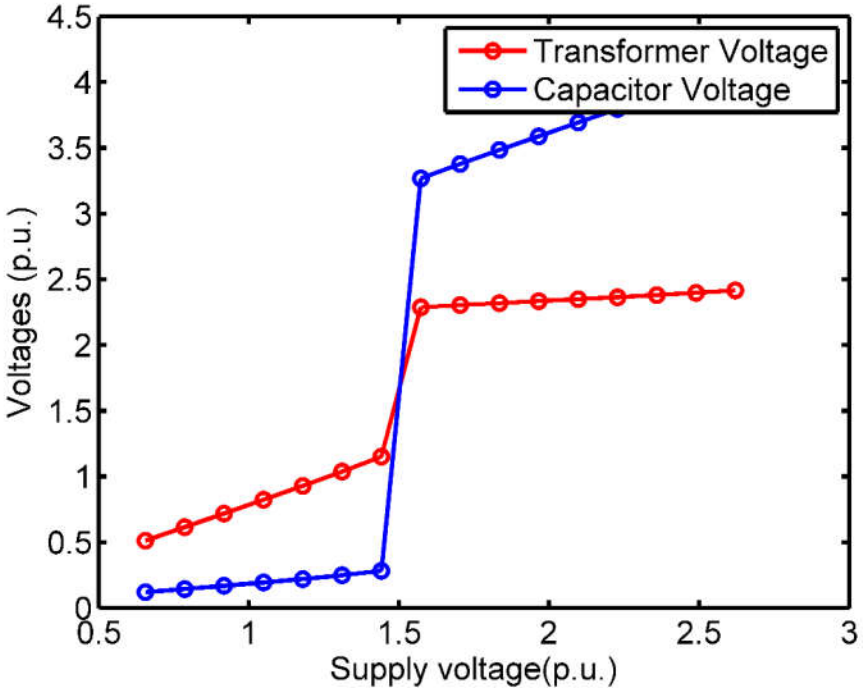

(a)

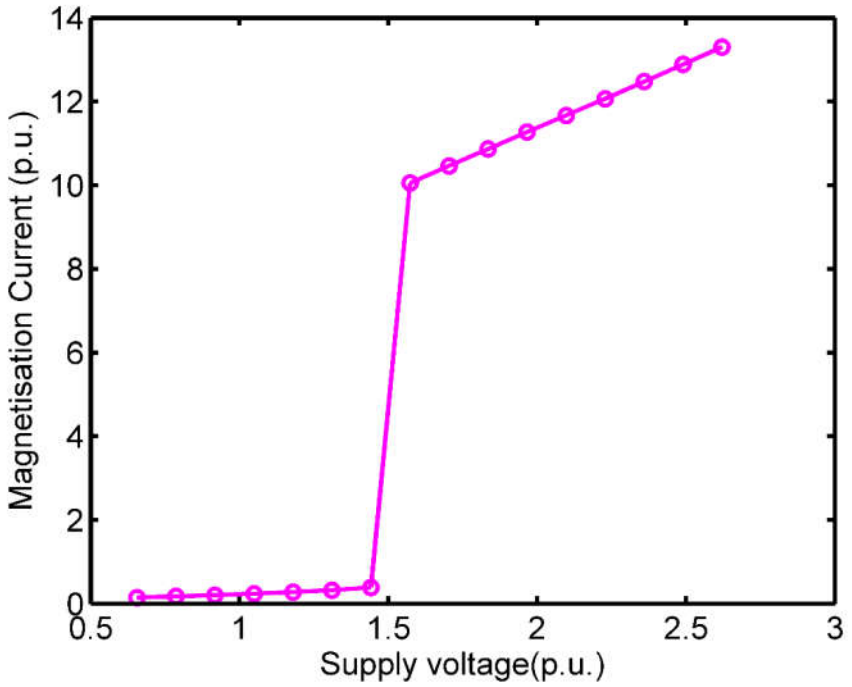

(b)

Fig. 5.27. Ferroresonance jump in (a) voltages and (b) current with initial $\lambda = 0$

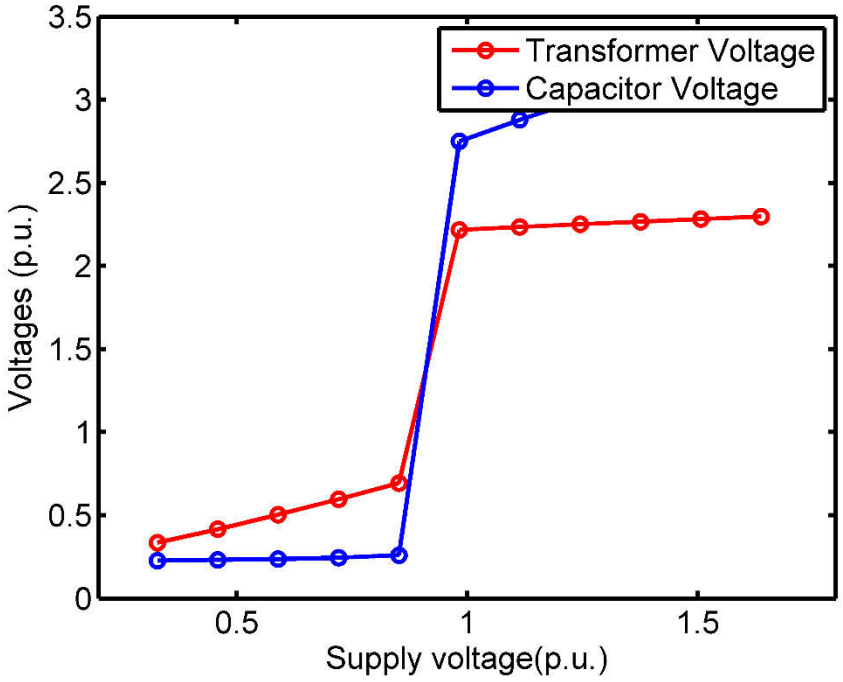

(a)

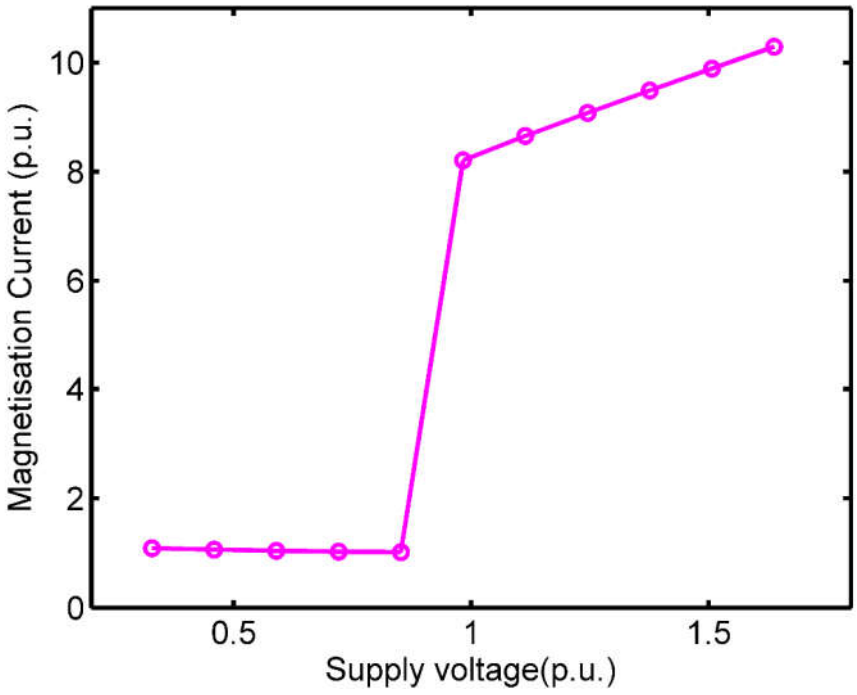

(b)

Fig. 5.28. Ferroresonance jump in (a) voltages and (b) current with initial $\lambda = +2$

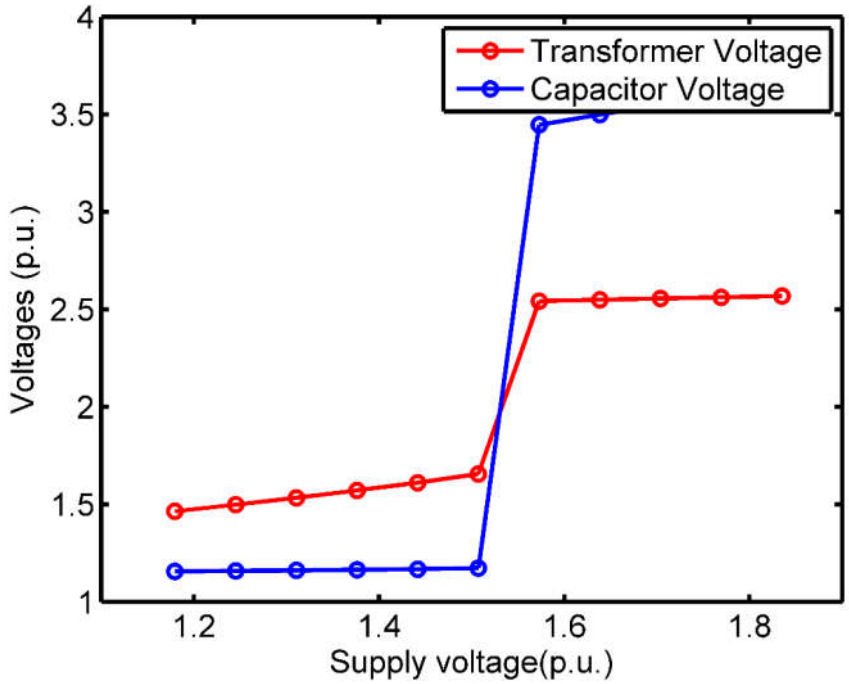

(a)

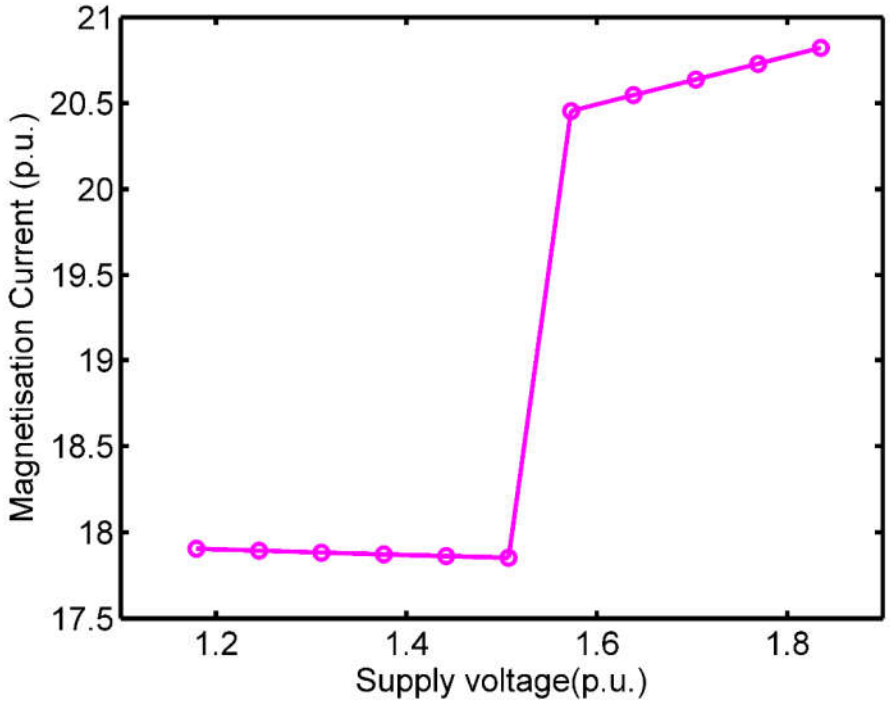

(b)

Fig. 5.29. Ferroresonance jump in (a) voltages and (b) current with initial $\lambda = +3$

Table 5.6: Occurrence of ferroresonance with the variation of initial flux linkage (λ)

Initial flux linkage (λ)	P.U. Supply voltage where ferroresonance occurs
-3	0.83
-2.5	1.51
-2	0.72
-1.5	1.54
-1	1.66
-0.5	1.62
0	1.51
0.5	1.25
1	1.00
1.5	0.68
2	0.96
2.5	0.68
3	1.52

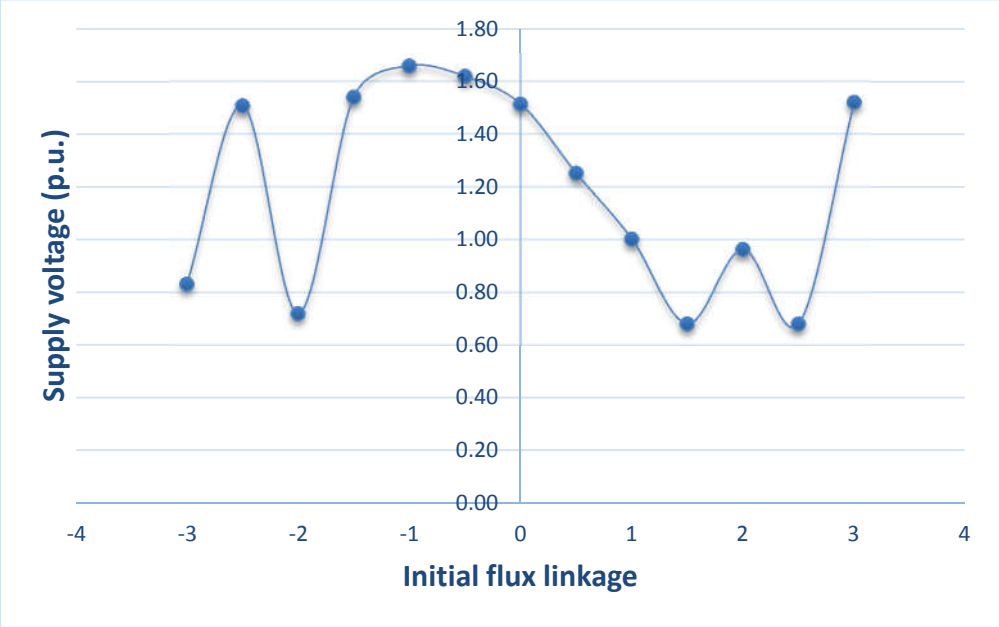

Fig. 5.30. Supply voltage where ferroresonance occurs for different initial flux linkage

5.9 Summary

The MATLAB model for ferroresonance created in the previous chapter is used to continue the study in this chapter. Here, a few circuit parameters are adjusted, and the voltage across the series capacitor and transformer for ferroresonance is observed. These parameters include supply voltage, supply frequency, series capacitance, core loss resistance of the transformer, degree of transformer core saturation, and initial flux linkage in the transformer core. In every instance, it has been shown that voltages increase to a high value at ferroresonance at a specific moment when the circuit parameter and other conditions coincide. It has been demonstrated how the stable operating point of the system moves from the first to third quadrant of the V-I characteristic and generates ferroresonance oscillation using Rudenberg's graphical analysis.

6. Nonlinear Dynamical Systems

6.1 Nonlinear Dynamical Systems

Previous chapters have done a simulation study on the occurrence of ferroresonance and the dependency of circuit parameters on that. In the next phase of the work, the objective is to study the behavior of the system under ferroresonance conditions. At this stage, one has to rely on the simulation study as the experimental study cannot be carried out with sustained overvoltage and overcurrent. As the system equation developed in Chapter 4 carries non-linear components, the knowledge of non-linear mathematics is essential to understand the system behavior. Stability domain analysis has been found in the literature [62] where the nonlinear dynamical method is compared with a two-dimensional brute-force bifurcation diagram and defined as a safety margin for operation. The Electro-Magnetic Transient Program (EMTP) program is used to obtain the bifurcation diagram of a ferroresonance circuit in [76]. Bifurcation with different circuit capacitance is discussed in [77]. However the detailed analytical approach is avoided may be due to the complexity of nonlinear mathematics.

A nonlinear dynamical system is a mathematical model that defines the behavior of a system that cannot be expressed as a simple sum of its parts or as a linear combination of inputs and outputs. That means, the behavior of a nonlinear dynamic system changes over time and is influenced by multiple factors that interact in complex ways.

Examples of nonlinear dynamic systems can be found in many different fields, including physics, biology, economics, and social sciences. For instance, weather patterns, stock market fluctuations, population growth, and the behavior of living organisms are all examples of systems that can be described using nonlinear dynamic models.

One key characteristic of nonlinear dynamic systems is that they often exhibit what is known as "chaotic" behavior. This suggests, a small changes in the initial conditions may generate completely different outcomes as time elapsed. That is why, predicting the behavior of a nonlinear dynamic system is challenging.

Overall, nonlinear dynamic systems are important tools for understanding and modeling complex phenomena, but their behavior can be difficult to predict and understand due to their nonlinear and chaotic nature.

6.1.1 Differential Equations

Differential equations describe how a variable or a set of variables changes with time, depending on the rate of change of those variables. These equations express the relationship between the function and its derivatives or differential coefficients and are used to express a wide variety of physical, biological, and social phenomena in mathematical models [78].

Differential equations again can be categorized into ordinary differential equations (ODEs), partial differential equations (PDEs), and stochastic differential equations (SDEs), depending on the number of independent variables in the system being modelled.

ODEs define the rate of change of a single variable with respect to time and are often used to model phenomena such as population growth, radioactive decay, and electrical circuits. PDEs express the rate of change of a function with respect to multiple variables and are used to model physical phenomena like heat transfer, fluid dynamics, and electromagnetic fields. SDEs describe the rate of change of a variable that is subject to random fluctuations and are used to simulate phenomena like Brownian motion and financial markets.

In nonlinear dynamics, an autonomous system refers to a set of differential equations independent of time. This means that the behavior of the system is solely determined by its current state and not influenced by any external factors or time-varying parameters.

Mathematically, an autonomous system can be represented in the following way:

$dx/dt = f(x)$

where vector x represents the state variables of the system, and $f(x)$ is a set of nonlinear functions that describe the dynamics of the system.

A non-autonomous system refers to a set of differential equations that explicitly depend on time. In this case, the behavior of the system is influenced by time-varying parameters or external forcing.

Mathematically, a non-autonomous system can be represented in the following way:

$dx/dt = f(x, t)$

where vector x represents the state variable of the system, t is time, and $f(x, t)$ is a set of nonlinear functions that define the dynamics of the system and explicitly depend on time.

6.1.2 Difference Equations

A difference equation describes how a variable changes with time, based on its previous values and the values of other variables. In contrast to differential equations, which describe the rate of change of a variable at an instant, difference equations describe the discrete-time evolution of a variable.

Difference equations can be linear or nonlinear. It depends on the relationship between the variable and its past values as a linear or nonlinear function. They can also be time-invariant or time-varying, depending on whether the equation is constant over time or changes over time.

A discrete-time dynamic system can be expressed with the following equation

$x(n+1) = f\big(x(n)\big), n = 0,1,2 \ldots.$

Here the function f maps the state vector $x(k)$ to the next state $x(k+1)$. This equation describes how the sequence evolves with time, depending on its past values.

Difference equations are used in many different fields, like physics, engineering, economics, and computer science. For modeling systems that evolve over discrete time intervals, such as digital signal processing, discrete-time control systems, and discrete event simulations difference equations are very useful.

6.2 Phase Plane

A phase plane is an approach to represent the behavior of the system in a reduced-dimensional space graphically, typically a 2D or 3D space. The phase plane is a powerful tool for visualizing and analyzing the trajectories of the system and understanding its dynamics. The concept of a phase plane works as follows:

In a nonlinear dynamical system, we often have multiple state variables that describe the state of a system at any given time. For simplicity, consider a 2D system having two state variables, denoted as x and y.

$\dot{x} = f(x, y)$

$\dot{y} = g(x, y)$

At any given time, the state of the system can be represented as a point in a multi-dimensional space known as the phase space. Each point in the phase space represents a specific combination of the state variables (x, y).

As the system evolves, it traces out a path or trajectory in the phase space. This trajectory represents how the state of the system evolves. The phase plane is a 2D projection of the phase space. It can be created by plotting one of the state variables against the other. For example, if a system has state variables x and y, a phase plane can be created by plotting x against y.

Some significant characteristics of phase portrait are:

1. The equilibrium points or fixed points like A, B, and C in Fig 6.1 are special points in the phase plane where the state of the system does not change over time. For a 2-dimensional system having fixed points (x^*, y^*) will satisfy the condition $f(x^*, y^*) = 0$ and $g(x^*, y^*) = 0$.
2. The closed paths, like D in Fig 6.1 indicate the periodic solutions. That means, for this type of system one can write $x(t + T) = x(t)$ and $y(t + T) = y(t)$for all t, for $T > 0$. These closed orbits are called limit cycles.
3. Vector field that indicates the direction and magnitude of state changes at different points. For instance, in Fig. 6.1, the flow pattern at A and C is distinct from that near B but otherwise comparable.
4. The decision on the closed orbits' and fixed points' stability or instability can be taken easily from phase portrait. In this case, the closed orbit D is stable but the fixed points A, B, and C are unstable since surrounding trajectories tend to move away from them.

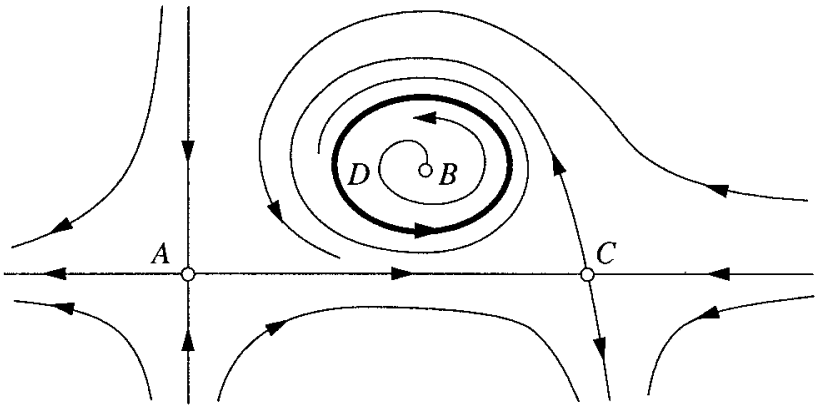

Fig. 6.1: Phase plane plot

By visualizing the system in a phase plane, one can analyze its behavior, identify fixed points, determine stability, and understand how trajectories evolve. This graphical representation is particularly useful for nonlinear systems because it allows you to gain insights into complex

behavior patterns, such as limit cycles, chaotic behavior, or bifurcations, by simply examining the flow pattern of the vector field in the phase plane.

6.3 Stability of Fixed Points

Consider the following dynamic system

$$\dot{x} = f(x, y)$$
$$\dot{y} = g(x, y) \quad (6.1)$$

If the system (6.1) has a fixed point at (x^*, y^*), then it must satisfy the condition

$$f(x^*, y^*) = 0$$
$$g(x^*, y^*) = 0 \quad (6.2)$$

There are different methods are available for analyzing the stability of the fixed point, depending on the type of system being studied. In general, stability analysis involves examining the behavior of nearby trajectories under small perturbations, and determining whether they diverge from the fixed point or converge towards it.

One common method for analyzing stability is linearization, which involves approximating the system near the fixed point as a linear function and examining its Eigenvalues to determine whether they are positive (unstable) or negative (stable).

For the system (6.1), a small deflection from a fixed point can be given as

$$u = x - x^*$$
$$v = y - y^* \quad (6.3)$$

Differential equations for u and v must be derived to observe whether the disturbance increases or decreases. Considering $the\ u$ equation first

$$\dot{u} = \dot{x}$$
$$\dot{u} = f(x^* + u, y^* + v)$$

By expanding the above equation using the Taylor series

$$\dot{u} = f(x^*, y^*) + u\frac{\partial f}{\partial x} + v\frac{\partial f}{\partial y} + O(u^2, v^2, uv)$$

Neglecting the quadratic terms $O(u^2, v^2, uv)$ in u and v to make the system linear and putting $f(x^*, y^*) = 0$

$$\dot{u} = u\frac{\partial f}{\partial x} + v\frac{\partial f}{\partial y} \quad (6.4)$$

Similarly for v equation

$$\dot{v} = u\frac{\partial g}{\partial x} + v\frac{\partial g}{\partial y} \tag{6.5}$$

The combination of equations (6.4) and (6.5) can be expressed in a matrix as

$$\begin{pmatrix} \dot{u} \\ \dot{v} \end{pmatrix} = \begin{pmatrix} \frac{\partial f}{\partial x} & \frac{\partial f}{\partial y} \\ \frac{\partial g}{\partial x} & \frac{\partial g}{\partial y} \end{pmatrix} \begin{pmatrix} u \\ v \end{pmatrix}$$

The matrix

$$J = \begin{pmatrix} \frac{\partial f}{\partial x} & \frac{\partial f}{\partial y} \\ \frac{\partial g}{\partial x} & \frac{\partial g}{\partial y} \end{pmatrix}_{(x^*, y^*)} \tag{6.6}$$

Is known as the Jacobian matrix at the fixed point (x^*, y^*) [79].

The stability conditions of the fixed point (x^*, y^*) can be obtained by examining the Eigenvalues λ_1, λ_2 of the Jacobian matrix. Fig. 6.2 shows all the criteria in one diagram. Here the y-axis shows the trace $\tau = \lambda_1 + \lambda_2$ and the x-axis denotes the determinant $\Delta = \lambda_1 \lambda_2$ of the matrix J.

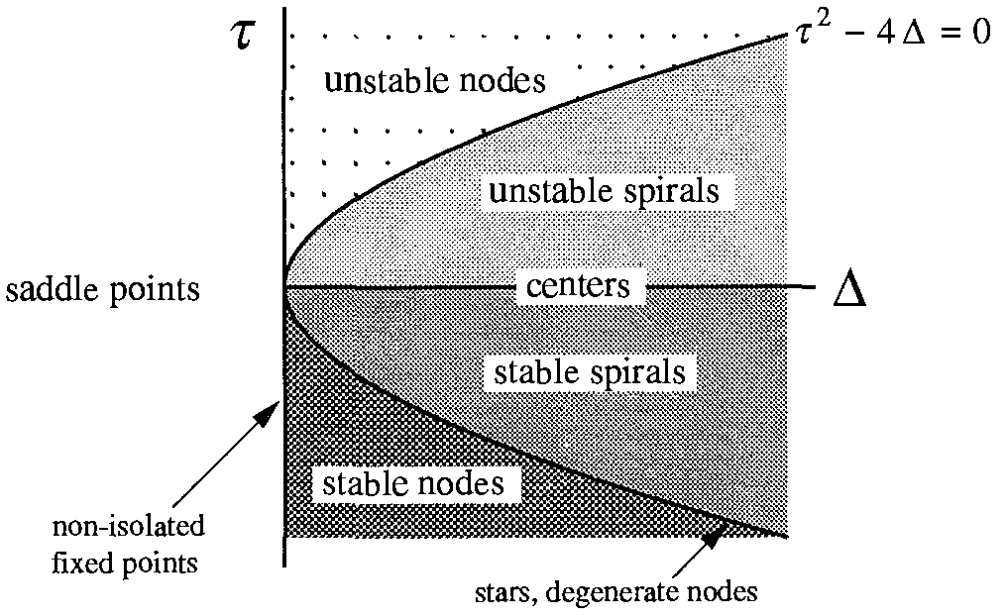

Fig. 6.2. Stability criteria of different fixed points

6.4 Limit Cycle

The tendency of a system to converge to its limit cycle even in the presence of minor perturbations or disturbances is known as the stability of the limit cycle. When the surrounding

trajectories of a system diverge from a limit cycle over time, it is considered unstable; otherwise, it is considered stable. [80].

Stable limit cycles are a significant concept in dynamical systems theory because they play a major role in shaping the long-term behavior of a system. A system having a stable limit cycle will tend to remain near that set over time, and its behavior will be predictable and consistent. On the other hand, if a system has an unstable limit cycle, its behavior will be highly sensitive to initial conditions, and small perturbations can lead to unpredictable and chaotic behavior.

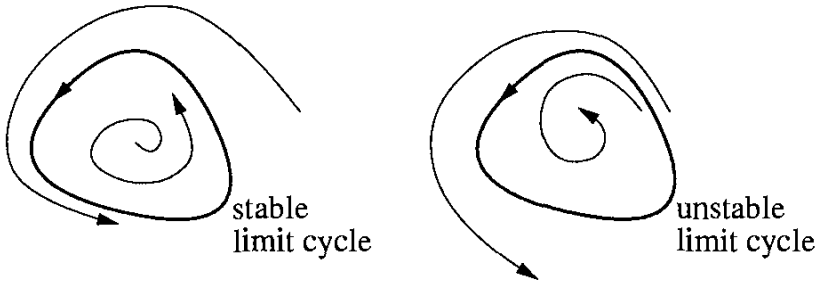

Fig. 6.3. Stability of a limit cycle

The mathematical model described in section 6.3 cannot be applied in the investigation of the stability of a limit cycle as it does not contain any fixed point. However, Poincare maps can be used to transform a limit cycle problem into a fixed point problem. This is discussed in the next section.

6.5 Poincare Maps

Poincare maps introduced by French mathematician Henri Poincare, are a mathematical tool used to analyze the dynamical systems, specifically for studying the behavior of systems that exhibit periodic or quasi-periodic motion.

A Poincare map is a two-dimensional plot that illustrates how a dynamical system behaves at regular time intervals, such as each time the system crosses a particular surface or boundary. The map consists of a set of discrete points that represent the state of the system at these intervals, and provides a way to visualize the evolution of the system over time [80].

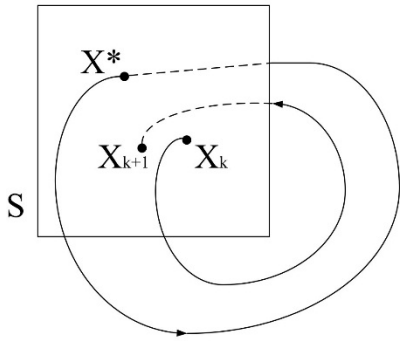

Fig. 6.4. Poincare map

Poincare maps are particularly convenient for studying systems whose behavior is chaotic or irregular, as they can reveal patterns and structures in the behavior of the system, that may be difficult to discern using other methods. Researchers can learn more about the underlying dynamics of the system and pinpoint key elements such as chaotic attractors, invariant sets, and stable and unstable periodic orbits by examining the geometry and topology of the Poincare map.

6.6 Stability of a Periodic Solution

The phase plane portrait of a periodic function is a limit cycle. To find out its stability by linearizing the system is difficult. Here comes the usefulness of the Poincare map. A limit cycle produces a fixed point in the Poincare map. The limit cycle problem is therefore transformed into a fixed point problem using a Poincare map.

In the discrete-time domain, a nonlinear system can be expressed as [81]

$$x_{i+1} = f(x_i, y_i) \tag{6.7}$$

$$y_{i+1} = g(x_i, y_i) \tag{6.8}$$

Let the fixed points of the above system be $x_i = x^*$ and $y_i = y^*$

As at a fixed point $x_{i+1} = x_i$ and $y_{i+1} = y_i$, one can write

$$x^* = f(x^*, y^*) \tag{6.9}$$

$$y^* = g(x^*, y^*) \tag{6.10}$$

To verify the stability of the system, a small perturbation

$$x_i = x^* + \xi_i \tag{6.11}$$

$$y_i = y^* + \eta_i \tag{6.12}$$

is injected such that

$$x_{i+1} = f(x^* + \xi_i,\ y^* + \eta_i) = x^* + \xi_{i+1} \tag{6.13}$$

$$y_{i+1} = g(x^* + \xi_i,\ y^* + \eta_i) = y^* + \eta_{i+1} \tag{6.14}$$

Expanding the function f and g in Taylor series at fixed point –

$$\xi_{i+1} = a\xi_i + b\eta_i \tag{6.15}$$

$$\eta_{i+1} = c\xi_i + d\eta_i \tag{6.16}$$

Here the higher-order terms are neglected with an assumption of small perturbation and $a, b, c, and\ d$ are the first derivatives evaluated at the fixed point.
In matrix form

$$\begin{bmatrix}\xi_{i+1}\\ \eta_{i+1}\end{bmatrix} = J\begin{bmatrix}\xi_i\\ \eta_i\end{bmatrix} \tag{6.17}$$

Where $J = \begin{bmatrix}a & b\\ c & d\end{bmatrix}$

Let λ_1 and λ_2 be the real Eigenvalues of the Jacobian matrix J. Now, the system will be stable if $-1 < \lambda_{1,2} < 1$, but unstable if $|\lambda_{1,2}| > 1$. If one of the Eigenvalues is 1, then the linear approximation is not adequate.

If λ_1 and λ_2 are complex conjugate

$$\lambda_1 = \alpha + j\beta = \rho e^{j\theta} \tag{6.18}$$

$$\lambda_2 = \alpha - j\beta = \rho e^{-j\theta} \tag{6.19}$$

If $\rho < 1$, the trajectory spirals inward and the fixed point will be called stable
If $\rho > 1$, the trajectory spirals outward and the fixed point will be called unstable
If $\rho = 1$, the linear approximation method fails.

It can also be observed [79] for periodic orbits of period $n = 2$

$$x_{i+2} = f\big(f(x_i, y_i)\big) = f^2(x_i, y_i) \tag{6.20}$$

$$y_{i+2} = g(g(x_i, y_i)) = g^2(x_i, y_i) \quad (6.21)$$

Here f^2 and g^2 are the notation only and not to be confused with the square of f or square of g. Thus, it is necessary to examine the functions f^2 and g^2 to assess the stability of a period 2 orbit. Eventually, for periodic orbits of period $n = k$

$$x_{i+k} = f^k(x_i, y_i) = x_i \quad (6.22)$$

$$y_{i+k} = g^k(x_i, y_i) = y_i \quad (6.23)$$

6.7 Bifurcation

A bifurcation is a qualitative shift in the behavior of a system that happens when a system parameter is changed in dynamical systems theory [82]. A bifurcation occurs when a small change in a system parameter ultimately leads to a large change in the behavior of the system. For example, a small change in the temperature of a system may lead to a transition from a stable equilibrium to a limit cycle or chaotic behavior.

There are two primary categories of bifurcations: local and global. When a minor change in a system parameter results in a qualitative shift in the behavior of the system close to an equilibrium point or periodic orbit, this is known as a local bifurcation. Examples are saddle-node bifurcations, transcritical bifurcations, and pitchfork bifurcations.

On the other hand, global bifurcations involve a qualitative change in the behavior of the system across a large region of the parameter space. Examples are homoclinic bifurcations, heteroclinic bifurcations, and period-doubling bifurcations.

Bifurcations play a significant role in understanding the behavior of complex systems. They can generate a wide range of phenomena, like oscillations, chaos, and pattern formation. Bifurcation analysis is a useful technique in many disciplines, such as physics, engineering, biology, and economics, for comprehending the behavior of dynamical systems.

6.7.1 Saddle-node Bifurcations

The generation or destruction of equilibrium points occurs in dynamical systems when stable and unstable equilibrium points collide and annihilate one another. This is known as saddle-node bifurcation. This type of bifurcation can occur in systems with one or more variables.

In a one-dimensional system, the bifurcation occurs when a stable fixed point collides with an unstable fixed point and disappears at a critical value of a parameter. The two fixed points at this bifurcation point, merge and form a saddle-node.

In a two-dimensional system, the saddle-node bifurcation occurs when there is a collision between a stable limit cycle and an unstable equilibrium point. This either creates or destroys the limit cycle. The stable limit cycle and the unstable equilibrium point coalesce to form a saddle-node at the bifurcation point.

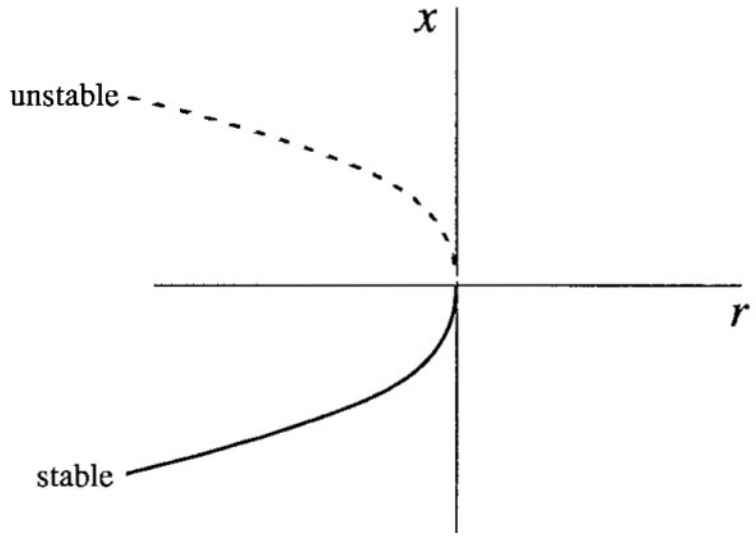

Fig. 6.5. Saddle-node Bifurcations

6.7.2 Transcritical Bifurcations

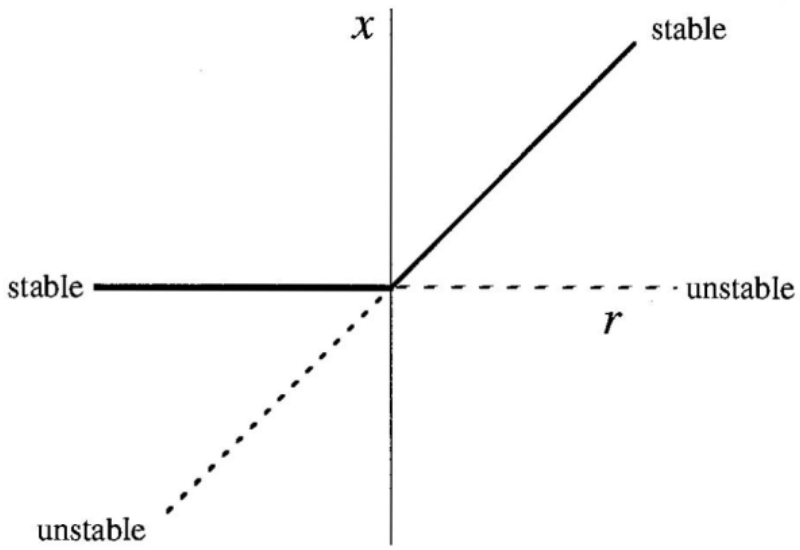

Fig. 6.6. Transcritical Bifurcations

In a one-dimensional system, when the stable and unstable fixed points collide and exchange their stability the transcritical bifurcation occurs. Equilibrium points are created or destroyed when the stable and unstable fixed points combine and swap stability at the bifurcation point. The resulting bifurcation diagram typically consists of two branches, with one branch for stable and the other branch for the unstable fixed point.

Transcritical bifurcations can influence the behavior of a system in several ways, depending on the characteristics and the parameters involved. They can give rise to bistability, where a system can exist in two stable states depending on the initial conditions, or hysteresis, where the response of the system to a change in a parameter depends on the direction of the change. Transcritical bifurcations are also important in the study of ecological and population dynamics, as they can give rise to alternative stable states and tipping points in ecosystems.

6.7.3 Pitchfork Bifurcations

A pitchfork bifurcation occurs in one-dimensional or two-dimensional dynamical systems when two new stable equilibrium points evolve from a stable equilibrium point, or when two unstable equilibrium points generate a new stable equilibrium point. Pitchfork bifurcations can occur in systems with one or more variables.

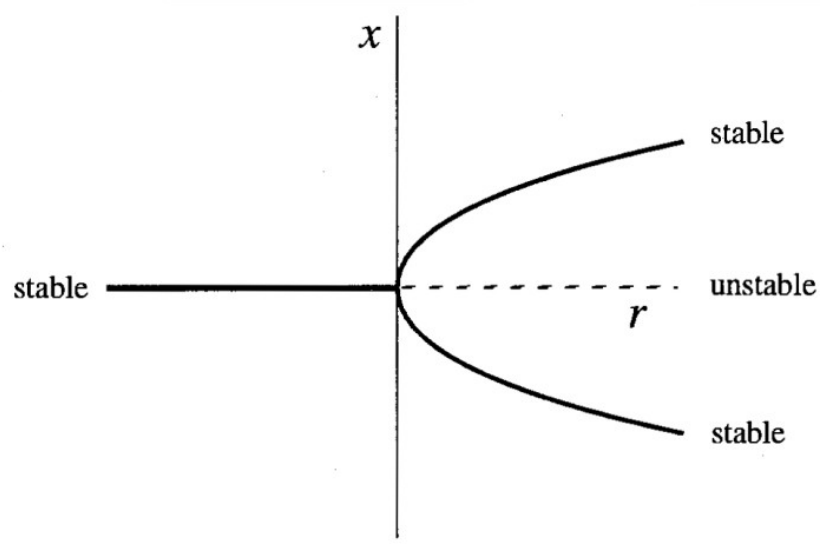

Fig. 6.7. Pitchfork Bifurcations

The bifurcation occurs in a one-dimensional system when a stable equilibrium point undergoes a symmetry-breaking transition and gives rise to two new stable equilibrium points

while a parameter is varied. A bifurcation diagram with three branches is produced when the first stable equilibrium point loses stability and two additional stable equilibrium points appear at the bifurcation point.

In a two-dimensional system, when two unstable equilibrium points undergo a symmetry-breaking transition and give rise to a new stable equilibrium point, the pitchfork bifurcation occurs. A bifurcation diagram with two branches is produced when the two unstable equilibrium points combine to form a single stable equilibrium point at the bifurcation point.

6.7.4 Homoclinic Bifurcations

A homoclinic bifurcation is a kind of global bifurcation that happens in dynamical systems when an unstable manifold collides with a stable equilibrium point or periodic orbit, creating or destroying a homoclinic orbit. A homoclinic trajectory connects an equilibrium point or periodic orbit to itself.

In a one-dimensional system, the bifurcation appears when a stable equilibrium point strikes its unstable manifold and creates a homoclinic orbit. The stable equilibrium point becomes unstable at the bifurcation point, and the homoclinic orbit emerges.

In a two-dimensional system, the homoclinic bifurcation appears when a stable periodic orbit strikes its unstable manifold and creates a homoclinic orbit. The stable periodic orbit becomes unstable at the bifurcation point, and the homoclinic orbit emerges.

6.7.5 Heteroclinic Bifurcations

A heteroclinic bifurcation occurs in dynamical systems while two or more equilibrium points or periodic orbits collide and exchange stability, resulting in the creation or destruction of heteroclinic orbits. A heteroclinic trajectory connects two or more different equilibrium points or periodic orbits.

In a one-dimensional system, when two or more equilibrium points collide and exchange stability, the bifurcation occurs, creating a heteroclinic orbit between them.

In a two-dimensional system, when two or more periodic orbits collide and exchange stability, the heteroclinic bifurcation occurs, creating a heteroclinic orbit between them.

6.7.6 Period-doubling Bifurcations

When a stable periodic orbit loses stability and gives rise to a new stable periodic orbit with double the period, this is known as a period-doubling bifurcation in dynamical systems. If the parameter is increased further, this process can continue endlessly, resulting in a series of period-doubling bifurcations and the creation of chaotic dynamics.

The period-doubling bifurcation in a one-dimensional system is the result of an unstable or stable periodic orbit giving rise to a new stable periodic orbit with twice the period. A bifurcation diagram with a series of period-doubling bifurcations is produced when the original periodic orbit loses stability at the bifurcation point and the new periodic orbit appears [83].

The period-doubling bifurcation can happen in a two-dimensional system when an unstable fixed point or periodic orbit collides with a stable limit cycle, creating a new stable limit cycle that has twice the period. A bifurcation diagram with a series of period-doubling bifurcations is produced when the original limit cycle loses stability at the bifurcation point and the new limit cycle appears.

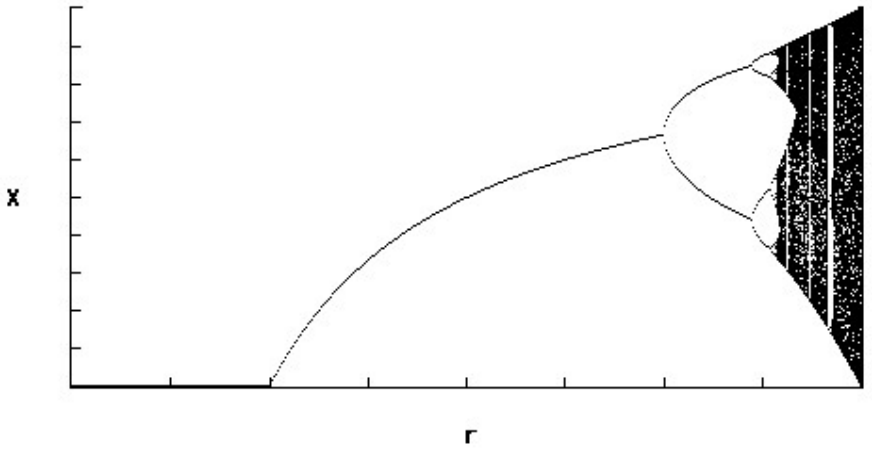

Fig. 6.8. Period-doubling Bifurcations

6.8 Bifurcation to Chaos

Fig. 6.8 shows that period-doubling bifurcation ultimately landed in to chaos. In a nonlinear dynamical system, chaos refers to a type of complex and unpredictable behavior that arises from the extreme sensitivity of the system to initial conditions. Chaotic systems exhibit complex, irregular, and aperiodic behavior. Unlike periodic or regular motion seen in stable systems, chaos

is characterized by trajectories that appear random and never repeat exactly. This makes it difficult to forecast the behavior of chaotic systems after a long time.

Chaotic systems often exhibit strange attractors, which are complex, self-replicating, and non-periodic structures in phase space that characterize the behavior of the system in the long term.

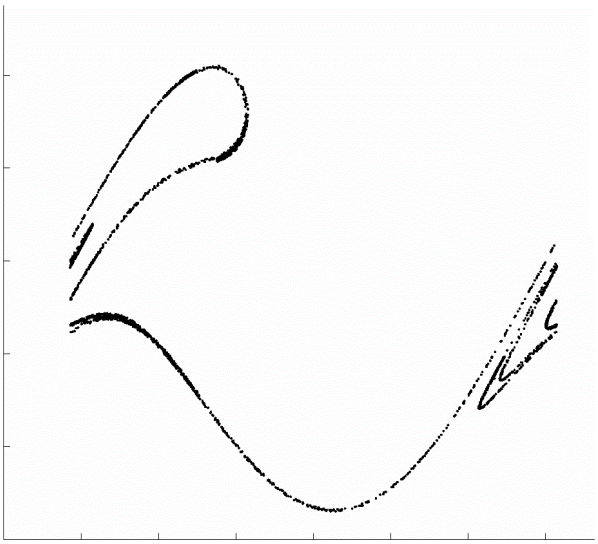

Fig. 6.9. Strange attractor - Poincare map for a chaotic system

One well-known route to chaos occurs by repeated flip bifurcations. A fixed point creates a period 2 orbit at $r = R_1$ then this period 2 orbit bifurcates to a 4-periodic orbit at $r = R_2$, and this continues as shown in Fig. 6.10.

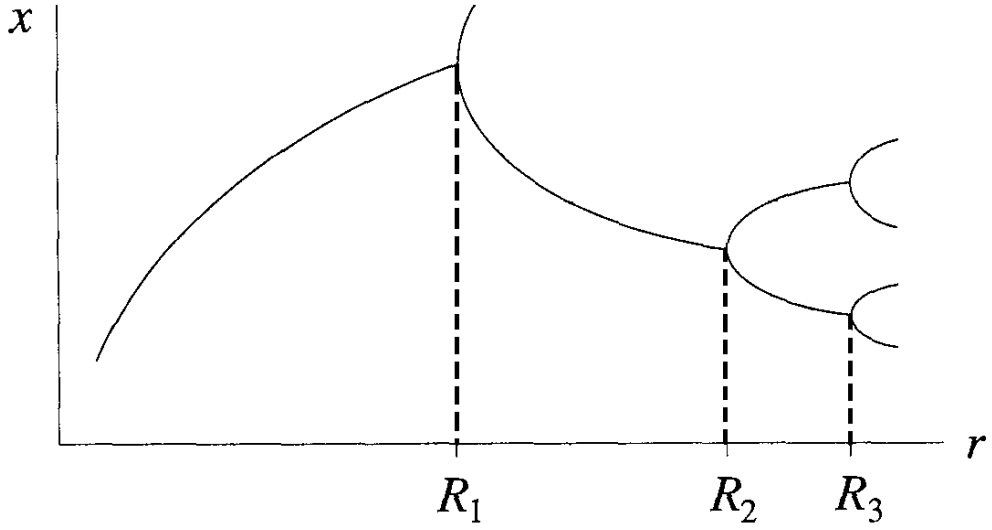

Fig. 6.10. Calculation of Feigenbaum constant

This sequence finally accumulated to a point R_∞ which involves an infinity of periodic orbits. These universal features were discovered quantitatively by Feigenbaum [84].

As per Feigenbaum, the ratios

$$\delta_n = \frac{R_n - R_{n-1}}{R_{n-1} - R_n} \tag{6.24}$$

approaches to the universal number $\delta_n = 4.66920\ldots$ as n tends to ∞. As δ_∞ is independent of the particular map, it is called universal. Several specific examples [85] have established its validity.

6.9 Summary

In this chapter, the theory of nonlinear dynamics has been discussed in detail. An overview of nonlinear dynamic systems, Poincare maps, bifurcation diagrams, limit sets, and their stability properties was given. It was demonstrated that the Poincare map technique was a potent instrument for analyzing the dynamic behavior of the system under ferroresonance. This will help to investigate the stability of the ferroresonance circuit while any of the circuit parameters is varied gradually.

7. Investigation on the Stability of an Electric Power Circuit under Ferroresonance Based on the Nonlinear Dynamic Model of Transformer

7.1 The System Equation

In Chapter 5, the simulation carried out with the nonlinear system equation. Only the occurrence of ferroresonance due to circuit parameter change was discussed. Now, to investigate how the system behaves if one of the parameter is keep on changing deep in to the ferroresonance and how the stability of the ferroresonance circuit is changing, one has to examine the Phase-Plane diagram and Poincare plot of the system. For that flux linkage (λ) and transformer-voltage $\left(\frac{d\lambda}{dt} = v\right)$ are taken as the system variables. So the following equation obtained in Chapter 5

$$\frac{d^2\lambda}{dt^2} = \frac{dV_s}{dt} - \frac{1}{C}\left(\frac{v}{R_C}\right) - \frac{1}{C}(a\lambda + b\lambda^7) \qquad (5.5)$$

can further be simplified as follows:

Let

$x = \lambda$

$y = \frac{d\lambda}{dt} = \dot{x}$

$V_S = E \sin \omega t$

$\frac{dV_S}{dt} = E\omega \cos \omega t = K \cos \omega t$

$\mu = \frac{1}{R_C}$

$\varepsilon = \frac{1}{C}$

Then (5.5) can be written as

$$\dot{x} = y \qquad (7.1)$$

$$\dot{y} = K \cos \theta - \mu\varepsilon y - \varepsilon(ax + bx^7) \qquad (7.2)$$

Equations (7.1) and (7.2) are the differential equations of a two-dimensional system. The phase plane plot of the system will be obtained by plotting flux linkage along the x-axis and transformer voltage along the y-axis.

7.2 Phase-plane Plot

The Simulink model described in Chapter 4 is used to obtain the Phase-plane diagram of the system. The model is first made to run at a particular supply voltage for a predefined time interval. Then the data of flux linkage and transformer voltage are extracted from the model. To get the response at a steady state only, the data of the first few cycles are neglected. The remaining data are plotted with flux linkage along the x-axis and transformer voltage along the y-axis. Fig. 7.1 shows the phase-plan plot at 0.66 p.u. supply voltage.

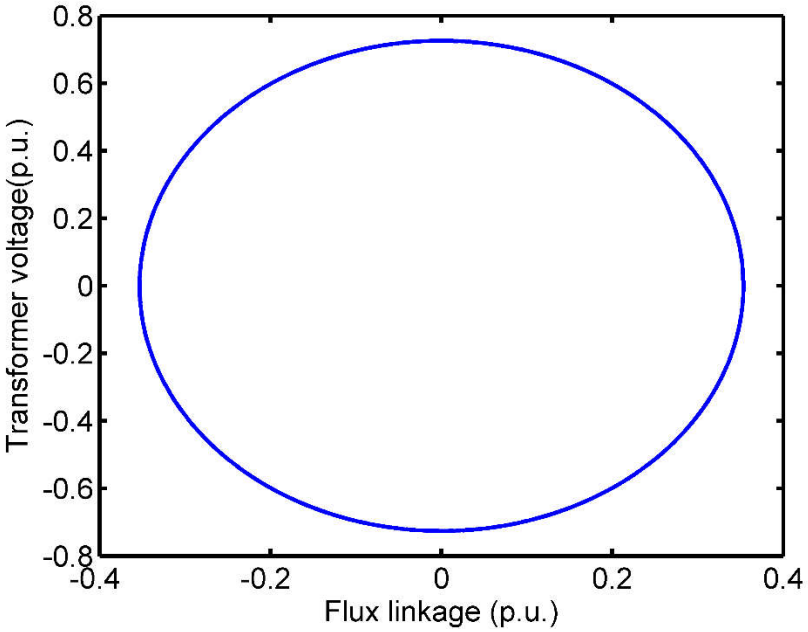

Fig. 7.1. Phase plane plot at 0.66 p.u. supply voltage

While increasing the supply voltage in steps, ferroresonance appeared at a certain voltage. These observations are already recorded in Table 5.1. In this part of the study, the limit cycles are also recorded. Fig. 7.2 (b) and 7.3 (b) show the phase plane plot obtained just before and after ferroresonance while varying the supply voltage in steps. A clear deformation in the shape of the limit cycle can be observed from these two plots.

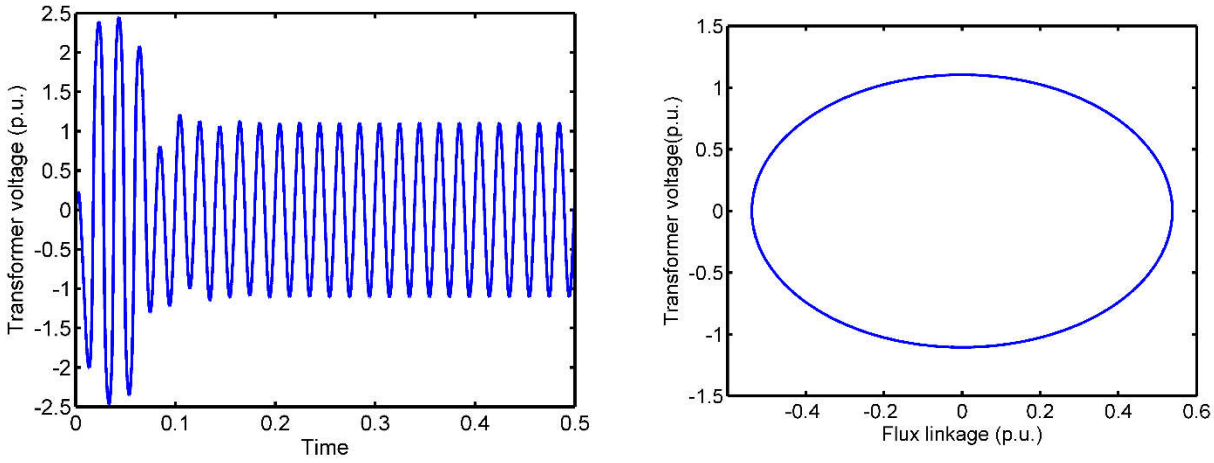

(a) **(b)**

Fig. 7.2. Transformer voltage (a) and Phase plane plot (b) before ferroresonance

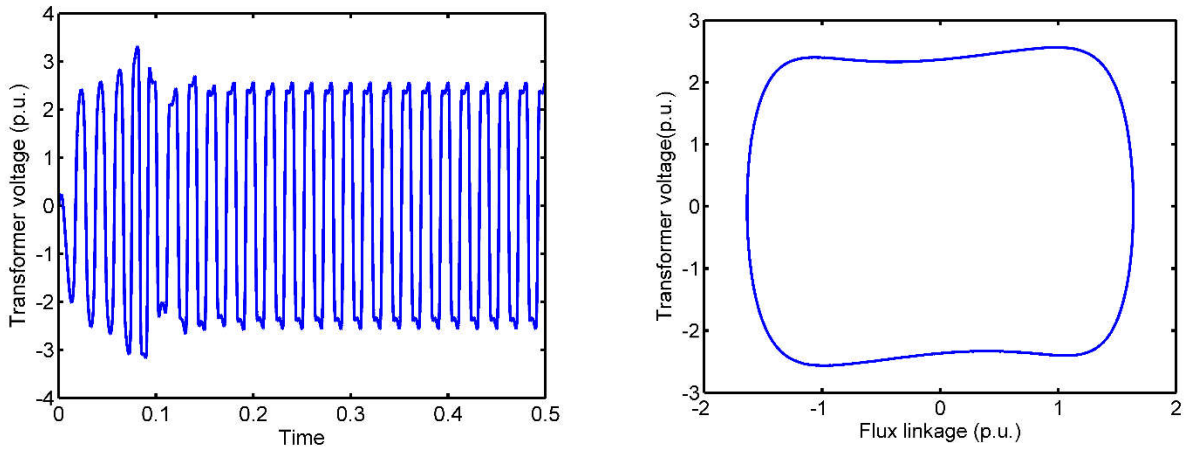

(a) **(b)**

Fig. 7.3. Transformer voltage (a) and Phase plane plot (b) after ferroresonance

Further increases in the supply voltage show a kind of deformation first and then the creation of a loop in the phase plane diagram. This is shown in Fig. 7.4 and 7.5 with 3.93 p.u. and 6.24 p.u. supply voltage respectively. The existence of period-2 oscillation can be observed from 5.90 p.u. supply voltage (Fig. 7.6). Period-4 and period-8 oscillation can be observed at 6.08 p.u. and 6.13 p.u. supply voltage respectively. These are shown in Fig. 7.7 and 7.8. Ultimately at 6.51 p.u. supply voltage the phase plane plot shows a very clumsy output as shown in Fig. 7.9. This can be the chaotic output. For further investigation, the Poincare plot is created and discussed in the next section.

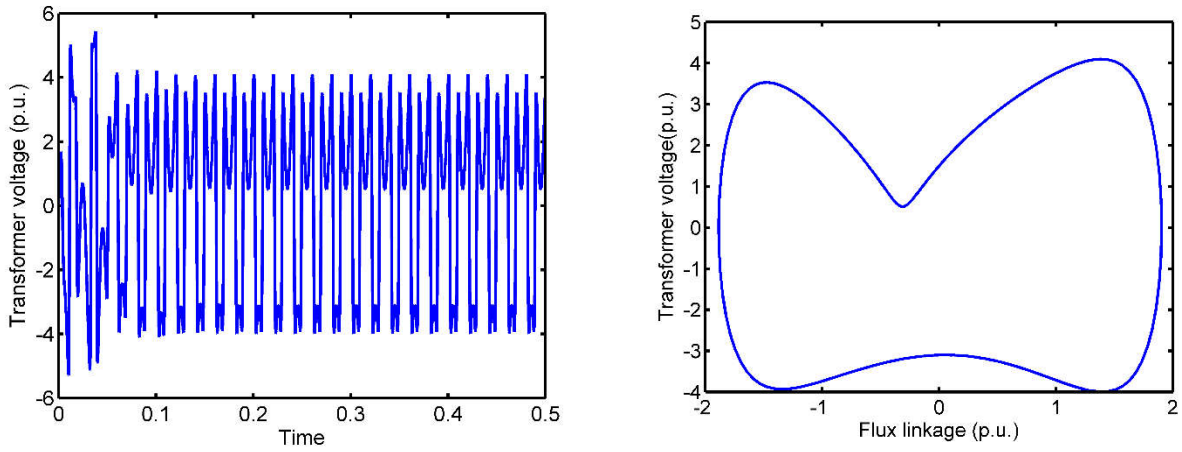

(a) **(b)**

Fig. 7.4. Transformer voltage (a) and Phase plane plot (b) at 3.93 p.u. supply voltage

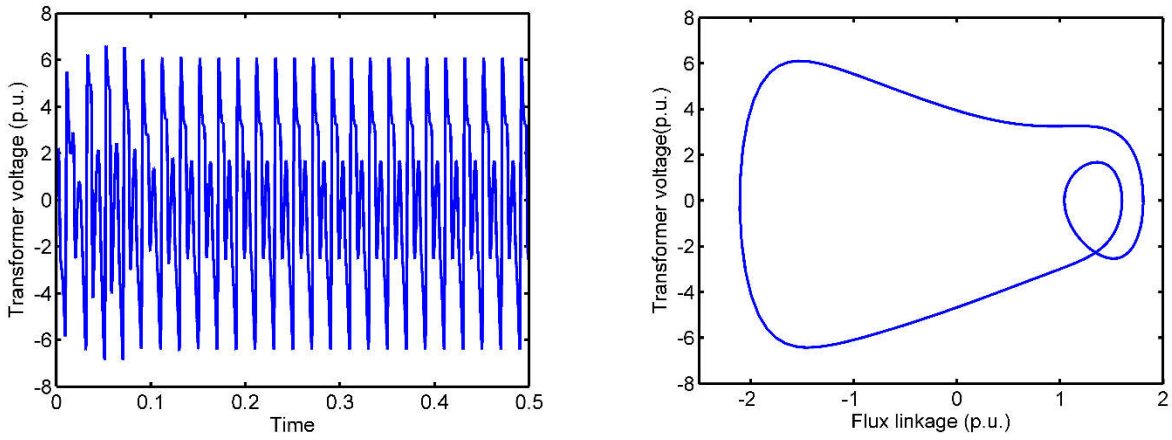

(a) **(b)**

Fig. 7.5. Transformer voltage (a) and Phase plane plot (b) at 5.24 p.u. supply voltage

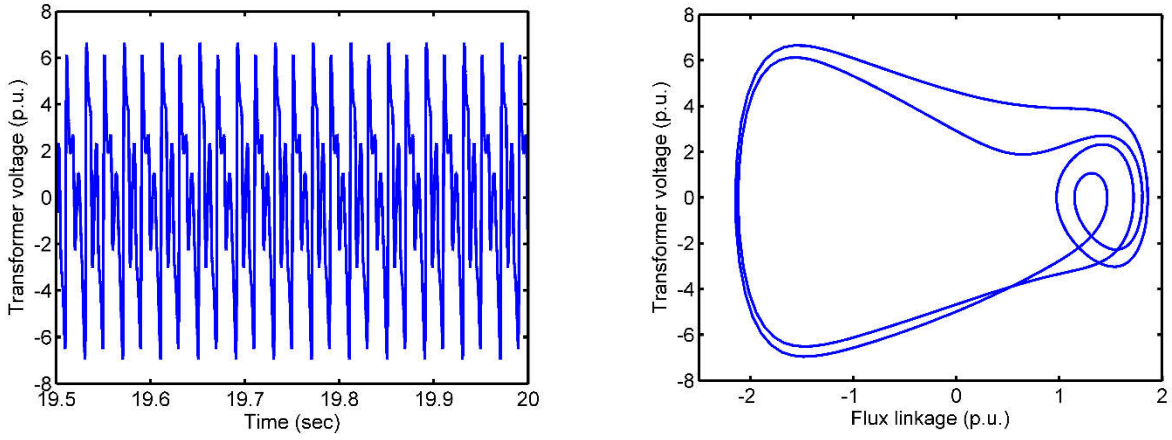

(a) **(b)**

Fig. 7.6. Transformer voltage (a) and Phase plane plot (b) at 5.90 p.u. supply voltage

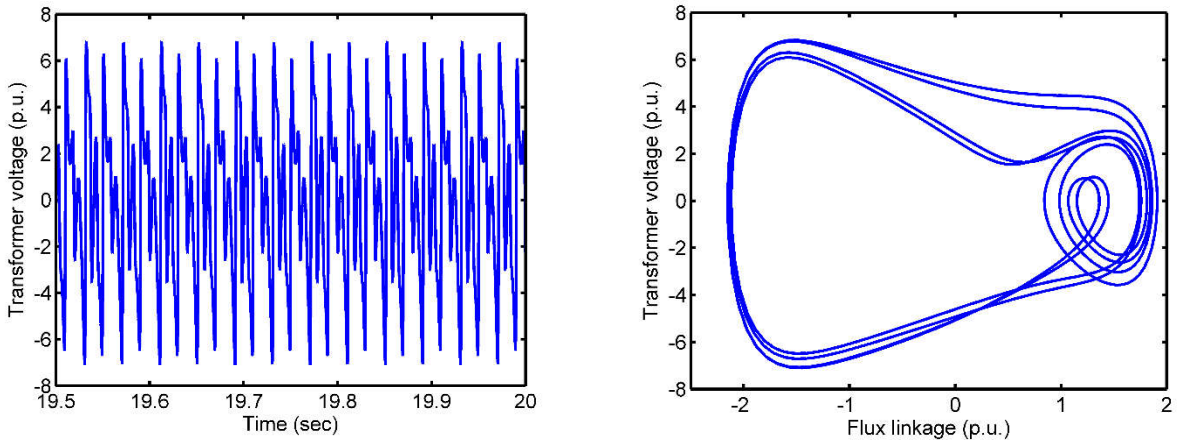

(a) **(b)**

Fig. 7.7. Transformer voltage (a) and Phase plane plot (b) at 6.08 p.u. supply voltage

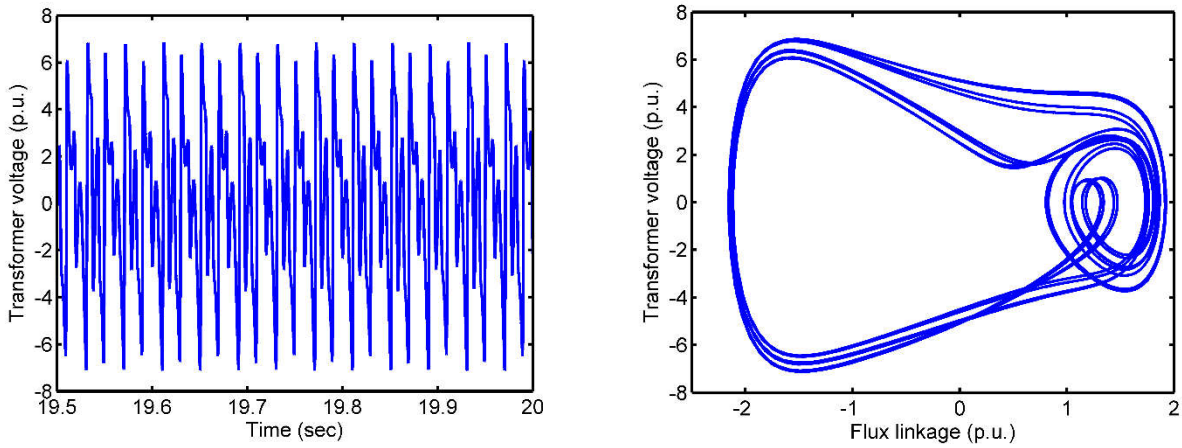

(a) **(b)**

Fig. 7.8. Transformer voltage (a) and Phase plane plot (b) at 6.13 p.u. supply voltage

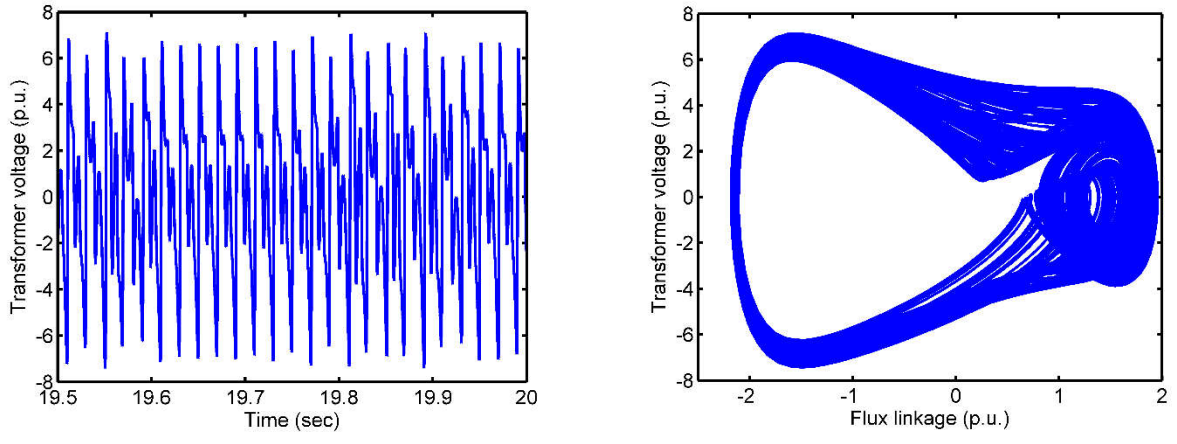

(a) **(b)**

Fig. 7.9. Transformer voltage (a) and Phase plane plot (b) at 6.51 p.u. supply voltage

7.3 Poincare Plot

To determine the Poincare Map for the system, the flux linkage is plotted against the transformer voltage at a regular interval [82]. The interval is taken as the time period of the supply voltage. Fig. 7.10 shows the data collection process for the Poincare plot. From the flux linkage and transformer voltage waveform data has been collected at 20 ms intervals. Those data are shown as red bubbles in Fig. 7.10 (a) and (b). Now the sampled data thus obtained is plotted on a graph with flux linkage along the x-axis and transformer voltage along the y-axis.

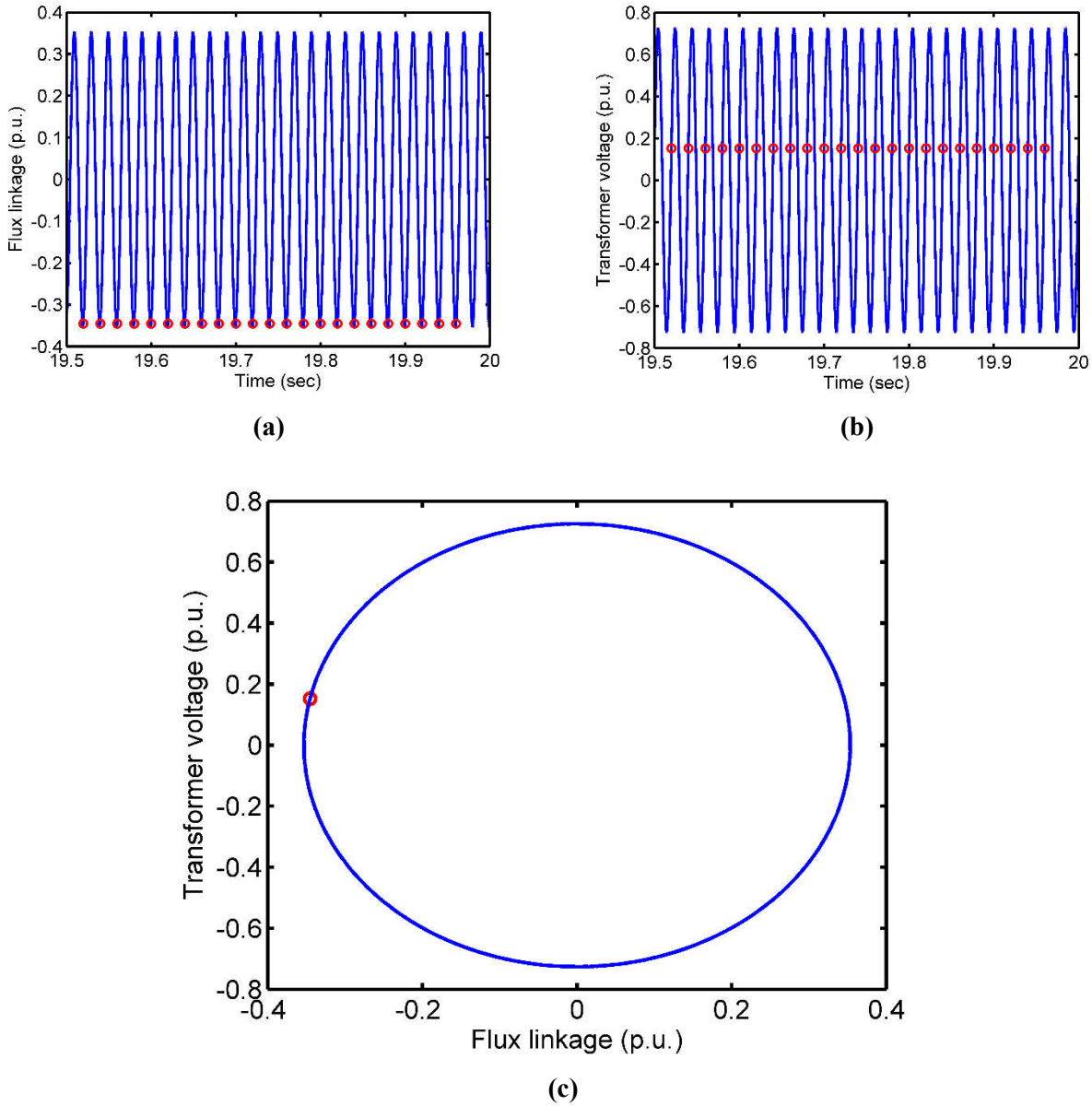

Fig. 7.10. Finding the Poincare plot for 0.66 p.u. supply voltage

Fig. 7.10 (c) shows the phase plane plot along with the Poincare plot at 0.66 p.u. supply voltage. It appears as a single point on the phase plane. That means after each cycle of the supply voltage, the system returns to the previous values of flux linkage and transformer voltage.

Thus the Poincare Plot can be viewed as the fixed point representation of the limit cycle. The tendency of the fixed point to return to its earlier value will establish a stable limit cycle.

In this way, the Poincare plots can be obtained for different supply voltages. A single point was observed in the Poincare section until at a supply voltage of 5.68 p.u., where the Poincare plot shows two points instead of one (Fig. 7.11).

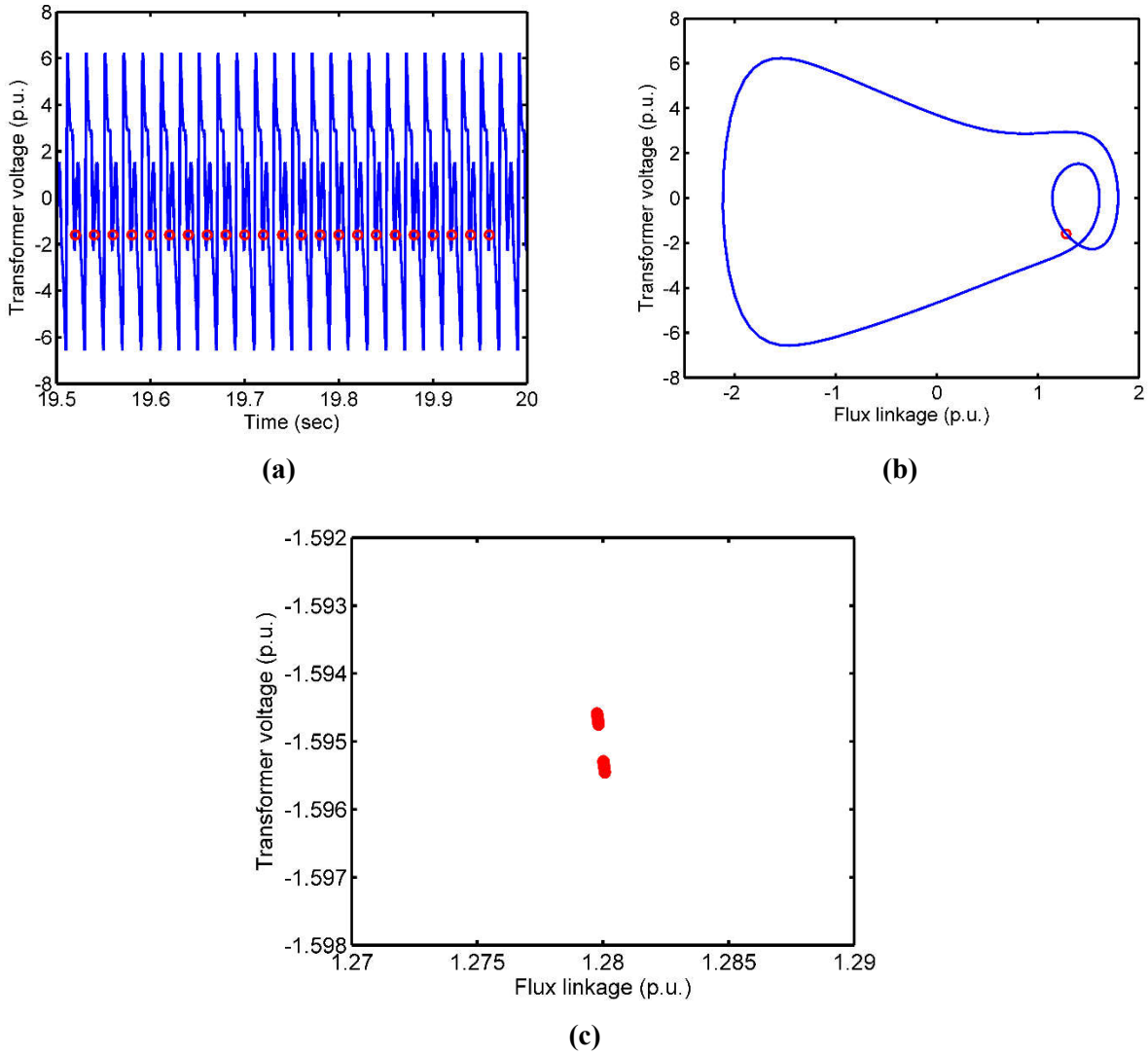

Fig. 7.11. Transformer voltage (a) Phase plane plot (b) and Poincare plot (c) at 5.68 p.u. supply voltage

However, it is very difficult to identify from the transformer waveform or phase plane plot as the two Poincare points are very close to each other. The change was prominent at 5.90 p.u. supply voltage (Fig. 7.12). The Poincare plots show the clear existence of period-2 orbits. The limit cycle shows two notable loops. Four and eight distinguished Poincare points can be observed at 6.08 and 6.13 p.u. supply voltages (Fig. 7.13 and 7.14). Fig. 7.15 shows a very strange behavior of the Poincare plot. It is haphazard and does not follow any trend. This observation can be termed a strange attractor. This suggests that the system enters into a chaotic mode. The transformer voltage waveform and the limit cycle also establish this fact.

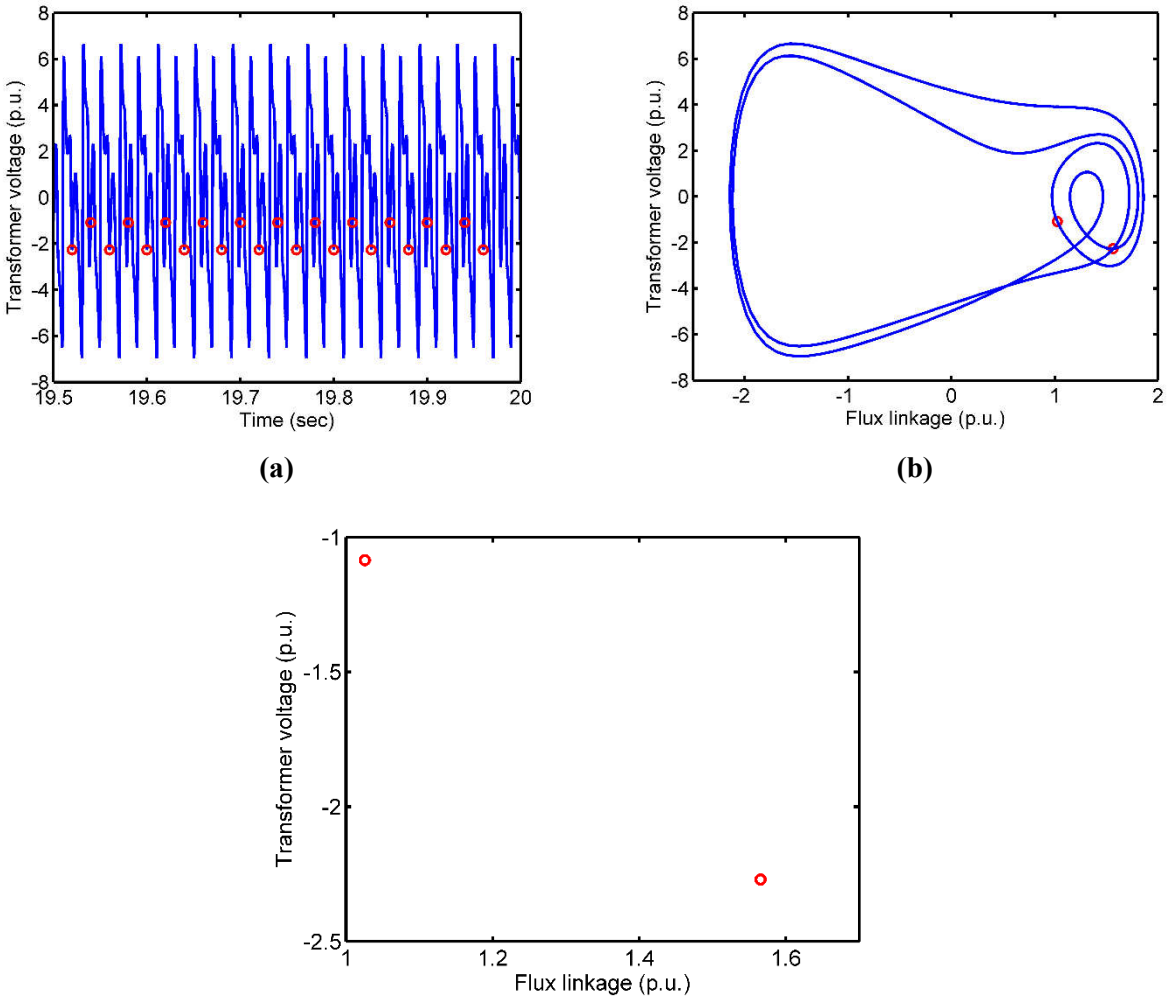

Fig. 7.12. Transformer voltage (a) Phase plane plot (b) and Poincare plot (c) at 5.90 p.u. supply voltage

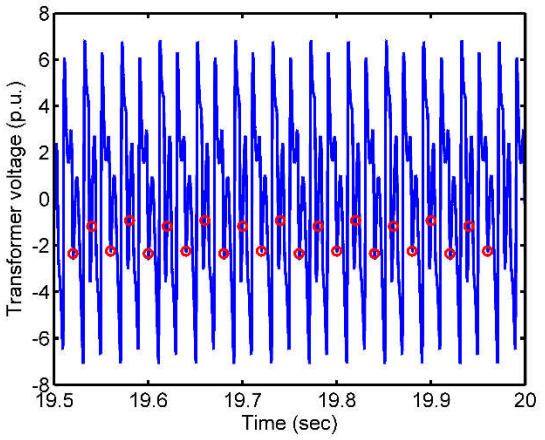

(a)

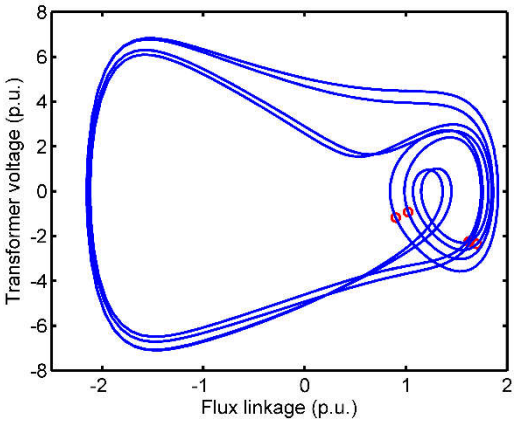

(b)

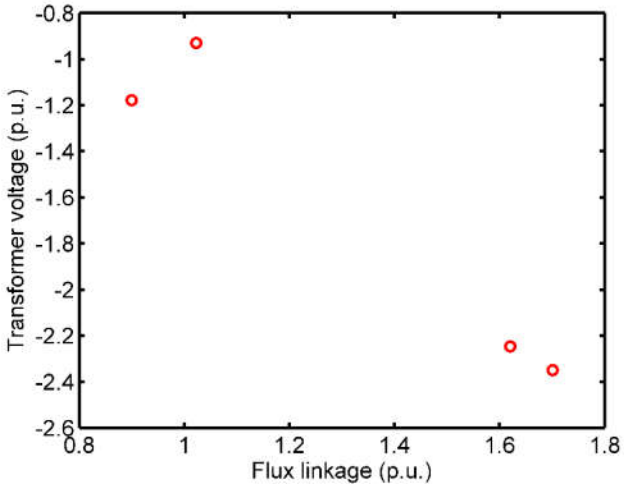

(c)

Fig. 7.13. Transformer voltage (a) Phase plane plot (b) and Poincare plot (c) at 6.08 p.u. supply voltage

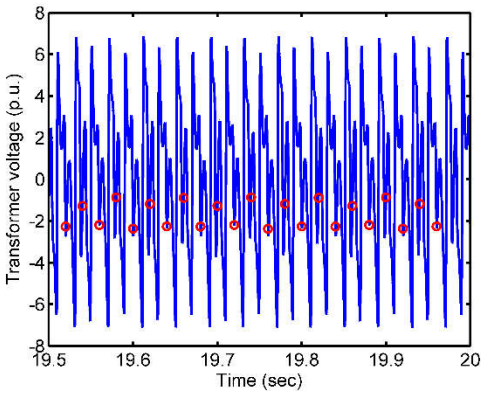

(a)

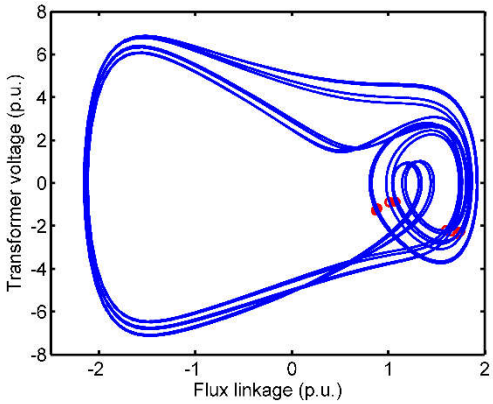

(b)

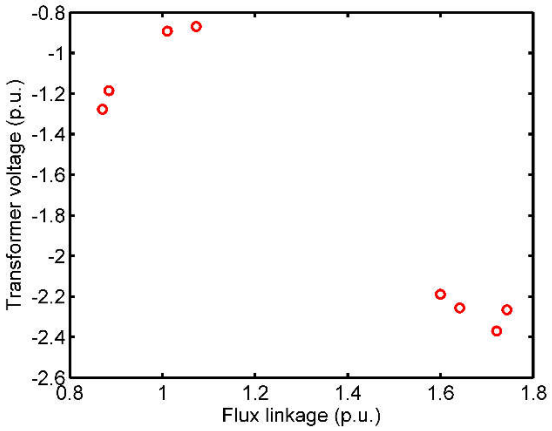

(c)

Fig. 7.14. Transformer voltage (a) Phase plane plot (b) and Poincare plot (c) at 6.13 p.u. supply voltage

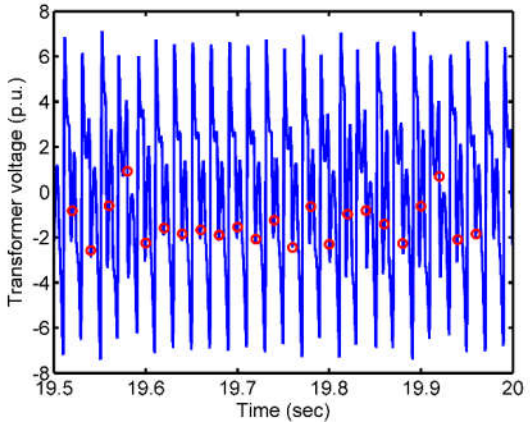

(a)

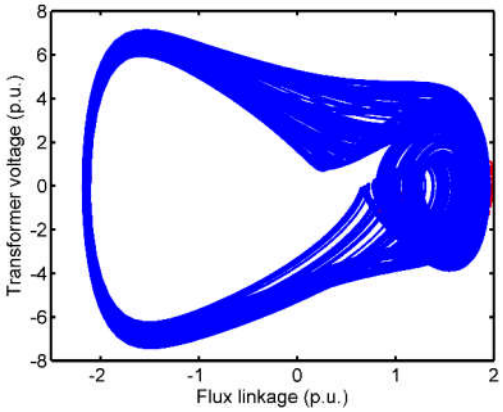

(b)

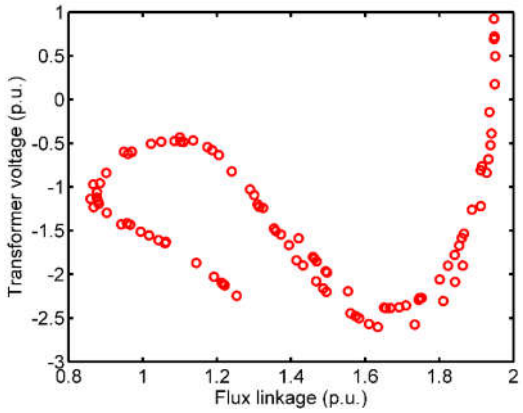

(c)

Fig. 7.15. Transformer voltage (a) Phase plane plot (b) and Poincare plot (c) for 6.51 p.u. supply voltage

All the above Poincare observations indicate that the system experienced several changes in its stability while the supply voltage was increased gradually. This can be considered as bifurcation. To capture this transition graphically, the help of bifurcation diagram has been taken.

7.4 Bifurcation Plot

To obtain the bifurcation diagram, flux linkage is taken as the bifurcation parameter. For a particular supply voltage, the flux linkage values are sampled at a specific interval. Then all the sampled values are plotted with supply voltage along the x-axis and flux linkage along the y-axis. It will appear as a single point or several points along a line parallel to the y-axis. Next, a higher supply voltage value is chosen and corresponding sampled flux linkage values are plotted on the same graph. The methods are repeated for several supply voltage values. Fig. 7.16 shows the bifurcation diagram with supply voltage as the variable parameter.

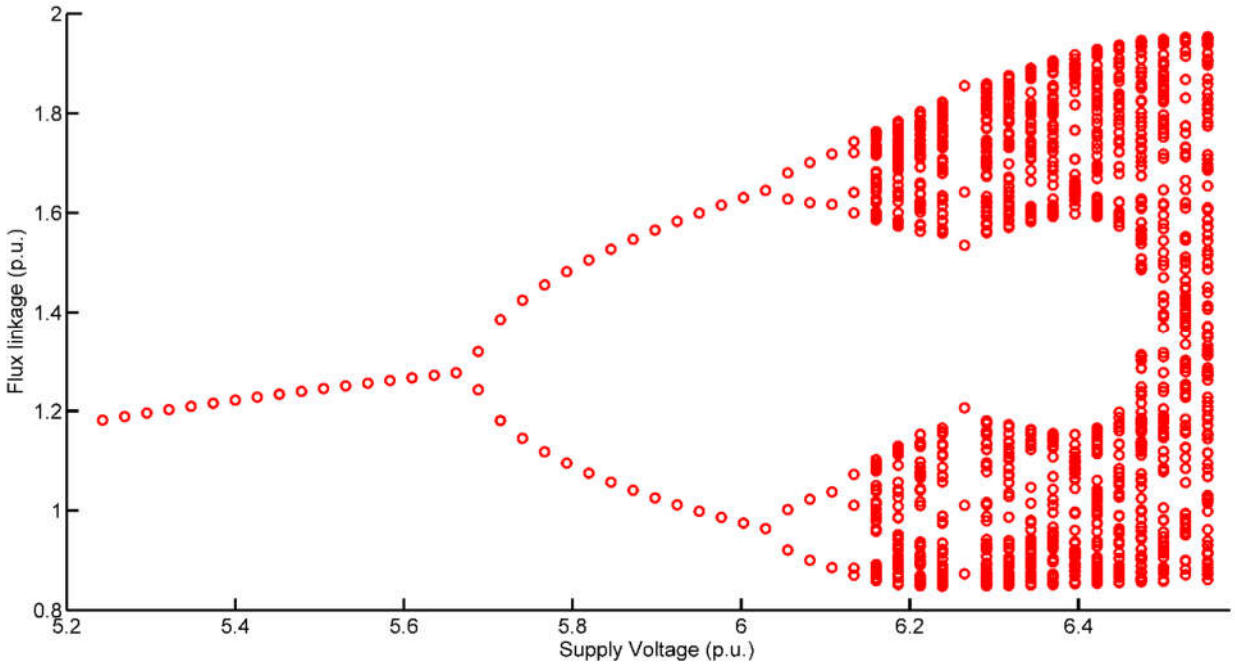

Fig. 7.16. Bifurcation plot

Fig. 7.16 shows single Poincare plots for initial supply voltages. Suddenly from the 5.67 p.u. supply voltage two Poincare plots started to appear per voltage. Then again from 6.03 p.u. supply voltage each branch creates two new branches. These 4 branches again bifurcate near 6.11 p.u. supply voltage. These bifurcation continues. However, it becomes difficult to identify

the Poincare plots because of the precision of the plots created. After 6.5 p.u. supply voltage almost continuous spectrum was observed. We can say that the system undergoes several period-doubling and in the end it reaches chaos. A similar bifurcation diagram also can be seen in earlier literature [8]. The analysis of the bifurcation plot is done in the next sections.

7.5 Chaos

With the increase of the supply voltage, the Poincare plot shows more fixed point generation. Fig. 7.13 and 7.14 shows the Poincare plot for period 4 and period 8. At a very high value, there appears a haphazard pattern confined in a region of the phase-plane. This is called the strange attractor (Fig 7.15) which indicates the existence of chaos. The corresponding phase-plane plot is displayed in Fig. 7.15 (b).

Fig. 7.17 to 7.19 displays the transformer voltage, capacitor voltage and flux linkage variation with time at chaotic mode. In all the cases the system was made to run for at least 20 sec and the output of the last 0.5 sec was shown. This has been done to avoid the initial transient and to capture the steady-state response.

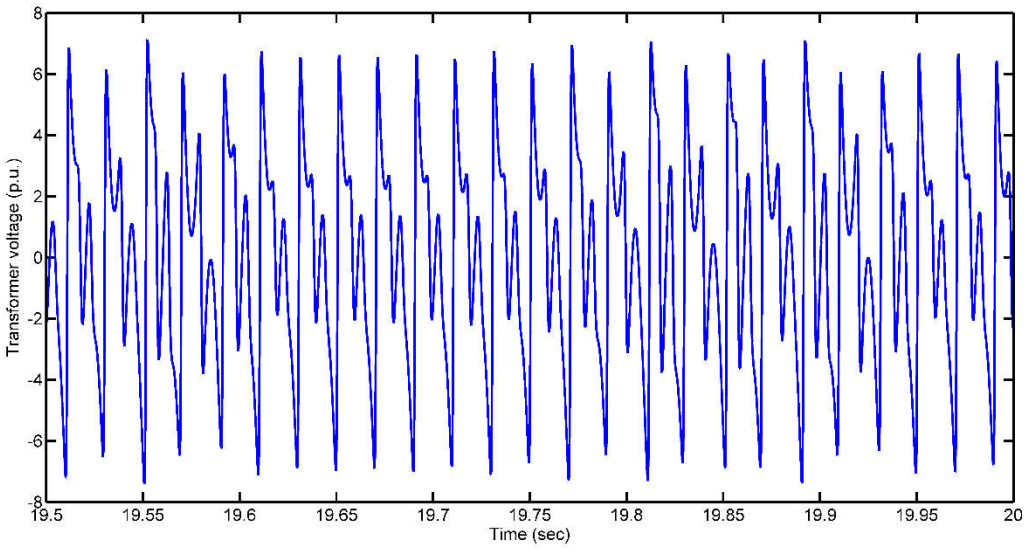

Fig. 7.17. Transformer voltage at chaos

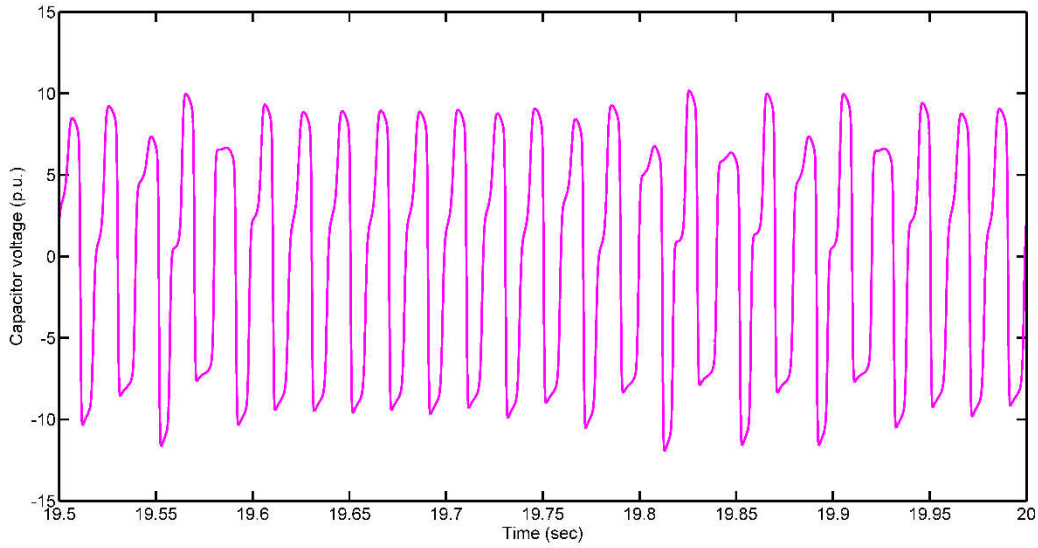

Fig. 7.18. Capacitor voltage at chaos

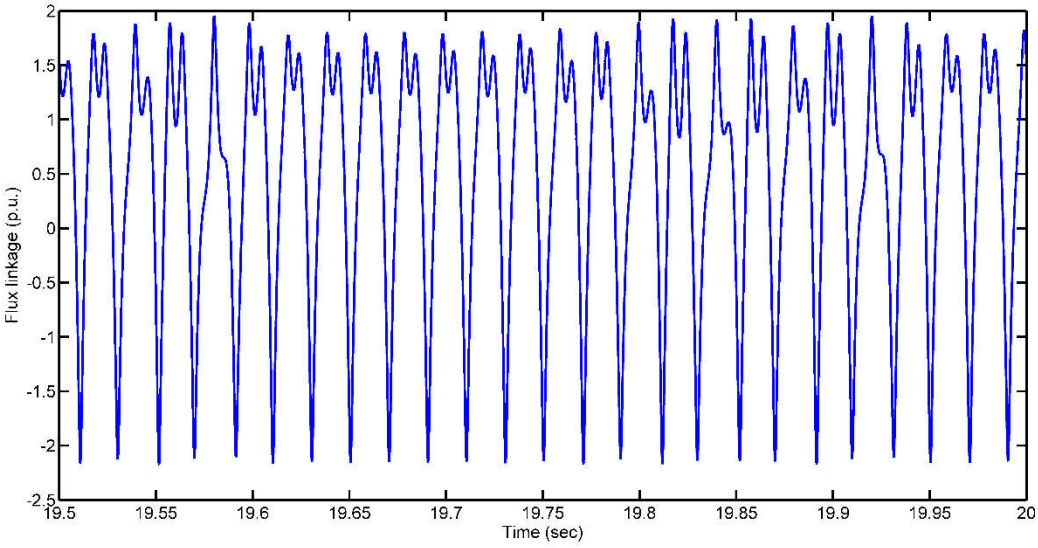

Fig. 7.19. Flux linkage at chaos

The spacing between period-doubling transitions becomes rapidly smaller as the order of the transition increases. Let us define E_n to be the value of the supply voltage at which the transition to period 2n occurs. The decrease of the occurrence gap between two successive bifurcations can be described by the Feigenbaum constant [84]

$$\delta_n = \frac{E_n - E_{n-1}}{E_{n-1} - E_n} \qquad (7.3)$$

The value of δ_n is nearly 4.669. For period 2 transition, our system gives

$E_1 = 5.69$ p.u.

$E_2 = 6.04$ p.u.

$E_3 = 6.12$ p.u.

Thus from (7.3)

$\delta_2 = 4.5$

This value of δ is very close to the Feigenbaum constant. The successive constants can also be calculated from more precise plot settings.

7.6 Bifurcation Plot with Capacitance as a Parameter

Next in our study, we consider series capacitance as the bifurcation parameter. For that, a supply voltage is taken, and then for a fixed capacitor value, flux linkage is sampled at a regular interval. All these sampled values are then plotted on a graph against that capacitor value. These processes are repeated for several capacitance values, and in each case, the sampled flux linkage values are plotted on the same graph.

For lower values of supply voltages, no significant bifurcation was observed with the capacitor as the bifurcation parameter. For example at 1.31 p.u. supply voltage the following bifurcation diagram shown in Fig. 7.20 was obtained when series capacitance was varied from 1 to 10 μF.

Output at 2.62 p.u. supply voltage is shown in Fig. 7.21 below. It shows period-3 oscillation between 2 to 6 μF. Some known period-doubling bifurcation is observed at 5.90 p.u. supply voltage (Fig. 7.22). But here period doubling bifurcation, instead of cascading further, it returned to period-1 oscillation at a higher value of the capacitance. A prominent period doubling is observed at 6.22 p.u. supply voltage (Fig. 7.23). The system shows a cascade period doubling at a lower value of capacitance. It ultimately reaches chaos at 1.5 μF. After that with further increase of the capacitance, system falls back from chaos to period-1 oscillation. However, it takes a longer time to reach from period-2 to period-1 oscillation.

The chaotic region widens further at supply voltage 6.55 p.u. Fig. 7.24 shows a bifurcation plot for capacitance values up to 1 μF. This gives a clear idea of how the system

enters into chaos through a period-doubling bifurcation. Fig. 7.25 shows bifurcation plot up to 5 μF. This shows that the system returns to period-1 by following the reverse steps from chaos.

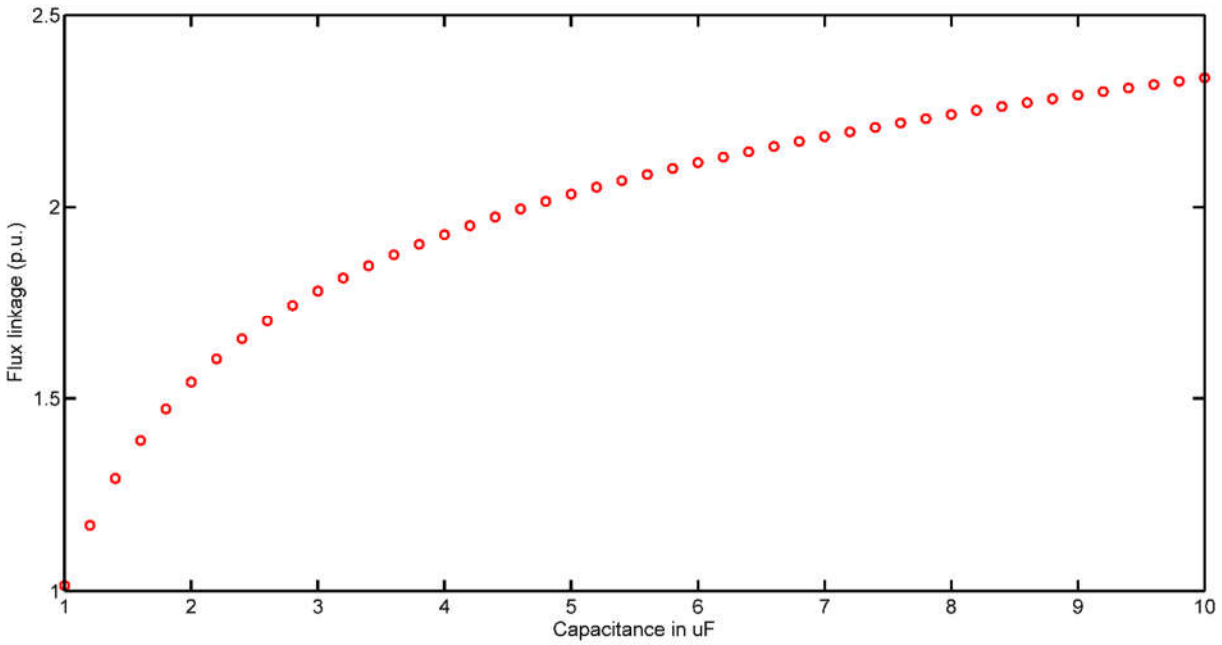

Fig. 7.20. Bifurcation plot with supply voltage 1.31 p.u.

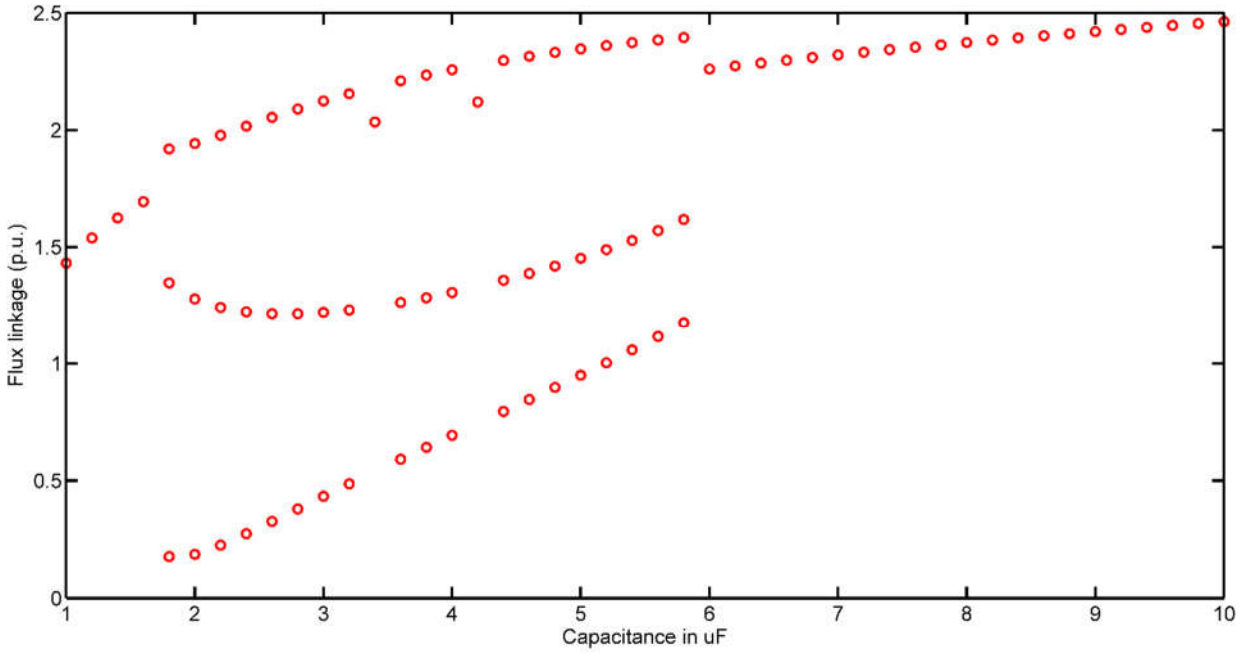

Fig. 7.21. Bifurcation plot with supply voltage 2.62 p.u.

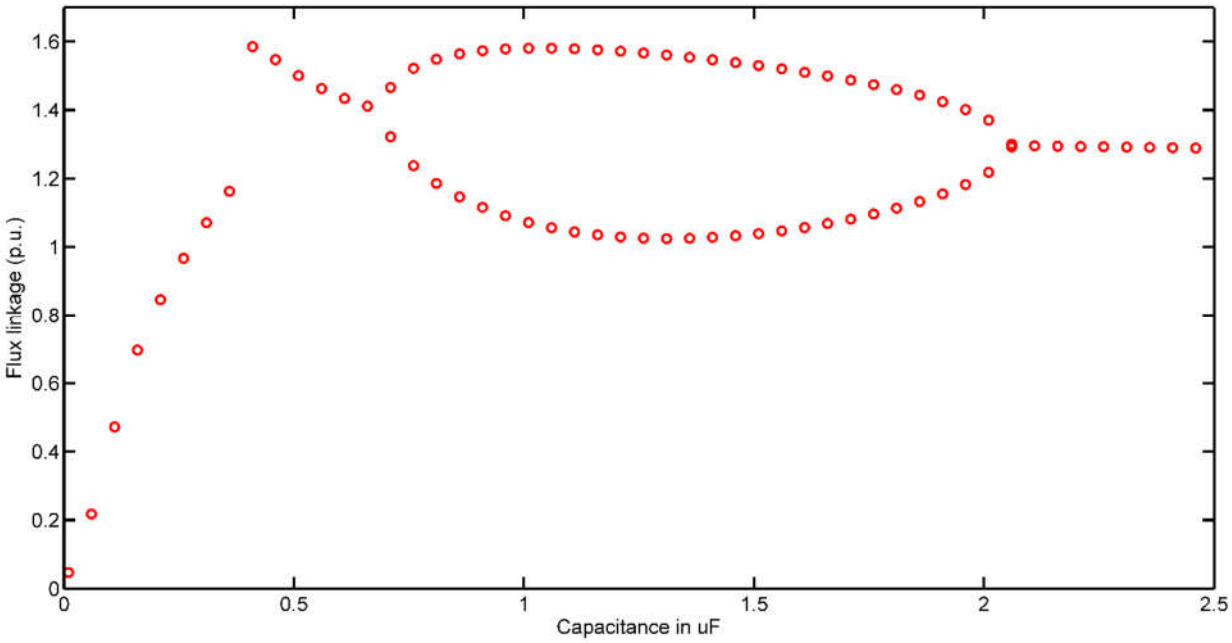

Fig. 7.22. Bifurcation plot with supply voltage 5.90 p.u.

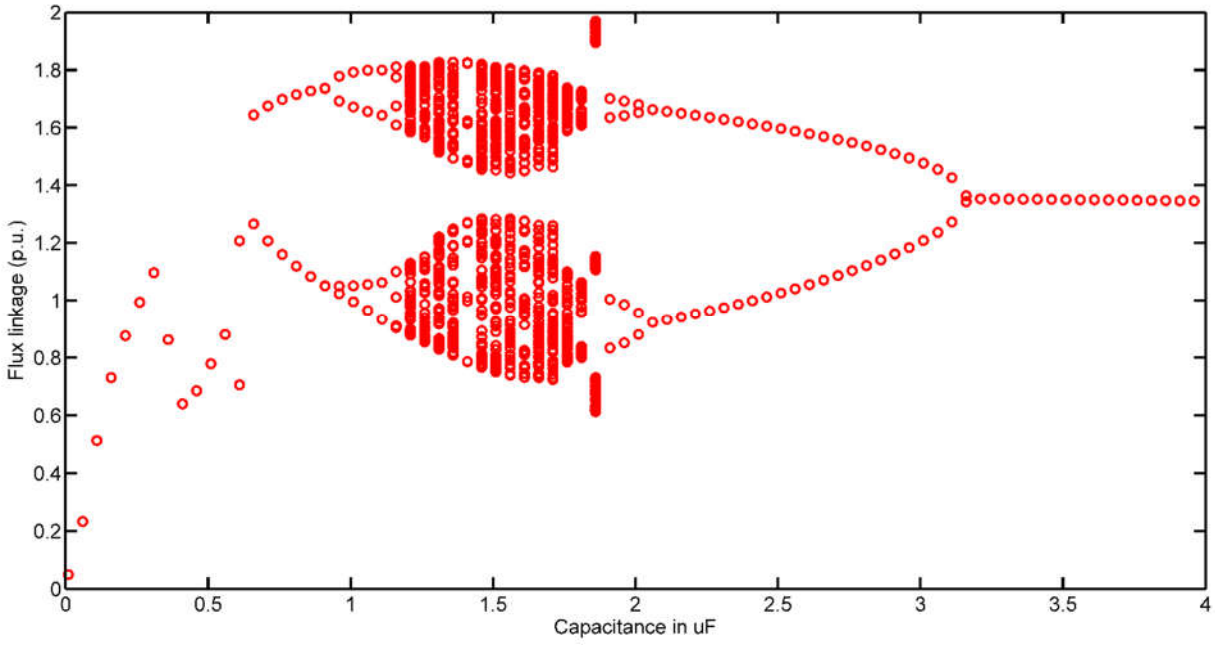

Fig. 7.23. Bifurcation plot with supply voltage 6.22 p.u.

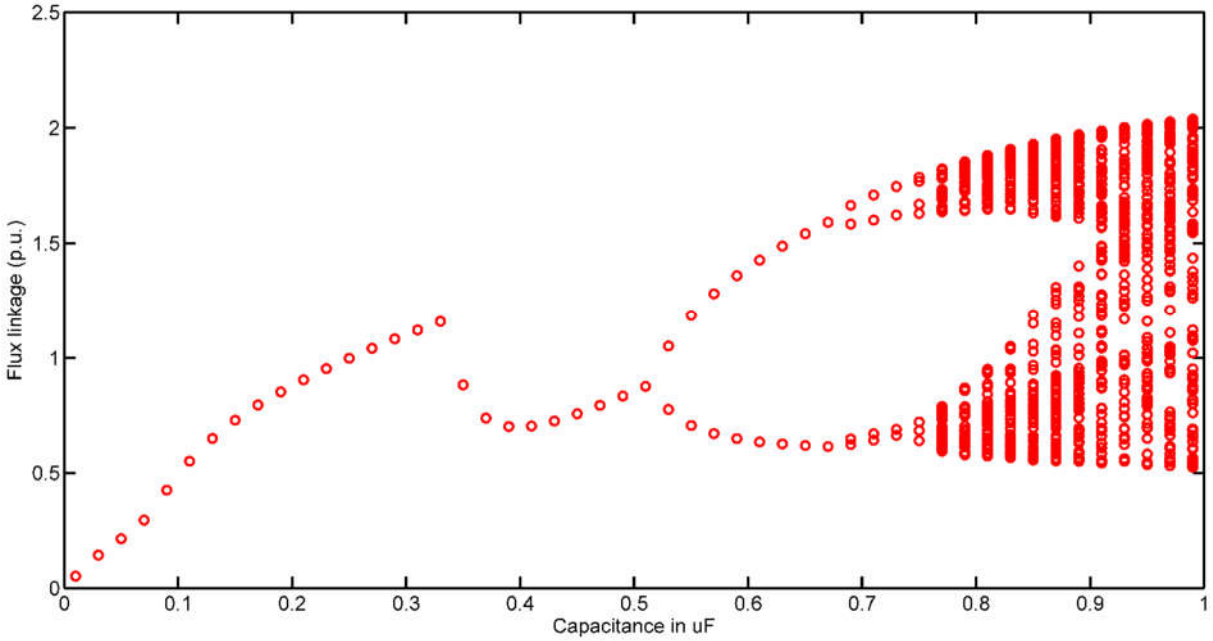

Fig. 7.24. Bifurcation plot with supply voltage 6.55 p.u. up to 1 μF

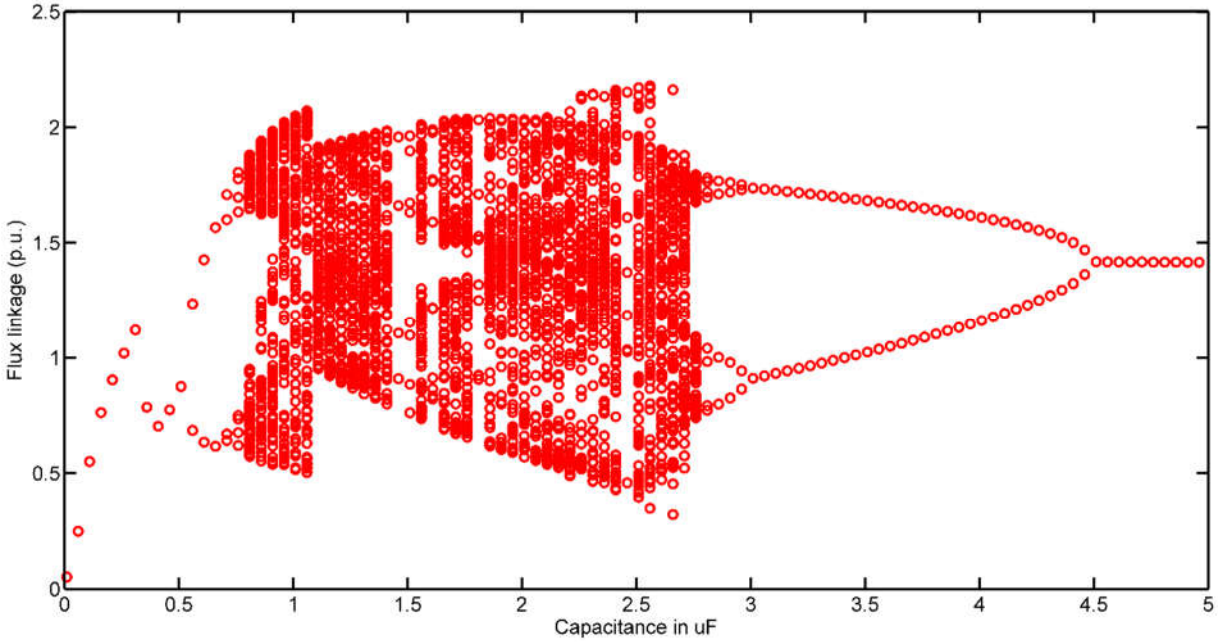

Fig. 7.25. Bifurcation plot with supply voltage 6.55 p.u. up to 5 μF

7.7 Summary

The ferroresonance model of the transformer is examined under the variation of the supply voltage. To find the stable point, the Poincare method is used. The model under consideration shows a period-doubling bifurcation and then a chaotic behaviour at a very high value of supply voltage. Since at ferroresonance, the system oscillates with a voltage up to 4 to 5 times the rated value and current up to 8 to 9 times the rated value, it is difficult to re-establish the process in the laboratory environment. So only verification of the results discussed in this chapter is possible with another analytical method. In the next chapter, the stability analysis method with the Jacobian matrix and corresponding Eigenvalues is attempted.

8. Verification of Period-Doubling Behavior of Ferroresonance Circuit with the Jacobian Matrix and Eigenvalues

8.1 Period Doubling Bifurcation

The generation of the bifurcation diagram is discussed in the previous chapter. A closer look (Fig. 8.1) in the bifurcation diagram reveals that as the value of supply voltage increases, the system bifurcates near 5.68 p.u. supply voltage. Before bifurcation, the system had one stable point. But after bifurcation there appeared two stable points. This transition from period-T solution orbit to 2T-period solution is known as a period-doubling bifurcation [80]. This chapter uses a perturbation method to check how and when the system is losing its period-1 stability and enters into the period-2 region. In this method, a small deflection in the circuit parameter is injected intentionally for a very small amount of time. If the system returns to its original limit cycle, then the system will be called stable, otherwise unstable. Two regions were chosen, one from period-1 oscillation and another from period-2 oscillation for analysis.

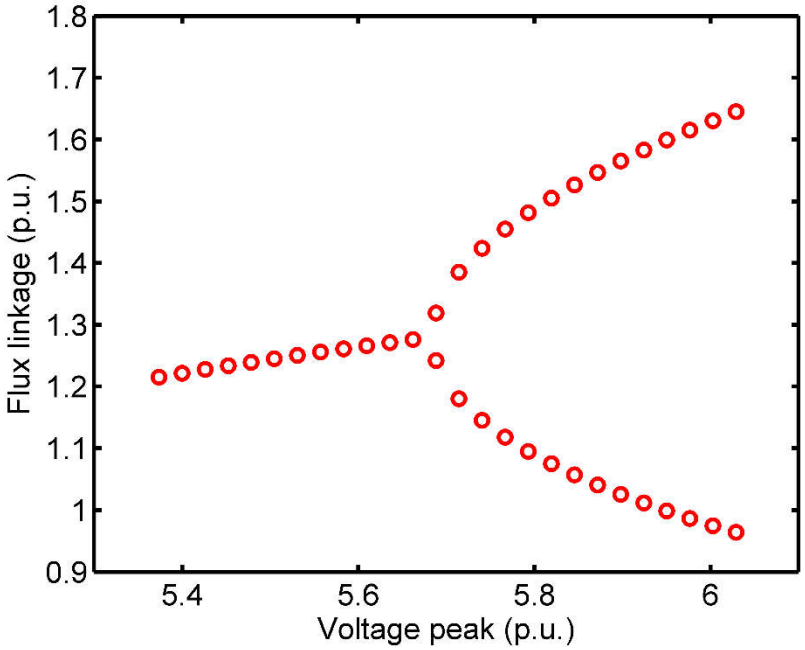

Fig. 8.1. Bifurcation plot – first period double

8.2 Stability Analysis in Period-1 Region

To analyze the stability of the system in the period 1 region, a pulse disturbance is applied to the flux linkage for a duration of 10 s (approx.) while the system was operating in a steady state with a supply voltage of 5.67 p.u. The phase plane diagram and Poincare section before and after the disturbance are shown in Fig 8.2 and 8.3 respectively.

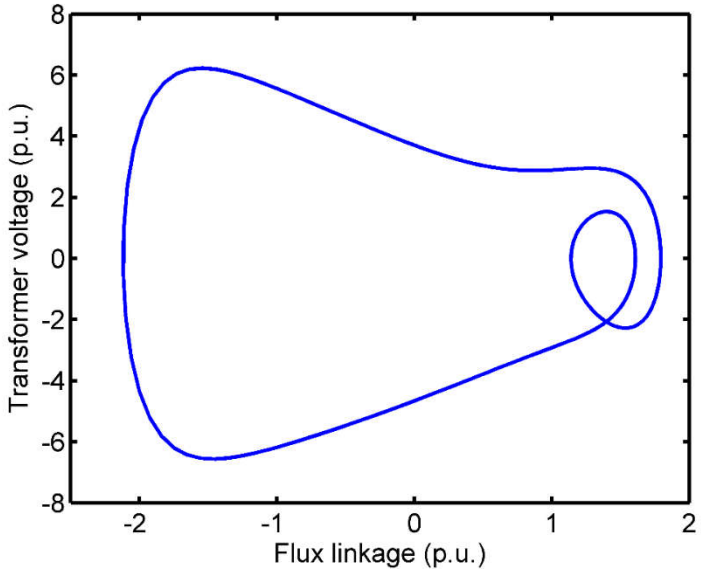

(a)

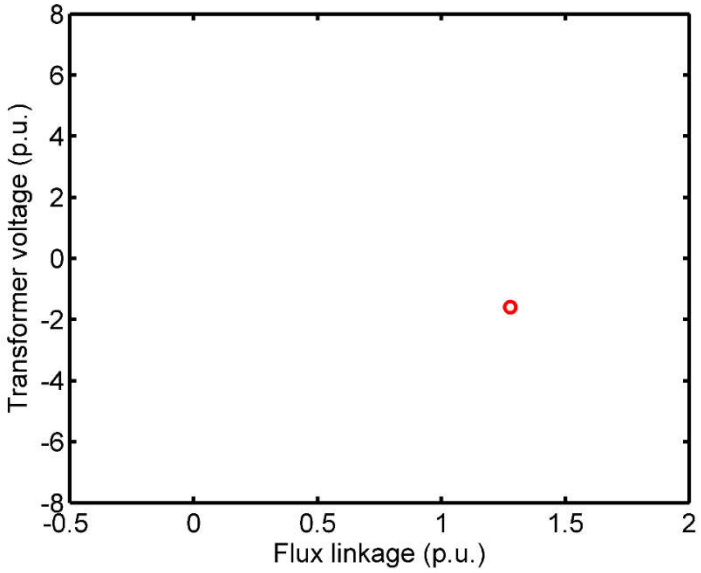

(b)

Fig. 8.2. (a) Phase plane and (b) Poincare plot for period-1 without disturbance at 5.67 p.u. supply voltage

From the phase plane and Poincare plot, it can be declared that the fixed point is stable as the system dynamics iterates back to its original value. Fig 8.4 shows the variation of flux linkage before and after the perturbation is applied. Before the deflection was produced, the flux linkage was single-valued. After the deflection, after some fluctuations, it slowly tends to a single value again.

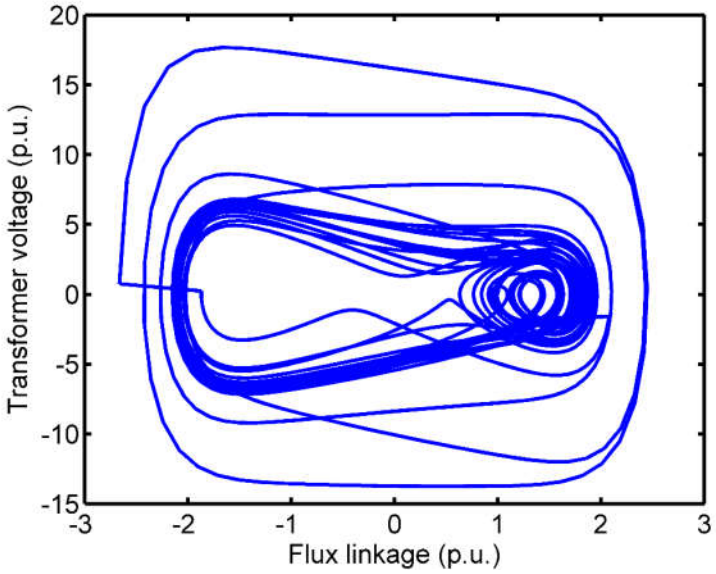

(a)

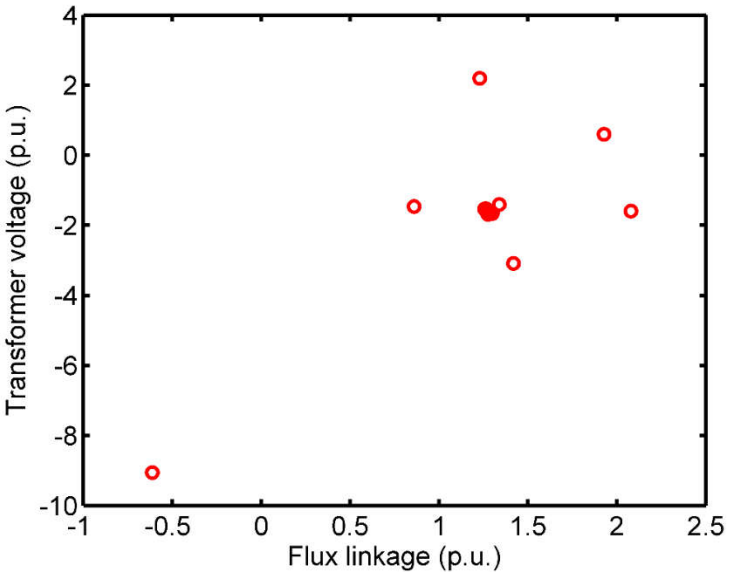

(b)

Fig. 8.3. (a) Phase plane and (b) Poincare plot for period-1 with disturbance at 5.67 p.u. supply voltage

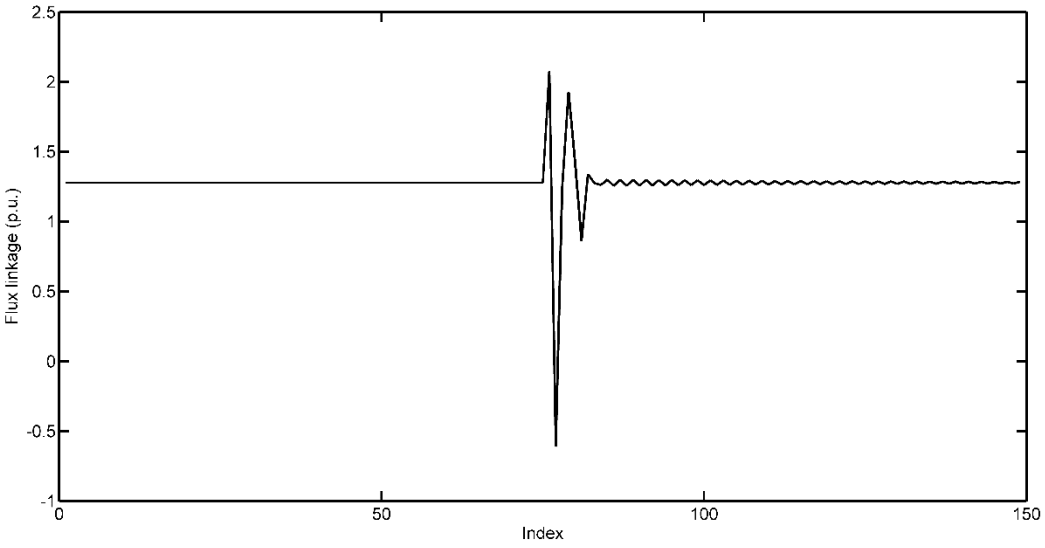

Fig. 8.4. Flux linkage before and after deflection at 5.67 p.u. supply voltage

Now, for mathematical calculation, it is required to linearize the system near the perturbation point [79]. Sample data for the two state variables flux linkage and transformer voltage are collected near the zone of perturbation. Sampled points are shown in Table 8.1.

Table 8.1. Sampled state variables under period one orbit

Sample No.	Flux linkage p.u. (X)		Transformer voltage p.u. (Y)	
1	2.07927671	= X1	-1.594282704	= Y1
2	-0.612320495	= X2	-9.051427855	= Y2
3	1.228435587	= X3	2.195326068	= Y3
4	1.927391217	= X4	0.600884605	= Y4
5	1.418744493	= X5	-3.086420391	= Y5
6	0.859506257	= X6	-1.462468601	= Y6
7	1.33854273	= X7	-1.399784538	= Y7
8	1.275014575	= X8	-1.685345435	= Y8
9	1.261568262	= X9	-1.522394629	= Y9
10	1.298825601	= X10	-1.661162055	= Y10
11	1.255304395	= X11	-1.532163542	= Y11

Table 8.1. Sampled state variables under period one orbit (Contd.)

Sample No.	Flux linkage p.u. (X)		Transformer voltage p.u. (Y)	
12	1.2998043	= X12	-1.656187809	= Y12
13	1.255735244	= X13	-1.535447976	= Y13
14	1.29897871	= X14	-1.653220442	= Y14
15	1.256682894	= X15	-1.538082754	= Y15
..	….	..	….	..
..	….	..	….	..

The first Jacobian matrix J1 is calculated from the first three sets of sampled data (sample no. 1, 2, and 3). Followed by matrix J2 derived from samples no. 2, 3, and 4, and so on for matrices J3, J4 …… …...

For example, from the first three sample data, one can obtain

$$\begin{pmatrix} \mathrm{X2} \\ \mathrm{Y2} \end{pmatrix} = (J1) \begin{pmatrix} \mathrm{X1} \\ \mathrm{Y1} \end{pmatrix} \tag{8.1}$$

$$\begin{pmatrix} \mathrm{X3} \\ \mathrm{Y3} \end{pmatrix} = (J1) \begin{pmatrix} \mathrm{X2} \\ \mathrm{Y2} \end{pmatrix} \tag{8.2}$$

Solving (8.1) and (8.2), the first Jacobian matrix $J1$ will be

$$J1 = \begin{pmatrix} -0.3789 & -0.1101 \\ -4.3153 & 0.0494 \end{pmatrix}$$

Corresponding Eigenvalues will be -0.8865 and 0.5570

Similarly from

$$\begin{pmatrix} \mathrm{X3} \\ \mathrm{Y3} \end{pmatrix} = (J2) \begin{pmatrix} \mathrm{X2} \\ \mathrm{Y2} \end{pmatrix} \tag{8.3}$$

$$\begin{pmatrix} \mathrm{X4} \\ \mathrm{Y4} \end{pmatrix} = (J2) \begin{pmatrix} \mathrm{X3} \\ \mathrm{Y3} \end{pmatrix} \tag{8.4}$$

2nd Jacobian matrix $J2$ is calculated as

$$J2 = \begin{pmatrix} 2.0606 & -0.2751 \\ 1.0495 & -0.3135 \end{pmatrix}$$

Corresponding Eigenvalues will be 1.9321 and -0.1850

After calculating all the Eigenvalues, the average Eigen Values come out as $(0.9703 + 0.0492\mathrm{i})$ with magnitude 0.9716 and $(-0.4889 - 0.0492\mathrm{i})$ with magnitude 0.4914.

As both the magnitudes fall within the unit cycle, as per the stability criteria discussed in Chapter 6, the system can be declared as stable.

8.3 Stability Analysis in Period-2 Region

Now to analyze the stability of the system in the period-2 region, $E = 5.68$ p.u supply voltage is taken. The phase plane and Poincare plots are shown in Fig 8.5 and 8.6 respectively. As the value of E chosen is very close to period-1 oscillation, the period-2 characteristic is not prominent in the limit cycle view (Fig. 8.5). But it can be observed from Poincare view in Fig. 8.6. Poincare plots show two points very close to each other.

A similar kind of pulse disturbance as discussed in the previous section is applied when the system is operating at a steady state for a few seconds. The resultant phase plane diagram and Poincare section of the system are shown in Fig 8.7 and 8.8. From Fig. 8.9 it can be observed that the oscillation of flux linkage value between two fixed points is more prominent after the deflection.

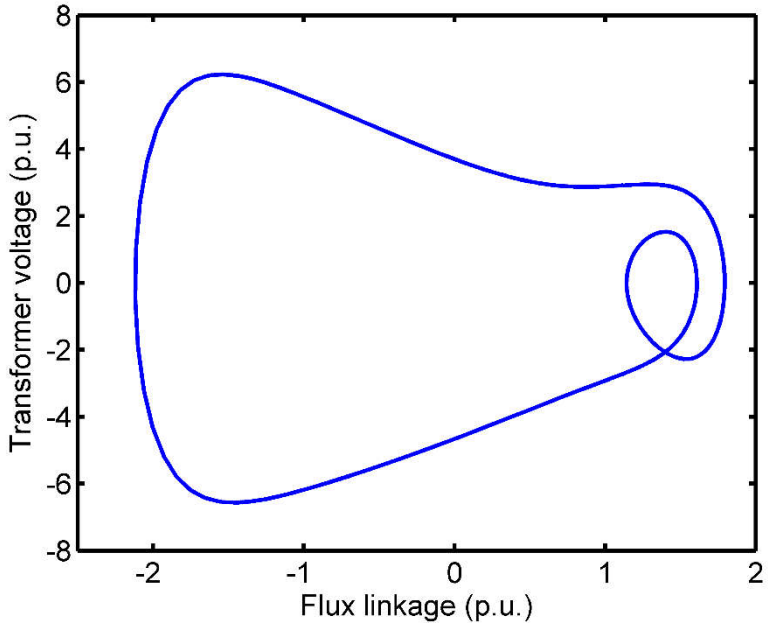

Fig. 8.5. Phase plane plot for period-2 without disturbance at 5.68 p.u supply voltage

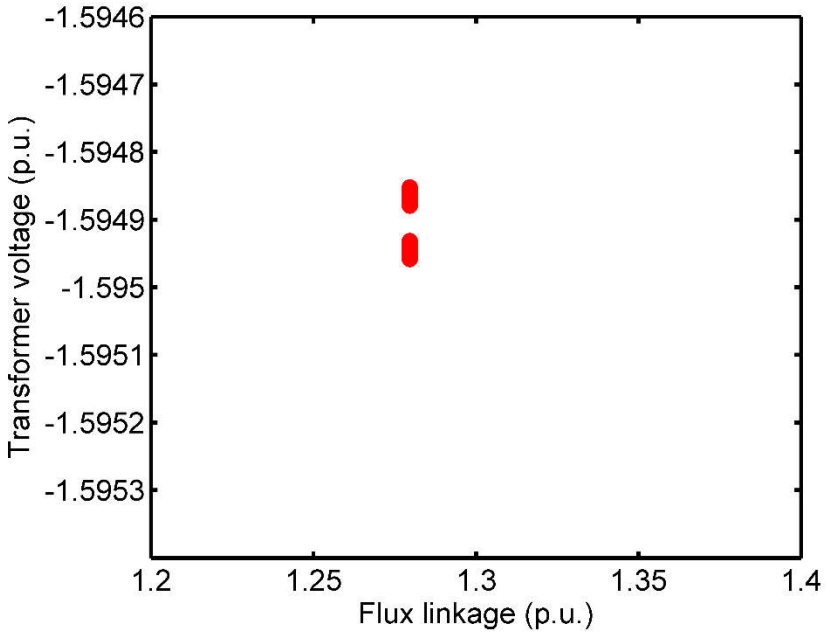

Fig. 8.6. Poincare plot for period-2 without disturbance at 5.68 p.u supply voltage

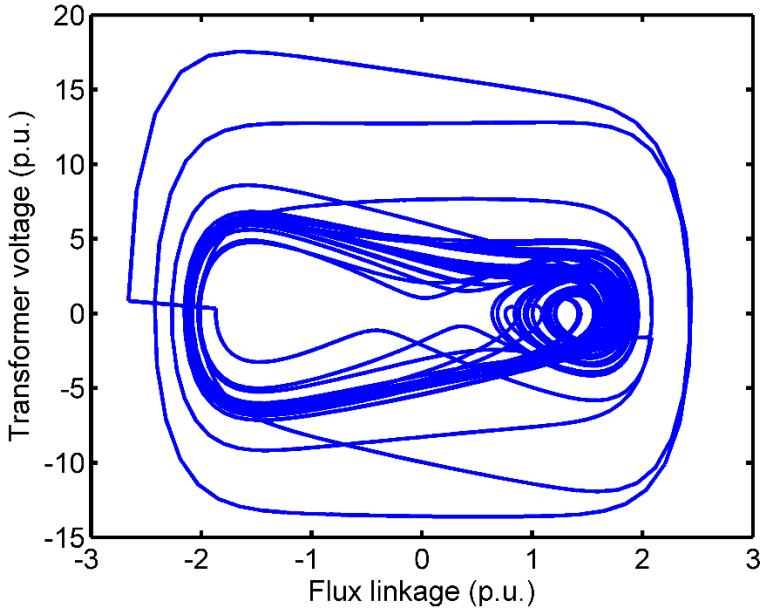

Fig. 8.7. Phase plane plot for period-2 with disturbance at 5.68 p.u supply voltage

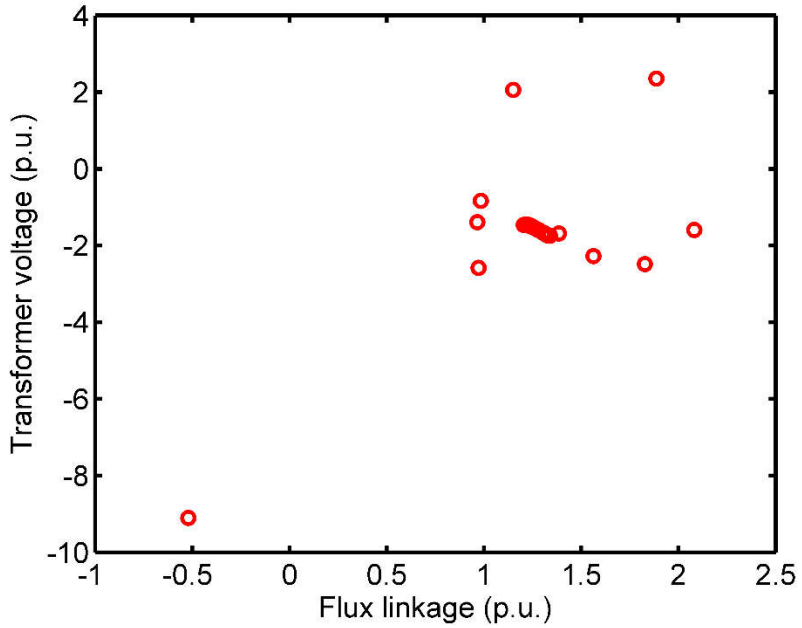

Fig. 8.8. Poincare plot for period-2 with a disturbance at 5.68 p.u supply voltage

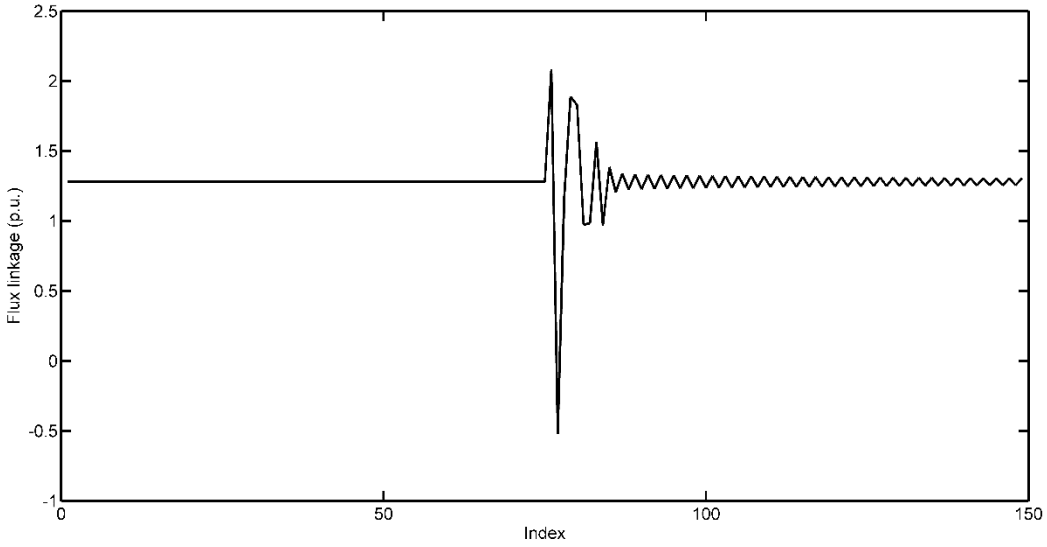

Fig. 8.9. Flux linkage before and after deflection at 5.68 p.u supply voltage

8.3.1 Method 1: Using $x_{(i+1)} = x_i$ and $y_{(i+1)} = y_i$

At first, the numerical analysis of the stability of this fixed point is analyzed with the period-1 assumption that at the fixed point $x_{(i+1)} = x_i$ and $y_{(i+1)} = y_i$.

Sampled sets of state variables are shown in Table 8.2.

Table 8.2. Sampled state variables at 5.68 p.u supply voltage

Sample	Flux linkage p.u. (X)		Transformer voltage p.u. (Y)	
1	2.081102098	= X1	-1.594860753	= Y1
2	-0.520953187	= X2	-9.096901129	= Y2
3	1.150539455	= X3	2.058664022	= Y3
4	1.886833705	= X4	2.35099459	= Y4
5	1.826918684	= X5	-2.483128939	= Y5
6	0.971329085	= X6	-2.580041764	= Y6
7	0.984076893	= X7	-0.832163191	= Y7
8	1.563244769	= X8	-2.272473526	= Y8
9	0.965275802	= X9	-1.389018612	= Y9
10	1.384716974	= X10	-1.686385016	= Y10
11	1.203930223	= X11	-1.462197139	= Y11
12	1.337696864	= X12	-1.741934431	= Y12
13	1.223567095	= X13	-1.455801832	= Y13
14	1.331421156	= X14	-1.740933099	= Y14
15	1.227129305	= X15	-1.459476837	= Y15
..	….	..	….	..
..	….	..	….	..

The Jacobian matrices and corresponding, eigenvalues are derived from the sampled state vectors. For example, from the first 3 samples, the first Jacobian matrix will be

$$J1 = \begin{pmatrix} -0.3327 & -0.1074 \\ -4.3536 & 0.0230 \end{pmatrix}$$

And corresponding Eigenvalues are -0.8614 and 0.5518

From samples no. 2, 3, and 4 the 2nd Jacobian can be obtained as

$$J2 = \begin{pmatrix} 2.0793 & -0.2456 \\ 2.7278 & -0.3825 \end{pmatrix}$$

And corresponding Eigenvalues are 1.7678 and -0.0710

Calculating Jacobian and corresponding all Eigenvalues, the average eigenvalues thus obtained are $(1.9847 + 0.0156i)$ with magnitude 1.9848 and $(-1.7526 - 0.0156i)$ with magnitude 1.7527.

As the magnitudes of both the Eigenvalues are greater than one, as per the criteria discussed in Chapter 6 it can be concluded that the system has lost its period one stability.

To observe the movement of the eigenvalues of the system while increasing the supply voltage gradually near bifurcation, a plot is created as shown in Fig 8.10. Here it is found that all the Eigenvalues fall below the unity line when the supply voltage is smaller than 5.68 p.u. So the system is stable. But the Eigenvalues fall beyond the unity line for supply voltage 5.68 p.u. This suggests the system transforms from period-1 to period-2 oscillation when the supply voltage is around 5.68 p.u. The conversion from period-1 to period-2 oscillation as observed from the Eigenvalue movement map matches the bifurcation diagram (Fig 8.1).

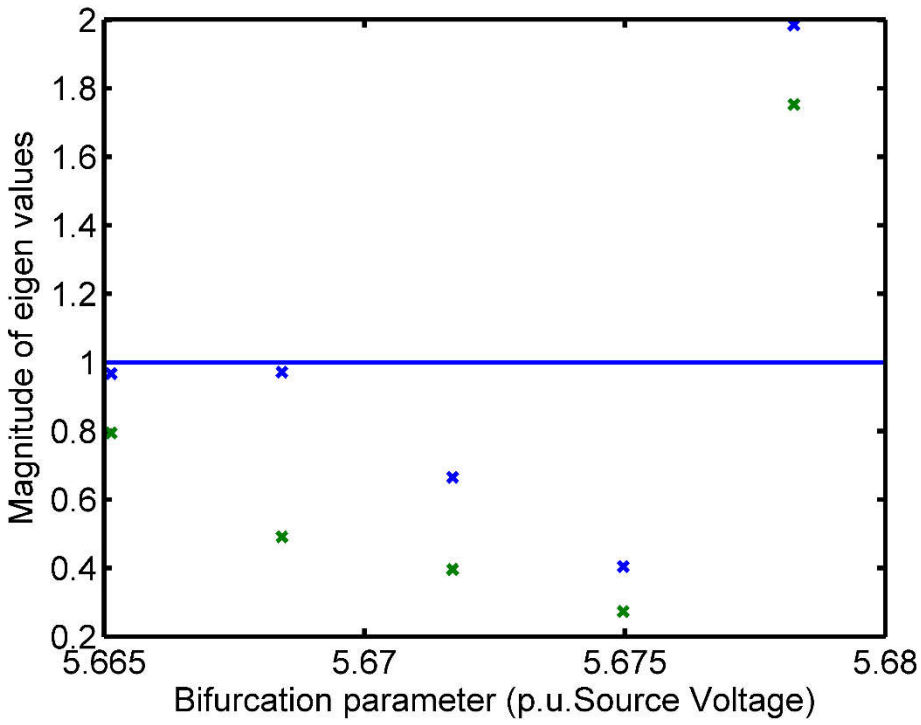

Fig. 8.10. Eigenvalue movement with the supply voltage for period 1 to period 2 transition

8.3.2 Method 2: Using $x_{(i+2)} = x_i$ and $y_{(i+2)} = y_i$

Now to establish that the system enters into the period-2 state, the numerical analysis of the stability is carried out again with the new assumption that at fixed points

$$x_{(i+2)} = x_i \tag{8.5}$$

$$y_{(i+2)} = y_i \tag{8.6}$$

So sample numbers 1, 3, and 5 from Table 8.2 are used to calculate the 1st Jacobian matrix.

$$J1 = \begin{pmatrix} 0.8632 & 0.4050 \\ 0.0454 & -1.2316 \end{pmatrix}$$

And its Eigenvalues are 0.8720 and -1.2403.

Samples 2, 4, and 6 are used to calculate the 2nd Jacobian as

$$J2 = \begin{pmatrix} 0.8326 & -0.2551 \\ -1.1257 & -0.1940 \end{pmatrix}$$

With Eigenvalues 1.0614 and -0.4227

Proceeding in this way, the average magnitudes of the two eigenvalues come out as 0.5998 and 0.3846 which are less than unity, which suggests the system is stable with period-2 orbit.

8.4 Transition from Period-2 to Period-4 Region

To check whether a similar argument can be carried out for the period-4 orbit or not the analysis continues in the period-2 region with increasing supply voltage in steps. For calculation of the Jacobian matrix and corresponding Eigenvalues, (8.5) and (8.6) are used. It has been found from the Eigenvalue movement map (Fig 8.11) that the system lost its period-2 stability at nearly 5.976 p.u. supply voltage where one of the Eigenvalues falls above the unity line.

For detailed analysis, the sampled values after the perturbation are collected in Table 8.3. Following (8.5) and (8.6), first Jacobian is calculated with samples no. 1, 3, and 5. The second Jacobian is calculated with sample no. 2, 4, 6 and it is continued for all sample data.

The average Eigenvalues obtained as $0.8791 + 0.0093i$ and $-1.4752 - 0.0093i$ with magnitudes 0.8791 and 1.4752. The 2nd Eigenvalue is greater than unity which makes the system unstable. So this calculation suggests that the system have lost its period-2 stability, which is also supported by the observation of Fig. 8.11.

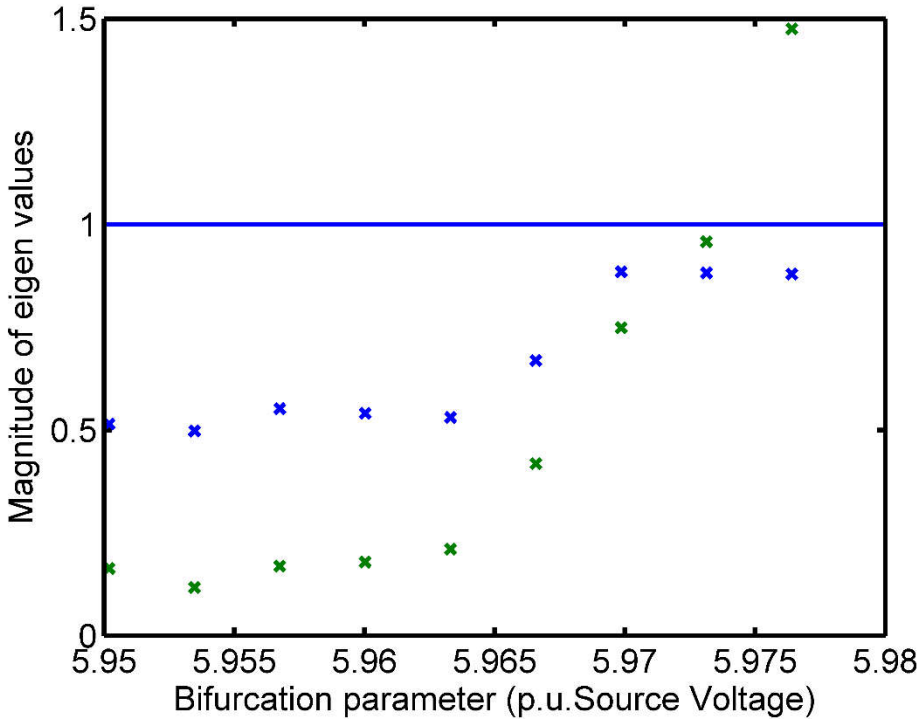

Fig. 8.11. Eigenvalue movement with the supply voltage for period 2 to period 4 transition

Table 8.3. Sampled state variables at 5.976 p.u. supply voltage

Sample	Flux linkage p.u. (X)		Transformer voltage p.u. (Y)	
1	1.78789810348851	= X1	-1.05940640597933	= Y1
2	1.42191650919052	= X2	-2.83075384367083	= Y2
3	1.04078579532347	= X3	-0.807363505686182	= Y3
4	1.68432242186280	= X4	-2.37519856494942	= Y4
5	0.891909777467130	= X5	-1.30564309422846	= Y5
6	1.51949771378432	= X6	-2.01756878630015	= Y6
7	1.13289030926556	= X7	-1.07486522320690	= Y7
8	1.56116160592545	= X8	-2.34614051596635	= Y8
9	1.04188139870732	= X9	-0.981070670153005	= Y9
10	1.62906242255780	= X10	-2.37162816356809	= Y10

Table 8.3. Sampled state variables at 5.976 p.u. supply voltage (Contd.)

Sample	Flux linkage p.u. (X)		Transformer voltage p.u. (Y)	
11	0.960108555789587	= X11	-1.09737569865386	= Y11
12	1.60382938290393	= X12	-2.27559229350964	= Y12
13	1.00593751133016	= X13	-1.03779503051941	= Y13
14	1.61983038225809	= X14	-2.33222706427226	= Y14
15	0.977747177602682	= X15	-1.07013365557150	= Y15
..	….	..	….	..
..	….	..	….	..

As the bifurcation diagram suggest that at 5.976 p.u. supply voltage the system enter in to period-4 oscillation, the analysis is performed again with the following fixed point relations

$$x_{(i+4)} = x_i \tag{8.7}$$

$$y_{(i+4)} = y_i \tag{8.8}$$

That means first Jacobian is calculated with sample no. 1, 5, 9. Second Jacobian with sample no. 2, 6, 10, and so on. The magnitude of average Eigenvalues was obtained as 0.7368 and 0.3779. These values are well below the unity line so it can be concluded that the system enters into period-4 stability.

This analysis can be further carried out for period-8 with the relations

$$x_{(i+8)} = x_i \tag{8.9}$$

$$y_{(i+8)} = y_i \tag{8.10}$$

And so on for the consecutive periods. However, the behavior after period-8 is difficult to track due to the resolution of the diagram.

8.5 Summary

In this chapter, the nonlinear behavior of the transformer operating under ferroresonance conditions was analyzed. The stability characteristic of the system at different stages was

investigated in detail with the help of computer simulations and appropriate numerical analysis tools.

The analysis showed how the transformer autonomous dynamic system loses its period-n stability to period-2n stability due to a small change in the supply voltages. The input voltage was used to examine the nonlinear behavior of the transformer.

As the ferroresonance condition demands sustained overvoltage and overcurrent for a finite amount of time, it may be dangerous for laboratory equipment. The stability of the period-1, 2, and 4 oscillations were thus analyzed by simulation only. Both graphical and numerical means and an overview of the shifting of the eigenvalues of the Jacobian matrices of the system from stable to unstable regions of operation were presented. The results of the stability analysis match well with the system bifurcation diagrams drawn in the previous Chapter.

9. System Modelling Using Finite Element Method

9.1 Finite Element Analysis

The Finite Element Method (FEM) is a numerical method for solving partial differential equations (PDEs) that arise in many areas of engineering and science. It is particularly useful in solving problems involving complex geometries or boundary conditions, where analytical solutions may not be possible.

The FEM solves problems by breaking them down into smaller, simpler pieces, each of which can be described by a set of equations. These equations are then coupled to form a series of algebraic equations that can be solved using matrix algebra techniques. The FEM can be used to solve a wide range of problems, including heat transfer, fluid flow, structural analysis, and electromagnetic fields.

The FEM has several advantages over other numerical techniques. First, it can handle complex geometries and boundary conditions, making it useful in many practical engineering applications. Second, it can provide accurate solutions with relatively few elements, making it computationally efficient. Finally, it can easily be extended to include more complex physics or materials models.

However, the FEM also has some limitations. It requires a significant amount of computational resources, particularly for large-scale problems. It can also be difficult to ensure the accuracy and reliability of the results, as errors can arise from various sources, including element discretization, numerical integration, and solution algorithms. Despite these challenges, the FEM remains one of the most extensively used numerical approaches in engineering and science for solving PDEs.

In the previous chapters, the simulation of ferroresonance was carried out using the non-linear dynamical equation of the transformer. But those analysis could not provide a satisfactory answer to the distribution of magnetic field during critical ferroresonance conditions. To investigate the change that occurs in the core magnetic field distribution during ferroresonance, the finite element method may be a good choice. The application of FEM in the ferroresonance study can be found in some literature [86-89].

9.2 Computational Method

Fundamentally the Finite Element method comprises four steps:

- partitioning the solution region into a finite number of elements,
- generating governing equations for a typical element,
- assembling all elements in the solution region, and
- solving the generated system of equations.

The first step in the finite element method is to subdivide or elementize the structure or solution region. The shapes of the elements should be such that the combination of them could be as close to the original body or domain as possible. For a 2-dimensional body, a triangular element requires the least computational complexity. But for closer representation the original body size should be chosen smaller.

The size of the elements is directly related to the convergence of the solution. The smaller the elements, the more accurate the final solution. However, using smaller-sized elements will increase computational time. Different sizes of elements may have to be used in the same body at times. [90].

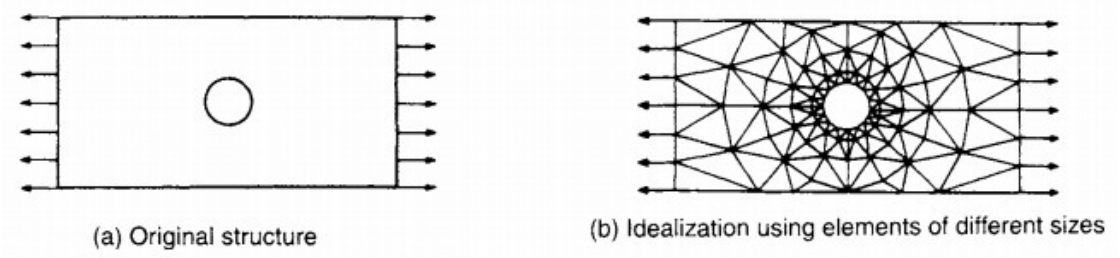

Fig. 9.1. Generation of mesh structure

Then, within an element, a suitable solution is assumed to approximate the unknown solution. In general, a linear polynomial can be the simplest solution or the interpolation model.

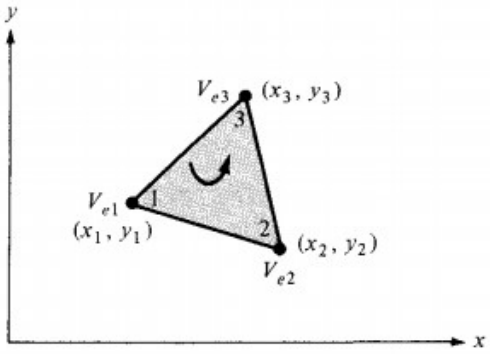

Fig. 9.2. Triangular element

For example in a triangular element shown in Fig. 9.2 it can be assumed that the potential varies linearly with the position as

$$\tilde{\varphi} = a + bx + cy \tag{9.1}$$

At three vertices

$$\widetilde{\varphi_1} = a + bx_1 + cy_1 \tag{9.2}$$

$$\widetilde{\varphi_2} = a + bx_2 + cy_2 \tag{9.3}$$

$$\widetilde{\varphi_3} = a + bx_3 + cy_3 \tag{9.4}$$

If the three values of the potentials are given, it is possible to solve for constants *a*, *b,* and *c* and the unknown potential of the m-th triangular element can be expressed as [91]

$$\widetilde{\varphi_m} = \sum_{i=1}^{n} v_i(x, y)\tilde{\varphi}_i \tag{9.5}$$

Where n is the number of nodes in an element and v_i are the shape functions or interpolating functions.

To formulate the characteristic matrices and vectors of finite elements any one of the following approaches can be used:

- Direct approach
- Variational approach
- Weighted residual approach

A good understanding of the governing equations of the physical system is required in the direct approach method. It is the most common implementation of FEM where the element properties are established from direct physical reasoning. This approach is only applicable to simple types of elements [90].

The variational approach is a method of finding the approximate solution to a differential equation by minimizing a functional. A functional is a function of functions, and in finite element analysis, the total potential energy of the system is typically chosen as the functional. The variational approach is based on the principle of minimum potential energy, which states that to find the actual solution to a differential equation, the total potential energy is to be minimized.

The variational approach can be a very efficient approach to solve problems with a large number of degrees of freedom. It is a very robust approach that can solve problems with complex boundary conditions. This is the reason why the variational approach is vastly used in

electromagnetic analysis [92, 93]. One significant limitation of the method is that it needs the physical problem to be defined in a variational form, which is not always possible.

In the calculus of variations the extrema (maxima and minima) or stationary values of functionals are determined. That means in variational calculus one needs to find a function *φ(x)* which makes the functional *I* stationary.

$$I = \int_{x_1}^{x_2} F(x, \varphi, \varphi', \varphi'')\, dx \tag{9.6}$$

Here, x is the independent variable,

$$\varphi' = \frac{dy}{dx},\ \varphi'' = \frac{d^2y}{dx^2}$$

I and F are called functionals. In most of the applications the functional *I* has a clear physical meaning.

Any approximate solution $\tilde{\varphi}(x)$ can be expressed as the summation of the exact solution *φ(x)* and the variation of φ.

$$\tilde{\varphi}(x) = \varphi(x) + \delta\varphi(x) \tag{9.7}$$

For the *I* to be stationary, the variation in *I* must be zero.

$$\delta I = \int_{x_1}^{x_2} \left(\frac{\partial F}{\partial \varphi}\delta\varphi + \frac{\partial F}{\partial \varphi'}\delta\varphi' + \frac{\partial F}{\partial \varphi''}\delta\varphi''\right) dx = 0 \tag{9.8}$$

This gives,

$$\frac{\partial F}{\partial \varphi} - \frac{d}{dx}\left(\frac{\partial F}{\partial \varphi'}\right) + \frac{d^2}{dx^2}\left(\frac{\partial F}{\partial \varphi''}\right) = 0 \tag{9.9}$$

Equation (9.9) is called the Euler-Lagrange equation or simply the Euler equation [90] and this will be the principal equation for the given problem.

If *I* is a quadratic functional of $\tilde{\varphi}$, the element equations can be found as

$$\frac{\partial I^{(m)}}{\partial \tilde{\varphi}^{(m)}} = \left[K^{(m)}\right]\tilde{\varphi}^{(m)} - \tilde{P}^{(m)} \tag{9.10}$$

Where $[K^{(m)}]$ is called the element characteristic matrix and $\tilde{P}^{(m)}$ is the characteristic vector. So the overall equations of the system will be,

$$\frac{\partial I}{\partial \tilde{\varphi}} = [K]\tilde{\varphi} - \tilde{P} = 0 \tag{9.11}$$

Applying the boundary conditions (9.11) can be solved and the nodal unknowns φ can be found.

The weighted residual approach in finite element analysis is a technique of finding the approximate solution to a differential equation by minimizing the weighted residual of the equation. The weighted residual is the difference between both sides of the equation, and it is

weighted by a function that is chosen to make the minimization problem well-posed. The weighted residual approach is very efficient and robust. Some examples of weighted residual methods are the Galerkin method, least squares method, etc.

For the magnetostatics Poisson equation, residual can be defined as,

$$R(A) = \nabla.\left(\frac{1}{\mu}\nabla\tilde{A}\right) + J_e \qquad (9.12)$$

Which goes to zero when an exact solution of A is achieved. As per distribution theory, one has to find the variable A that satisfies the statement

$$\int R(A) w d\Omega = 0 \qquad (9.13)$$

Where w is called a weighting function and Ω is the domain of the problem. In the Galerkin Method, the shape function (v_i) in (9.5) is taken as the weighting function (w).

$$\int \frac{1}{\mu}\nabla\tilde{A}.\nabla v_i d\Omega - \int v_i J_e = 0 \qquad (9.14)$$

Equation (9.14) is the finite element equation for a single element. The system or overall equations can be obtained by assembling these element equations.

The concept of assembling the element matrices and vectors is as follows: the value of the unknown nodal degree of freedom or variable at any node is to be considered as same for all the elements connecting at that node.

Let E be the total number of elements in a given system and M denotes nodal degrees of freedom. Then the assembled characteristic matrix and characteristic vector will be of order $M \times M$ and $M \times 1$ respectively. Again consider the element characteristic matrix $[K^{(e)}]$ is of the order $n \times n$ and the element characteristic vector $P^{(e)}$ is of the order $n \times 1$. Thus, the global characteristic matrix $[K]$ and the global characteristic vector P will be calculated from the element matrix by including zeros in the remaining locations and adding algebraically [90].

$$[K] = \sum_{e=1}^{E}[K^{(e)}] \qquad (9.15)$$

$$P = \sum_{e=1}^{E} P^{(e)} \qquad (9.16)$$

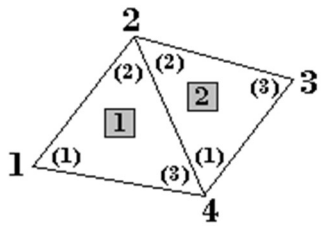

Fig. 9.3 Two triangular elements

For an example, consider a two-element system as shown in Fig. 9.3. The element characteristic matrices for elements 1 and 2 using the local node numbering scheme will be

$$\left[S^{(1)}\right]=\begin{bmatrix} S_{11}^{(1)} & S_{12}^{(1)} & S_{13}^{(1)} \\ S_{21}^{(1)} & S_{22}^{(1)} & S_{23}^{(1)} \\ S_{31}^{(1)} & S_{32}^{(1)} & S_{33}^{(1)} \end{bmatrix} \tag{9.17}$$

$$\text{And } \left[S^{(2)}\right]=\begin{bmatrix} S_{11}^{(2)} & S_{12}^{(2)} & S_{13}^{(2)} \\ S_{21}^{(2)} & S_{22}^{(2)} & S_{23}^{(2)} \\ S_{31}^{(2)} & S_{32}^{(2)} & S_{33}^{(2)} \end{bmatrix} \tag{9.18}$$

Now the global element characteristic matrix using the global node numbering scheme will be.

$$\left[S\right]=\left[S^{(1)}\right]+\left[S^{(2)}\right]=\begin{bmatrix} S_{11}^{(1)} & S_{12}^{(1)} & 0 & S_{13}^{(1)} \\ S_{21}^{(1)} & S_{22}^{(1)}+S_{22}^{(2)} & S_{23}^{(2)} & S_{23}^{(1)}+S_{21}^{(2)} \\ 0 & S_{32}^{(2)} & S_{33}^{(2)} & S_{31}^{(2)} \\ S_{31}^{(1)} & S_{32}^{(1)}+S_{12}^{(2)} & S_{13}^{(2)} & S_{33}^{(1)}+S_{11}^{(2)} \end{bmatrix} \tag{9.19}$$

There are two methods available for solving the system equations: direct and iterative. Direct approaches yield a precise solution in a limited number of simple arithmetic operations. Since a computer has a finite word length, round-off and truncation errors may occur. Gaussian elimination is the fundamental method for direct solutions.

Iterative procedures begin with an approximation and progress to the true solution through successively better approximations. The accuracy and rate of convergence of iterative approaches vary depending on the algorithm used. The fundamental benefit of iterative approaches is that they are ideally adapted to digital computers.

9.3 Finite Element Analysis of Transformer

For the analysis of a transformer, a suitable transformer model is required. This model must include the winding characteristics and the saturable core characteristics. Fig. 9.4 shows an equivalent circuit of a transformer. So one has to first find out all the components of the equivalent circuit to use the transformer model for analysis purposes.

As the Hysteresis and Eddy current losses ultimately produce heat in the transformer core, it is common practice to use a non-linear resistor to represent the core losses. The non-

linearity or saturation behavior of the transformer core can be captured by a non-linear inductor constructed from the hysteresis loop or open circuit test results.

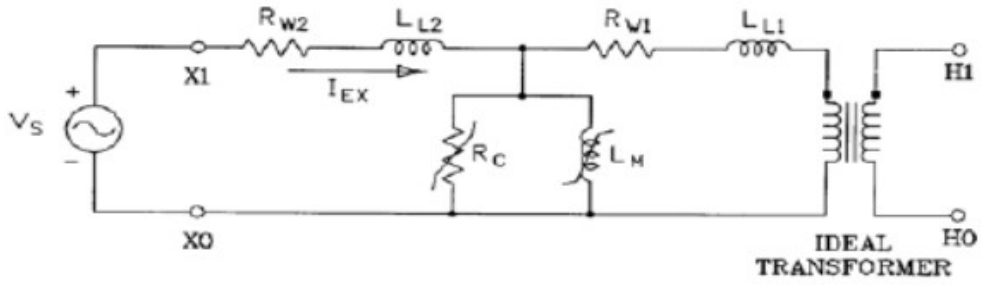

Fig. 9.4. Equivalent circuit of a transformer

Fig. 9.5(a) shows a single-phase core-type transformer and Fig. 9.5(b) shows a single-phase shell-type transformer.

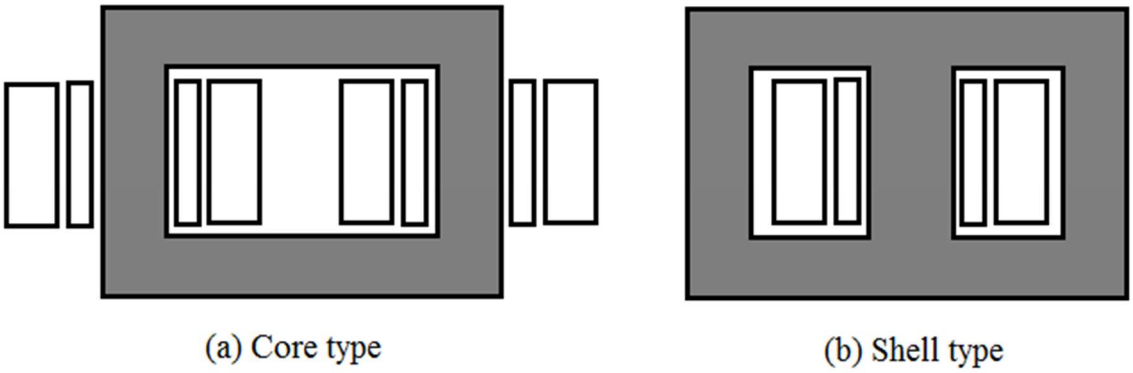

Fig. 9.5. Single phase transformer

To cut down the computational time, the analysis of the transformer can be carried out on a part of the whole structure [94]. In the core type transformer the flux line must be symmetrical about the axis *Y*. Then the analysis can be carried out only on the part of the structure drawn in Fig. 9.6.

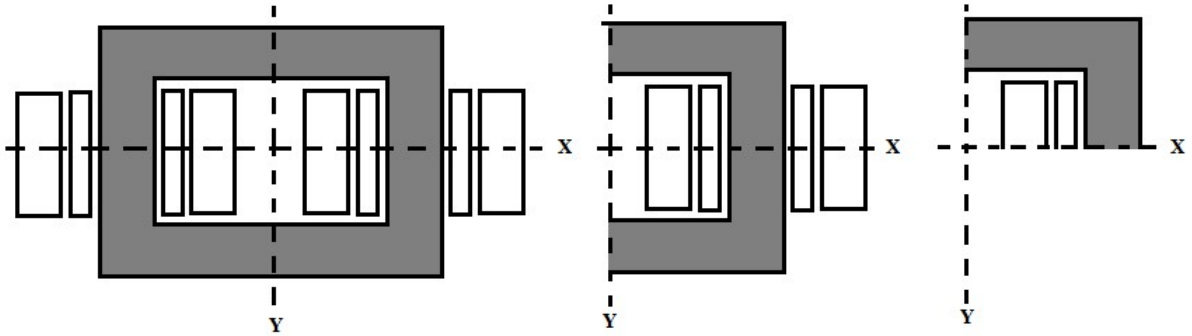

Fig. 9.6. Core type transformer

Similarly, in shell type line *X* plays the role of symmetrical axis, so the analysis is reduced to the section part illustrated in Fig. 9.7.

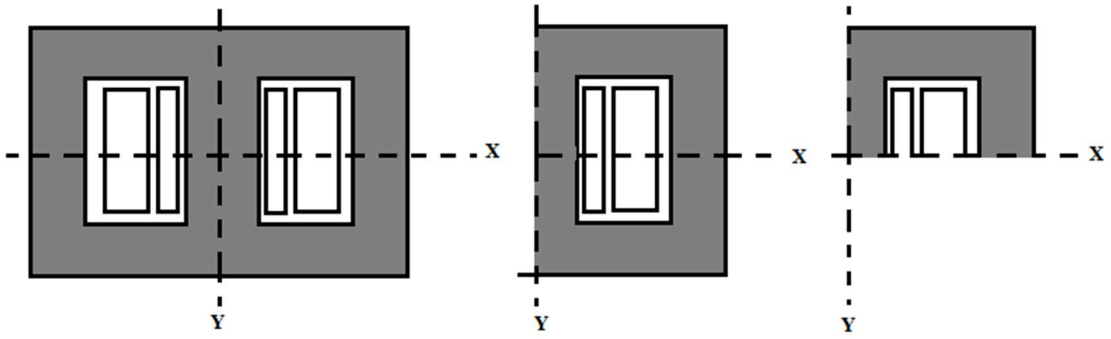

Fig. 9.7. Shell type transformer

The simulation, that is carried out is equivalent to the no-load test of the transformer. The primary winding current (I_{EX}) at no load is imposed as the excitation parameter and the secondary winding current is put to zero. Corresponding voltages are computed across the two windings of the transformer.

Once the problem is solved, the stored magnetic energy density can be calculated as

$$W_m = \frac{1}{2}\vec{B}.\vec{H} = \frac{1}{2}\mu H^2 \quad (9.20)$$

Since the 2D problem is analyzed, stored magnetic energy can be obtained by taking the surface integral of (9.20) and multiplying it with the iron length of the transformer (L_{Fe}).

$$W_m = 4L_{Fe}\iint \frac{1}{2}\mu H^2 \quad (9.21)$$

'4' is multiplied as only a quarter of the transformer is analyzed.

The main flux is obtained by integrating the normal component of the flux density as

$$\Phi_0 = L_{Fe}\int \vec{B}.\hat{n}dl \quad (9.22)$$

For core type transformer and

$$\Phi_0 = 2L_{Fe}\int \vec{B}.\hat{n}dl \quad (9.23)$$

For shell type transformer.

The no-load inductance and mutual inductance now can be calculated as

$$\mathrm{L}_0 = \frac{N_1\Phi_0}{I_0} \quad (9.24)$$

$$M = \frac{N_2\Phi_0}{I_0} \quad (9.25)$$

The leakage inductances can be determined from a short circuit test. The simulation can be carried out by imposing a winding current equal to the rated current such that two MMFs result in equal and opposite i.e. $N_1 i_1 = -N_2 i_2$.

Thus the leakage flux linkages

$$\lambda_1 = L_1 i_1 \quad (9.26)$$

$$\lambda_2 = L_2 i_2 \quad (9.27)$$

If the transformer operates in the saturation zone of its core characteristic, then the permeability cannot be considered constant. This problem then can be solved by representing the core characteristic with a suitable nonlinear equation.

9.4 Analysis of Ferroresonance with FEM

9.4.1 Setup the System for Finite Element Analysis

The following setup has been created in the simulation environment.

Rated power = 200 VA

Primary voltage = 220 V

Secondary voltage = 24 V

Frequency = 50 Hz

Core material = silicon steel GO 3%

Primary turn = 416 with wire diameter 1.02 mm

Secondary turn = 45 with wire diameter 2.71 mm

The 2D analysis has been chosen as this can solve the issue of convergence of 3D design and can save computational time [95]. For that, the shell-type transformer with concentric winding as shown in Fig. 9.8 has been created in Comsol Multiphysics software. Equation (4.1) is incorporated as the B-H characteristic of the core material. Fig. 9.9 shows the BH relation that is used for analysis. To build up the ferroresonance circuit shown in Fig. 4.2, it is required to couple the circuit study with the field study. Previous literature [96] has done this using an electromagnetic transients program for the circuit part and a finite element magnetic field solver for the field part. In our program of Comsol Multiphysics Electric Circuit interface is coupled with the Magnetic Fields interface. As the flux density vector B will only have the tangential component along the axis of symmetry PQ (Fig. 9.8), Dirichlet's boundary condition is assigned along this line.

In the next step triangular mesh has been generated as shown in Fig. 9.10. To make a balance between the computational time and accuracy of the result element size is taken as 'fine' with 1916 domain elements and 274 boundary elements. The system is simulated for 998 degrees of freedom.

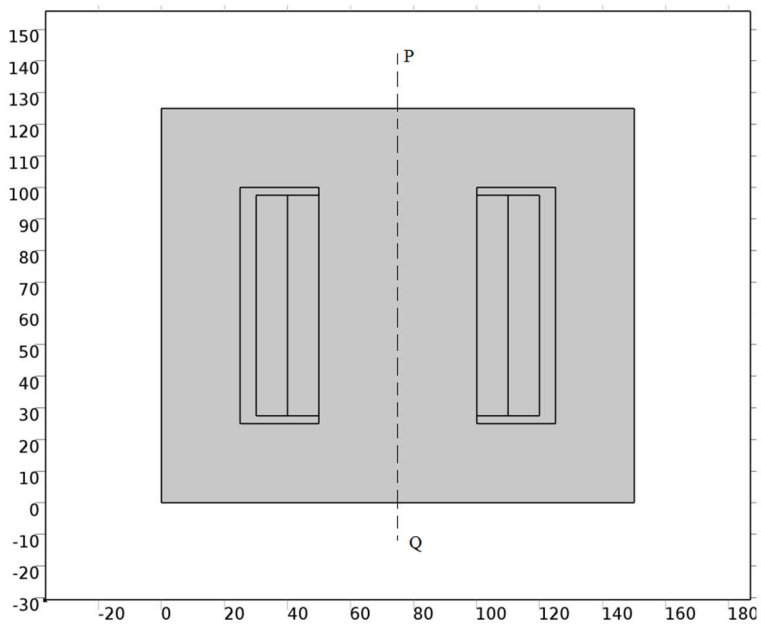

Fig. 9.8. Transformer for finite element analysis (units in mm)

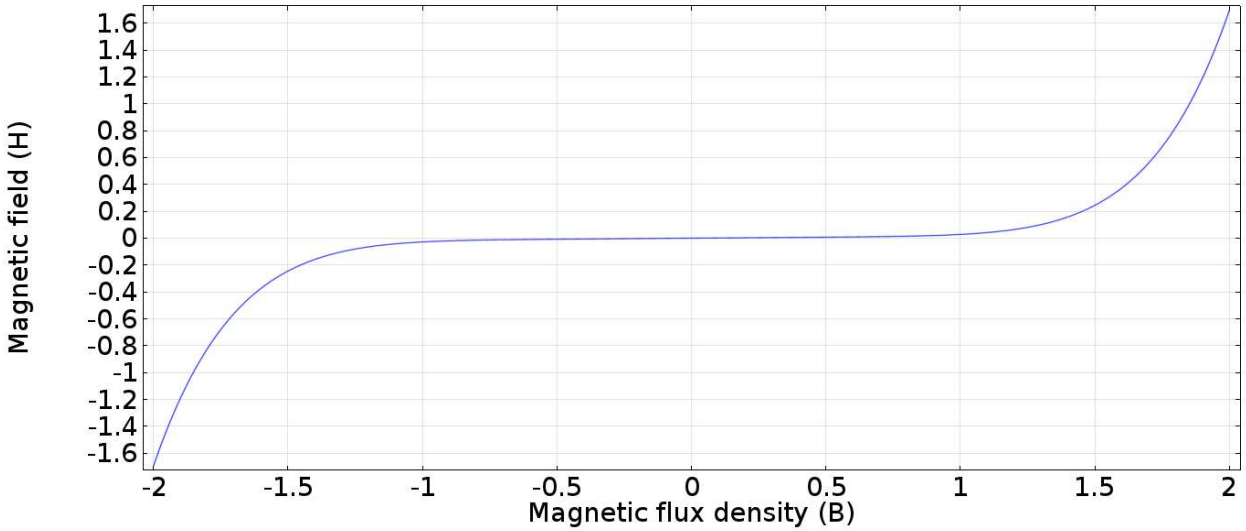

Fig. 9.9. B-H curve of the transformer core

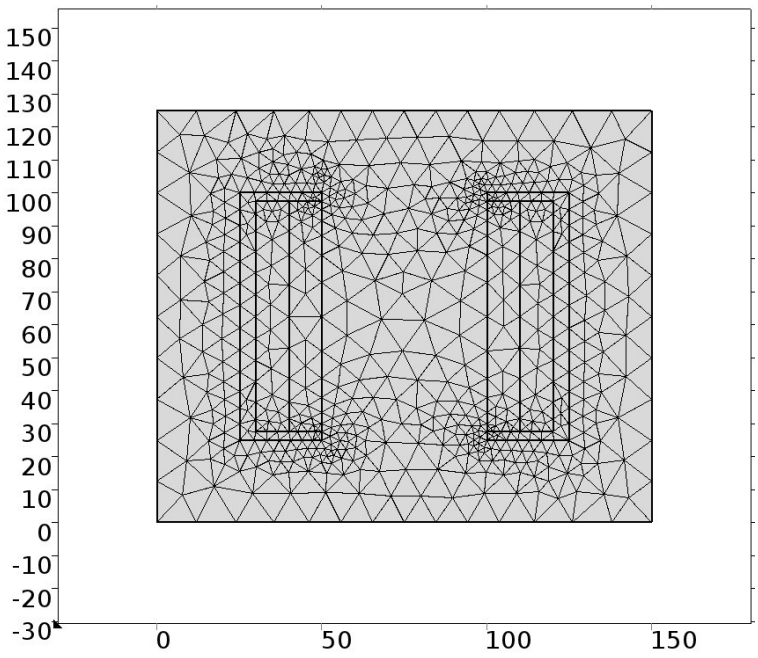

Fig. 9.10. Mesh generation for finite element analysis (units in mm)

For quasi-static analysis of magnetic and electric fields, displacement current density can be assumed as zero. With this Ampere's law can be rewritten as:

$$\nabla \times \boldsymbol{H} = \sigma \boldsymbol{E} + \boldsymbol{J_e} \tag{9.28}$$

Here $\boldsymbol{J_e}$ is the current density generated externally.

From the definitions of the potentials one can have,

$$\boldsymbol{B} = \nabla \times \boldsymbol{A} \tag{9.29}$$

$$\boldsymbol{E} = -\nabla V - \frac{\partial \boldsymbol{A}}{\partial t} \tag{9.30}$$

Incorporating (9.29) and (9.30) in (9.28)

$$\sigma \frac{\partial \boldsymbol{A}}{\partial t} + (\nabla \times \boldsymbol{H}) + \sigma \nabla V = \boldsymbol{J_e} \tag{9.31}$$

Equations (9.29) and (9.30) are not sufficient to define both the potentials uniquely.

Consider two new potential functions

$$\widetilde{\boldsymbol{A}} = \boldsymbol{A} + \nabla \Psi \tag{9.32}$$

$$\tilde{V} = V - \frac{\partial \Psi}{\partial t} \tag{9.33}$$

also produce the same magnetic and electric fields.

To obtain a unique solution, constraints can be put on the scalar Ψ such that the solution becomes unique. It is also suitable for computation to select a Ψ such that only the magnetic

vector potential exists and the scalar electric potential disappears. This approximation is known as gauge transformation.

From (9.31) the magnetic vector potential $\boldsymbol{A}$ is calculated by applying the finite element method. The primary winding current is taken as the excitation parameter. Secondary winding terminals are kept open. Time dependent automatic highly nonlinear (Newton) method with 25 maximum iteration is used for solution. The voltages across two windings are computed. The components of magnetic flux density are derived from the vector potential. The observations are listed in the next section.

9.4.2. Results and Analysis

The supply voltage is increased gradually and the transformer and capacitor voltages are observed. Taking the transformer primary voltage as base voltage, up to 0.66 per unit (p.u.) supply voltage system shows no ferroresonance. Fig. 9.11 shows the build-up of capacitor voltage. For comparison, the capacitor voltage waveform obtained from laboratory experiments is also shown in Fig. 9.12. The steady-state capacitor and transformer voltages are shown in Fig. 9.13. The circuit behaves like an inductive circuit as the transformer voltage is greater than the capacitor voltage. Fig. 9.14 shows the phase trajectory on the phase plane for below ferroresonance state and Fig. 9.15 shows the magnetic flux density distribution at all points of the core surface. After reaching the steady state the magnetic flux density attains a peak value of 1.18 T at no-ferroresonance conditions.

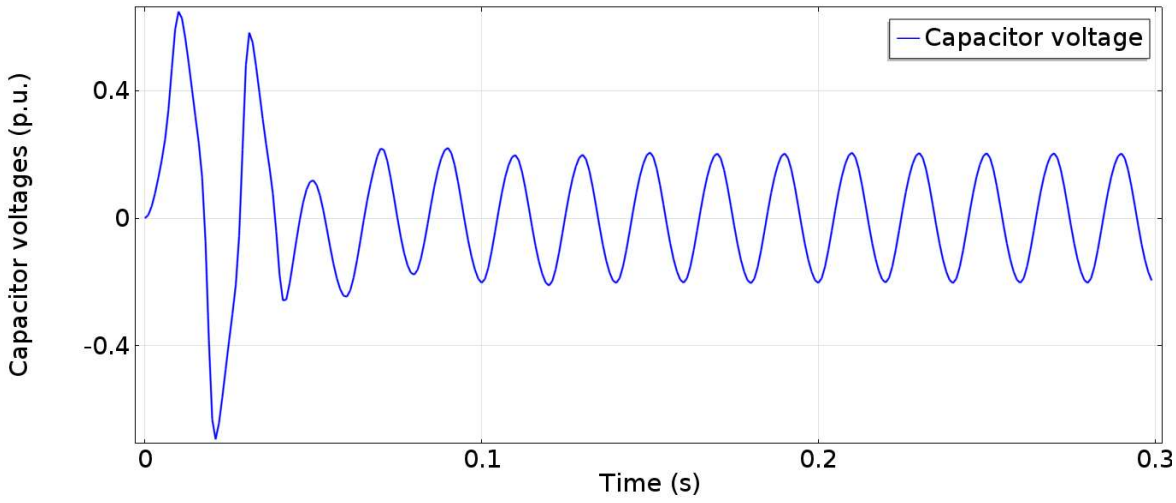

Fig. 9.11. Capacitor Voltage plot at 0.66 p.u. supply voltage – no ferroresonance

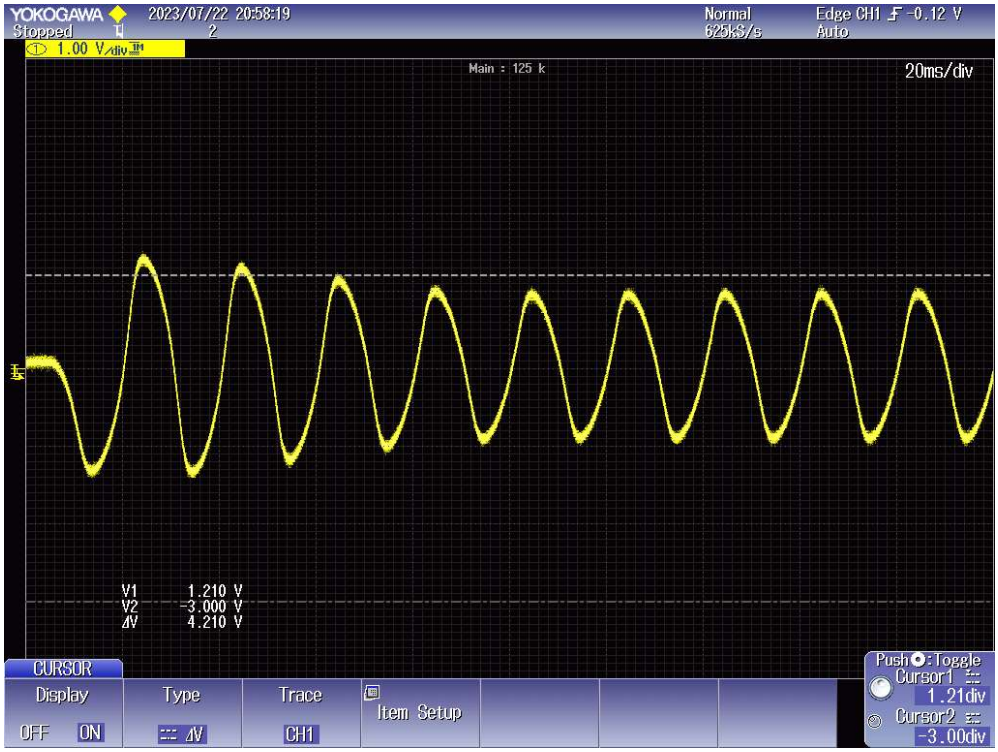

Fig. 9.12. Capacitor voltage at 0.66 p.u. supply voltage – observation from the laboratory experiment where no ferroresonance was observed

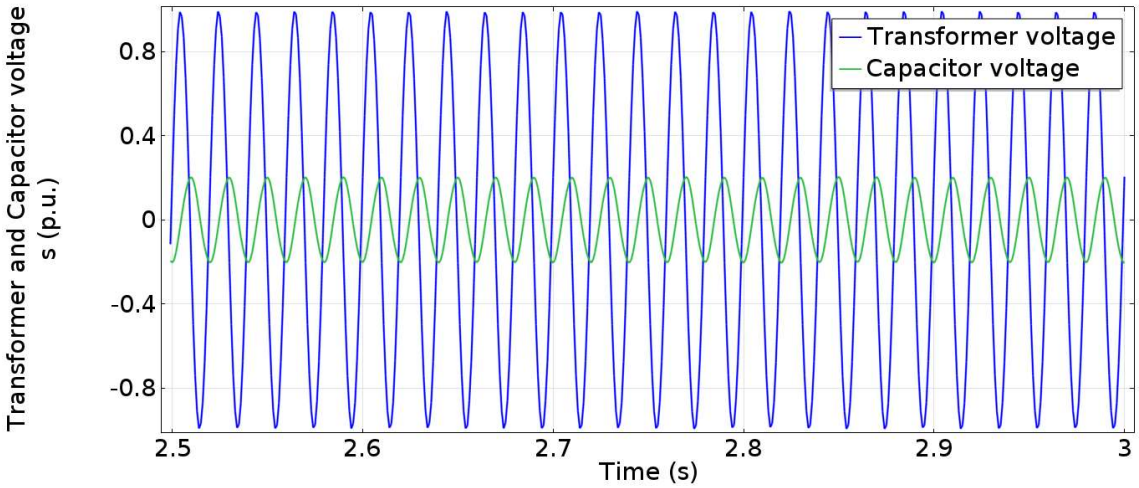

Fig. 9.13. Steady-state voltages at 0.66 p.u. supply voltage – no ferroresonance

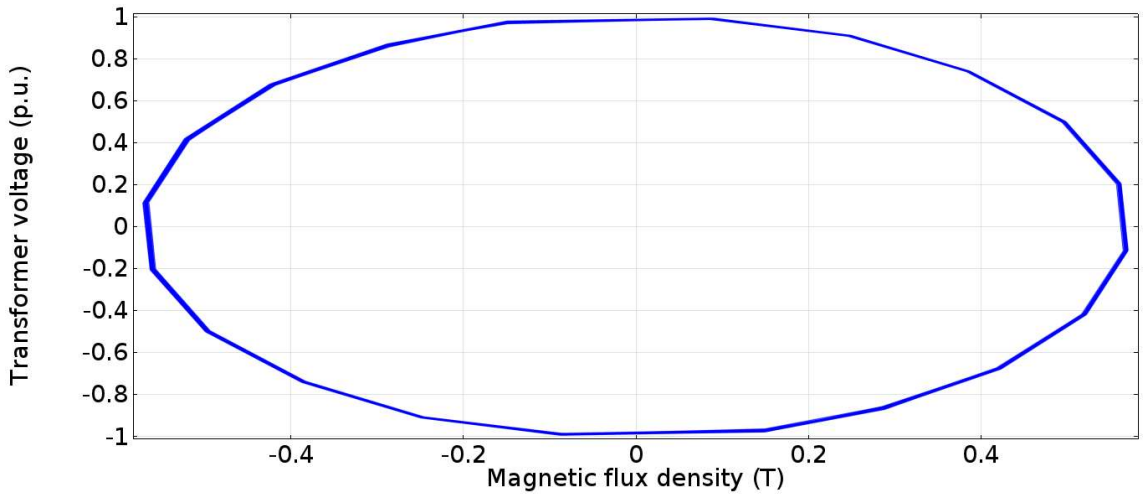

Fig. 9.14. Phase plane plot at 0.66 p.u. supply voltage – no ferroresonance

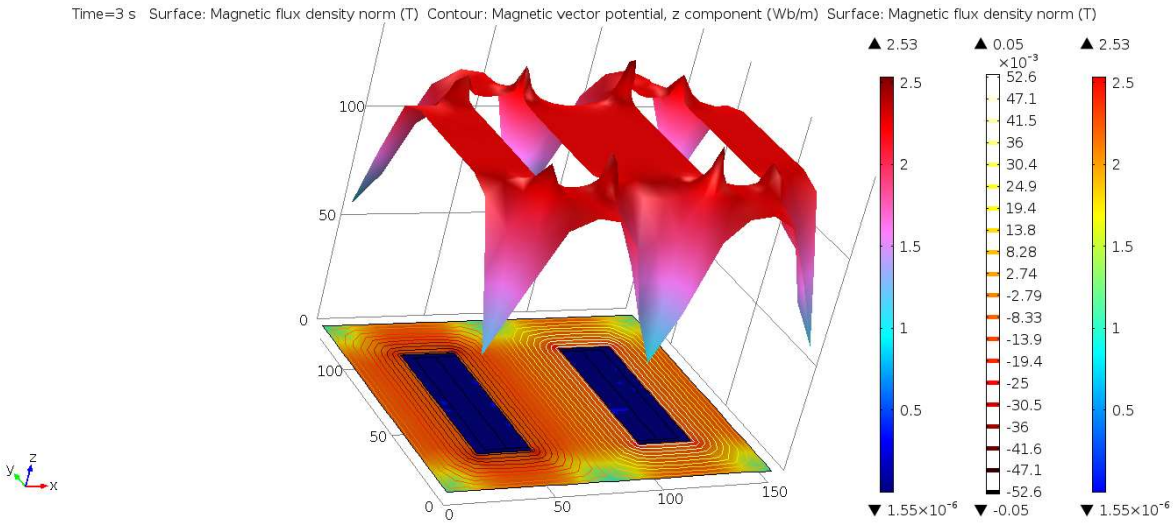

Fig. 9.15. Magnetic flux density at 0.66 p.u. supply voltage – no ferroresonance

At 0.67 p.u. supply voltage, ferroresonance is observed. Fig. 9.16 shows the build-up of capacitor voltage. The nature matches with the waveform obtained in the laboratory experiment (Fig. 9.17). However, the ferroresonance occurs with a little higher voltage in the experimental setup. Fig. 9.18 shows that the capacitor voltage peak value extended almost 2.4 p.u. whereas transformer voltage reached 1.6 p.u peak value at steady state. The circuit becomes capacitive. It was expected as per Rudenberg's graphical analysis [3]. Fig. 9.19 shows the phase plane plot. Fig. 9.20 shows the magnetic flux density distribution under ferroresonance. In this case, the flux density achieved a peak value of 2.47 T after the initial transient decay down. This is well above

the saturation value of GO steels which is 1.7 T [97]. The flux density peak obtained in ferroresonance is 2.1 times the no ferroresonance condition. Fig. 9.21 shows the change of flux density peak while the system enters into the ferroresonance condition from the non-ferroresonance condition.

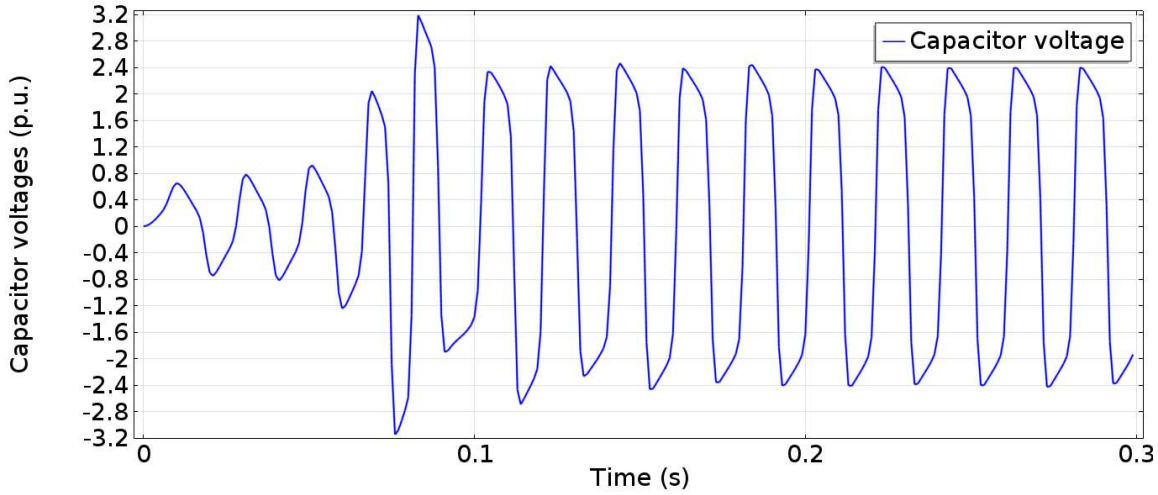

Fig. 9.16. Capacitor Voltage plot at 0.67 p.u. supply voltage – with ferroresonance

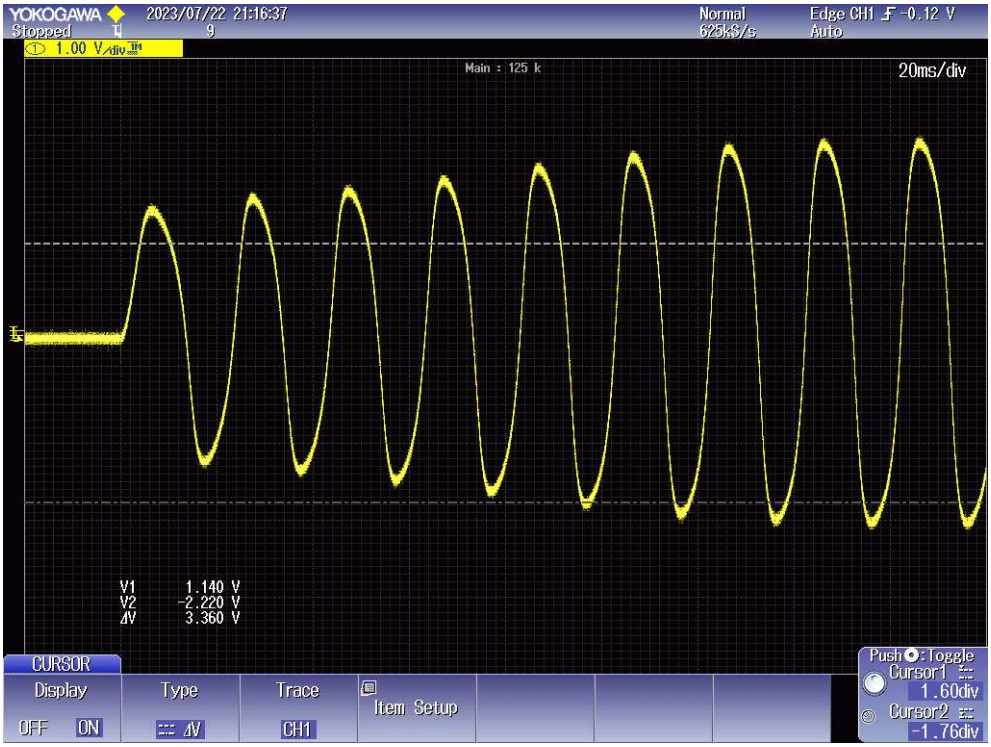

Fig. 9.17. Capacitor voltage at 0.69 p.u. supply voltage – where the first ferroresonance occurs in laboratory experiment

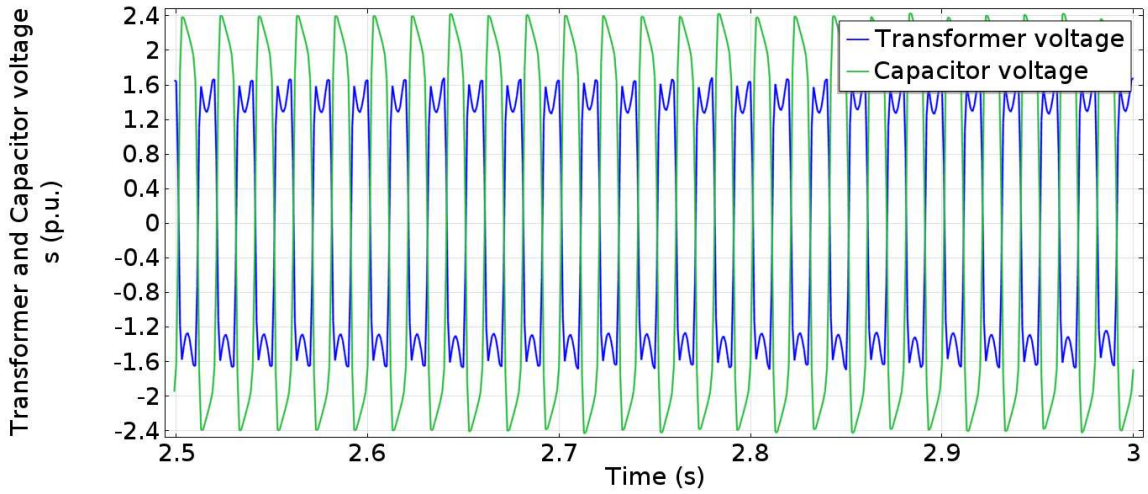

Fig. 9.18. Steady-state voltages at 0.67 p.u. supply voltage – with ferroresonance

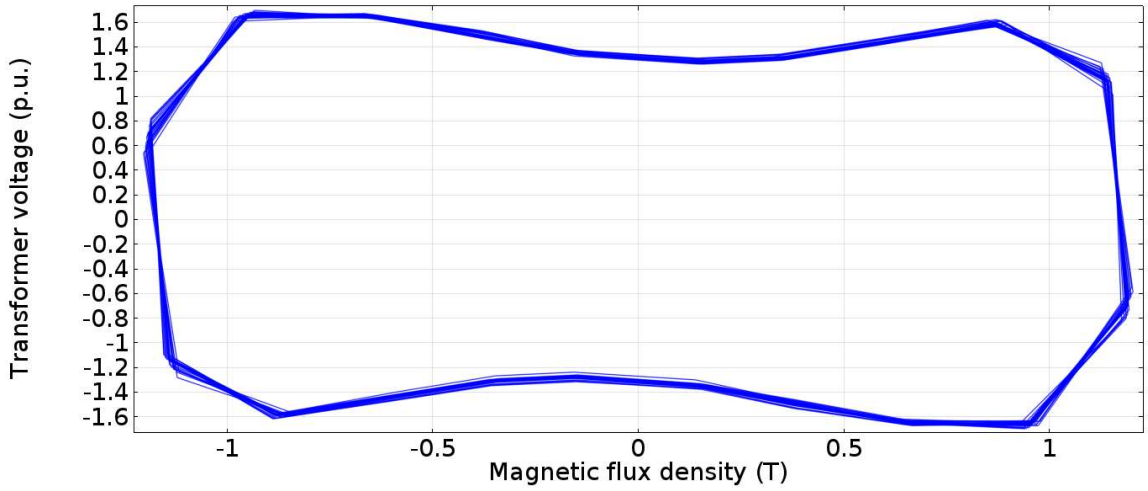

Fig. 9.19. Phase plane plot at 0.67 p.u. supply voltage – with ferroresonance

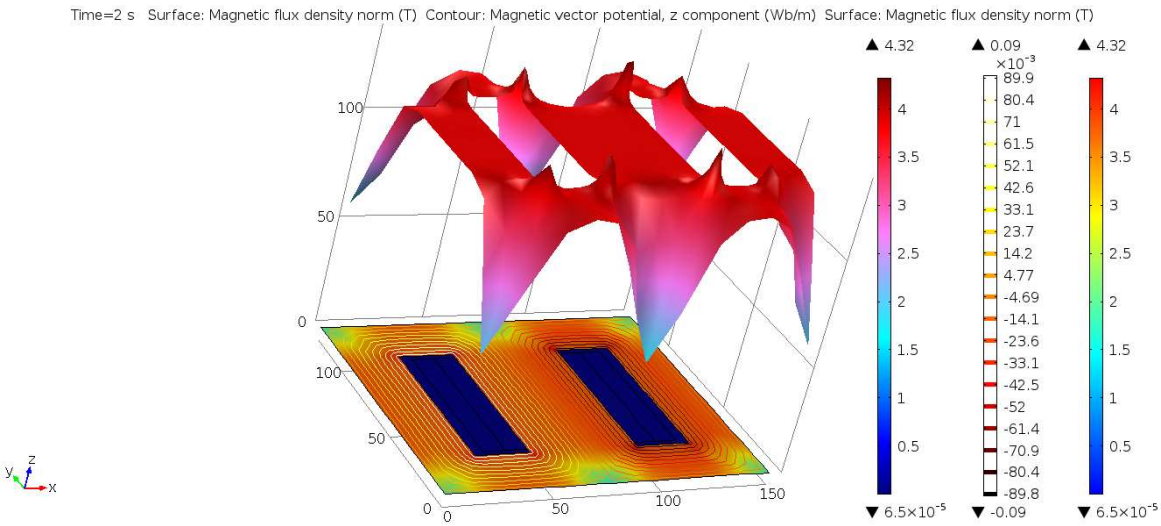

Fig. 9.20. Magnetic flux density at 0.67 p.u. supply voltage – with ferroresonance

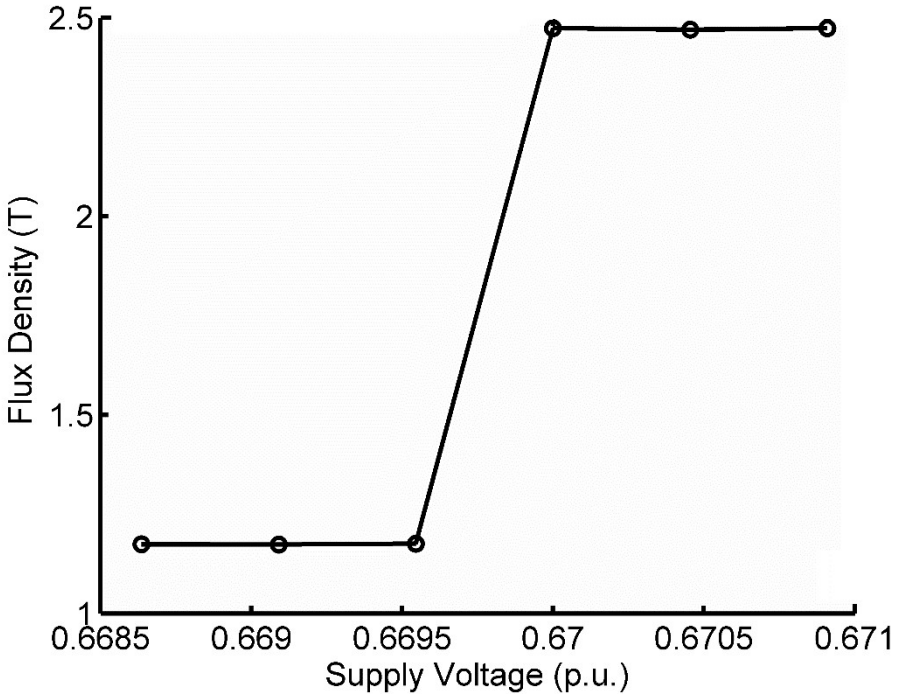

Fig. 9.21. Change of magnetic flux density with supply voltage

A detailed study of magnetic flux density shows that during ferroresonance the flux density raised to 2.1 times. This may throw the core of the transformer deep into the saturation. This will permanently magnetize the core material. Also increases the core losses. The jump in magnetic flux density also makes it difficult to rebuild the condition under a laboratory environment as it may permanently damage the core of the transformer under test.

9.5 Summary

The finite element method is used on the ferroresonance circuit in this chapter. The hysteresis curve of the core material of the transformer is represented by a nonlinear equation which was obtained from experimental results. A successful ferroresonance observation has been captured with the finite element model. The supply voltage at which the ferroresonance jump was observed in the laboratory setup almost matches with that in the finite element simulation. The finite element method also aids in understanding the magnetic flux dynamics in the core body before and after ferroresonance.

10.1 Conclusion

The following observations can be made from the works undertaken here by the author in addition to knowledge related to ferroresonance science and can be treated as contributions.

Chapter 1 gives an overall introduction to the thesis. Various causes of ferroresonance configurations are identified after a suitable review of works in ferroresonance. Ferroresonance may be generated in a 3-phase power system when the following conditions arise due to a fuse blown or unsynchronized 3-phase switching device that failed to connect all phases:

- 3-phase system grounded at the source, but having no ground at the transformers banks or vice versa.
- Underground cable length or overhead conductor length is sufficient to create the capacitance necessary.
- The degree of nonlinearity in the magnetic characteristics of the transformer.
- Transformers are unloaded or lightly loaded.
- VT is energized through the grading capacitance of the circuit breaker when circuit breakers disconnect the phases.

It discusses the current scenario of the ferroresonance study and the necessity of the proposed work. This is explained in a nutshell with the basic works that have been performed under the current thesis.

Chapter 2 on the definition of ferroresonance. It discusses the effects of ferroresonance that have been listed in different publications. The study says that the circuit consists of saturable inductance, and capacitance, and an alternating voltage source is prone to ferroresonance. How this combination can be achieved in the power system that also discussed in this chapter. In 1950, a German engineer R. Rudenberg presented a graphical analysis of ferroresonance which is the stepping stone of ferroresonance analysis. **This chapter provides an overview of Rudenberg's analysis.** Analysis shows, how the system jumps into ferroresonance from normal value while changing any of the circuit parameters. At the end of this chapter, a comprehensive study is made on the different types of works on ferroresonance that have been performed for

decades. Four main categories have been discussed - examples & and case studies, experimental investigations, damping, and analysis of ferroresonance.

Chapter 3 describes the details of **a laboratory experiment** that has been developed and performed to observe ferroresonance in a controlled environment. At first, the core magnetic characteristics of the transformer under the ferroresonance test are extracted from the open circuit test of the transformer. The series capacitance value is designed and calculated using R. Rudenberg's graphical method. To protect the digital oscilloscope a potential divider made of capacitor is used. To prevent the line equipment from extended exposure to overvoltage at ferroresonance, an auto cut-off switch is used which cuts off the circuit after a pre-defined time. The ferroresonance incident has been captured successfully. Time domain Waveform of capacitor voltage and transformer voltage at different source voltages are taken on the creation of ferroresonance at various line conditions. **So it is being concluded from the experimental results a sustained over-voltage will appear across the line equipment which will damage the lightning arrester in the power system and after which burning of transformers etc. in the system.**

Chapter 4 explains the process of **building up the simulation model of ferroresonance** incorporating experimental transformer magnetic characteristics. A wide experimental study on ferroresonance in a real setup is difficult and also hazardous for the equipment used as it involves power frequency and very high overvoltages. So for further study of ferroresonance, a suitable simulation model is developed. The B-H loop data of the transformer obtained from the experiment is used to find an approximated mathematical equation to represent the transformer core magnetism for the ferroresonance circuit model. Then mathematical nonlinear differential equations for **ferroresonance are simulated in a MATLAB software** platform. The ferroresonance result obtained from the simulation model is compared with the experimental results where both the results match with a minor deviation. This modeling method is based on real transformer data obtained by experiment and this explains the technique of development of a non-linear mathematical science for electrical devices; transformers.

Chapter 5 continues the study with the MATLAB model for ferroresonance developed in the previous chapter. Here some circuit parameters like **supply voltage, supply frequency, series capacitance, core loss resistance of transformer, degree of transformer core saturation, and initial flux linkage** in the transformer-core are varied and the voltage across

series capacitor and transformer for ferroresonance are observed. For each of the cases it has been found at a certain point when the circuit parameter and other conditions match, voltages jump to a high value at ferroresonance. Using Rudenberg's graphical analysis it has been shown how the stable operating point of the system switches from 1st quadrant to 3rd quadrant of V-I characteristic and builds up ferroresonance oscillation. **So this chapter contributes a verification of ferroresonance using Rudenberg's graphical analysis versus nonlinear system analysis at various system conditions.**

Chapter 6 briefs the nonlinear dynamical method and its application for ferroresonance in the thesis work. It describes the use of a phase plane diagram in the analysis of a nonlinear system. For a periodic function for nonlinear ferroresonance, the **'Phase-Plane'** analysis produces **'Limit Cycles'**. The method to determine the **'Stability'** of a nonlinear ferroresonance system is to provide a small **'Perturbation'** at a steady state and if the system returns to its previous 'Phase Plane' path then the system will be called **'Stable'** otherwise **'Unstable'**. So a **'Stability domain of nonlinear ferroresonance'** has been studied. Mathematically, the linearization method that is used to determine the **'Stability of a Fixed Point'** cannot be applied to the **'Stability of Limit Cycles'**. The **''Stability of Limit Cycles'** problem has been converted into a 'Stability of a Fixed Point' problem by using the concept of **'The Poincare method and Floquet theory for the stability of periodic orbit**. The study of the Poincare plot also reveals how a system '**Bifurcate from one Stable state to another Stable state'**. So this **Limit Cycles study provides us with the quality of the ferroresonance system or a power system actually: a power system is a nonlinear system.**

Chapter 7 shows the simulation study of the model ferroresonance system used in Chapter 5. In this case, the system is under ferroresonance and the supply voltages are increased in steps. The Poincare plots of different ferroresonance system voltages are also observed. At first system generates a single point on the Poincare plane. As the supply voltage is increased, it generates two points, then four, eight and so on leading to **the Period-Doubling Behavior of Ferroresonance**. At a very high supply voltage, the Poincare plot shows a **'Strange Attractor'** which changes with the change of initial condition. The behavior of the system at this stage is moving to '**Chaos**'. The bifurcation plot, which holds all the Poincare plots for all supply voltages in a single diagram, shows a period-doubling behavior of the system. The calculation of **'The Feigenbaum Constant'** also establishes the fact that the system will ultimately land in

chaos after **successive period doubling**. In the end, the bifurcation study with series capacitance as the **'Bifurcation'** parameter is also made.

Chapter 8 deals with the stability of the system at different **periodic oscillation**s as obtained in the **bifurcation diagram** in the previous chapter. For determining the stability at the period-1 region of the bifurcation diagram, a small perturbation is injected in the flux linkage while the system is in a steady state. Poincare plots and phase plane diagram shows that the system iterates back to its previous operating condition. To verify this condition mathematically, **the Jacobian matrix was calculated with the Poincare values near perturbation**. The magnitude of the **Eigenvalues of the Jacobian matrix** falls within the unity value. A similar investigation was carried out in the period-2 region and mathematical calculation shows the **system lost its period-1 stability**. **For period-2 oscillation**, the relations $x_{(i+2)} = x_i$ and $y_{(i+2)} = y_i$ hold, and the **Eigenvalues of the Jacobian matrix fall within the value 1**. Analysis with **period-4 oscillation** is also performed and verified.

Chapter 9 gives the details of **finite element analysis done on the ferroresonance** circuit. To know the **magnetic field distribution in the core of the transformer** during ferroresonance conditions, the finite element method is used. The **transformer model is built up in the Comsol Multiphysics** simulator. The core characteristic equation that was used in the previous chapters is injected into the core properties. Then to build up the ferroresonance circuit, **the magnetic field model of the transformer is coupled with the electric circuit** model consisting of an alternating voltage source, capacitor in series, and resistance in parallel which will act as core loss resistance. The current developed in the circuit is used as the excitation parameter of the primary of the transformer keeping the secondary of the transformer open. The simulation was done with different supply voltages. At a certain supply voltage ferroresonance is observed. **The results match with the experimental outputs** given in Chapter 3. **The magnetic flux density distribution during ferroresonance is also observed.**

All experiments in the laboratory have been performed with a supply of 230V/phase or 440V/line voltage and 250V tapping of the transformer is used as it is rated for 440V. The value of series capacitance used to obtain ferroresonance is 1.272 μF.

Now for the 11 kV line, the value of this capacitance can be calculated as

$= 1.272 \times (440/11000) \times (440/11000) = 2035.2\, pF$

Similarly, for the 33 kV line, the value will be $= 226.13\, pF$ and

For the 220 kV line, the value will be $= 5.088\ pF$.

So the above calculations indicate that **a small capacitance in the order of nano-farad is sufficient to generate ferroresonance in the high voltage lines. So when system voltage increases, the ferroresonance risk factor increases in the line. The ferroresonance capacitance depends on the length of the transmission line of a particular power system. Hence a safe length can be calculated using this laboratory test method and this should be a proper guideline for mitigating the ferroresonance in the line design stage.**

So the transformers fed via capacitive coupling from 3-phase sources at open-phase conditions have been considered a prospective ferroresonance system in the power system. To simulate ferroresonance - a non-linear system is formed by a transformer and line capacitance in series. A non-linear model of the magnetizing characteristics of transformers is built using the magnetizing characteristics of core-type transformers, which are recorded in a digital recorder in the laboratory. Several simulations of ferroresonance oscillations in the time domain that result in high voltage/current in the line elements of the non-linear system are examined, and the different outcomes demonstrate fundamental frequency, sub-harmonic, and chaotic ferroresonance.

The ferroresonance experimental recorded wave-form of over-voltages across transformer and capacitor are slightly different than the wave-form obtained by the model simulating ferroresonance. This may be due to imperfections in the model developed. However, it is very difficult to model transformer magnetizing characteristics exactly as practically as it behaves, because the residual magnetism, saturation, hysteresis, eddy current, magnetostriction, and frequency all affect the magnetic, electrical, and mechanical properties of the ferromagnetic material that makes up the transformer core. However, there is a consistency and similarity in the magnitude and quality of over-voltages on ferroresonance obtained in experimental and model simulation results.

The results of the simulation demonstrate that even a small change in applied voltage (0.1 mV) can produce a voltage across the capacitor and transformer that is significantly greater than the supply voltage. This can cause a persistent ferroresonance over-voltage in the line, where the voltage of the capacitor is higher than the voltage of the transformer. So a minute variation of the system parameter in a nonlinear system can result in a different state of operations and that has been explained by R. Rudenberg's graphical method. However, recent analytical techniques

applied to nonlinear systems (repeated solution of the nonlinear differential equations of the system) have demonstrated that various ferroresonance voltages can arise from variations in the value of the equivalent circuit parameters, potentially due to system configuration changes. It has also been demonstrated that chaotic ferroresonance states are likely to arise within a wide range of system parameters, even though fundamental frequency and sub-harmonic ferroresonance situations may occur under common-place operating settings.

It is highly desired for engineers to have a thorough understanding of these ferroresonance possibilities so they may plan for the expansion of their systems without increasing the likelihood of ferroresonance and operate their systems outside of hazardous areas. The work described, together with recent studies of ferroresonance as a nonlinear phenomenon with involved terminology such as '**Phase-Space', 'Trajectory', 'State variables', 'Limit-cycle', 'Aperiodic', 'Chaotic'**, although these terms have wide applications for a nonlinear dynamical system in mathematical science. However, the observations of a minute variation of the system parameter (suppose source voltage) in a **nonlinear system** can result in different states of operations. For example; **period one** response with small amplitude producing a **circular** small **stable orbit (limit-cycle)** in the phase–space {transformer voltage $\left(\frac{d\lambda}{dt} = v\right)$ vs. flux linkage (λ)} and a minute variation of the system parameter (suppose source voltage) results in another big **non-circular stable orbit (limit-cycle)** in phase-space producing high voltage in the system. This type of multiple stable operation and behavior cannot be seen in a linear system i.e. if a linear inductor in series with linear capacitor excited from alternating voltage source and that is a period one response. But when there are **2-loops** in phase-space then that is **period-2** response which is called as **sub-harmonic** response and various sub-harmonic responses are found in this simulation results of ferroresonance. When the response has **period-infinity,** that is, **an aperiodic** response known as a **chaotic** ferroresonance solution, the phase-space shows a trajectory that will **never close** onto itself.

The **Poincare map** is a simple replica of the phase plane trajectory recorded as a sequence of discrete points at constant time intervals and if the frequency of the forcing function (i.e. the frequency of the supply voltage) is taken as the sampling frequency then, the Poincare map will show only one point for a periodic waveform. This is shown in the simulation results. The Poincare mapping is a valuable tool to confirm the periodicity of ferroresonance response. A chaotic response will produce a Poincare map with a haphazard set of points restricted to a

particular region of the phase plane. The Poincare mapping can give important information about the frequency ratio of the forcing function to the real response frequency of the system.

The simulation results do not yet provide a comprehensive understanding of the nonlinear system and chaos. Many questions are still to be answered from the standpoint of nonlinear science for chaos.

10.2 Future Work

The analysis and explanations of this thesis offer a solid starting point for future studies on ferroresonance systems powered by alternating voltage sources.

Several difficult yet valuable domains where this study can be used and leveraged for subsequent research include the following

1. A study of ferroresonance circuits has been done with series capacitance only. But in power networks, there are possibilities of parallel capacitive effect also. Implementation of a parallel connected capacitor in the ferroresonance circuit by both computer simulations and experimental testing can be a good prospect.
2. It has been found that the system reaches chaotic behavior while changing one of the system parameters. Due to time restrictions, the chaotic behavior of the system could not be studied in detail, which can be done in future work.
3. FEM has been used here to predict the transformer condition during ferroresonance this study can be improved further with a 3-phase transformer which is used in a power system. That also may be a future scope of work.

References

[1] Bethenod, J., "Sur le Transformateur à Résonance", L'Éclairage Électrique, vol. 53, Nov. 30, 1907, pp. 289-96.

[2] Boucherot, P.,"Éxistence de Deux Régimes en Ferrorésonance", Rev. Gen. de L'Élec., vol. 8, no. 24, December 11, 1920, pp. 827-828.

[3] R. Rudenberg, "Transient Performance of Electric Power System," New York: McGraw-Hill, 1950, pp. 642–656.

[4] Mork BA. "Understanding and Dealing with Ferroresonance". Minnesota Power Systems Conf. November 7-9, 2006

[5] P. Sakarung, T. Bunyagul and S. Chatratana, "Investigation and Mitigation of Overvoltage Due to Ferroresonance in the Distribution Network", Journal of Electrical Engineering and Technology, vol. 2, no. 3, pp. 300-305, 2007

[6] Yunge Li, Wei Shi, Rui Qin and Jilin Yang, "A Systematical Method for Suppressing Ferroresonance at Neutral-Grounded Substations", IEEE Transactions on Power Delivery, vol. 18, no.3, July 2003.

[7] Hamid Radmanesh and Mehrdad Rostami, "Effect of Circuit Breaker Shunt Resistance on Chaotic Ferroresonance in Voltage Transformer", Advances in Electrical and Computer Engineering, vol. 10, no. 3, 2010.

[8] F. Wornle, D. K. Harrison and Chengke Zhou, "Analysis of a ferroresonant circuit using bifurcation theory and continuation techniques," in IEEE Transactions on Power Delivery, vol. 20, no. 1, pp. 191-196, Jan. 2005, doi: 10.1109/TPWRD.2004.835529.

[9] Zhang Bo and Lu Tiecheng, "Application of Nonlinear Dynamic on Ferroresonance in Power System", Proceedings of Asia-Pacific Power and Energy Engineering Conference, pp. 1-4, Wuhan China, 27-31 March 2009

[10] M. Stosur, W. Piasecki, M. Florkowski and M. Fulczyk, "ATP/EMTP Study of Ferroresonance Involving HV Inductive VT and Circuit Breaker Capacitance", Electrical Power Quality and Utilization Journal, vol. 14, no. 2, 2008.

[11] Anbarri, K., Ramanujam, R. Rao, CH. Subba, Kuppusamy, K., "Effect of Circuit Configuration on Chaotic Ferroresonance in a Power Transformer", Electric Power Components and Systems, vol 30, pp. 1015–1031, 2002, doi: 10.1080/15325000290085334

[12] K. Al-Anbarri, R. Ramanujam, R. Saravanaselvan, K. Kuppusamy, "Effect of iron core loss nonlinearity on chaotic ferroresonance in power transformers", Electric Power Systems Research, Volume 65, Issue 1, 2003, Pages 1-12, doi:10.1016/S0378-7796(02)00210-9.

[13] Kumar, Goutham; Rajan, Saravanaselvan; and Rangarajan, Ramanujam "Analysis of Ferroresonance in a Power Transformer with Multiple Nonlinearities," International Journal of Emerging Electric Power Systems: Vol. 7, Issue. 2, 2006. doi: 10.2202/1553-779X.1119

[14] Madhab Roy and Chinmay Kanti Roy, "A Study on Ferroresonance with a varying Initial Conditions using a Nonlinear Model of Transformer", Proceedings of Third International Conference on Power Systems, no. 213, India, 2009.

[15] M. Roy and C. K. Roy, "A study on ferroresonance and its depedence on instant of switching angle of the source voltage," 2009 International Conference on Power Systems, Kharagpur, India, 2009, pp. 1-6. doi: 10.1109/ICPWS.2009.5442704.

[16] M. L. Prasad, M. Roy and C. K. Roy, "Analysis of Ferroresonant Oscillations in a Nonlinear Circuit," 2008 IEEE Region 10 and the Third international Conference on Industrial and Information Systems, Kharagpur, India, 2008, pp. 1-6. doi: 10.1109/ICIINFS.2008.4798433.

[17] M. Roy and C. K. Roy, "Experiments on Ferroresonance at Various Line Conditions and Its Damping," 2008 Joint International Conference on Power System Technology and IEEE Power India Conference, New Delhi, India, 2008, pp. 1-8. doi: 10.1109/ICPST.2008.4745305

[18] V. Valverde, G. Buigues, A. J. Mazón, I. Zamora, I. Albizu, "Ferroresonant Configurations in Power Systems", International Conference on Renewable Energies and Power Quality (ICREPQ'12), Spain, March, 2012

[19] R. J. Rusch and M. L. Good, "Wyes and wye nots of three-phase distribution transformer connections," Papers Presented at the 33rd Annual Conference Rural Electric Power Conference, Colorado Springs, CO, USA, 1989, pp. C2/1-C2/7, doi: 10.1109/REPCON.1989.95535.

[20] P. E. Sutherland and T. A. Short, "Effect of Single-Phase Reclosing on Industrial Loads," Conference Record of the 2006 IEEE Industry Applications Conference Forty-First IAS Annual Meeting, Tampa, FL, USA, 2006, pp. 2636-2644, doi: 10.1109/IAS.2006.256912.

[21] Zhu Xukai, Yang Yihan, Lian Hongbo and Tan Weipu, "Study on ferroresonance due to electromagnetic PT in ungrounded neutral system," International Conference on Power System Technology, PowerCon 2004. Singapore, 2004, pp. 924-929 Vol.1, doi: 10.1109/ICPST.2004.1460126.

[22] M. Monadi, A. Luna, J. I. Candela, J. Rocabert, M. Fayezizadeh and P. Rodriguez, "Analysis of ferroresonance effects in distribution networks with distributed source units," IECON 2013 - 39th Annual Conference of the IEEE Industrial Electronics Society, Vienna, Austria, 2013, pp. 1974-1979, doi: 10.1109/IECON.2013.6699434.

[23] D. Braun, M. Delfanti, M. Palazzo and R. Zich, "Harmonic distortion in power stations due to ferroresonance," 2012 Asia-Pacific Symposium on Electromagnetic Compatibility, Singapore, 2012, pp. 101-104, doi: 10.1109/APEMC.2012.6237886.

[24] G. Kaur and M. Y. Vaziri, "Effects of distributed generation (DG) interconnections on protection of distribution feeders," 2006 IEEE Power Engineering Society General Meeting, Montreal, QC, Canada, 2006, pp. 8 pp.-, doi: 10.1109/PES.2006.1709551.

[25] K. Laohacharoensombat, K. Tuitemwong, S. Jaruwattanadilok, C. Wattanasakpubal and K. Kleebmek, "Case study of ferroresonance in 33 kV distribution network of PEA Thailand," 2004 IEEE Region 10 Conference TENCON 2004., Chiang Mai, Thailand, 2004, pp. 417-420 Vol. 3, doi: 10.1109/TENCON.2004.1414796.

[26] K. Al-Anbarri, R. Ramanujam, T. Keerthiga, K. Kuppusamy, "Analysis of nonlinear phenomena in MOV connected transformer", IEE Proceedings - Generation, Transmission and Distribution, vol. 148, Issue 6, November 2001, pp. 562 – 566, doi: 10.1049/ip-gtd:20010571

[27] M. Esmaeili, M. Rostami, G. B. Gharehpetian and C. P. McInnis, "Ferroresonance After Islanding of Synchronous Machine-Based Distributed Generation," in Canadian Journal of Electrical and Computer Engineering, vol. 38, no. 2, pp. 154-161, Spring 2015, doi: 10.1109/CJECE.2015.2411713

[28] Abdelmalik Djebli, Faouzi Aboura, Lazhar Roubache, Omar Touhami, "Impact of the eddy current in the lamination on ferroresonance stability at critical points", International Journal of Electrical Power & Energy Systems, Vol. 106, 2019, pp. 311-319, doi:10.1016/j.ijepes.2018.10.008.

[29] A. Rezaei-Zare, M. Sanaye-Pasand, H. Mohseni, S. Farhangi and R. Iravani, "Analysis of Ferroresonance Modes in Power Transformers Using Preisach-Type Hysteretic Magnetizing Inductance," in IEEE Transactions on Power Delivery, vol. 22, no. 2, pp. 919-929, April 2007, doi: 10.1109/TPWRD.2006.877078.

[30] V. Simha and W. -j. Lee, "Transient Behavior of Three-Phase Shell Transformers in a Distribution Feeder," Conference Record of the 2006 IEEE Industry Applications Conference Forty-First IAS Annual Meeting, Tampa, FL, USA, 2006, pp. 741-746, doi: 10.1109/IAS.2006.256609.

[31] J. Pienaar and P. H. Swart, "Ferro-resonance in a series capacitor system supplying a submerged-arc furnace," IEEE AFRICON. 6th Africon Conference in Africa, George, South Africa, 2002, pp. 785-789 vol.2, doi: 10.1109/AFRCON.2002.1160014.

[32] A. Noosuk et al., "Commissioning experience of the 300 MW Thailand-Malaysia Interconnection project," IEEE/PES Transmission and Distribution Conference and Exhibition, Yokohama, Japan, 2002, pp. 1004-1009 vol.2, doi: 10.1109/TDC.2002.1177614.

[33] P. E. Sutherland and R. Manning, "Ferroresonance in a 13.8 kV Distribution Line," Conference Record of the 2006 IEEE Industry Applications Conference Forty-First IAS Annual Meeting, Tampa, FL, USA, 2006, pp. 2238-2241, doi: 10.1109/IAS.2006.256853.

[34] Ta-Peng Tsao and Chia-Ching Ning, "Analysis of ferroresonant overvoltages at Maanshan Nuclear Power Station in Taiwan," in IEEE Transactions on Power Delivery, vol. 21, no. 2, pp. 1006-1012, April 2006, doi: 10.1109/TPWRD.2005.860268.

[35] D. A. N. Jacobson, "Examples of ferroresonance in a high voltage power system," 2003 IEEE Power Engineering Society General Meeting (IEEE Cat. No.03CH37491), Toronto, ON, Canada, 2003, pp. 1206-1212 Vol. 2, doi: 10.1109/PES.2003.1270499.

[36] R. C. Dugan, "Examples of ferroresonance in distribution," 2003 IEEE Power Engineering Society General Meeting (IEEE Cat. No.03CH37491), Toronto, ON, Canada, 2003, pp. 1213-1215 Vol. 2, doi: 10.1109/PES.2003.1270500.

[37] M. Rioual and C. Sicre, "Energization of a no-load transformer for power restoration purposes: modeling and validation by on site tests," 2000 IEEE Power Engineering Society Winter Meeting. Conference Proceedings (Cat. No.00CH37077), Singapore, 2000, pp. 2239-2244 vol.3, doi: 10.1109/PESW.2000.847704.

[38] J. Z. Vernieri, M. B. Barbieri and P. L. Arnera, "Consequence of an unbalanced supplying condition on a distribution transformer," 2001 IEEE Porto Power Tech Proceedings (Cat. No.01EX502), Porto, Portugal, 2001, pp. 6 pp. vol.4-, doi: 10.1109/PTC.2001.964865.

[39] S. Mišák and J. Fulneček, "The influence of ferroresonance on a temperature of voltage transformers in undeground mines," 2017 18th International Scientific Conference on Electric Power Engineering (EPE), Kouty nad Desnou, Czech Republic, 2017, pp. 1-4, doi: 10.1109/EPE.2017.7967361.

[40] D. Femandes, W. L. A. Neves, J. C. A. Vasconcelos and M. V. Godoy, "Comparisons Between Lab Measurements and Digital Simulations for a Coupling Capacitor Voltage Transformer," 2006 IEEE/PES Transmission & Distribution Conference and Exposition: Latin America, Caracas, Venezuela, 2006, pp. 1-6, doi: 10.1109/TDCLA.2006.311664.

[41] Yunge Li, Wei Shi, Rui Qin and Jilin Yang, "A systematical method for suppressing ferroresonance at neutral-grounded substations," in IEEE Transactions on Power Delivery, vol. 18, no. 3, pp. 1009-1014, July 2003, doi: 10.1109/TPWRD.2003.813858.

[42] M. Graovac, R. Iravani, Xiaolin Wang and R. D. McTaggart, "Fast ferroresonance suppression of coupling capacitor voltage transformers," in IEEE Transactions on Power Delivery, vol. 18, no. 1, pp. 158-163, Jan. 2003, doi: 10.1109/TPWRD.2002.803837.

[43] P. Picher, L. Bolduc, B. Girard and V. N. Nguyen, "Mitigation of Ferroresonance Induced by Single-Phase Opening of a Three-Phase Transformer Feeder," 2006 Canadian Conference on Electrical and Computer Engineering, Ottawa, ON, Canada, 2006, pp. 482-485, doi: 10.1109/CCECE.2006.277410.

[44] Z. Bo, L. Tiecheng, G. dong and D. Xiaolei, "Application of Equivalent Linearization Algorithm on Voltage Transformer Protection during Fundamental Resonance in Power System," 2006 IEEE 8th International Conference on Properties & applications of Dielectric Materials, Bali, Indonesia, 2006, pp. 361-364, doi: 10.1109/ICPADM.2006.284190.

[45] W. Piasecki, M. Florkowski, M. Fulczyk, P. Mahonen and W. Nowak, "Mitigating Ferroresonance in Voltage Transformers in Ungrounded MV Networks," in IEEE Transactions on Power Delivery, vol. 22, no. 4, pp. 2362-2369, Oct. 2007, doi: 10.1109/TPWRD.2007.905383.

[46] Y. Zan, W. Qian, D. Jiandong and T. Wangjing, "Nonlinear dynamic analysis and ZnO-based suppression of ferroresonance overvoltage in distribution network," 2015 5th International Conference on Electric Utility Deregulation and Restructuring and Power Technologies (DRPT), Changsha, China, 2015, pp. 1321-1325, doi: 10.1109/DRPT.2015.7432434.

[47] H. Radmanesh, A. Heidary, S. H. Fathi, G. B. Gharehpetian, “Dual function ferroresonance and fault current limiter based on DC reactor”, IET Gener. Transm. Distrib., 2016, Vol. 10, Iss. 9, pp. 2058–2065, doi: 10.1049/iet-gtd.2015.1032

[48] A. Ben-Tal, V. Kirk and G. Wake, "Banded chaos in power systems," in IEEE Transactions on Power Delivery, vol. 16, no. 1, pp. 105-110, Jan. 2001, doi: 10.1109/61.905606.

[49] Z. Emin, B. A. T. Al Zahawi, Yu Kwong Tong and M. Ugur, "Quantification of the chaotic behavior of ferroresonant voltage transformer circuits," in IEEE Transactions on Circuits and Systems I: Fundamental Theory and Applications, vol. 48, no. 6, pp. 757-760, June 2001, doi: 10.1109/81.928158.

[50] B. Tanggawelu, R. N. Mukerjee and A. E. Ariffin, "Ferroresonance studies in Malaysian utility's distribution network," 2003 IEEE Power Engineering Society General Meeting (IEEE Cat. No.03CH37491), Toronto, ON, Canada, 2003, pp. 1216-1219 Vol. 2, doi: 10.1109/PES.2003.1270501.

[51] Yunge Li, Wei Shi and Furong Li, "Novel analytical solution to fundamental ferroresonance-part I: power frequency excitation characteristic," in IEEE Transactions on Power Delivery, vol. 21, no. 2, pp. 788-793, April 2006, doi: 10.1109/TPWRD.2005.859303.

[52] K. Milicevic and Z. Emin, "Initiation of Characteristic Ferroresonance States Based on Flux Reflection Model," in IEEE Transactions on Circuits and Systems II: Express Briefs, vol. 60, no. 1, pp. 51-55, Jan. 2013, doi: 10.1109/TCSII.2012.2234897.

[53] Hamid Reza Abbasi Fordoei, Ahmad Gholami, Seyyed Hamid Fathi, Ataollah Abbasi, “A new approach to eliminating of chaotic ferroresonant oscillations in power transformer”, Electrical Power and Energy Systems, vol. 67, pp. 152–160, 2015, doi: 10.1016/j.ijepes.2014.11.021

[54] N. A. Janssens, "Magnetic cores modeling for ferroresonance computations using the harmonic balance method," 2003 IEEE Power Engineering Society General Meeting (IEEE Cat. No.03CH37491), Toronto, ON, Canada, 2003, pp. 1644-1649 Vol. 3, doi: 10.1109/PES.2003.1267402.

[55] M. Moradi and A. Gholami, “A Harmonic Balance Based Stability Domain Analysis of Period-1 Ferroresonance”, Electric Power Components and Systems, vol. 39, no. 12, 2011, pp. 1315-1328. doi: 10.1080/15325008.2011.567218

[56] J. A. Martinez and B. A. Mork, "Transformer modeling for simulation of low-frequency transients," 2003 IEEE Power Engineering Society General Meeting (IEEE Cat. No.03CH37491), Toronto, ON, Canada, 2003, pp. 1223-1225 Vol. 2, doi: 10.1109/PES.2003.1270503.

[57] A. Tokic, V. Madzarevic and I. Uglesic, "Numerical calculations of three-phase transformer's transients," 2003 IEEE Bologna Power Tech Conference Proceedings,, Bologna, Italy, 2003, pp. 7 pp. Vol.2-, doi: 10.1109/PTC.2003.1304644.

[58] A. Rezaei-Zare, H. Mohseni, M. Sanaye-Pasand, S. Farhangi and R. Iravani, "Performance of various magnetic core models in comparison with the laboratory test results of a ferroresonance test on a 33 kV voltage transformer," 2006 IEEE Power Engineering Society General Meeting, Montreal, QC, Canada, 2006, pp. 8 pp.-, doi: 10.1109/PES.2006.1709624.

[59] S. Jazebi et al., "Duality Derived Transformer Models for Low-Frequency Electromagnetic Transients—Part I: Topological Models," in IEEE Transactions on Power Delivery, vol. 31, no. 5, pp. 2410-2419, Oct. 2016, doi: 10.1109/TPWRD.2016.2517327.

[60] J. A. Corea-Araujo, F. González-Molina, J. A. Martínez, F. Castro-Aranda, J. A. Barrado-Rodrigo and L. Guasch-Pesquer, "Single-phase transformer model validation for ferroresonance analysis including hysteresis," 2015 IEEE Power & Energy Society General Meeting, Denver, CO, USA, 2015, pp. 1-5, doi: 10.1109/PESGM.2015.7285872.

[61] A. Rezaei-Zare, "Equivalent Winding Capacitance Network for Transformer Transient Analysis Based on Standard Test Data," in IEEE Transactions on Power Delivery, vol. 32, no. 4, pp. 1899-1906, Aug. 2017, doi: 10.1109/TPWRD.2016.2578047.

[62] D. A. N. Jacobson, P. W. Lehn and R. W. Menzies, "Stability domain calculations of period-1 ferroresonance in a nonlinear resonant circuit," in IEEE Transactions on Power Delivery, vol. 17, no. 3, pp. 865-871, July 2002, doi: 10.1109/TPWRD.2002.1022816.

[63] Seker, S., Akinci, T.C. & Taskin, S. Spectral and statistical analysis for ferroresonance phenomenon in electric power systems. Electr Eng 94, 117–124 (2012), doi:10.1007/s00202-011-0224-4

[64] M. Moradi and A. Gholami, "Numerical and experimental analysis of core loss modeling for period-1 ferroresonance," Eur. Trans. Elect. Power, no. 21, pp. 18–26, 2011, doi: 10.1002/etep.408

[65] I. D. Mayergoyz, Mathematical Models of Hysteresis and Their Applications. New York: Academic Press/Elsevier, 2003

[66] A. Tokić and J. Smajić, "Modeling and Simulations of Ferroresonance by Using BDF/NDF Numerical Methods," in IEEE Transactions on Power Delivery, vol. 30, no. 1, pp. 342-350, Feb. 2015, doi: 10.1109/TPWRD.2014.2346766.

[67] Yunge Li, Wei Shi and Furong Li, "Novel analytical solution to fundamental ferroresonance - part II: criterion and elimination," in IEEE Transactions on Power Delivery, vol. 21, no. 2, pp. 794-800, April 2006, doi: 10.1109/TPWRD.2005.859302.

[68] Hamdi Abdi, Shahriar Abbasi, Mohammad Moradi, "Analyzing the stochastic behavior of ferroresonance initiation regarding initial conditions and system parameters", International Journal of Electrical Power & Energy Systems, Vol. 83, 2016, pp 134-139, doi:/10.1016/j.ijepes.2016.04.016.

[69] Bikash Patel, Sankar Das, C.K. Roy, M. Roy, "Simulation of Ferroresonance with Hysteresis Model of Transformer at No-load Measured in Laboratory", TENCON 2008, IEEE Conference

[70] Kruno Miličević, Zia Emin, "Impact of initial conditions on the initiation of ferroresonance", International Journal of Electrical Power & Energy Systems, Volume 31, Issue 4, 2009, Pages 146-152, doi: /10.1016/j.ijepes.2008.10.015

[71] H. Li, Y. Fan and R. Shi, "Chaos and Ferroresonance," 2006 Canadian Conference on Electrical and Computer Engineering, Ottawa, ON, Canada, 2006, pp. 494-497, doi: 10.1109/CCECE.2006.277616.

[72] R. A. Walling, "Ferroresonance in low-loss distribution transformers," 2003 IEEE Power Engineering Society General Meeting (IEEE Cat. No.03CH37491), Toronto, ON, Canada, 2003, pp. 1220-1222 Vol. 2, doi: 10.1109/PES.2003.1270502.

[73] Chang H, Chun Y, Yeong HCh, Faa J, Chao M, Jau GL, "Effect of Magnetostriction on the core loss, noise, and vibration of flux gate sensor composed of amorphous materials". IEEE Trans Magn, 2013, 49(7), doi: 10.1109/TMAG.2013.2248702

[74] Njafi A, Iskender I, "Impacts of amorphous core to reduce the losses in distribution transformer based on time stepping finite element method". Int J Tech Phys Probl Eng (IJTPE), 2015, 7(3), pp:53–57

[75] I. M. Yulistya Negara, I. G. Ngurah Satriyadi Hernanda, D. A. Asfani, D. Fahmi, M. Wahyudi and R. Hidayat, "Comparison of Ferroresonance Response on Three Phases Transformer with Different Core Material: M5 and ZDKH," 2018 International Seminar on Intelligent Technology and Its Applications (ISITIA), Bali, Indonesia, 2018, pp. 129-134, doi: 10.1109/ISITIA.2018.8710895.

[76] P. Sakarung, "Bifurcation diagram with Electromagnetic Transient Program (EMTP) for ferroresonance analysis," ECTI-CON2010: The 2010 ECTI International Confernce on Electrical Engineering/Electronics, Computer, Telecommunications and Information Technology, Chiang Mai, Thailand, 2010, pp. 289-292.

[77] J. A. Corea-Araujo, F. González-Molina, J. A. Martínez, J. A. Barrado-Rodrigo and L. Guasch-Pesquer, "Tools for Characterization and Assessment of Ferroresonance Using 3-D Bifurcation Diagrams," in IEEE Transactions on Power Delivery, vol. 29, no. 6, pp. 2543-2551, Dec. 2014, doi: 10.1109/TPWRD.2014.2320599.

[78] John H. Hubbard, Beverly H. West, "Differential Equations: A Dynamical Systems Approach", Springer, 1995. doi: 10.1 007/978-1-4612-4192-8

[79] S. Banerjee and G. C. Verghese, Nonlinear Phenomena in Power Electronics, New York: IEEE Press, July 2001.

[80] Steven H. Strogatz, "Nonlinear Dynamics and Chaos: With Applications to Physics, Biology, Chemistry, and Engineering", Perseus Books Group, 2001

[81] J. M. T. Thompson and H. B. Stewart, Nonlinear Dynamics and Chaos, John Wiley & Sons, 2002, pp 169-172

[82] Nicholas J. Giordano, Hisao Nakanishi, "Computational Physics" 2nd Edition, Prentice Hall, 2006, pp 58-69

[83] Ali H. Nayfeh, Balakumar Balachandran, "Applied Nonlinear Dynamics, Analytical, Computational, and Experimental Methods" 1st edition, Wiley-VCH, 1995

[84] Feigenbaum, M. J, "Quantitative universality for a class of nonlinear transformations", Journal of Statistical Physics, vol. 19, pp. 25-52, 1978, doi: /10.1007/BF01020332

[85] Collet, P., Eckmann, J.P. & Koch, H. Period doubling bifurcations for families of maps on ℝn Journal of Statistical Physics vol. 25, pp.1–14 (1981). doi:10.1007/BF01008475

[86] V. D. Lebedev, A. V. Makarov and A. A. Yablokov, "Modeling of ferroresonance phenomena in software products Simulink," 2014 International Conference on Computer Technologies in Physical and Engineering Applications (ICCTPEA), St. Petersburg, Russia, 2014, pp. 93-94, doi: 10.1109/ICCTPEA.2014.6893298.

[87] M. Mikhak-Beyranvand, B. Rezaeealam , J. Faiz, A. Rezaei-Zare, "Impacts of ferroresonance and inrush current forces on transformer windings", IET Electric Power Applications, vol. 13, no. 7, pp. 914-921, 2019, doi; 10.1049/iet-epa.2018.5193

[88] Charalambos A. Charalambous, Zhongdong Wang, Paul Jarman, Jonathan Peter Sturgess, "Time-domain finite-element technique for quantifying the effect of sustained ferroresonance on power

transformer core bolts", IET Electr. Power Appl., 2014, vol. 8, no. 6, pp. 221–231, doi: 10.1049/iet-epa.2013.0330

[89] Behrooz Rezaeealam, Behzad Norouzi, "Investigating Ferroresonance Phenomenon in a Single Phase Transformer with the Effect of Magnetic Hysteresis", Indonesian Journal of Electrical Engineering and Computer Science, vol. 2, no. 2, May 2016, pp. 248 - 258, doi: 10.11591/ijeecs.v2.i2.pp248-258

[90] Singiresu S. Rao, "The Finite Element Method in Engineering", Elsevier Science & Technology Books, 2004, pp. 53-68, pp 235-270.

[91] Sheppard J. Salon, "Finite Element Analysis of Electrical Machines" Springer, 1995, pp. 1-10

[92] E. Lange, F. Henrotte and K. Hameyer, "A Variational Formulation for Nonconforming Sliding Interfaces in Finite Element Analysis of Electric Machines," in IEEE Transactions on Magnetics, vol. 46, no. 8, pp. 2755-2758, Aug. 2010, doi: 10.1109/TMAG.2010.2043075.

[93] M. M. Botha and Jian-Ming Jin, "On the variational formulation of hybrid finite element-boundary integral techniques for electromagnetic analysis," in IEEE Transactions on Antennas and Propagation, vol. 52, no. 11, pp. 3037-3047, Nov. 2004, doi: 10.1109/TAP.2004.835140.

[94] Nicola Bianchi, "Electrical Machine Analysis Using Finite Elements" Taylor & Francis, 2005, pp. 25-59 and 95-122

[95] Rosa Ana Salas, and Jorge Pleite. "Nonlinear Modeling of E-Type Ferrite Inductors Using Finite Element Analysis in 2D" Materials 2014, vol. 7, no. 8, pp. 5454-5469, doi:10.3390/ma7085454

[96] E. Melgoza, R. Escarela-Perez, J. L. Guardado and M. A. Arjona-López, "Strong Coupling of an Electromagnetic Transients Program and a Finite Element Magnetic Field Solver Including Eddy Currents," in IEEE Transactions on Power Delivery, vol. 32, no. 3, pp. 1414-1421, June 2017, doi: 10.1109/TPWRD.2016.2604225.

[97] S. E. Zirka, Y. I. Moroz, A. J. Moses and C. M. Arturi, "Static and Dynamic Hysteresis Models for Studying Transformer Transients," in IEEE Transactions on Power Delivery, vol. 26, no. 4, pp. 2352-2362, Oct. 2011, doi: 10.1109/TPWRD.2011.2140404

Rajat Shubhra Pal
18.1.24

18.01.2024

Associate Professor
Electrical Engg. Dept.
Jadavpur University
Kolkata - 700 032